

Fatigue behavior of resin and steel reinforced resin used in IBCs



Master's Thesis

Konstantinos Roupakas

Faculty of Civil Engineering and Geosciences

Delft University of Technology

June 2019, Delft



Fatigue behavior of resin and steel reinforced resin used in IBCs

By

Konstantinos Roupakas

in partial fulfilment of the requirements for the degree of

Master of Science

in Civil Engineering

at the Delft University of Technology,

to be defended publicly on Friday June 28, 2019 at 11:00

Supervisor:	Prof. dr.	M. Veljkovic	TU Delft
Thesis committee:	Dr.	O. Çopuroğlu	TU Delft
	Dr.	H. Xin	TU Delft
	Ir.	M.P. (Martin) Nijgh	TU Delft

An electronic version of this thesis is available at <http://repository.tudelft.nl/>.



Preface

This Thesis is submitted as the final requirement to obtain a Master's degree in Civil Engineering at Delft University of Technology. The topic of the thesis is an experimental and numerical investigation of fatigue properties of epoxy resin and recently developed steel reinforced resin with a tailor-made for this research test set-up. Structural resins are used in injected bolted connections in civil engineering steel structures applications.

I started working on my Thesis in September 2018 focusing on state of the art and preliminary testing of specimens aiming to optimise the assembly and testing process. For a fatigue experimental program, a significant number of specimens, tested in thousands of cycles is demanded and a large amount of data have to be handled. Therefore, I used the testing rig continuously until April 2019, testing most of specimens for at least 1 day and some of them for 3-10 days. The months of April and May 2019 have been used for statistical evaluation of the data and finalizing my Thesis towards to graduation on June 2019.

First of all, I would like to express my deep gratitude to all the members of my Assessment Committee, prof. dr. M. Veljkovic, dr. H. Xin and ir. M.P. (Martin) Nijgh from department of Steel and Composite structures of T.U Delft and dr. O. Çopuroğlu from department of Materials and Environment. Their professional guidance and advice were valuable assets through my research. I would like to thank dr. W.F. Gard for his collaboration and finally the laboratory staff members F.J.P Schilperoort, G. Stamoulis and K. Mouthaan. for their aid in execution of experiments.

Of course, last but not least I would like to thank my family and friends for being helpful, supportive and for inspiring me to follow my dreams despite all difficulties during my studies.

Konstantinos Roupakas

Delft, May 2019

Abstract

Injection Bolts have been preferred for several reasons over other alternatives for the rehabilitation of old riveted steel bridges since 1970's. More recently they have been used to obtain slip critical shear connections in new structures such as new bridges, large roofs, storm barriers and other structures exposed to cyclic loading. In addition, they are tested as a feasible alternative to traditional shear connectors in steel-concrete composite flooring systems, in combination with oversized holes in the flange of steel girder to allow reusability. On the grounds of this research a novel injection material was developed at T.U Delft, namely steel reinforced resin as an alternative to conventional resin allowed in the Netherlands for structural applications without compromising stiffness of connection.

Due to limited research on fatigue of resins used in structural applications, in this study an initial attempt to investigate the cyclic behaviour of conventional and steel reinforced resin subjected to uniaxial compressive cyclic bearing stress, in confined conditions is performed.

First, for this objective an experimental program using a tailor-made test setup was carried out, and the fatigue response in terms of slip over number of cycles for resin and steel reinforced resin in oversized holes of 6mm and 10mm was obtained. With this specimen configuration, is intended to reproduce as possible the stress state of double lap shear connection without endanger the fatigue cracking of steel parts. Frequency, stress ratio and other testing parameters that can influence the results have been chosen based on relative literature and assembly of setup. Three stress ranges used, with the maximum related to the recommended long term bearing stress for conventional resin, while the failure criterion was set at 0.3mm slip which is related to this long term bearing strength at the end of working life.

Secondly, a numerical model of test set-up to investigate the static and quasi-static behaviour of specimens was developed and validated by the quasi static experimental results of initial stiffness of connection. Finally, through statistical treatment of test results fitted curves obtained, and characteristic curves with 95% probability of survival are proposed for both resin types and hole clearances based on probabilistic model of ASTM standard and probabilistic model proposed by Schneider and Maddox, using Student's t distribution.

On the basis of experimental results, large scattering was observed for both type of resins, and more prominent for the larger hole clearance and higher stress range. The reasons for this scatter are discussed and recommendations for future improvement of set-up are proposed. Due to scatter the results could not fully support the expectations that fatigue behaviour of steel reinforced resin is superior to that of conventional, as it is the case in static and creep behaviour. From a selection of specimens with limited scatter in 6mm oversized holes, a trend that connections with steel reinforced resin lead to less slip due to cyclic loads after 500.000 cycles was observed.

From the numerical research on static models of specimens it was verified that the bearing stress state of resin layer is almost identical to that of the double lap shear connection of EN 1090-2 indicating a similar stress transfer mechanism. From the statistical evaluation of test data with ASTM probabilistic model the use of steel reinforced resin leads to higher fatigue endurance related to conventional resin in 10mm oversized hole, while the fatigue life of specimens with conventional resin decreased with larger hole clearance namely from 6 to 10mm.

Contents

List of Figures	ix
List of Tables	xiv
1 Introduction	1
1.1 Problem definition	1
1.2 Research questions.....	2
1.3 Methodology of research	3
1.4 Outline of thesis	3
2 Literature review	4
2.1 Injection Bolts.....	4
2.1.1 Components of injection bolts.....	4
2.1.2 Advantages of injection bolts	8
2.2 Static creep and fatigue behaviour of Resin Injected Bolted Connections (RIBC's).....	9
2.2.1 Static behaviour of IBCs.....	9
2.2.2 Fatigue behaviour of IBCs.....	11
2.3 Application examples with resin injected bolts.....	14
2.3.1 Repair of riveted connections in old steel bridges with injection bolts	14
2.3.2 Maeslant Storm Surge Barrier.....	15
2.3.3 Johan Cruijff Arena - New Stadium of Ajax in Amsterdam	17
2.3.4 Glass roof structure in bus station near Amsterdam Central Station	18
2.3.5 Demountable steel-concrete systems – a new field of research	19
2.4 Oversized and slotted Holes.....	21
2.5 Slip critical joints.....	24
2.6 Fatigue testing of epoxy resins	25
2.6.1 Examples of fatigue tests on resins for various applications.....	25
2.6.2 Testing parameters	28
2.7 Statistical evaluation of experimental results	29
3 Experimental work	33
3.1 Description of the specimens.....	33
3.1.1 Geometry of specimens.....	33
3.1.2 Lower steel (female) plate	34
3.1.3 Upper (male) steel plate.....	35
3.1.4 Threaded bolt part (pin) – M8x80 Hex Bolts – Side Steel plates	37
3.2 Materials.....	38

3.2.1 Resin	39
3.2.2 Steel Reinforced Resin	40
3.2.3 Steel	41
3.3 Assembly of specimens	42
3.4 Test Set-up	53
3.4.1 Loading pattern	54
3.4.2 Control Mode of machine	55
3.4.3 Stress Ratio	56
3.4.4 Cyclic Loading Frequency and Temperature	56
3.4.5 Failure Criterion	56
3.4.6 Stress Range	58
3.4.7 Specimen Designation	58
3.4.8 Loading phases of specimens	59
3.5 Summary of experimental procedure	61
4 Numerical Analysis	62
4.1 Model Description	62
4.1.1 Geometry, material properties and assembly	62
4.1.2 Boundary conditions and interaction	65
4.1.3 Mesh of finite elements	67
4.1.4 Loading Step	68
4.2 Calculation of initial stiffness	69
4.3 Numerical verification of set-up	73
4.4 Parametric Investigation of confinement conditions provided by side plates....	76
4.5 Quasi-static numerical analysis of yielding of upper (male) steel plate.	79
4.6 Conclusions of numerical analysis	82
5 Experimental Results	83
5.1 Initial stiffness from quasi-static loading phase	83
5.2 Results of Fatigue loading phase	87
5.2.1 Slip vs Number of cycles	87
5.3 Possible reasons for scattering in the experimental results and recommendations for future improved set-up	100
5.4 Behaviour of specimens in high cycle fatigue	107
5.5 Conclusions of experimental results	108
6 Statistical evaluation of test results	110
6.1.1 Overview of S-N curves obtained by test data	110
6.1.2 Comparison of two failure criteria	116
6.1.3 Comparison between different hole clearances for the same injection material	118

6.2 Summary and Conclusions of statistical evaluation of experiments.....	121
7 Discussion	122
7.1 Scatter in experimental results.....	122
7.2 Selected parameters for fatigue testing and statistical limitations.....	124
7.3 Linking resin material properties to fatigue performance	125
8 Conclusions and Recommendations.....	126
8.1 Conclusions.....	126
8.2 Recommendations for future research	128
9 Bibliography	129
10 Annex A - Input data for ABAQUS.....	133
A.1 Resin conventional	133
A.2 Steel reinforced resin	134
A.3 Steel plates and bolts	134
11 Appendix B – Probabilistic models.....	135
B.1 Schneider and Maddox.....	135
12 Appendix C – Materials.....	139
C.1 Resin conventional	139
C.2 Metric threads M20x2.5.....	140

List of Figures

Figure 1.1: Cut of a Double Lap Shear connection using injection bolt (Koper 2017 [1])	1
Figure 2.1: Injection hole layout [3]	4
Figure 2.2: Conventional resin (left) and steel reinforced resin (right) after dismantling of double lap shear injected connection specimens [5]	6
Figure 2.3: Injection bolt layout [2]	8
Figure 2.4: t_1 and t_2 definition	10
Figure 2.5: Bearing stress distribution for $l/d > 3$ [2]	10
Figure 2.6: Comparison of S-N fatigue data from the single shear connections made of the material from the Trezói bridge (similar to S355) [14]	11
Figure 2.7: Comparison of S-N fatigue data from the double shear connections made of the material from the Fão bridge (puddle iron) [14]	12
Figure 2.8: Comparison of EC3 detail category 90 for preloaded injected single lap connections with the experiments	13
Figure 2.9: Left-Cross section detail of Oranienburg bridge. Right-Visible corrosion on the web of steel supporting girder [20]	14
Figure 2.10: Left: Injection procedure of the M24 injection bolts. Right View of the strengthening plates with injection bolts on the web of main girder of the bridge [20]	15
Figure 2.11: Front view of Maeslant Barrier while it is open [22]	16
Figure 2.12: Image of connection between trusses and ball bearings with injection bolts in Maeslant Storm Surge Barrier [5]	16
Figure 2.13: Johan Cruijff Arena	17
Figure 2.14: Drawing of steel removable roof [23]	17
Figure 2.15: View of the glass roof steel structure from the inside of bus station [24]	18
Figure 2.16: Detail of the connection where injection bolts were applied [24]	18
Figure 2.17: Up: Cross section of a composite structure. Down: Beam with and without composite action (M. von Arnim 2017 [28])	19
Figure 2.18: Right: Demountable shear connectors [31] Left: Innovative Bolted shear connector with embedded coupler [28]	20
Figure 2.19: Gap between bolt and hole [28]	22
Figure 2.20: Bolt t unfavourable position inside the bolt according to EN 1090-2 [3] (in this case bolt with $d_o=20\text{mm}$ and hole with $d=22\text{mm}$ are depicted) [1]	23
Figure 2.21: Comparison between initial connection stiffness for double lap shear connections with slotted and oversize round holes in the center plate. Bolt (M20) located in most negative position with respect to connection slip [5]	24
Figure 2.22: Representation of a unidirectional FRP material [48]	26
Figure 2.23: Temperature increase in epoxy and polyester resins vs increasing frequency [43]	27
Figure 2.24: S-N curves for Sinka-52 and Sinka-30 obtained from statistical evaluation [50]	27
Figure 2.25: Most characteristic loading types for fatigue testing	28
Figure 2.26: Relationship between stress range and number of cycles to failure in conventional axes (left) and in logarithmic axes (right)	30
Figure 3.1: Front view of lower plates D30, D26, D22 from left to right (dimensions in mm)	34
Figure 3.2 Left-Side view of lower plates (dimensions in mm), Right-Grip of the lower plate by wedges	35
Figure 3.3: Lower (female) plate of specimen in reality and in 3D visualization	35

Figure 3.4: Drawings of front and side view of upper loading male steel plate (dimensions in mm)	36
Figure 3.5: Upper loading male plate of specimen in reality and in 3D visualization	36
Figure 3.6: Cutting of bolt parts from threaded M20 rod	37
Figure 3.7: Drawing of front view of the steel side plates (dimensions in mm)	37
Figure 3.8: Side plate of specimen in reality and in 3D visualization.....	38
Figure 3.9: M8x 80 Hex bolts with their nut in reality and in 3D visualization as designed in FEA environment without the threads	38
Figure 3.10: Left-Resin components RENGEL SW 404 and REN HY 2402 allowed by Rijkswaterstraat, Right-Resin components RENGEL SW 404 and REN HY 2402 used in the experiments	40
Figure 3.11: Steel shot used as the reinforcing material of steel reinforced resin used in experiments	41
Figure 3.12: Fatigue plates used for the assembly of specimens	43
Figure 3.13: Materials used for the assembly of specimens. From left to right: a) ACMOS 82-2405 release agent, b) Clay and small steel plates to facilitate assembly, c) Perspex glass plates with drilled holes for injection	44
Figure 3.14: Grinding of bolt threaded part.....	44
Figure 3.15: Bolt threaded part placed on the most unfavorable position inside the hole – a) in a specimen prior to injection with conventional resin, b) in a specimen prior to injection with steel reinforced resin, c) drawing of the most unfavorable position of bolt part in the hole	45
Figure 3.16: Desired distance between upper and lower plate to keep bolt part in most unfavorable position for the resin under testing	45
Figure 3.17: Positioning of small steel plates between upper plate and lower plate of specimens ready for injection to secure that the position of the bolt part will be the most unfavorable for the resin	46
Figure 3.18: Maximum thickness of resin part for the three different geometry types of specimens.....	46
Figure 3.19: Specimen D30 ready for injection after the tightening of Perspex plates with drilled hole	47
Figure 3.20: Insertion of steel shot reinforcement (left) in the hole through glass plate using funnel.....	48
Figure 3.21: Mixing of resin SW404 and catalyst HY 5159 in ratio 8:1 using a scale and a mixing paddle.....	48
Figure 3.22: Hand-operated caulking gun with a caulk tube containing the mixed injection material [5].....	49
Figure 3.23: Air escape channels positioned such to prevent air inclusions within the volume that is injected for horizontal injection [5].....	49
Figure 3.24: Repair of visible defects of resin part in injected specimens	50
Figure 3.25: Injected specimen before the positioning of side plates.....	50
Figure 3.26: Visualization of contact friction surfaces (in yellow) between steel plates during loading	51
Figure 3.27: Visible effects of friction in surface of side plates after preliminary experiments	51
Figure 3.28: Teflon sheets placed in the expected friction surfaces (right after the dismantling of specimen, left at a specimen assembled and ready for testing).....	52
Figure 3.29: Assembled specimens with the sticker indicating their designation ready for testing (Left). Visualization of assembled specimen in Abaqus (Right). In green colour the resin part can be seen.....	52

Figure 3.30: Hydraulic Wedge Grip Machine (Left-Upper wedge gripping upper plate of specimen, Right- Lower Wedge gripping lower fatigue plate of specimen)	53
Figure 3.31: Specimen on testing machine with 2 LVDTs at each side measuring the vertical slip between upper and lower plate	54
Figure 3.32: Constant amplitude compression-compression sinusoidal loading history chosen for the experiments	55
Figure 3.33: Machine operation for fatigue test	55
Figure 3.34: Slip accumulation of specimen D26R125-2 with the number of cycles to reach failure criterion indicated	57
Figure 3.35: Force vs Slip diagram of specimen after the quasi-static loading phase.....	59
Figure 3.36: Calculation of initial stiffness (kN/mm) of specimen from Force-Slip diagram of quasi static loading phase after the remove of 1 st <<setting>> circle.....	60
Figure 4.1: Left: Actual 2-D geometry of the specimen. Right: 2-D Geometry of specimen as designed for FEA Analysis	63
Figure 4.2: Uniform distribution of stresses after the change in geometry of upper and lower plate in full model after the application of maximum load of experiments	63
Figure 4.3: Geometry of primary components of specimen in Abaqus part module	65
Figure 4.4: Geometry of secondary components of specimen in Abaqus part module.....	65
Figure 4.5: Tie constraint between nuts and M8 Bolts	66
Figure 4.6: Meshed lower-female plate (left) and upper-male plate (right).....	67
Figure 4.7: Meshed M20 bolt part-pin (left) and resin part (right).....	68
Figure 4.8: Meshed M8 bolt (top-left), nut (top-right) and side plate (bottom)	68
Figure 4.9: Relationship between force and slip measured between the upper and lower plate of setup in the same way as the experiments (mean) zoomed on the range 0-0.1mm from which the numerical initial stiffness was calculated	69
Figure 4.10: Initial stiffness of set-up vs Hole diameter diagram for conventional and steel reinforced resin according to Numerical analysis. The increase of stiffness with decrease of diameter is not linear.....	71
Figure 4.11: Comparison of initial stiffness for conventional resin with varying hole clearance	71
Figure 4.14: Comparison of initial stiffness for steel reinforced resin with varying hole clearance	72
Figure 4.13: Comparison of initial stiffness for same hole clearance and varying injection material.....	72
Figure 4.14 Overview of double lap shear connection (left) and proposed set-up used for cyclic experiments (right) [67].....	73
Figure 4.15: Longitudinal bearing stress on resin along bolt/pin perimeter (left) and path of stresses in the resin along bolt part perimeter part as it was taken from Abaqus model D26R (right)	74
Figure 4.16: Longitudinal bearing stress on resin along bolt/pin length (left) and path of stresses in the resin along bolt part length part as it was taken from Abaqus model D26R of test set-up (right).....	74
Figure 4.17: Initial stiffness of set-up vs Hole diameter diagram for conventional resin according to Numerical analysis of set-up (solid) and Double Lap Shear Connection by Nijgh	75
Figure 4.18: Stiffness of set-up vs Hole diameter diagram for conventional resin according to numerical analysis of set-up (solid lines) and numerical analysis with fully confined conditions (dashed lines)	77
Figure 4.19: Longitudinal bearing stress on resin along pin perimeter for D30R set-up.....	77
Figure 4.20: Longitudinal bearing stress on steel reinforced resin along pin perimeter for D30SR set-up	78

Figure 4.21: Von Mises stresses vs True distance along inner surface of side plate (left) and path of stresses in the side plate as it was taken from Abaqus model D30SR Parametric (right)	78
Figure 4.22: Plot of Von Mises stresses (up) and path of stresses on upper plate (down) ...	79
Figure 4.23: Plastic material model for all steel plates S355.....	80
Figure 4.24: Difference in slip between upper and lower plate within each cycle vs Number of cycles.....	81
Figure 4.25: Plastic strains in set-up are zero everywhere (left) except a zone in upper steel plate (right).....	81
Figure 4.26: Plastic Strain in upper steel plate vs Number of cycles.....	82
Figure 5.1: Comparison between Numerical and Experimental (mean) results for Initial Stiffness vs Hole diameter in lower plate.....	86
Figure Figure 5.2: Comparison between experimentally obtained initial stiffness for different injection material	86
Figure 5.3: Slip vs Number of Cycles for D30R180 series.....	87
Figure 5.4: Slip vs Number of Cycles for D30SR180 series.....	88
Figure 5.5: Slip between loading plates vs Number of Cycles for D30R135 series.....	88
Figure 5.6: Slip between loading plates vs Number of Cycles for D30SR135 series	89
Figure 5.7: Slip between loading plates vs Number of Cycles for D30R90 series.....	89
Figure 5.8: Slip between loading plates vs Number of Cycles for D30SR90 series	90
Figure 5.9: Slip between loading plates vs Number of Cycles for D26R180 series.....	90
Figure 5.10: Slip between loading plates vs Number of Cycles for D26SR180 series.....	91
Figure 5.11: Slip between loading plates vs Number of Cycles for D26R135 series.....	91
Figure 5.12: Slip between loading plates vs Number of Cycles for D26SR135 series.....	92
Figure 5.13: : Slip between loading plates vs Number of Cycles for D26R90 series.....	92
Figure 5.14: Slip between loading plates vs Number of Cycles for D26SR90 series	93
Figure 5.15: Comparison of mean slip line of specimens with geometry D30 with resin and steel reinforced resin.....	93
Figure 5.16: Comparison of mean slip line of specimens with geometry D26 with resin and steel reinforced resin.....	94
Figure 5.17: Relative displacement between loading plates as a function of the number of applied loading cycles at a nominal bearing stress range of 90 MPa for a specimen with Ø26 mm hole.....	95
Figure 5.18: Relative displacement between loading plates as a function of the number of applied loading cycles at a nominal bearing stress range of 135 MPa for a specimen with Ø26 mm hole	96
Figure 5.19: Relative displacement between loading plates as a function of the number of applied loading cycles at a nominal bearing stress range of 180 MPa for a specimen with Ø26 mm hole	97
Figure 5.20: Comparison of mean lines of slips of selected specimens for all stress ranges	98
Figure 5.21: Influence of scatter in an S-N curve [59] for steel details(p corresponds to the probability of failure; r_f is the fatigue limit stress)	100
Figure 5.22: Specimen ready for injection. Highlighted in red the injection hole in first Perspex plate, and in green the escape hole in the second Perspex plate in the back side of specimen	101
Figure 5.23: Average Slip vs Number of Cycles for specimen series D30R180 (left) and D30SR180 (right) where the scatter is more prominent.....	101
Figure 5.24: Left-Air inclusions in resin samples. Right- Visualization of air inclusions and future alternative escape path [67]	102
Figure 5.25: CT-scan of sample with injection resin part around a bolt part with void in resin layer.....	102

Figure 5.26: The examined in the CT scan sample with the outside missing resin part at the side	103
Figure 5.27: Alternative air escape path (left) and compact resin specimens after the application of the improved solution	103
Figure 5.28: Results of slip vs number of cycles for the specimens with the alternative escape path which mitigate the scatter	104
Figure 5.29: Left-Drawing of angle defect (not to scale). In blue the lower plate not in straight line with the red upper pate. Right-The defect in an actual specimen.....	104
Figure 5.30: Crack due to misalignment after the position of specimen to the wedges, highlighted in red. The specimen was placed in machine fixed by wedges and removed before start of loading revealing the cracks	105
Figure 5.31: Visualization of proposed base (in red) for assembly of specimen.....	105
Figure 5.32: Visualization of the defect of position of the bolt part in the reception of upper male plate	106
Figure 5.33: Improved upper plate for future specimens (visualization)	106
Figure 5.34: Plot of Slip vs Number of cycles for specimen D30R90-5 which left in the machine for 6 million cycles	107
Figure 5.35 Plot of Slip vs Number of cycles for specimen D30SR90-5 which left in the machine for 4 million cycles	108
Figure 6.1: Statistical analysis of D30-R specimens with failure criterion 0.3mm	110
Figure 6.2: Statistical analysis of D30-R specimens with failure criterion 0.25mm	111
Figure 6.3: Statistical analysis of D26-R specimens with failure criterion 0.3mm	112
Figure 6.4: Statistical analysis of D26-R specimens with failure criterion 0.25mm	112
Figure 6.5: Statistical analysis of D30-SR specimens with failure criterion 0.3mm	113
Figure 6.6: Statistical analysis of D30-SR specimens with failure criterion 0.25mm	114
Figure 6.7: Statistical analysis of D26-SR specimens with failure criterion 0.3mm	114
Figure 6.8: Statistical analysis of D26-SR specimens with failure criterion 0.25mm.....	115
Figure 6.9: Comparison of S-N curves of D30-R specimens for 2 different failure criteria .	117
Figure 6.10: Comparison of S-N curves of D26-R specimens for 2 different failure criteria	117
Figure 6.11: Comparison of S-N curves of D30-SR specimens for 2 different failure criteria	118
Figure 6.12: Comparison of the effect of oversized holes in fatigue strength of specimens injected with conventional resin.....	118
Figure 6.13: Comparison of the effect of oversized holes in fatigue strength of specimens injected with steel reinforced resin	119
Figure 6.14: Comparison of fatigue strength for same geometry (D30) and varying injection material	120
Figure 6.15: Comparison of fatigue strength for same geometry (D26) and varying injection material.....	120
Figure 7.1: Left-Specimen ready for injection highlighted with red the entrance hole and with green the air escape hole on side plates. Right- Large air inclusion in top of the resin part	122
Figure 7.2: Air escape channel at the top position of steel plate to limit the air inclusions .	123
Figure 7.3: Crack due to misalignment during assembly and forced alignment by wedges of machine	123
Figure 11.1: Student's t distribution used in Schneider and Maddox model.....	137
Figure 11.2: Linear regression analysis equations and parameters for ASTM model	138
Figure 11.3: Parameters and equations used to establish characteristic curves with ASTM model.....	138
Figure 12.1: Product sheet of RENGEL	140
Figure 12.2: Standard dimensions of metric threads M20x2.5 according to ISO.....	140

List of Tables

Table 2.1: Resin properties according to manufacturer [10]	7
Table 2.2: Values of β and t_b , resin as a function of ratio t_1/t_2 [3] in double lap shear connections. The definition of t_1 and t_2 is given in Figure 2.3.	10
Table 2.3: Fatigue detail categories for double lap and single lap connections preloaded/non-preloaded, injected-non-injected according to EN 1993-1-9 [13].....	11
Table 2.4: Normal and oversized holes for standard bolts [3].....	22
Table 2.5: Reduction factor for shear connections due to oversized holes according to EN 1993-1-8 [4]	23
Table 3.1: Specimen type distinction according to geometry of lower plate	34
Table 3.2: Functions of resin and particles in a steel reinforced resin injected connection [5]	40
Table 3.3 Steel grade per component used in specimens (EN 1993-1-1).....	42
Table 3.4: Order list of steel plates of the specimens	42
Table 3.5: Maximum and minimum applied forces of the sinusoidal loading history	58
Table 3.6: Designation system of specimens	59
Table 4.1: Geometrical simplifications in numerical analysis	64
Table 4.2: Results of Initial Stiffness (kN/mm) of set-up from Numerical Analysis	69
Table 4.3: Results of static numerical analysis	70
Table 4.4: Initial stiffness of set-up vs Hole diameter diagram for conventional resin according to Numerical analysis of set-up (solid) and Double Lap Shear Connection by Nijgh	75
Table 4.5: Results of parametric study regarding initial stiffness	76
Table 5.1: Overview of fatigue experimental program	83
Table 5.2: Results of experimental initial stiffness of test set-up specimens D30 R-SR and comparison with numerical values.....	84
Table 5.3: Results of experimental initial stiffness of test set-up specimens D26 R-SR and comparison with numerical values.....	85
Table 5.4: Comparison of cyclic behaviour between DS6R90 and D26SR90 selected specimens.....	95
Table 5.5: Comparison of mean cyclic behaviour between DS6R135 and D26SR135 selected specimens	96
Table 5.6: Comparison of cyclic behaviour between DS6R180 and D26SR180 selected specimens.....	97
Table 5.7: Summary of results in mean slip after 400.000 cycles for geometry D26 (6mm hole clearance)	98
Table 10.1: Density and Elasticity for conventional resin.....	133
Table 10.2: Drucker Prager criterion parameters for conventional resin	133
Table 10.3: Drucker Prager Hardening for conventional resin	133
Table 10.4: Density and Elasticity for steel reinforced resin	134
Table 10.5: Drucker Prager criterion parameters for steel reinforced resin.....	134
Table 10.6: Drucker Prager Hardening for steel reinforced resin.....	134
Table 10.7: Density and Elasticity for steel grade S355.....	134
Table 10.8: Plasticity of steel grade S355	135
Table 10.9: Density and Elasticity for steel grade 10.9.....	135
Table 11.1: Linear regression analysis equations and parameters for Schneider and Maddox model.....	136
Table 11.2: Parameters and equations used to establish characteristic curves with Schneider and Maddox model	136

1 Introduction

1.1 Problem definition

Injected bolted shear connections (IBCs) have been used for the renovation of old metallic riveted bridges with faulty rivets, and corrosion problems. Riveting is no longer widely used leading to lack of skilled labour and materials, while another good solution to preserve null slip namely the fitted bolts, are considered expensive. High strength friction grip bolts (HSFG) are not preferred due to unknown friction coefficient of faying surfaces, while welding is avoided on site due poor weldability properties of corroded steel. The first application of such technique occurred in the Netherlands in 70's and it is common practice for the rehabilitation of old bridges, as well as for the erection of new structures when slip critical connections are demanded. New railway and road bridges, large roofs, windmills, wave barriers and others have been erected using shear IBCs (Figure 1.1). The increased traffic conditions in case of bridges and the cyclic nature of loads to which these structures are exposed led to the need of fatigue assessment of injected bolted connections but the research to that extend is limited. Even more limited is the research on fatigue behaviour of structural resins used in this kind of applications. Fatigue behaviour of resins is important to be investigated, for the use of results in numerical models for prediction of fatigue strength of resin IBC's.



Figure 1.1: Cut of a Double Lap Shear connection using injection bolt (Koper 2017 [1])

More recently a wide research has been carried out, aiming to replace traditional headed welded studs to steel concrete composite flooring systems which used in decks of bridges and multi-storey buildings. Traditional shear connectors are an economic and standardized in their use solution, but their application excludes the possibility of deconstruction and reuse. For this reason, demountable shear connectors with injection bolts and oversized holes in the flange of steel girder have been investigated as a sustainable alternative. Research has shown that

in this case use of oversized holes is necessary to ensure proper fabrication tolerances and allow re-erection process.

Considering this research on demountability of composite structures using injection bolts and oversized holes, a new injection material was developed at T.U Delft, namely the steel reinforced resin, as an alternative to conventional epoxy resin recommended by Dutch Ministry of Infrastructure for structural applications. In this novel material, steel shot is used to fill the hole clearance before the injection with conventional resin SW404/HY2404. The small steel spherical particles act like reinforcement, while the epoxy resin acts as matrix filler material, forming a final material with higher Youngs Modulus (approx. 2.5 times higher) than that of conventional resin. Therefore it can be used instead of conventional resin without compromising the connection stiffness. Also, it has been proven that leads to lower creep deformation.

In present Master Thesis the behaviour of these 2 resin products (conventional and steel reinforced resin) in uniaxial cyclic loading and under confined conditions is investigated using a tailor-made for this reason test setup. This setup is a simple pin connection, trying to simulate the bearing stress state of a double lap shear connection when cyclic loading is applied, but without risk of fatigue cracks in steel parts (bolt and steel plates) which is the common failure mode in fatigue testing of Injected Bolted Connections. An experimental program was designed for that reason with testing parameters selected based on previous research on fatigue testing on IBCs and current assembly of specimens. The specimen tested had oversized holes to be in accordance with the research of using injection bolts for demountability. Furthermore, numerical modelling of test set-up was used to investigate the static (define initial stiffness) and quasi static behaviour of specimens. Finally, a statistical evaluation with probabilistic models of ASTM, and a more conservative model by Schneider and Maddox recommended from IIW (International Institute of Welding) was performed. Through linear regression analysis the fitted curves are plotted and through probabilistic analysis with confidence level of 95% characteristic curves are proposed.

1.2 Research questions

The main aim of this thesis is to investigate the fatigue behaviour of resin and steel reinforced resin used in IBC's by carrying out experiments with a tailor made test-up where the deformation over cycles built-up is attributed to deterioration of material properties of resin layer exposed to cyclic loads. An effort was made to answer the following research questions during the thesis.

- Is the non-standardized novel test set-up verified compared to standard double lap shear connection
- What is the behavior of tested resins with the novel set-up:
 - a) In a quasi-static loading scheme
 - b) In a fatigue loading scheme
- How the hole clearance affects the fatigue behaviour of tested resins
- Is the fatigue behaviour of Steel-Reinforced resin superior to that of Conventional resin

1.3 Methodology of research

Literature review on the current state of the art on resin injected bolted connections in static and fatigue loads, applications of IBCs in civil engineering and fatigue testing of epoxy resins is performed.

Testing of conventional and steel reinforced resin with the proposed custom test setup is performed in oversized holes with 3 different stress ranges of uniaxial compressive cyclic loading in two phases. A quasi-static phase to capture initial stiffness of connection and fatigue loading phase to investigate the slip accumulation over number of testing cycles due to the deterioration of mechanical properties of resin layer.

Finite element analysis on static and quasi-static loading of test set up is performed with models validated from experiments, mainly to investigate if it is reliable to use the test-set up compared to real double-lap shear connections with injection bolts as described in Eurocode.

Finally, a fatigue probabilistic analysis was conducted to obtain S-N curves and propose characteristic S-N curves of resin and steel reinforced resin in tested geometries based on selected confidence levels.

1.4 Outline of thesis

This thesis is organized in 8 chapters

Chapter 1 provides general information about the topic and research question as well as methodology of research are presented

Chapter 2 summarizes the state of art on application of resin injection bolts in civil engineering, the use of oversized holes and slip critical joints. Main focal points are the fatigue testing of injected bolted connections and epoxy resins, and the testing parameters used in fatigue experimental programs with injection bolts and the material properties of tested resins to be used in numerical analysis.

Chapter 3 presents the tailor-made test set-up, finalizes the testing parameters to be used and describes the assembly and testing process.

Chapter 4 presents the results of static numerical analysis and the numerical verification of novel test set-up compared to standardized double lap shear connection of EN 1090-2.

Chapter 5 describes the results of the experiments in quasi-static and fatigue phase, a selection of data is performed to mitigate scatter and draw conclusions and an investigation in possible reasons of scattering to improve the test set-up for future experiments is carried out

Chapter 6 provides a statistical evaluation of the test results based on two probabilistic models

Chapter 7 presents a discussion on the conclusions and the research limitations

Chapter 8 provides main conclusions of the research conducted and recommendations for future work.

2 Literature review

In this section an overview of the state of the art in the field of injection bolts, connections with injection bolts both in static and fatigue loading, applications with resin injection bolts are presented. Also, previous research on fatigue testing of epoxy resins and statistical methods to evaluate test data are mentioned.

2.1 Injection Bolts

According to ECCS [2] the definition of injection bolts is the following. Injection Bolts are bolts in which the cavity produced by the clearance between the bolt and the wall of the hole is completely filled up with a two-component resin. Filling of the clearance is carried out through a small hole in the head of the bolt. After injection and complete curing, the connection is slip resistant. Normative regulations for injection bolts can be found in Annex G of EN 1090-2 [3] and in EN 1993-1-8 [4].

2.1.1 Components of injection bolts

- **Bolts**

For injected bolted connections (IBC's) bolts of strength class 8.8 or 10.9 may be used. A hole with prescribed dimensions and position (see Figure 2.1), should be placed in the head of the bolt to allow for the injection of the resin with use of an injection gun. Injection bolts can be found in the market or they can be fabricated in shop according to the regulations of Eurocode 1090-2 [3]. They can be preloaded or non-preloaded but in case of preload, tightening should be carried out prior to the injection of the resin. A small amount of pretension of steel plates which has no structural use is recommended in any case to prevent possible leakage of the resin between the plates.

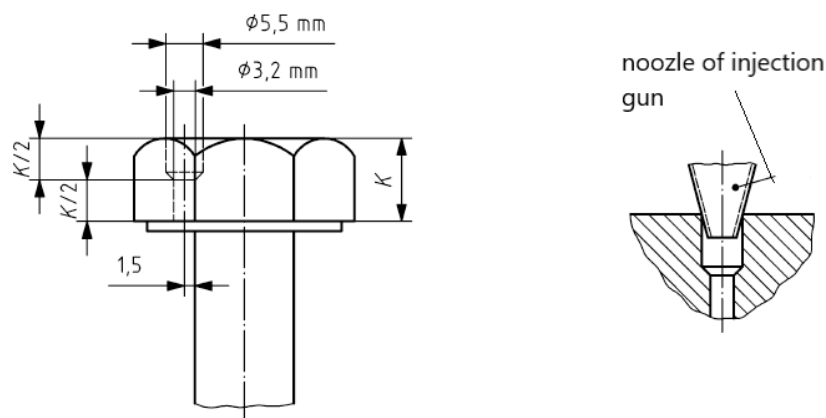


Figure 2.1: Injection hole layout [3]

- **Resin**

A certain resin to be used for injection bolt applications is not defined in EN 1090-2. It is defined that a 2-component epoxy resin should be used with pot life at least 15 minutes and a viscosity such all the clearances of the connection are filled sufficiently and the resin should not flow out of the bolt after the injection in room temperature is stopped (EN 1090-2 [3]). If there are not available data, tests should be performed in order to determine the suitable resin temperature and curing time. The temperature of the resin should be in the range of 15-25°C. One of the most used 2-component epoxy resin, which is in fact the only allowed for use in infrastructural works by the Dutch Ministry of Infrastructure (Rijkswaterstaat) is Araldite/RenGel SW 404 which is combined with hardening agent Ren HY 2404.

An extensive research on possible resins to be used for injection bolt applications has been carried out by Koper [1]. In this research the application of various resins was investigated, namely SW404+HY2404, Sinkadur30, Sinka Injection 451, Edilon Dex R2K, and Edilon Dex G20 based on parameters such as viscosity, pot life, glass transition temperature T_g and mechanical properties after curing. Considering all these parameters author concluded that RenGel SW 404/HY 2404 best performs related to alternatives.

Nijgh [5] has also investigated the feasibility of different injection materials for use in oversized holes regarding the short and long term behaviour of the connections, and invented a novel injection material, the steel reinforced resin which consists of a steel particles skeleton and a conventional epoxy resin (SW404/HY2404) used as matrix. He proposed that the most suitable material to use for steel skeleton is steel spherical shot like the one used in steel blasting. This innovative material offers an increased connection stiffness (+71%) and a decrease in creep deformation (-35%) for the geometry of standard double lap shear connection tests recommended in EN 1090-2 [3].

These two materials namely the conventional RenGel and the steel reinforced resin made from the conventional epoxy resin plus the steel shot will be used in this research for a preliminary investigation of their fatigue properties (further information also can be found in section 3.2). The material properties of both materials are briefly referred below.

The product sheet of SW404/HY2404 epoxy resin indicates a compressive strength of 110-125 Mpa and a Young's Modulus of 9-9.5 GPa but various values are mentioned for this material in literature. For example Kortis (2011 [6]) indicates a value of 4-5.5GPa while de Freitas et al. (2012 [7]) report a value of 3.2 GPa. Nijgh (2017 [5]) suggested $E=4.25$ GPa in the numerical study of his test set-up of the injected double lap shear connections. A Poisson's ratio of 0.3 for conventional resin is commonly used.

In the most recent work at TU Delft (M. Nijgh, H. Xin and M. Veljkovic ([8], [9]) the material properties of resin and steel reinforced resin are defined using analytical and numerical homogenization methods and small scale specimens in confined and unconfined conditions subjected to uniaxial static compression loading. From this research for conventional resin in unconfined conditions $E=5640$ MPa, $\nu=0.3$ and compressive strength of 167 MPa are proposed. It is mentioned that natural confinement provided by connection components has a positive effect on strength and stiffness of the resin and decreases the creep deformation. For steel reinforced resin in unconfined conditions the material properties are the following: $E=15700$ MPa $\nu=0.22$ and compressive strength of 120.3 MPa.

The authors in the above-mentioned research ([8], [9]) concluded that due to good agreement between the numerical and experimental results in their research, these material properties proposed for resin and steel reinforced resin may be used safely for Finite Element

simulations. Therefore, in the current research for the numerical analysis which is presented in Chapter 4 these material properties for resin and steel reinforced resin are adopted.

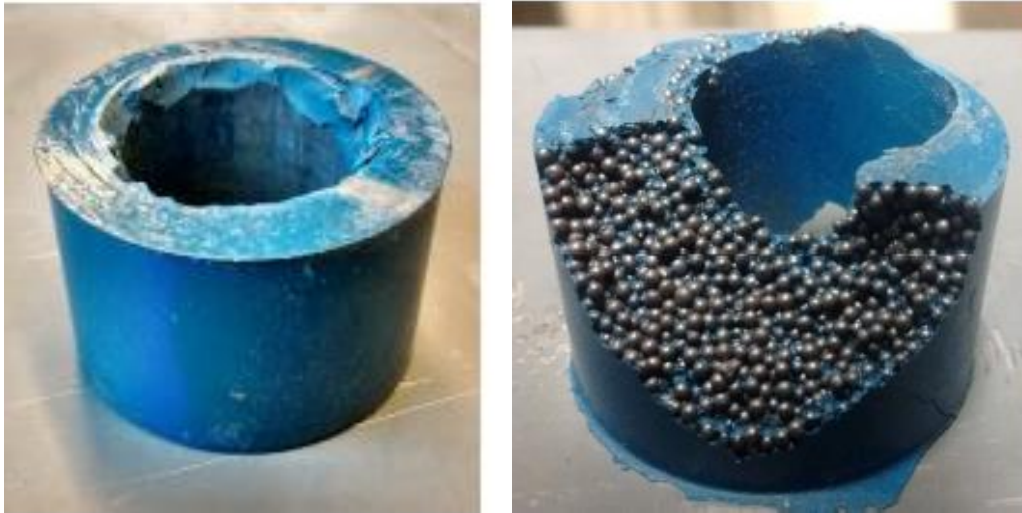


Figure 2.2: Conventional resin (left) and steel reinforced resin (right) after dismantling of double lap shear injected connection specimens [5]

- **Hardener**

As already mentioned a 2-component epoxy resin product consists of a polymer epoxy resin combined with a hardener which in in case of Araldite is the SW404 and HY2404 respectively. The hardener is a reactive chemical which starts the reaction between polymer chains of resin molecules (Koper 2017 [1]). This reaction is called curing and is defined as the chemical reaction where the viscosity of mixture increases from the moment that resin and hardener come in contact until the resin turns to a solid state at the end of reaction.

For technical reasons the speed of this rise of viscosity is important and is defined as pot life of the resin. Pot life is the time in which the initial viscosity of resin doubles. Another way to describe the reaction speed is working time which is defined as the time after that the resin has a viscosity such it cannot be applied any more, therefore working life is dependent every time on the application (dimensions, tolerances etc.) (Koper, 2017 [1]).

Firstly, the hardener HY 404 was used for Araldite resin but it was discovered that has negative effects in human health and was replaced by the today's widely used HY 2404. Another option that can be used for the same epoxy resin system is hardener HY 5159. This hardener offers an increase pot life related to HY 2404, without compromising the mechanical properties of final product. The mixing ratios and the material properties of the two hardeners with the same resin SW404 as defined by the manufacturer can be found in Table 2.1.

Mix ratio	Parts by weight	
RenGel [®] SW 404	100	100
Ren [®] HY 2404	10	-
Ren [®] HY 5159	-	8

Resin/Hardener mix:	Volume	Unit	SW 404 HY 2404	SW 404 HY 5159
Appearance			Blue	Blue
Pot life at 25°C	250 ml	min	15	50
Demoulding time		h	12	12

Density	ISO 1183	g/cm ³	1.8	1.8
Hardness	ISO 868	Shore D	85-90	85-90
Deflection temperature	ISO 75	°C	80	100
Abrasion	Taber	mm ³ /100U	4-6	4-6

Table 2.1: Resin properties according to manufacturer [10]

The advantage of hardener with higher pot time is that gives the worker the flexibility to finish the application of a larger portion of resin and therefore leads to a reduced working time. It is obvious that the hardener HY 5159 facilitates the technical procedure of injection in terms of feasibility and workability. Indeed this was confirmed in the research of Girbacea [11] who investigated the influencing factors in assembly and disassembly of large steel concrete composite flooring systems with multiple injection bolts used as shear connectors. In this research both type of hardeners used in the experiments and author concluded that the use of HY 5159 reduced the injection time by a factor of 5 compared to HY 2404. Therefore, the former hardener will be used in the experimental program of current Thesis.

- Release agent

A research conducted at TU Delft already from 70's mentioned that it possible to deconstruct components of IBC's if a release agent would be applied in advance (L. P. Bouman, 1972 [12]). In cases when the demountability of injected bolted connections is an issue of importance, such as in demountable-reusable composite structures, all surfaces in contact with resin need to be treated with a release agent prior to injection. This is needed since epoxy resin is highly adhesive and without protective measures, the bolt with the resin part around it cannot be removed after hardening. An experimental research on demountability of IBC's was conducted by Nijgh [5]. Wax spray, silicon spray and PVA solution used as alternatives for release agents and author concluded that the use of wax-based spray as a release agent is most suitable for IBC's. Although the performance of silicon spray is similar to that of wax spray, silicon is not chosen since the presence of silicon may degrade the material properties of the resin.

2.1.2 Advantages of injection bolts

Application of injection bolts provide important advantages in repair and strengthening techniques of old structures as well as in the construction of new structures where slip critical joints are required. An overview of positive aspects of injection bolts related also to other solutions for slip-critical joints is presented below:

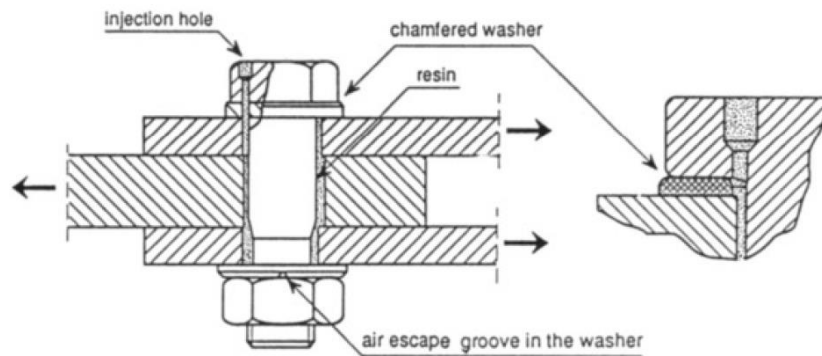


Figure 2.3: Injection bolt layout [2]

- In rehabilitation of old corroded steel riveted structures, the use of injection bolts is a very good alternative to replace damaged rivets. They offer a similar behaviour with fitted bolts but with lower costs since application of fitted bolts demands special preparation of holes. Use of rivets is avoided due to lack of equipment and skilled workers, while welding of strengthening plates is avoided due to poor weldability properties of old corroded steel. HSFG bolts also are not preferred due to unknown friction coefficient of contact surfaces.
- A good corrosion resistance is ensured with use of injection bolts since the resin completely fills the cavity of clearance (important for old and new structures).
- Injection bolts resist effectively sudden slip in case of overload. In connections with HSFG sudden slip in case of load higher than slip resistance of connection is possible (important for both old and new structures).
- There is no need of special requirements when applying injection bolts compared to application of HSFG, such as requirements for connected surfaces (use of certain paint layers to achieve certain slip factor), and not controlled tightening in case of non-preloaded injection bolts.
- Possibility of compact connections when the desired load transfer is very high, and the available space is small. Using preloaded injection bolts in such cases could offer the solution since the design resistance is the sum of slip resistance plus the bearing resistance of the resin.
- In case of connecting materials with different geometrical tolerances (i.e. in steel-concrete composite structures) the use of injection bolts with oversized holes is a very good alternative to traditional shear connectors

Examples of the advantages offered by IBC's in real applications can be found in following section 2.3

2.2 Static creep and fatigue behaviour of Resin Injected Bolted Connections (RIBC's)

Behaviour of bolted connections with injection bolts have been studied by various authors mainly in monotonic and creep loads, and secondly in fatigue loads. A brief overview of studies available in literature as well as the code provisions for fatigue and static loading are presented in this section. Calculation rules for the design resistance of the connections with resin injected bolts can be found in EN 1993-1-8 [4] while executional information on the bolt detailing and the bolt hole can be found in EN 1090-2 [3].

2.2.1 Static behaviour of IBCs

Resin injected bolted connection have a design static resistance which depends on the shear connection category according to EN 1993-1-8 [4]. For bearing type, non-preloaded shear connection which falls to Category A, with bolts of strength class 4.6 - 10.9, the static design resistance is the minimum between the design shear resistance of the bolt $F_{v,Rd}$ and the design bearing resistance of the resin $F_{b,Rd,resin}$ according to (Equation 2.1)

$$F_{Rd,A} = \min (F_{v,Rd}, F_{b,Rd,resin})$$

(Equation 2.1)

For slip-resistant at Serviceability Limit State (Category B) and for slip-resistant at Ultimate Limit State (Category C), preloaded shear connection with bolts class 8.8 or 10.9, the static design resistance should not exceed the minimum between the design shear resistance of the bolt $F_{v,Rd}$, the design bearing resistance of the resin $F_{b,Rd,resin}$ plus the design slip resistance of the bolt $F_{s,Rd}$ and the design bearing resistance $F_{b,Rd}$ as shown in (Equation 2.2)

$$F_{Rd,B} = F_{Rd,C} = \min (F_{v,Rd}, F_{b,Rd,resin} + F_{s,Rd}, F_{b,Rd})$$

(Equation 2.2)

The design bearing resistance of the resin $F_{b,Rd,resin}$ is calculated according to the following (Equation 2.3):

$$F_{b,Rd,resin} = \frac{k_t \cdot k_s \cdot d \cdot t_{b,resin} \cdot \beta \cdot f_{b,resin}}{\gamma_{M4}}$$

(Equation 2.3)

Where

k_t : for SLS is equal to 1.0 and for ULS is equal to 1.2

k_s : is equal to 1.0 for holes with normal clearances or 1.0-0.1 m for oversized holes

m : is the difference expressed in mm between the normal and oversized hole dimensions. In case of short slotted holes m is equal to half the difference between the hole length and width

$t_{b,resin}$: is the length over which the resin is considered to be effective and is given in Table 2.2

β : is a coefficient which depends on the thickness ratio of the connected plates and is given in Table 2.2

$f_{b,resin}$: is the bearing strength of the resin calculated according to Annex G of EN 1090-2 [3]

t_1/t_2	β	$t_{b,resin}$
$\geq 2,0$	1,0	$\min(2t_2; 1,5d)$
$1,0 \leq t_1/t_2 \leq 2,0$	$1,66 - 0,33(t_1/t_2)$	$\min(t_1; 1,5d)$
$\leq 1,0$	1,33	$\min(t_1; 1,5d)$

Table 2.2: Values of β and $t_{b,resin}$ as a function of ratio t_1/t_2 [3] in double lap shear connections. The definition of t_1 and t_2 is given in Figure 2.4.

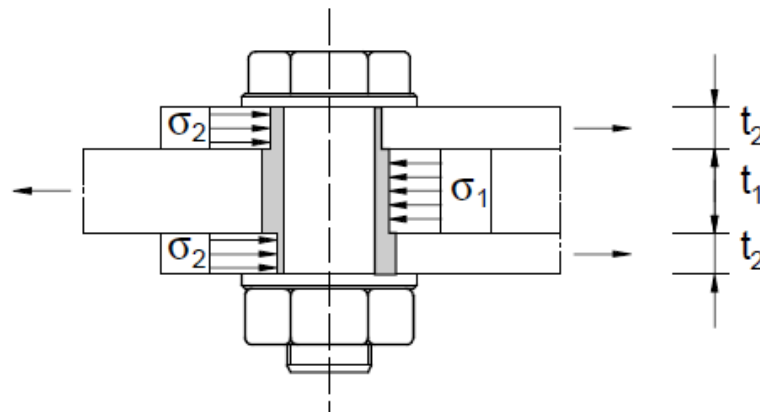


Figure 2.4: t_1 and t_2 definition

It should be mentioned that according to EN 1993-1-8 [4] for ratio $l/d > 3$ where l is the length of plate package and d is the diameter of injection bolt the stress distribution in resin layer is not uniform due to bending deformation of the bolt as it can be seen from the following figure.

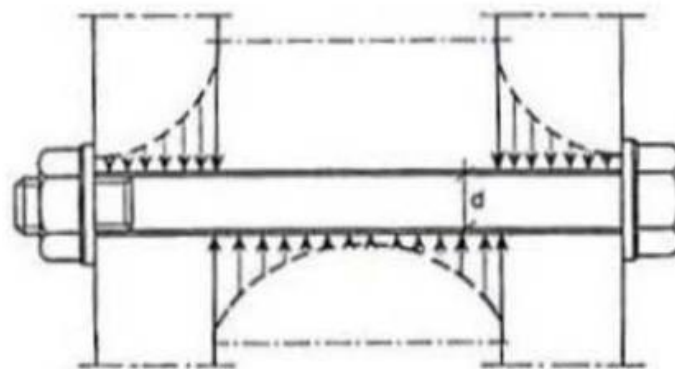


Figure 2.5: Bearing stress distribution for $l/d > 3$ [2]

2.2.2 Fatigue behaviour of IBCs

Fatigue detail categories of resin injected bolted connections with or without preload are defined by EN 1993-1-9 [13]. Eurocode suggests the same detail category (112) for preloaded conventional and preloaded resin injected bolts.

Connection Type	Non-preloaded		Preloaded	
	Double Lap	Single Lap	Double Lap	Single Lap
Non-injected	50	50	112	90
Injected	90	80	112	90

Table 2.3: Fatigue detail categories for double lap and single lap connections preloaded/non-preloaded, injected/non-injected according to EN 1993-1-9 [13]

An experimental study carried out by de Jesus, da Silva et al. (2016) [14] for the fatigue behaviour of double and single lap shear preloaded connections with injection and normal bolts and steel plates from old riveted bridges to simulate strengthening application conditions. The goal of authors was to investigate in what extend the same detail category for preloaded injected or not connections is correct. For double lap shear connections and single lap shear connections, a puddle iron material from Fao bridge and a mild steel similar to S355 from Terzoi bridge in Portugal were used respectively. The researchers revealed after experiments and statistical analysis with probabilistic model proposed in ASTM standards to obtain S-N curves, that the use of preloaded injection bolts leads to a fatigue strength reduction compared to standard preloaded bolts. As it can be seen in Figure 2.6 where the S-N curve for preloaded standard bolts, is higher compared to that for preloaded resin injected bolts used in single lap shear connections.

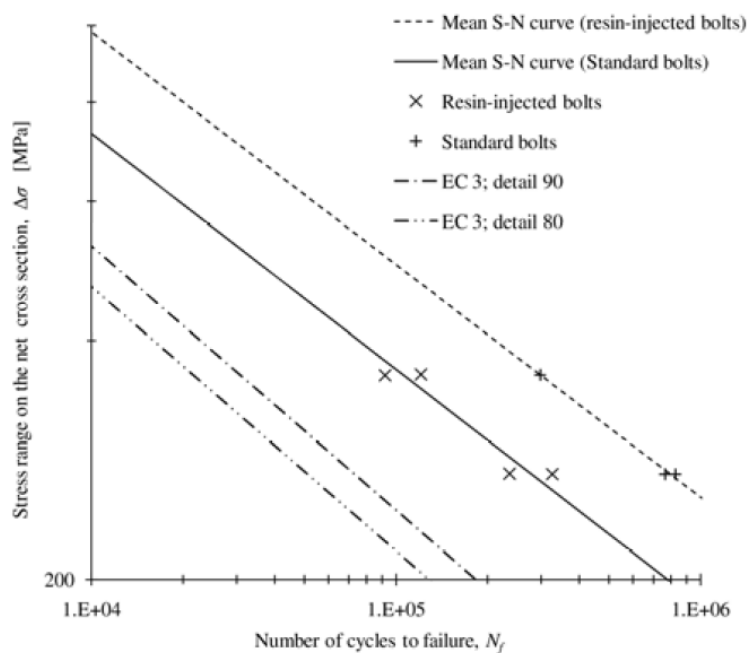


Figure 2.6: Comparison of S-N fatigue data from the single shear connections made of the material from the Trezói bridge (similar to S355) [14]

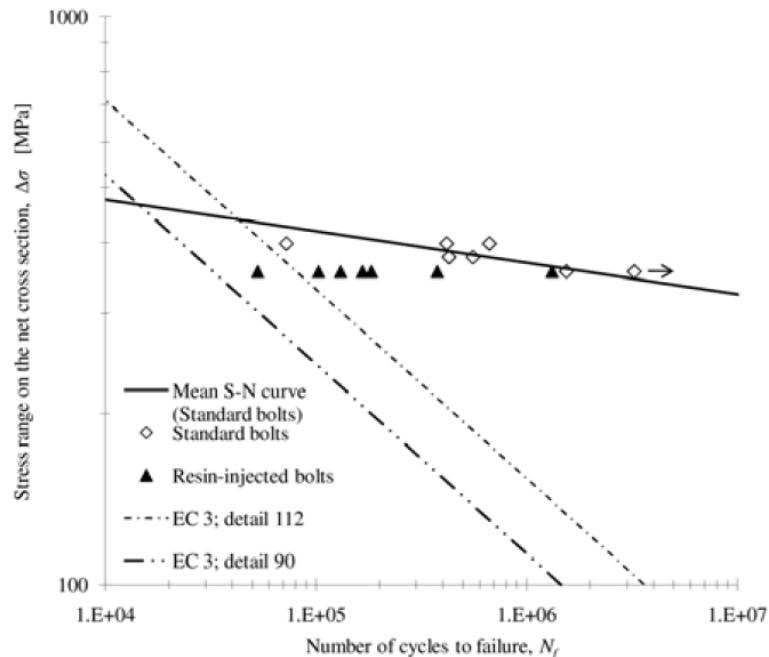


Figure 2.7: Comparison of S-N fatigue data from the double shear connections made of the material from the Fão bridge (puddle iron) [14]

After fatigue failure of all specimens the epoxy resin (which was Sinkadur 30), was undamaged according to authors. Comparing code-based S-N curves for single shear lap joints (80,90 MPa) to mean S-N curves from single-lap joints with steel Terzoi bridge (Figure 2.6), it can be observed that first all obtained curves have same slope with Eurocode curves which is logic since material of Terzoi bridge was similar to steels used today. Secondly Eurocode curves are conservative and finally there is a fatigue strength reduction when using preloaded injection bolts compared to standard preloaded bolts as.

This is also verified by experiments for double lap shear connections made of iron material of Fao bridge (Figure 2.7). The difference in that case is that S-N curve is no longer parallel to standard from Eurocode curves which may be justified to the different material properties of iron related to steels used today, resulting to different crack propagation which is the basis of the definition of S-N code curves. Also in this case the test data of preloaded injection bolts were lower than test data of preloaded standard bolts indicating fatigue strength reduction. The results are considered from the authors as surprising since Eurocode does not propose lower detail category for resin injected bolts.

However from a more recent research numerical research has been carried out by the same researchers (J. Correia et al [15]), with standard and resin injected bolts it was concluded that the use of adhesive resins produce an improvement on the fatigue life in the crack initiation phase which is in contradiction with the previous experimental work. This statement agrees with the current research at TU Delft.

This partly agrees also with another study by B. Pedrosa et al. (2017) [16] where single shear connection configuration was investigated to access resistance when using injected bolts in comparison to non-injected bolts. The material of plates was S355 and old iron material from Eiffel bridge in Portugal (Figure 2.8). The epoxy resin used was Sinkadur52 and bolts were

M24 10.9 to 26mm holes. Run-outs were excluded from statistical analysis as indicated in ASTM standards [17]

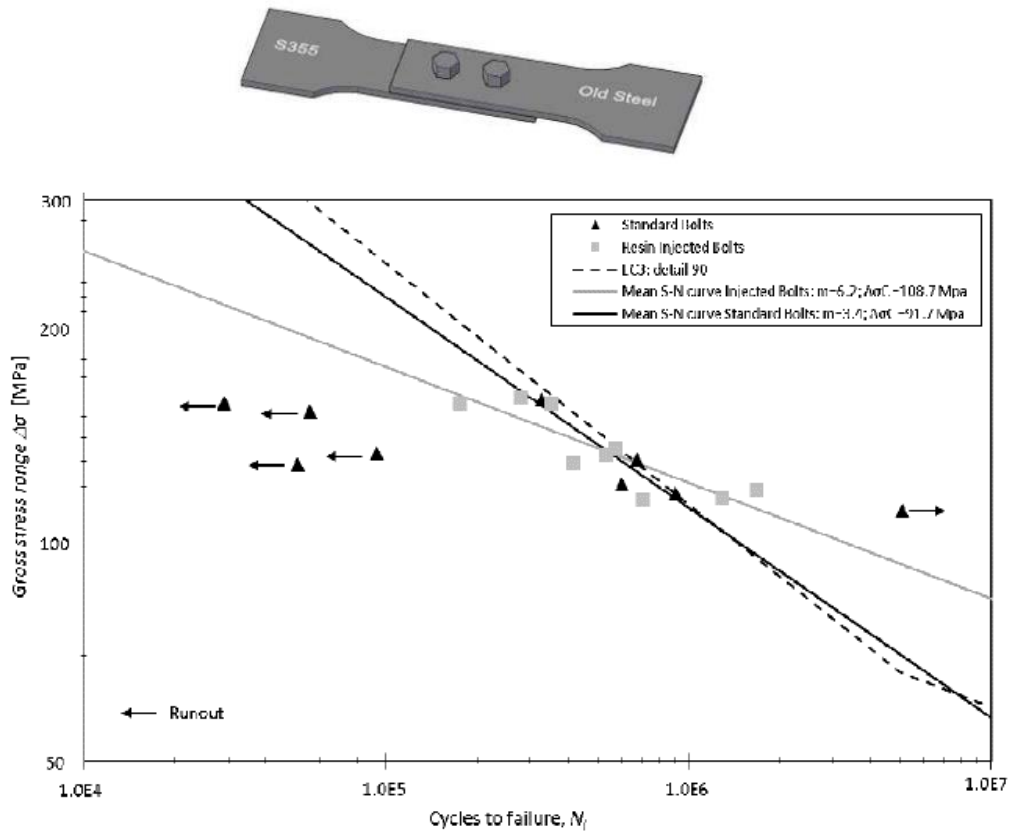


Figure 2.8: Comparison of EC3 detail category 90 for preloaded injected single lap connections with the experiments

The main conclusion of this study was that resin improved the fatigue strength of single lap connections in high cycle fatigue regime. The scatter of experimental data may be attributed to the inclusions of resin and to heterogeneities and defects of old iron material. The slopes of mean S-N curves are different from EC3 category 90 for preloaded single shear due to different material properties, but the slope of curve obtained for standard bolts has a similar slope with code curve.

2.3 Application examples with resin injected bolts.

This section discusses four real projects and one large experimental project where resin injected bolted connections were used. More application examples can be found in sources [2] and [18].

2.3.1 Repair of riveted connections in old steel bridges with injection bolts

According to American Institute of Steel Construction [19] riveting is considered as one of the oldest ways of joining steel structures and was one of the most popular methods in steel construction during the first decades of 20th century. Nevertheless, after the introduction of high strength bolts their use was decreased sharply and currently rivets are almost never used in new structures where either welds or bolts are preferred. However, there are still many old damaged or outdated rivetted railway or road bridges across the world, and there is lack of experienced technical staff for retrofitting of such structures. To repair rivetted structures alternative slip-resistant fasteners are thus considered such as HSFG (High Strength Grip Bolts), Fitted bolts and Injection bolts. Fitted bolts is an expensive solution due to the necessary preparation of the holes, while the use of HSFG is considered as unreliable since corrosion of old steel plates and paint layers lead to an unknown friction coefficient of contact surfaces. For this reason in the Netherlands it is standard practice to repair old railway or road bridges with injection bolts as a replacement for damaged rivets [2],[18],[20]. Injection bolts are used as connection method also for construction of new railway and road Dutch bridges [18].

According to A. Gresnigt et. al [20], injection bolts used successfully to repair an old (constructed in 1934) rivetted bridge crossing river Havel in Oranienburg, Germany. Inspection revealed serious corrosion problems in the web of the main girder, where from the original thickness of 14mm, only 9mm in average remained, and even 0mm at some places. A detail of the cross section and a picture of the corroded steel plates can be seen in the following Figure 2.9

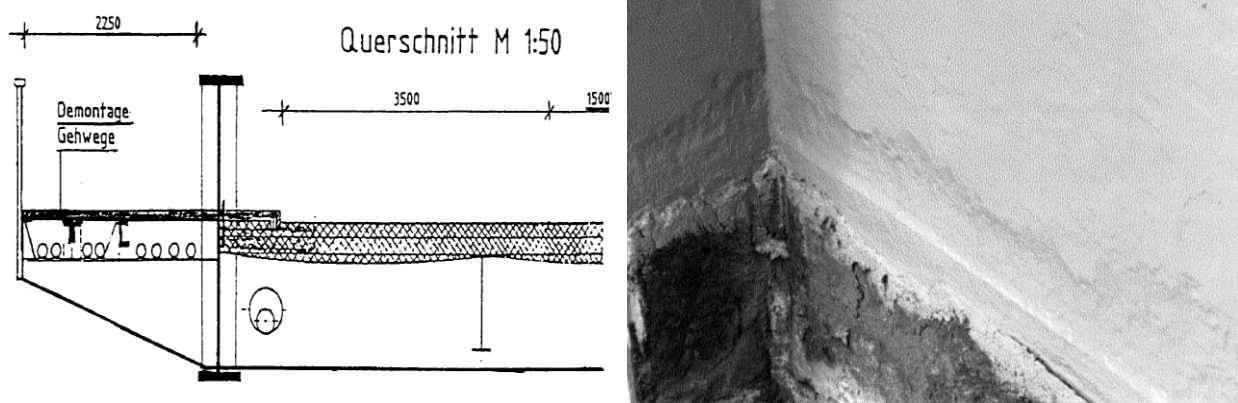


Figure 2.9: Left-Cross section detail of Oranienburg bridge. Right-Visible corrosion on the web of steel supporting girder [20]

For this project, ministry of traffic of the county Brandenburg in Germany decided to apply injection bolts to strengthen the bridge, and for this reason a research was carried out in TU Delft Stevin Lab with accordance of RWTH Aachen [20]. The results of long duration creep tests conclude that the application of injection bolts in old bridges is an excellent alternative to repair damaged rivets. Also, even though a design bearing stress of $\sigma_b=130 \text{ N/mm}^2$ is recommended by ECCS Recommendations (1994) [2], it was decided to use a design bearing

stress of $\sigma_b=150 \text{ N/mm}^2$, since test results proved the safety of the applied design value for the bearing stress in the bridge. This means that the slip of the bolt in the hole at a bearing stress of $\sigma_b=150 \text{ N/mm}^2$ is less than 0.3mm which is the same limit used for HSFG and Fitted bolts by EN 1993-1-8 [4]. Moreover, according to results of tests in specimens with maximum service temperature of 70° C , high temperatures have a non-significant effect on slip. In total 700 injection bolts with size M24, and steel plates were used for the strengthening of the web and their application can be seen in following figure. Another known successful application of resin injected bolts is the rehabilitation of a metallic bridge in Portugal at the bridge over the Mondego River in Figueira da Foz [21]. It should be noted that according to numerical study by J. Kortis [6] the replacement of rivets with injection bolts leads to a rise of load transferred by adjacent rivets. This can be attributed to the relatively low stiffness of resin related to stiffness of steel.

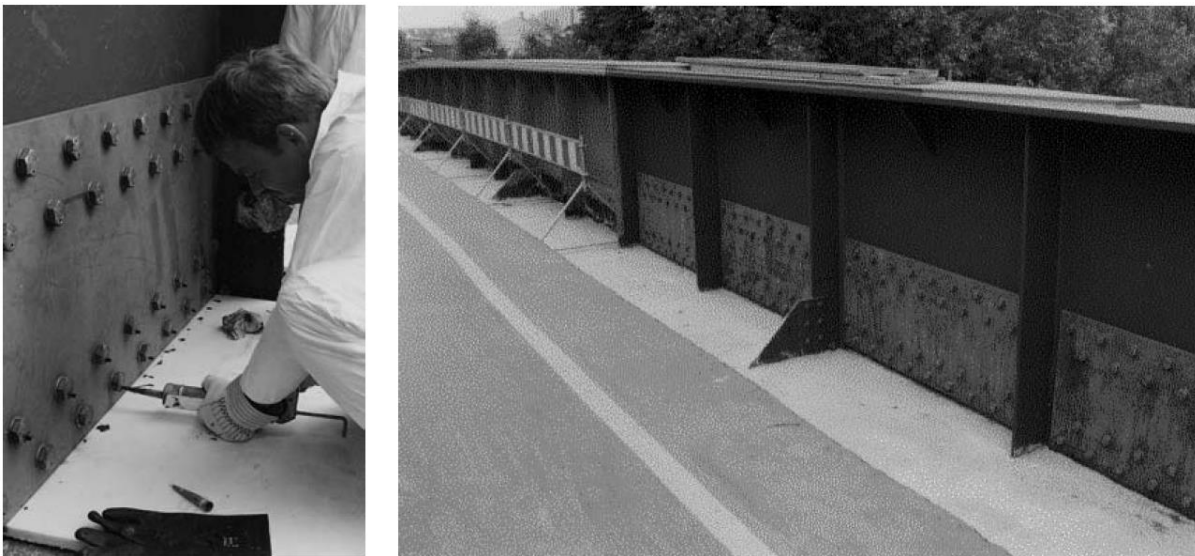


Figure 2.10: Left: Injection procedure of the M24 injection bolts. Right View of the strengthening plates with injection bolts on the web of main girder of the bridge [20]

2.3.2 Maeslant Storm Surge Barrier

Maeslant storm surge barrier (Figure 2.11) located in the end of the Rhein-Meuse river close to Hook of Holland, is part of Delta Works, a huge infrastructural project which protect the South regions of the Netherlands from seawater after the fatal floods of 1953. It was constructed between 1991-1997 and according to Dutch Ministry of Infrastructure (Rijkswaterstaat) [22] no other flood barrier in Netherlands has larger movable parts than Maeslant Barrier. Normally the Barrier is open, but it closes if the water level is predicted to reach the critical point of 3m above NAP (which is the reference height for measurements in Low Countries), to protect a population of 2 million in Zuid-Holland Province. This can happen every decade, and the gate closed for the first time at 2007. It is noted that it can withstand storm tides up to 5m above NAP which can create very large forces. It is consisted of two doors, each 210m long and 22m high and steel trusses of 237m welded at each gate increasing the weight at 6800 tonnes for each gate, which can transfer the huge sudden forces when the gates are closed to one single hinge ball joint at the end of every gate. The forces must be transferred through steel trusses to ball bearings and from there safely to the ground. The engineers wanted to prevent any slip in the connections between trusses and bearings (Figure 2.12) in combination with high design resistance for each bolt and protection from corrosion due to environmental conditions. For these reasons M80, M72, M64, M56 8.8

preloaded injection bolts were used instead of conventional preloaded bolts, since the resin protects the bolt and hole from corrosion and with HSFG there is a danger of sudden slip if load is higher than maximum friction resistance. The reason why big bolt sizes were chosen is because the steel plates are quite thick due to big dimensions of structure and large forces, and the engineers wanted to stay in the limit $l/d < 3$ to achieve uniform bearing stress distribution in the resin (Nijgh, 2017 [5]).



Figure 2.11: Front view of Maeslant Barrier while it is open [22]



Figure 2.12: Image of connection between trusses and ball bearings with injection bolts in Maeslant Storm Surge Barrier [5]

2.3.3 Johan Cruijff Arena - New Stadium of Ajax in Amsterdam

The new football stadium of Ajax in Amsterdam (Figure 2.13) was constructed between 1993-1996 by Royal BAM Group and Ballast Nedam and designed by Arcadis Bow/Infra, with a capacity of 55.000 spectators and a final cost of 140 million. The stadium has a removable roof steel structure consisting of two parts, each measuring 35 x 120 m, which can be opened or closed in less than half an hour (I. D. G. Mans and J. Rodenburg, 2000 [23]). The roof is normally opened but depending on weather conditions it can be closed. For this roof application there was the requirement that under no circumstance deformations are allowed at the connectors [18]. Therefore, the designers chose injection bolts as a slip resistant connection for the steel members of roof structure.



Figure 2.13: Johan Cruijff Arena

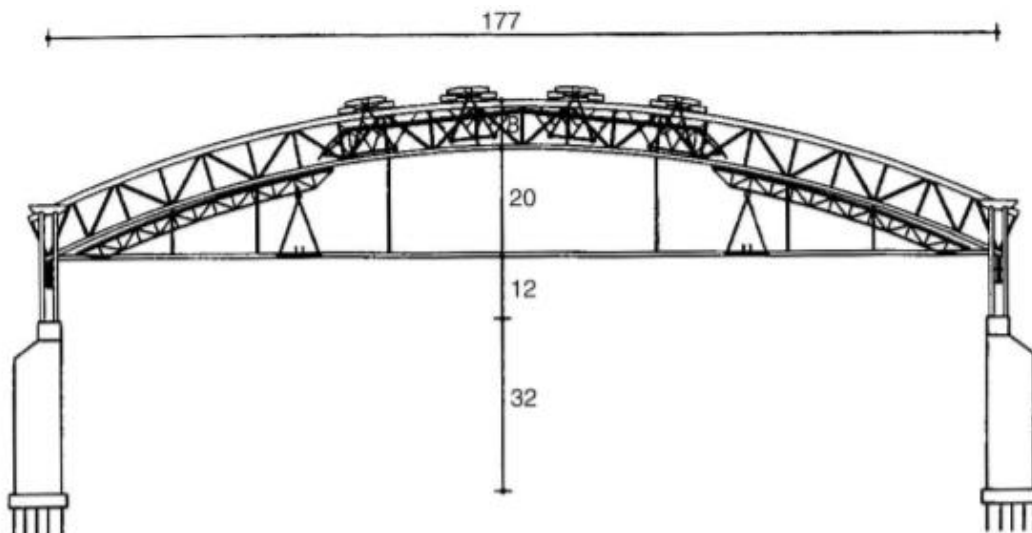


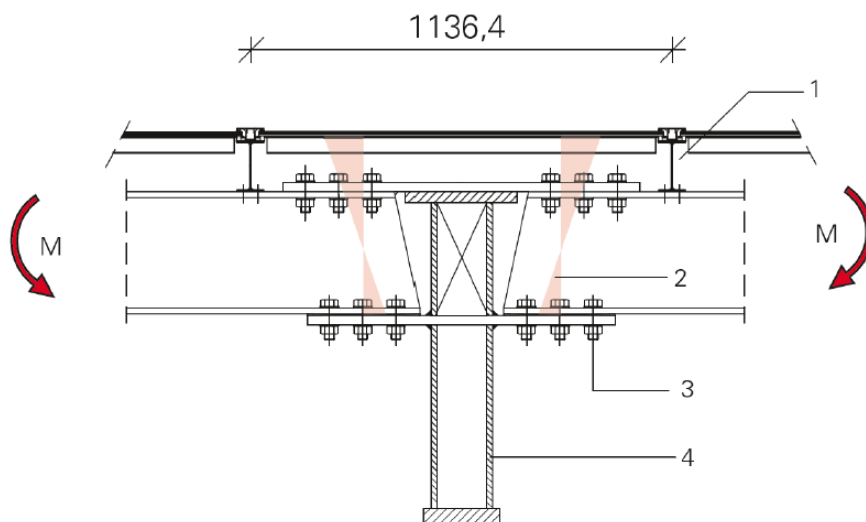
Figure 2.14: Drawing of steel removable roof [23]

2.3.4 Glass roof structure in bus station near Amsterdam Central Station

Another application of injection bolts can be found in the source [24] (H. J. Lint et al. 2012) regarding a glass roof structure which covers the IJ-sei bus station near Amsterdam Central Railway Station (Figure 2.15). The structure has a total length of 360m and maximum height of 22m, consisted from steel arc frames placed at equal distances of 12.5m and purlins which support the glass roof panels. The influence of deformations on this steel structure is greater in the connection between the purlins and the arc frame girder. A construction detail of the connection can be seen in Figure 2.15.



Figure 2.15: View of the glass roof steel structure from the inside of bus station [24]



1. Purlins IPE140
2. Horizontal displacement due to hole clearance
3. Injection bolts M27 10.9 in 30mm hole
4. Truss structure

Figure 2.16: Detail of the connection where injection bolts were applied [24]

In the detail (Figure 2.16), two purlins fixed in the flanges of frame girders are depicted. In loading situation with max SLS load the purlins subjected to an opposite angle of rotation at both sides of the connection. The bending moment can only be fully transferred if all contact surfaces are compact. With normal bolts the rotations are large. The angle of rotation can be limited using slip-resistant connections such as fitted bolts, preloaded bolts and injection bolts. As in the case of Oranienburg bridge (section 2.3.1) designers chose injection bolts since fitted bolts was considered an expensive solution, and with HSFG the design resistance depended on friction resistance which is affected by the friction coefficient between contact surfaces. For this project additional short and long duration test were carried out in TU Delft Stevin Lab and in University of Ljubljana according to recommended testing procedure by EN 1090-2 [3], to investigate the bearing resistance of the resin. The results of this research are available in publications [25] (N. Gresnigt et al.), [26] (D. Beg and N. Gresnigt). From this research it was concluded that the design long duration bearing resistance of resin RenGel SW404+HY2404 can be considered as $f_{b, resin, LT}=200\text{MPa}$ and design short duration bearing resistance $f_{b, resin, ST}=280\text{MPa}$. These values are greater than the recommended from ECCS Recommendations (1994) [2], which is $\sigma_b=130\text{MPa}$ and they agree with previous research for short duration bearing stress (L. P. Bouman, 1974 [27]), and for long duration bearing stress (A. Gresnigt et al. 2000 [20]) respectively.

2.3.5 Demountable steel-concrete systems – a new field of research

Composite structures with steel supporting girders and concrete deck are widely used throughout the world as a cost-efficient approach for flooring systems in structures such as bridges and multi-storey buildings. In composite structures both materials are used in their most favourable way. The strain distribution is continuous over the cross sections where steel provides tensile strength, concrete provides compressive strength resulting in increasing stiffness and load capacity. The most common way to ensure composite action is by using traditional headed welded studs which transfer the longitudinal shear forces in steel-concrete surface. (Figure 2.17)

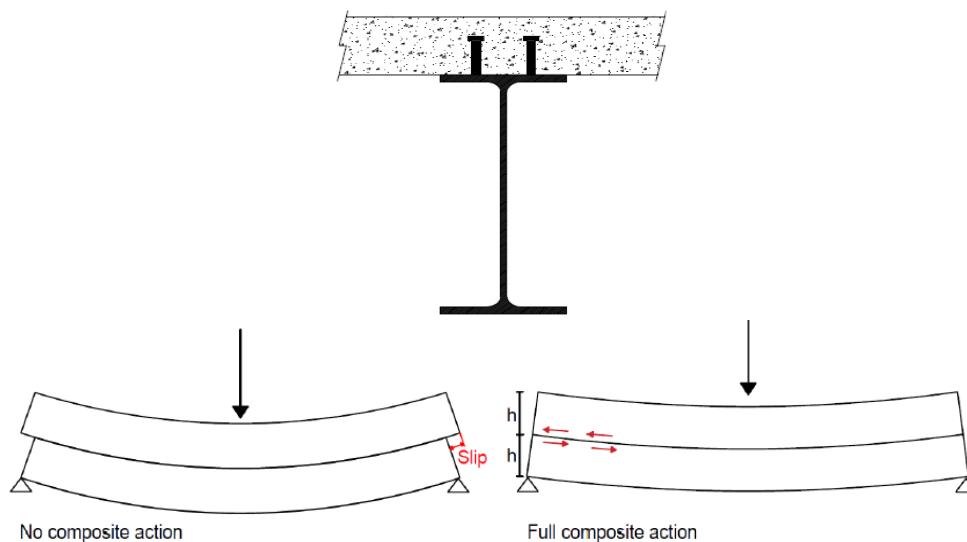


Figure 2.17: Up: Cross section of a composite structure. Down: Beam with and without composite action (M. von Arnim 2017 [28])

Currently the mayor disadvantage of welded-headed studs in terms of reusability, is that it is almost impossible to achieve a separation of concrete deck and steel girder without damaging the elements. Especially in the era of sustainability, where market moves from linear to circular economy the goal is to design structures with perspective of reuse. This becomes more prominent, since the construction industry uses 40% of primary energy production and is responsible for 40% of CO₂ emissions in industrialized countries (N. Jonas et al. 2007 [29]), while in Europe every year there are 450 million tonnes of construction and demolition waste, and only 25% of waste materials are reused (K. Kourmpanis et. al 2008 [30]).

For this reason, a wide research has been carried out in the field of demountability in construction industry, and especially for composite structures research focused on demountable shear connectors instead of welded headed studs. Demountable shear connectors which can be used towards a circular economy are bolted shear connectors with or without embedded nuts, friction grip bolts, and a novel connector i.e. resin-injected bolt-coupler systems (Figure 2.18). They can be used in combination with pre-fabricated concrete decks for even faster assembly without drying time for in-situ casted concrete.

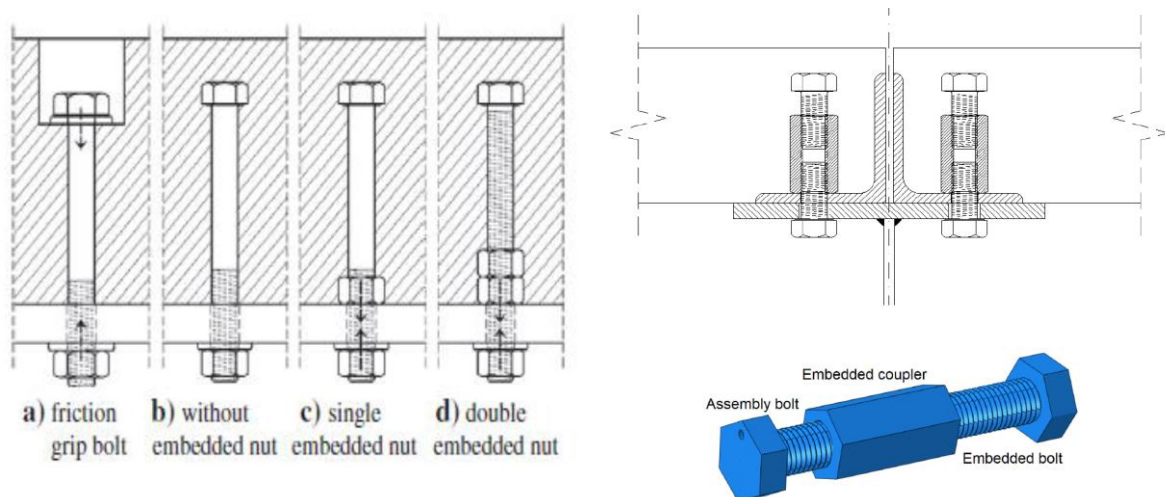


Figure 2.18: Right: Demountable shear connectors [31] Left: Innovative Bolted shear connector with embedded coupler [28]

According to Pavlovic [32] oversized holes are necessary to achieve an easy installation of precast deck to steel girder, and easy demounting. The cost of demountable connectors is higher related to traditional solution but still structure is cost-effective due to fast erection and considering the total life-cycle. However, a disadvantage of using oversized holes is the initial slip between concrete deck and steel girder especially when shear connectors are not pretensioned.

Friction grip bolts transfer shear forces through friction achieved by prestressing, but this prestress load introduces high compressive strength in the concrete around bolt and due to creep and shrinkage of concrete there is a loss of structural pretension with time. In addition, there is the danger of sudden slip if design loads overcome friction resistance.

Bolts without embedded nuts are not suitable as mechanical connectors according to M. Pavlović [32], due to reduced stiffness because of slip and possible rotation of bolt in the absence of nut. Bolts with embedded nuts have an increased stiffness related to those without nut but still lower than welded studs due to slip in the oversized hole, and a shear resistance almost equal to this of welded studs (M. Pavlovic et al. 2013 [33])

The innovative solution of resin-injected bolt coupler systems is a feasible solution since the resin allows for larger tolerances without compromising load-bearing capacity according to A. Kozma et al. [34]. Moreover, there is no danger to damage of elements since there are no extending parts as in regular embedded bolts which are vulnerable to transportation and the danger of sudden slip as in case of friction bolts is eliminated since resin fills the clearances. The system is consisted by a coupler and a bolt embedded in the prefabricated concrete deck and an assembly bolt which is placed at the construction site to connect steel girder to concrete deck (M. von Arnim [28]). The assembly bolt is injected from below to obtain a slip-resistant connection. The steel grade of assembly bolt is lower than this of coupler and internal bolt therefore in ULS will fail first without damaging the non-removable parts of the system.

Resin-injected bolt-coupler systems have been studied by various authors (A. Gritsenko [35]), (I. A. Gîrbacea [11]), (A. Sarri [36]), (M. P. Nijgh et al.[37]), (A. Kozma et al.[38]), (M. von Arnim [28]), and others mostly from TU Delft, University of Luxemburg, University of Bradford, Steel Construction Institute (UK), in the context of REDUCE project (Reuse and Demountability Using steel structures and Circular Economy). The project is founded by European Commission and aims to provide technical solutions, tools and guidance to assist in design for deconstruction as well as reuse, of multi-storey steel-composite structures.

According to a study of Nijgh et al. [37] it is proposed that the optimal method in terms material use, execution and deconstruction of composite car-park flooring system is to use tapered beams with 6mm oversized holes and injection bolts with embedded couplers. Experimental and numerical research by Gîrbacea [11] indicates that demountable composite flooring systems is feasible solution if construction tolerances are designed properly and resin injection of large oversized holes allows for higher manufacturing imperfections and reduced construction time while at the same time enables composite action by creating a slip-resistant connection. Finally it should be noted that reusability of elements would not be possible without precautions such as release agents which will prevent the adhesion between resin and steel (Nijgh [5]), (I. A. Gîrbacea [11]), (Koper [1]).

2.4 Oversized and slotted Holes

From the literature review so far, in the applications with resin injected bolts the importance of using oversized holes is becoming clear. Of course, the same occurs in many applications with conventional bolts.

Since the 1st application of high-strength bolts in 1947 bolt holes larger than bolts have been used for assembly according to G. L. Kulak et al. [19]. The same approach was adopted in USA and Japan where a hole diameter normally 2mm greater than bolt diameter became usual practice. When the hole diameter is restricted to values less than 2mm in excess of nominal bolt diameter, erection problems is easier to occur due to miss-alignment of elements in joint regions. A solution to avoid such problems is the preassembly of structures in steel shop from fabricators, but this increases the total cost. A larger hole size could minimize preassembly resulting in both time and money saving.

With an oversized hole the same clearance in all direction is provided to achieve tolerances during erection. When an adjustment on clearance needed only in one direction slotted holes can be used which are normally aligned parallel with respect to load direction. In TABLE 11 of EN 1090-2) [3] normal and oversized hole clearances are defined (Table 2.4 below).

Diameter of bolt or pin (mm)	12	14	16	18	20	22	24	27 and over
Normal hole clearance (mm)	1		2				3	
Oversized hole clearance (mm)	3		4				6	8
Long slotted holes (on length mm)	1.5d							

Table 2.4: Normal and oversized holes for standard bolts [3]

It should be mentioned that the provisions regarding the hole diameter for injected assemblies are the same as for regular bolted assemblies (H. Kolstein et al. [39]) and are laid down in Table 11 of EN 1090-2 (Table 2.4 above)

Bolt to hole clearance is defined as: $\varnothing_{hole} - \varnothing_{bolt}$

Bolt to hole gap for symmetrical assembly (concentric placement) inside the hole is defined as: $\frac{\varnothing_{hole} - \varnothing_{bolt}}{2} = \frac{clearance}{2}$

These definitions are depicted in Figure 2.19.

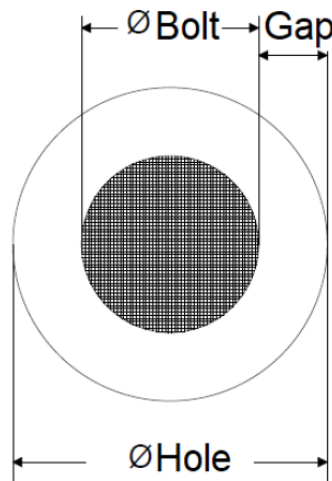


Figure 2.19: Gap between bolt and hole [28]

For prefabricated decks with demountable connectors (section 2.3.5) a larger hole diameter needed due to a big chance of misalignment and overlapping during fabrication, but this results in a reduced stiffness due to residual slip. According to G. L. Kulak et al. [19] care must be provided when large oversized or slotted holes used, to prevent an excessive slip at working loads. According to EN 1993-1-8 [4] the use of large oversized holes may lead to slip which results in large deformations and the connection can be specified as slip-critical. For this

reason Eurocode [4] provides reduction factors for shear resistance in connections with oversized holes (Table 2.5). Similar regulations provided in American codes [40].

	Bearing Connections	Friction Connections
Normal holes	1	1
Oversized holes	0.8	0.85

Table 2.5: Reduction factor for shear connections due to oversized holes according to EN 1993-1-8 [4]

Most unfavourable position of the bolt in bolt hole for IBC's

In EN-1090-2 (Annex G) [3] the testing procedure for Injected Bolted Shear Connections is specified. In this procedure the design resistance is specified with prescribed Double Lap Shear Connection specimens. The code defines that this procedure is used for testing of preloaded connections, but it can be used also for testing of various resins with injection bolts. For injection bolts the assembly of the specimens must be such that the bolt inside the hole is such that the most unfavourable position (Figure 2.20) of the bolt is achieved with respect to the resin layer. This is in accordance with the statement in ENV 1090-1[41]. This position creates the maximum potential for slip of the bolt in the hole since the resistance in EN 1090-2, is calculated in certain slip level (0.15mm) and therefore the resin layer loaded in compression is maximized.

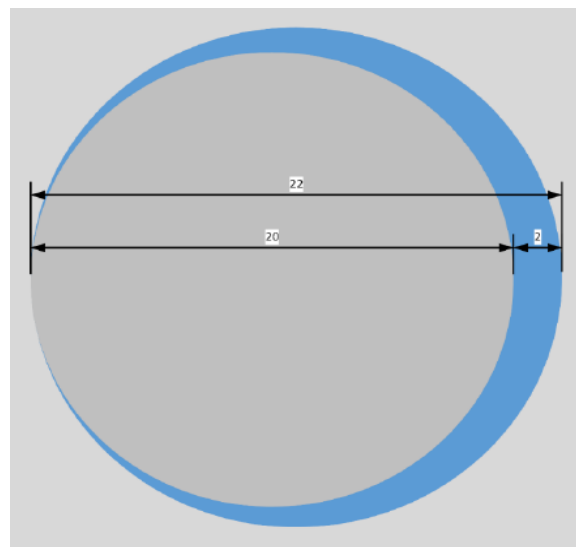


Figure 2.20: Bolt in unfavourable position inside the hole according to EN 1090-2 [3] (in this case bolt with $d_o=20\text{mm}$ and hole with $d=22\text{mm}$ are depicted) [1]

In the study of Kolstein et al. [39] the effect of slotted holes on long duration creep experiments on standard specimens with M20 bolts, according to the guidelines in EN 1090, Annex K [3]. Some specimens had round holes of 22mm and some had slotted holes of either 24 or 26mm. The displacements of the specimens with a normal round hole clearance are lower than displacements of specimens with slotted holes. In the same paper it is reported that the use of oversized holes reduces the maximum allowed bearing stress as a result of lower initial stiffness and increased slip.

Nijgh [5] created a numerical model for the evaluation of connections with resin injection bolts. In his parametric study the behaviour of the connections investigated with bolts placed in most unfavourable position is oversized round holes and slotted holes. The results indicate that the initial connection stiffness is always higher in case of oversized round holes than in case of slotted holes and the effect is more prominent for higher longitudinal clearances as it can be seen in Figure 2.21. In both cases for higher hole dimensions the stiffness decreases, which agrees with the numerical parametric study of Sarri [36] in push out experiments for specimens with steel beam sections and concrete decks, where it is indicated that the diameter of the steel section hole affects the stiffness.

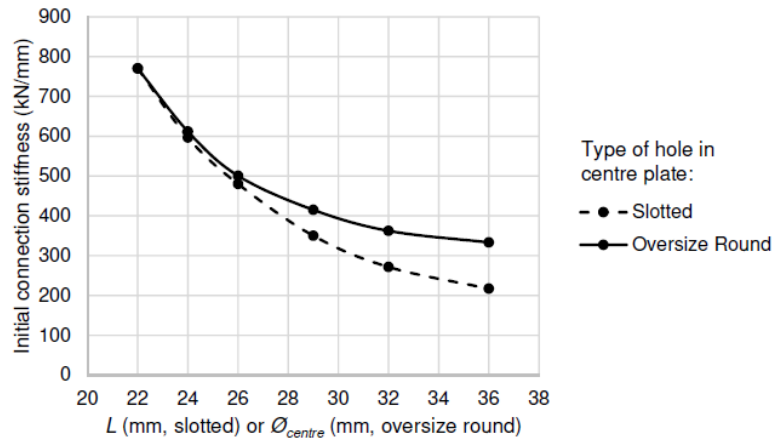


Figure 2.21: Comparison between initial connection stiffness for double lap shear connections with slotted and oversize round holes in the center plate. Bolt (M20) located in most negative position with respect to connection slip [5].

Based on this research it is recommended to use oversize round holes rather than slotted holes since besides the higher initial stiffness, oversized holes offer more favourable execution tolerances in all directions and lower or equal average bearing stresses resulting hypothetically in less creep. However, the latter reason contradicts with EN 1993-1-8 which allows higher bearing stresses for slotted holes.

2.5 Slip critical joints

As mentioned above, generally bolted connections are fabricated with hole clearances so that the fabrication process is easier. This in many cases results to initial slip occurring in the joints even before the application of significant loads. In applications such as those mentioned in section 2.3.5, where oversized or slotted holes must to be used to facilitate erection and demounting if necessary, or when there is a possibility of fatigue and load reversals in the structure these connections can be considered as slip-critical. These joints should have a rigid behaviour and the connectors must provide a slip-resistant connection.

There is no a strict definition of slip critical joints in Eurocodes but according to American Institute of Steel Construction (AISC) [42] slip critical joints are joints which have low probability of slip during the life of structure. Due to their increased cost related to bearing type or shear type connections, should be used only when it is expected that slip in the joints would endanger the serviceability of structure or would result in a decrease of ULS strength of structure. In RCSC (Research Council on Structural Connections) design guide [19] of AISC is suggested that slip-critical joints should be designed to prevent slip under serviceability loads and prevent rupture under ultimate loads. In ULS failure the slip resistant joint behaves as a bearing type joint and the forces are transferred through bolt shear or bearing of plates. Therefore, the failure of a slip-resistant joint is not a catastrophic failure necessarily, but it should be noted that significant slip in the joint may lead to second order effects and instability of connected structural members.

Summarizing slip critical joints should be used (according to G. Grondin et al. [42]) in cases when:

1. Joints subject to fatigue load with reversal of loading direction
2. Joints where oversized holes are used
3. Joints where slotted holes are used
4. Joints where slip at the faying surfaces may be harmful to the performance of structure

The mechanical fasteners to be used (according to RCSC design guide [19]) in slip-critical connections are:

- High Strength Friction Grip bolts (HSFG)
- Fitted bolts
- Rivets
- Injection Bolts

2.6 Fatigue testing of epoxy resins

2.6.1 Examples of fatigue tests on resins for various applications

Most of data and results of fatigue testing on epoxy resins available in literature, are from researches on composite FRP materials used in aerospace and mechanical engineering (L. J. Broutman [43]), (R. Talreja [44]), (P. T. Curtis [45]), (L. Lorenzo [46]), (D. Hughes [47]). In FRP the fibres (mostly made from carbon or glass) are embedded and supported by a matrix material which transfer the loads from fibre to fibre, protects fibres from damage and support fibres in compression (Figure 2.22). Matrices are made usually from epoxy or polyester resins, but the most common matrix materials for applications in automobile and aerospace engineering are 2-component epoxy resins due to their advanced chemical and mechanical properties, besides their high cost. Therefore, the increasing engineering applications of composites in the 70's created the need for better understanding of fatigue behaviour of their components to improve the design and reliability, and this draw the attention of many researchers.

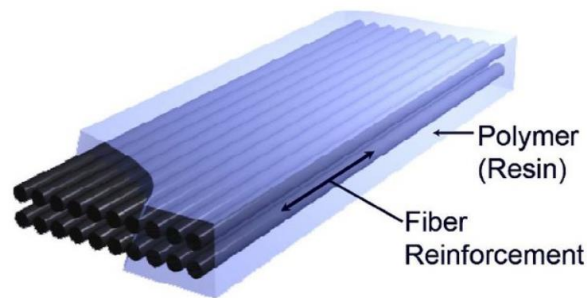


Figure 2.22: Representation of a unidirectional FRP material [48]

According to P.T Curtis [45] in a research on fatigue of composites, FRP fibres generally perform well in fatigue and it is usually the matrix that influences the development of fatigue damage in composites during fatigue loading. Furthermore, experimental evidence has shown that slopes of S-N curves of composites are determined by the stresses in matrix. A similar statement that fatigue behaviour of fibre composites is depended upon matrix materials, can be found in [49] (L. Sahu and J. Broutman et al.)

An extend research on fatigue behaviour of epoxy resins has been carried out by Broutman et al. [43] in 1972. Authors investigated several influencing factors for fatigue life in specimens made of epoxy resin/hardener Epon 828/MPDA subjected to cyclic fatigue tension-compression stresses (with mean stress=0).

The fatigue mechanisms of resins are difficult to understand because of their complex molecular structure, their hysteresis and viscoelastic response in cyclic loads and their environmental and temperature sensitivity. Because epoxies are polymers, they suffer from a temperature rise due to hysteresis loss when subject to cyclic loads. This temperature increase depends on stress range and cyclic frequency and according to Broutman experiments [43], fatigue life of epoxies increases with decreasing frequency. In high frequencies the temperature increases inside epoxy (Figure 2.23) and this decreases the strength and modulus of elasticity and the resistance to fatigue of the resin is lowered. Below a certain frequency there is no increase in temperature. The presence of water in the specimens had a beneficial effect on fatigue life of resins and this can be attributed to the cooling down of specimens subjected to high frequencies. Finally, after testing it was proved that fatigue behaviour of epoxy resins is similar to that of metals, in the sense that the endured number of cycles increases with decreased applied stress range. Lorenzo et. al [46], tested 2 epoxy resins with flexural cyclic loads, Epon815/Versamide140 and Epon828/Epon-Z and two failure mechanisms were identified namely viscoelastic creep ductile failure and nucleation of a main crack due to microcracks and defects in the resin which resulted in brittle failure.

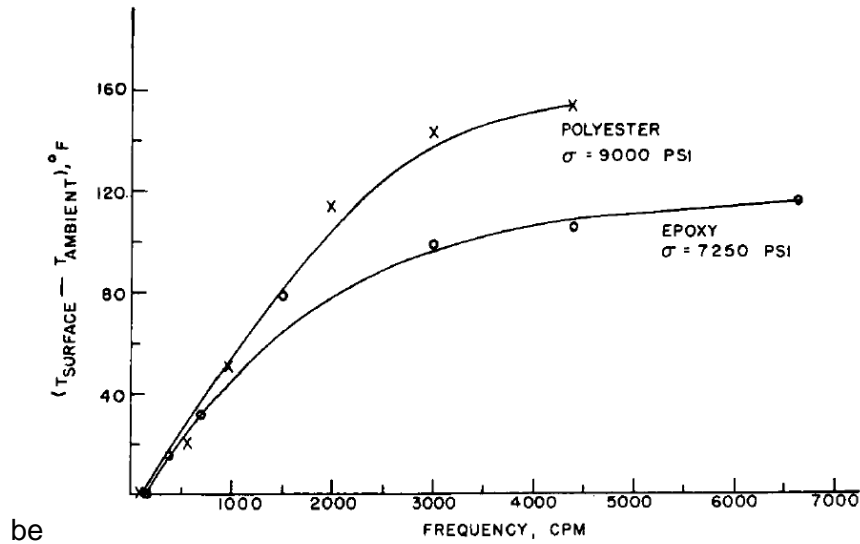


Figure 2.23: Temperature increase in epoxy and polyester resins vs increasing frequency [43]

In structural engineering the evaluation of fatigue behaviour of resins is important for use in numerical models to predict fatigue strength of resin injected bolted connections. M. Rodriguez and all [50] conducted experiments on specimens made of two resins used in structural applications namely Sinkadur 52 and Sinkadur 30, assembled according to ASTM standards [51]. To evaluate the results and obtain the S-N curves of adhesives a statistical analysis was performed according to the principles of the standard ASTM E739-91[52]. The obtained S-N curves from this experimental program can be found in Figure 2.24. The slope of S-N curve for Sinka-52 is $m=11$, while for Sinka-30 is $m=6$. It was concluded that Sinka-30 has higher stress range for same failure cycles in high cycle fatigue when compared to Sinka-52 while for low number of cycles this is reversed.

- The S-N characteristic equation for Sinka-30 is: $\log N = 14.45 - 11 \cdot \log \Delta \sigma$
- The S-N characteristic equation for Sinka-52 is: $\log N = 9.16 - 6 \cdot \log \Delta \sigma$

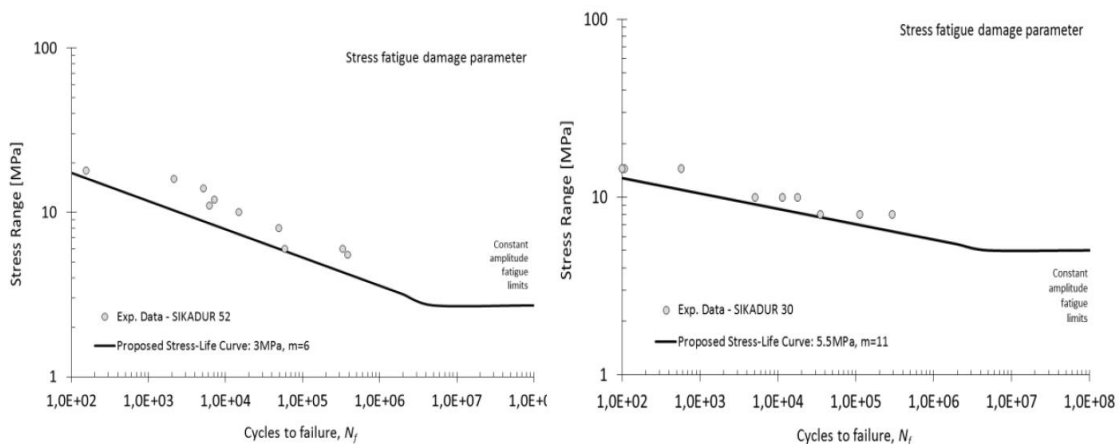


Figure 2.24: S-N curves for Sinka-52 and Sinka-30 obtained from statistical evaluation [50]

2.6.2 Testing parameters

From the above it is concluded that for a fatigue testing program in general and specially for fatigue experiments on epoxy resins, a consideration of several parameters is required and each of these can affect test results. Such influencing factors are the stress ratio $R_\sigma = \sigma_{\min} / \sigma_{\max}$, the cyclic frequency f , and the control mode and others which selection for current research is analysed also in Chapter 3. For this reason, a search in the literature was necessary to help the author to choose the parameters for the fatigue experiments of the current study.

The majority of experimental data reported for fatigue testing have been extracted using constant stress amplitude loading (B. Zafari et al. [53]). Moreover, fatigue tests for IBC's most often conducted under displacement control mode or force control mode, but the former results in material failure under fewer cycles. This is attributed to the continuous increase in deformation after the damage in the connection has initiated since the load is kept constant. It should be noted that in the experimental program of this Thesis, there is no possibility of failure in steel parts of the test assembly, and cracks are expected in the resin part therefore a force-control mode was chosen.

Another influencing parameter as mentioned above is the stress range R_σ . Stress range can take the following values depending on the loading of the specimens.

- $0 < R < 1$: in case both $\sigma_{\min}, \sigma_{\max}$ are tensile and mean stress is tensile
- $-1 < R < 0$: in case σ_{\max} is tensile and σ_{\min} is compressive and mean stress is tensile
- $-\infty < R < -1$: for same as previous but with mean stress is compressive
- $0 < R < 1$: in case both $\sigma_{\min}, \sigma_{\max}$ are compressive and mean stress is compressive
- $R = 0$ in case σ_{\min} is zero. In this case loading type is called repeated or one-directional

The most characteristic loading types for fatigue testing can be shown in following figure:

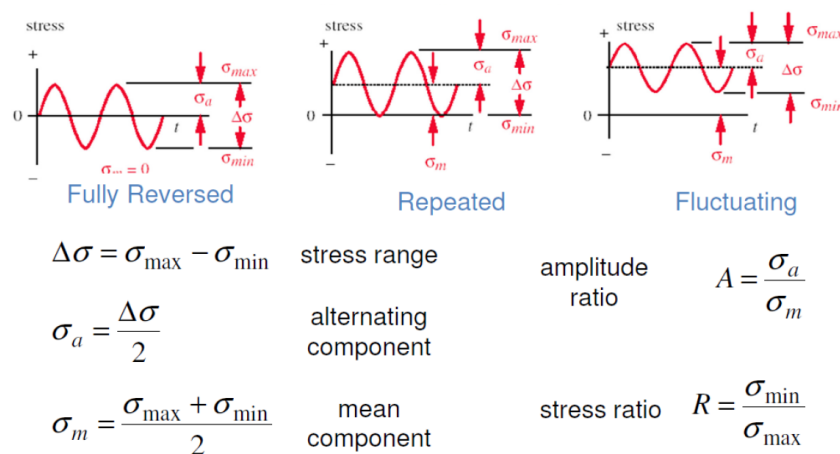


Figure 2.25: Most characteristic loading types for fatigue testing

As mentioned in previous section 2.6.1 the hysteresis heat energy dissipation which depends on cyclic frequency can have a significant influence on fatigue behaviour of resins. Therefore, the choose of frequency f is a key test parameter. For fatigue testing structural resins, ASTM

standard D7791-12 [51] proposes a testing frequency 1-25 Hz **but strongly recommends the use of value $f=5\text{Hz}$ or lower.**

Most of researchers followed these recommendations for fatigue testing of resin injected bolted connections or in resins itself. In fatigue experiments for IBCs in FRP (B. Zafari et al. [53]), a frequency $f=2$ Hz and a stress ratio $R=0.1$ (tension-tension) were used. Authors justified the selection of this stress ratio, since it offers a high-tension stress range so that interaction between creep and fatigue would be most severe and there is no stress reversal so that relaxation can be excluded.

De Jesus and Da Silva in [15] used $R=0.1$ and $f=4-6\text{Hz}$ for single lap shear IBC's and $R=0$ and $f=2.5$ for double lap shear IBC's with metals from Portuguese bridges. In a similar research of fatigue behaviour of single lap shear IBC's made of S355 and an old steel of Eiffel Bridge in Portugal [16] the parameters were $R=0.1$ and $f=5\text{Hz}$. For the testing of resins Sinkadur 52 and Sinkadur 30 which referred before (M. Rodrigues et al. [50]), stress range was $R=0$ while frequency was $f=5\text{Hz}$ for the former and $f=2.5\text{Hz}$ for the latter.

For fatigue tests of epoxy resins used as matrix for FRP's which conducted at the 70's and 80's for automobile and aerospace applications, values for R and f at the same range as the above mentioned are reported. In source [54] (R. Rahul and R. Kitey) for tests on resin specimens of DGEBA resin/MTHPA hardener $f=10\text{Hz}$ and $R=0.1$ (tension-tension), while in [55] (A. Lowe et al.) testing parameters were $f=1\text{Hz}$ and $R=0.1$ (tension-tension). For fatigue tests in [46] (L. Lorenzo et al.) the applied fatigue load was a sinusoidal wave form with $R=0.1$ (tension-tension) used with various frequencies in ambient temperature.

Given these facts from the literature search on fatigue testing parameters for experiments where epoxy resins were tested alone or as part of connections, it was decided to conduct the experiments of current Thesis in the Hydraulic Wedge Grip machine of TU Delft Stevin Laboratory with force control mode. The applied fatigue load chosen to be a sinusoidal wave load with constant amplitude and $R=0.1$ (compression-compression), frequency $f=5\text{Hz}$ and ambient test temperature were selected. More details for test set-up and more parameters like stress ranges, and failure criterion considered, can be found in section 3.4.

2.7 Statistical evaluation of experimental results

Many structural components may be subjected to repeated cyclic loads. Engineering experience has shown that materials, members and connection details may fail from fatigue even if the maximum applied stress is less than yield strength. The fatigue life of a material or detail can be obtained analytically using fracture mechanics, or by carrying out fatigue tests. So far, most knowledge of fatigue life of structural members and their connections has been obtained by testing representative details (G. L. Kulak et al. [19]).

According to Schneider and Madox (2003) [56] fatigue testing is the main basis of the relationship between the fatigue resistance of a given material, component or structural detail and cyclic loading. The results of such fatigue endurance tests are plotted on graphs relating applied loading (force, stress, strain, etc.) and the number of cycles to failure known in literature as S-N curves or Wöhler lines. Failure can be defined as structural failure of specimen or some predefined criterion such as certain crack size or certain displacement or slip based on the materials and testing conditions.

Research has shown that stress range is the dominant variable causing fatigue failure. According to DNVGL code [57], for new types of connections it is recommended to perform testing of at least 15 specimens in order to establish a new S-N curve and at least 3 stress ranges should be selected in the relevant S-N region such as the representative slope m can be determined. Based on that for the experiments on resin and steel reinforced resin of this Thesis 3 stress ranges selected and an effort has been made to have 15 specimens for each tested condition (for further information read section 3.4.6). The information about fatigue life provided by S-N curves has been obtained by testing of materials with cyclic loading of constant amplitude and constant mean value. This would be the case in current fatigue study.

It has been shown that relationship between stress range $\Delta\sigma$ (can be found also in literature as S or σ_r) and the number of cycles to failure is linear when each of two variables is expressed in logarithmic form (Figure 2.26). Therefore, data from fatigue tests are generally described using the relationship:

$N = A \cdot \sigma_r^m$ which in logarithmic form can be written as $\log N = \log A - m \log \sigma_r$, where:

- N is the number of cycles to failure (dependent variable)
- m is the slope of S-N curve (independent variable)
- σ_r (or S or $\Delta\sigma$) is the stress range
- $\log A$ is the intercept of line with x axis

It is noted that m and A are constants which depend on the material

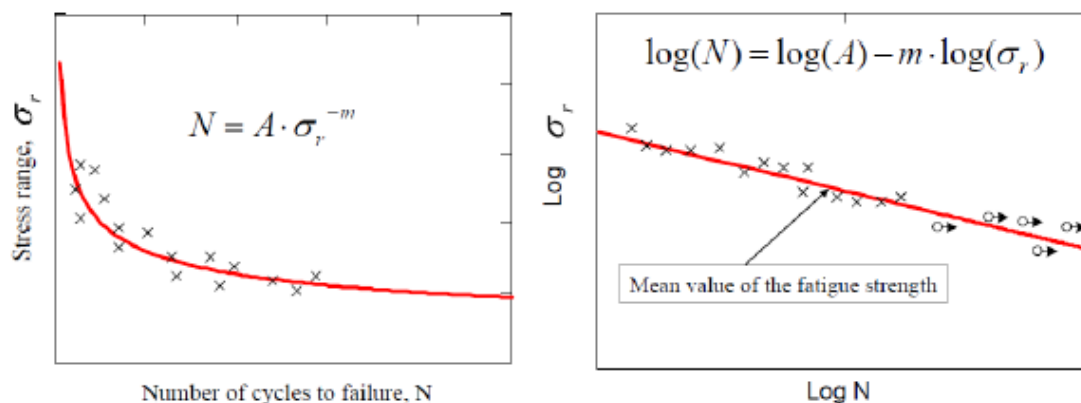


Figure 2.26: Relationship between stress range and number of cycles to failure in conventional axes (left) and in logarithmic axes (right)

If enough data from experiments are available, the mean S-N curve can be derived. Mean S-N curve is the fitted curve between the data points of results ($\log N$, $\log S$), and represents the 50% survival probability of all specimens according to G. L. Kulak et al. [19]. Special attention should be given to the fact that in curve fitting methods the standard approach is to assume that the parameter plotted on x-axis is the independent variable and the parameter plotted on y-axis is the dependent variable. However, the opposite is the case in fatigue approach where $\log N$ is treated as the dependent variable (C. Schneider and S. Maddox [56]).

The standard practice in fatigue analysis for constructing the fitted line (also called the mean line and an example can be seen in Figure 2.26 above), is to consider only the results from the specimens that failed (or reached the failure criterion). From these results the parameters $\log A$ and m of the best fit through the data are estimated by an ordinary linear regression. With

this method the values of parameters $\log A$ and m are chosen such as the sum of squared deviations of $\log N_i$ (or residuals) is minimized and according to [56] (C. Schneider and S. Maddox) is the basis to derive later the design curve for most of fatigue design rules in the word.

It must be mentioned that since test specimens and testing conditions are never identical, the resulting data are more or less scattered. Furthermore, in structural engineering fatigue problems are influenced by many parameters which are not always independent therefore design and evaluation procedures are in most of cases empirical. To overcome the scatter of S-N data besides the linear regression analysis to find the fitted curve, statistical methods have to be used so that the derived characteristic (also called design) curves for fatigue lifetime predictions, agree with the principles of structural integrity criteria. For this procedure besides a pure statistical approach, also some engineering judgment is needed to establish suitable safety levels for structural details or materials.

In the literature various probabilistic models can be found, that attempt to model the complete probabilistic fatigue field. Zao et al. [58] developed a model to predict fatigue life railway axle steels in high cycle regimes, assuming data follow a logarithmic normal distribution. Schijve [59] established a statistical distribution function for fatigue life of structures but it was valid only in certain parts of S-N field and not the full regime. Castillo and Fernandez [60] proposed a probabilistic model which is recommended for medium high and very high cycle fatigue.

In general, for design purposes, it is necessary to establish limits between which, a given proportion of the data lie. Typically a value of 95% for probability of survival is used (C. Schneider and S. Maddox [56]). EN 1993-1-9 adopts the same assumption since the characteristic fatigue curves in EC3-1-9 (2005) represent 95% probability of survival, which correspond to the lower 5% failure of the tested fatigue strength. In the literature, for fatigue studies of structural resins and injected bolted connections, researchers M. Rodrigues et al.[50], J. A. F. de O. Correia et al.[61], and B. Pedrosa et al. [16], adopted the probabilistic model of ASTM E739-91 [17] for the derivation of design curves. It should be noted that this procedure has a limited application for very-high cycle fatigue, also it is recommended not to extrapolate the curve outside the interval of testing, and the run-out specimens cannot be considered in the analysis.

In this procedure of ASTM the linear model to represent the S-N curve is described by the known equation:

$$Y = A + B \cdot X$$

Where dependent variable Y , and independent X , defined as

$$Y = \log N, \quad X = \log \Delta \sigma$$

The parameter A is the intercept $\log A$ and B is the slope m of the mean curve and can be estimated as:

$$A = \bar{N} - B \cdot \bar{\Delta \sigma}$$

$$B = \frac{\sum_{j=1}^k (\Delta \sigma_j^* - \bar{\Delta \sigma})(N_j^* - \bar{N})}{\sum_{j=1}^k (\Delta \sigma_j^* - \bar{\Delta \sigma})^2}$$

Where \overline{N} and $\overline{\Delta\sigma}$ are the mean values of the experimental data and $\Delta\sigma_j^* = \log \Delta\sigma_j$, $N_j^* = \log N_j$ respectively; and k is the number of tested specimens.

After the derivation of mean curve, for the derivation of characteristic curve rectilinear confident bands are used by shifting the mean S-N curve as expressed by next equation

$$N = A + B \cdot \Delta\sigma \pm a \cdot S$$

Where S is the standard deviation of residuals and a is an integer number that defines probability curves of failure according to normal distribution. In case of 95% probability of survival $a = 2$.

Another probabilistic model is proposed by Maddox and Schneider [56] and is adopted for the fatigue push-out tests in the research on fatigue push-out tests of shear connectors by R Hallmark et al. [62], uses a similar linear regression analysis for the derivation of mean S-N curve, based on the least square method proposed by Maddox in a separate publication [63]. The equations of this regression analysis can be found in Appendix B. For the characteristic curves in this model, can be written also in a linear form with 95% survival probability based on the equations:

$$\log N_{c,k} = (\log a + m \log \Delta\sigma) - t_{5\%} \sigma \sqrt{f}$$

$$f = 1 + \frac{1}{n} + \frac{(\log \Delta\sigma_c - \overline{\log \Delta\sigma})^2}{\sum_{i=1}^n (\log \Delta\sigma_i - \overline{\log \Delta\sigma})^2}$$

where:

- $\overline{\log \Delta\sigma}$ is the mean value of n values of $\log \Delta\sigma_i$
- $t_{5\%}$ is the t-score of a one sided 95% confidence interval in the student's t-distribution
- n_f the degrees of freedom which in this case is $n - 2$ since there are two coefficients in the regression line (m and $\log \Delta\sigma$) that have to be estimated
- σ is the standard deviation of the regression line

The equations of this probabilistic model and the values of students t distribution depending on the probability of survival can be found in Appendix B.

Based on this research on the literature for the statistical approaches used for the evaluation of fatigue of resins two models are chosen in the present Thesis for the shake of comparison. These models are the described above ASTM E739-91 [17], and the Maddox and Schneider model [56].

3 Experimental work

As mentioned before, injection bolts are used in applications such as repair of old riveted connection in steel bridges, construction of new bridges (common in the Netherlands), slip resistant connections in storm barriers and other structures, while they are a feasible solution for the construction of composite structures with demountable and reusable structural members mostly with oversized holes. In these injected bolted connections (IBCs), the void formed by the clearance between the bolt and the hole is filled up with resin, and hereby a slip-resistant and durable connection is achieved. The performance of IBC's preloaded or not, has been investigated in laboratory mainly by quasi-static and creep tests. There are very few studies on fatigue behavior of joints and even fewer in fatigue behavior of resins. This experimental work focuses on the deterioration of the connection stiffness and the slip build-up, which is mainly caused by the resin under cyclic loads.

For the purposes of the ongoing research of fatigue behaviour of resins, several cyclic tests had been carried out in Stevin Laboratory of TU DELFT using a Hydraulic Wedge Grip machine. The specimens used at the experiments were designed and constructed according to a tailor-made test set-up which allows testing of the resin under cyclic loads, without the risk of fatigue cracks of the injection bolt itself. The specimens were injected with the conventional resin (recommended by Dutch Ministry of Infrastructure-Rijkswaterstaat), as well as with a newly developed in TU DELFT, resin reinforced with steel shots, with a subsequently higher Young's Modulus (both described briefly in literature review section 2.1). Experiments with both resins had been carried out to examine in what extend the fatigue properties of steel reinforced resin are superior to those of conventional resin.

Specimens of two different geometries with respect to the diameter of the hole filled up with resin were tested, subjected in three different compressive stress ranges. Each experiment was divided into two phases to simulate as possible, a real loading scheme of a connection. For the first phase a quasi-static loading with a very low frequency was applied, which made possible the identification of the initial stiffness of the connection. For the second phase a fatigue loading in form of a sinusoidal compressive load was applied with a 100 times higher frequency with respect of that of the quasi-static phase. This cyclic loading scheme with higher frequency made possible the application of repeated compressive bearing stresses in the resin, for the investigation of stiffness degradation and slip accumulation of specimen due to fatigue of resin layer.

3.1 Description of the specimens

3.1.1 Geometry of specimens

Three different specimen geometries have been designed and constructed for the experimental phase of the research. In terms of geometry all specimen types have the same dimensions, except for the hole diameter in which the resin is injected. Each specimen consisted of a steel lower (female) plate with a bolt part in which the resin material is injected, an upper steel loading (male) plate, two orthogonal steel plates for each side of the hole tightened by M8x80mm Hex bolts to create a confinement for the resin and the threaded part of a M20 bolt placed in the most unfavourable position inside the hole. The dimensions of all parts of specimens are described below.

3.1.2 Lower steel (female) plate

Every specimen consisted of a steel lower plate with a hole in the upper side with diameter of 30 mm, 26 mm, 22 mm for each specimen type respectively. All the other dimensions of the lower steel plate are the same except for the diameter of the hole which differentiates the specimen type and can be shown in Figure 3.1 where the front view of the lower plates of the three different specimen's type is presented. In Table 3.1 the distinction of specimen type according to diameter of the hole can be found. The same designation with first capital letter D followed by the diameter of the hole in mm will be used later for the specimen designation at every experiment.

Specimen Designation	Diameter of hole	Radius	Distance from centre of the hole to upper edge	Nominal maximum thickness of resin part formed inside the hole
D30	30 mm	15 mm	25 mm	10 mm
D26	26 mm	13 mm	25 mm	6 mm
D22	22 mm	11 mm	25 mm	2 mm

Table 3.1: Specimen type distinction according to geometry of lower plate

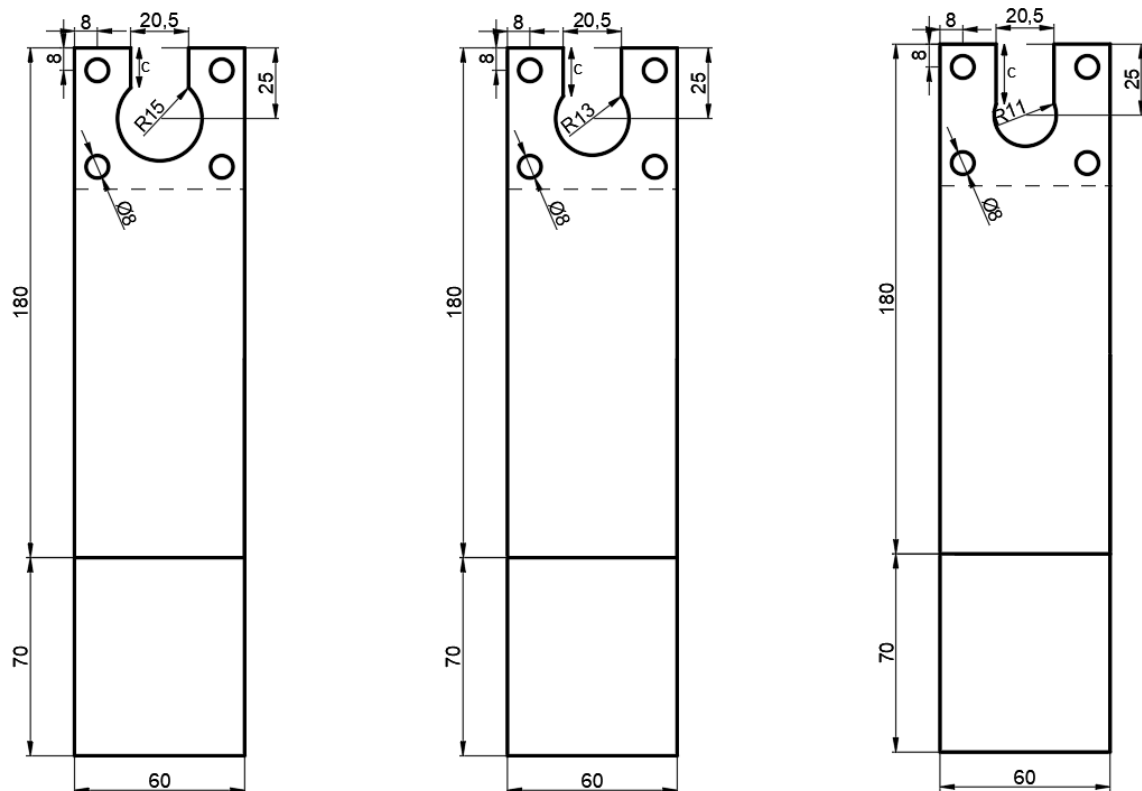


Figure 3.1: Front view of lower plates D30, D26, D22 from left to right (dimensions in mm)

In Figure 3.2 the side view of the plate can be seen. The thickness of the main body of the plate which accommodates the hole is 30mm with length of 180mm and a width of 60mm. There is an extension with length 70mm and thickness of 15mm which facilitates the fixing of the plate by the lower wedges of the loading machine as it can be shown. A similar extension with same dimensions was predicted for the upper lading pin plate as it will be explained in section 3.1.3. In Figure 3.3a 3D simulation of the lower plate D30 at the ABAQUS CAD environment is shown along with a picture of lower plate.

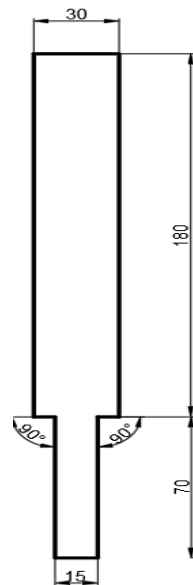


Figure 3.2 Left-Side view of lower plates (dimensions in mm), Right-Grip of the lower plate by wedges

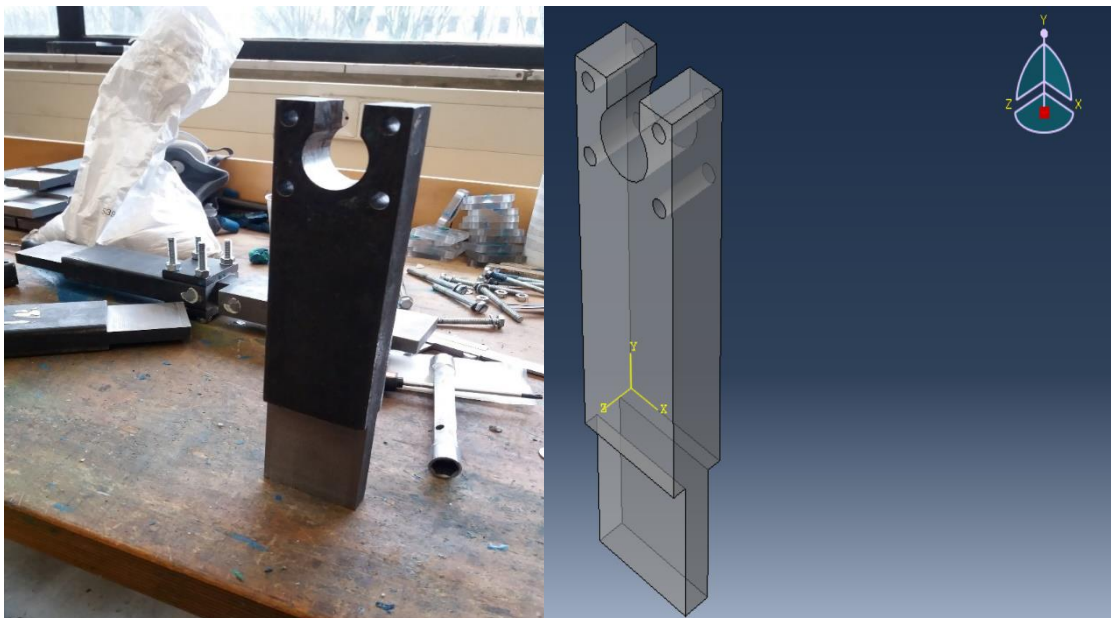


Figure 3.3: Lower (female) plate of specimen in reality and in 3D visualization

3.1.3 Upper (male) steel plate

All specimens have the same upper loading male plate through which the load is transferred to the bolt part and hereby to the resin under testing. Upper plates have a special designed extension at the lower edge of length 35 mm with an arch finishing which has engraved threads M20x2.5 of class 6H according to ISO (see Annex C) to accommodate the M20 threaded part

of the bolt (Figure 3.4). This extension enters to the opening of lower plate at the final specimen assembly. The width of the extension is 20 mm, while the width of the opening in the lower plate is 20.75 mm, in order to avoid the contact between steel surfaces during loading to limit the friction resistance. The length of the main body of upper plate is 120 mm, the width and the thickness of the main body is the same as of lower plate meaning 60 mm for the former and 30 mm for the later. Furthermore, as in the case of lower steel plate, the same extension of 70mm x 60mm x 15mm can be found on the upper side of the loading pin plate which serves the fixing of the plate by the wedges of the machine. The drawing of the upper plates with dimensions in mm can be shown in Figure 3.4 bellow. In Figure 3.5 a 3D simulation of the upper plate in the ABAQUS CAD environment is shown along with a picture of upper plate in reality

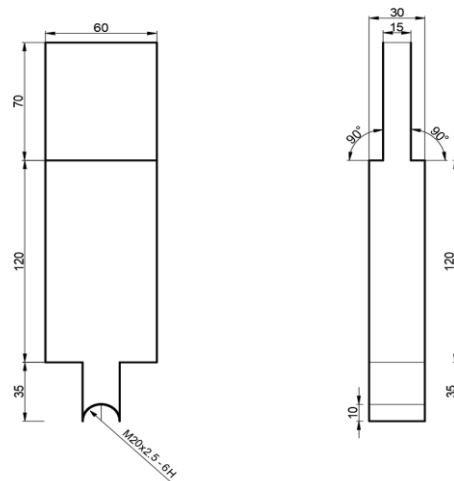


Figure 3.4: Drawings of front and side view of upper loading male steel plate (dimensions in mm)

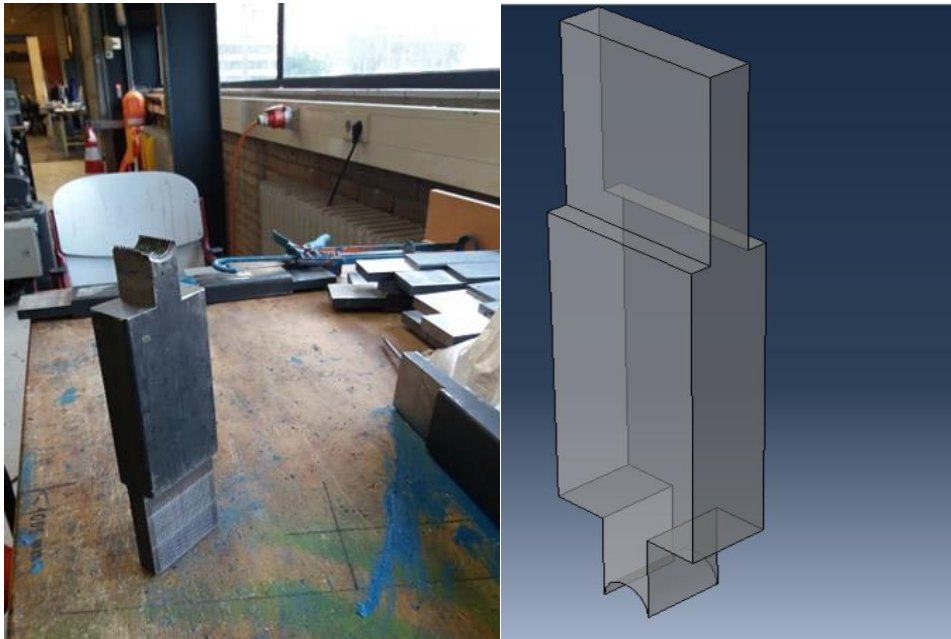


Figure 3.5: Upper loading male plate of specimen in reality and in 3D visualization

3.1.4 Threaded bolt part (pin) – M8x80 Hex Bolts – Side Steel plates

The remaining smaller steel parts of the specimen but also very important in terms of their function at the specimen, are the threaded M20 bolt parts which are attached to the upper plate's extension with the engraved M20x2.5 metric threads as well as the side plates which are tightened to the lower steel plate by M8x80 hex bolts fitted to four 8 mm diameter holes drilled in lower plate.

The M20 bolt parts (Figure 3.6) are cutted from a M20 threaded rod in lengths of 29.5 mm in order to be just smaller than the width of upper and lower plate which is 30 mm to avoid friction between the bolt part and the side plates. The bolt part serves a vital role, since it transfers the bearing stresses to the resin part under testing of each specimen. Along with the side plates which are tightened by the M8 bolts and confine the resin create a simulation of an injected bolted connection where the resin is confined inside the hole but at the same time facilitate the testing of the resin alone in fatigue loads, without the risk of the fracture of bolt.

The side plates are orthogonal with dimensions 50mm x 60mm and thickness of 10mm and with 4 drilled holes of diameter 8mm (Figure 3.7, Figure 3.8) Two side plates are used for each specimen each at one side of the hole to confine the resin. They are tightened with the use of M8x80mm Hex Bolts, by manually applying torque at the nuts. Note that the holes in side plates and in the lower steel plate have no threads and they have diameter of 8 mm therefore the bolts are fitted. Washers are used in the interface of side plates and the nuts of the M8 fasteners to reduce the compressive stresses applied to steel side plates due to tightening of bolts.

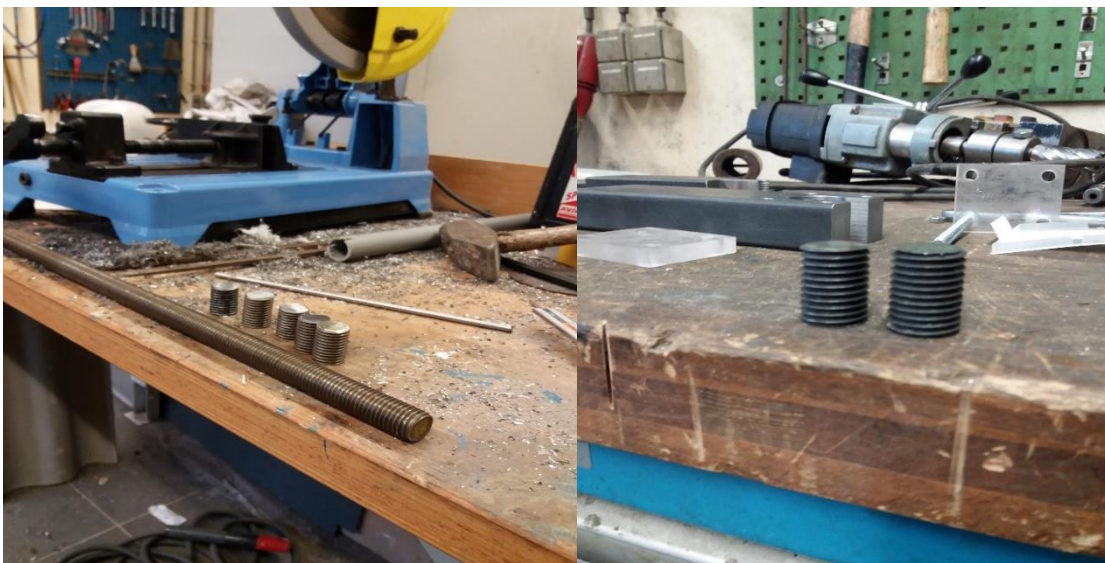


Figure 3.6: Cutting of bolt parts from threaded M20 rod

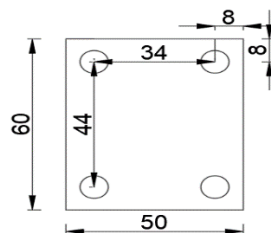


Figure 3.7: Drawing of front view of the steel side plates (dimensions in mm)

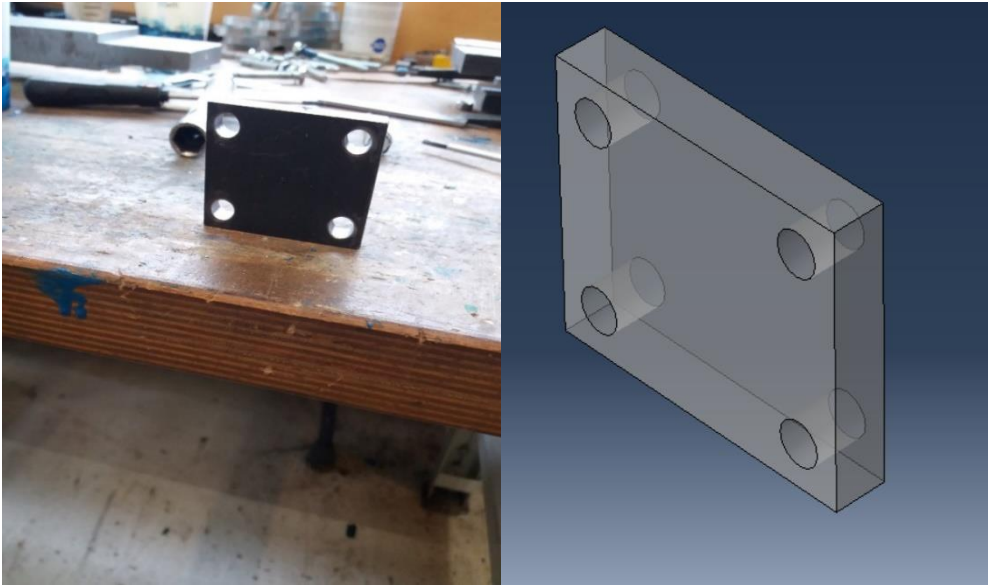


Figure 3.8: Side plate of specimen in reality and in 3D visualization

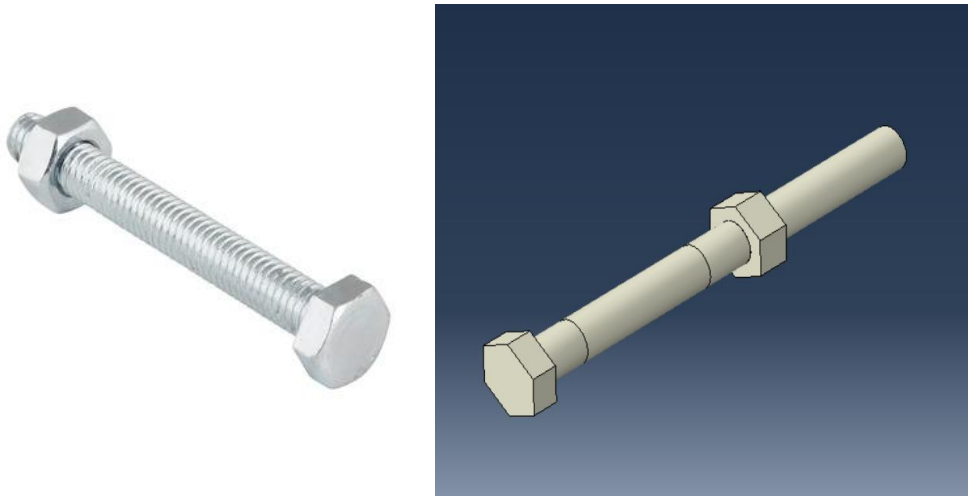


Figure 3.9: M8x 80 Hex bolts with their nut in reality and in 3D visualization as designed in FEA environment without the threads

3.2 Materials

The main materials used in the specimens are the resin (conventional and steel reinforced) which fills the void formed between the plates and the bolt part, and the steel from which all the plates and bolt parts are made of. Further information about resins can be found in the literature review

3.2.1 Resin

For injection bolt applications a two-component epoxy resin should be used for the injection of the hole clearance with a pot life at least 15 minutes. The resin must have a viscosity such as the filling of any cavities is achieved. The injection temperature should be between 15-24°C. Epoxy resins are thermosetting polymers and therefore they need a curing process for hardening. Curing is initiated by heat or radiation or by mixing with a catalyst. Once reach the solid state, a thermoset cannot be melted for change shape under the influence of heat but rather burns, in contrast to thermoplastic polymers.

The only resin product allowed from Dutch Ministry of Infrastructure (Rijkswaterstaat) for injection bolt applications is RenGel SW404 with hardener HY2404 which is also referred in literature as Araldite SW404/HY2404. The mixing ratio of the components is 10:1 (Resin RenGel SW404/Hardener HY2404) according to product sheet. The same resin product (RenGel SW404) is adopted for the experiments of current research but with a different hardener by the same manufacturer meaning HY 5159 with mixing ratio 8:1, which offers a higher pot life after mixing and therefore facilitates the injection process. At the same time the final product after curing has the same material properties as in the case of using HY 2404.

The most important parameters of resins for injection bolt applications are the following:

- Viscosity of resin
- Pot life of resin
- Heat deflection temperature of resin after hardening
- Mechanical properties of resin after hardening

Pot life is a defined time during which the viscosity of the mixed system doubles. Pot life of RenGel SW404 with hardener HY 5159 at room temperature is 50 min according to product sheet (while pot life of SW404+HY2404 is 15 min). The heat deflection temperature is 100°C. Although according to the manufacturer the resin is completely cured after 24 hours, a former research on the resin that conducted in TU Delft have shown that the strength and stiffness are developed after 3-4 hours [27].

Regarding the mechanical properties of resin the following adopted for this research namely $E=5640$ MPa and Poisson ratio $\nu=0.3$ defined for unconfined conditions according to M. Nijgh et al. [8],[9] as already has been reported in literature review.



Figure 3.10: Left-Resin components RENGEL SW 404 and REN HY 2402 allowed by Rijkswaterstraat, Right-Resin components RENGEL SW 404 and REN HY 2402 used in the experiments

3.2.2 Steel Reinforced Resin

Nijgh suggested reinforcing of epoxy resins with steel particles would have two positive effects [5]. Firstly, the decrease of the creep deformation since resins are susceptible to creep like all polymers and secondly the increase of initial connection stiffness. Since one of the most important research questions of this study is the comparison of the fatigue behaviour of conventional and steel reinforced resin, steel reinforced resin was used also for the specimens.

Small, strong and stiff particles are added to the hole and fill the clearance prior to injection of the conventional resin material. They act as reinforcement, as they form a continuous skeleton through the free volume, forming a load bearing path. The main function of the resin in that case is the filling of the small voids between the particles and the bonding of the particles. According to research of Nijgh [5] there are two options for the reinforcing steel particles. The first is steel shot particles of spherical shape which are used for shot peening which is an improvement technique of fatigue strength in welded connections. The second alternative is grit which is has an irregular shape. The steel spherical shots are preferred over grit due to their easy workability, since irregular shaped grit has lower mobility which makes harder the insertion in the clearance.

Therefore, spherical steel shot of size class S330 with a nominal diameter of 1mm (Figure 3.11) is used as load bearing skeleton and along with the resin RenGel SW 404 + HY 5159 form the steel reinforced resin material used in the present study.

Function of Particles	Function of Resin
Transfer load through direct particle to particle contact	Fills the residual free volume
Reduce the required resin volume (economic benefit)	Prevents any sudden free body movement of the particles
	Provides initial stiffness in case particles are not in direct contact with the fastener or hole surface
	Protects particles from degradation due to environmental influences such corrosion

Table 3.2: Functions of resin and particles in a steel reinforced resin injected connection [5]



Figure 3.11: Steel shot used as the reinforcing material of steel reinforced resin used in experiments

Regarding the material and mechanical properties of steel reinforced resin, a first consideration should be done for the mass of the material. According to Kepler conjecture theorem (1611), the maximum packing density of equally sized spheres is 74% which is still valid today.

$$\eta_{\text{Kepler}} = \frac{\pi}{3\sqrt{2}} \approx 0.74048 \approx 74.048\% \quad (\text{Kepler's conjecture})$$

However according to research of Scott and Kilgour [64] the packing density in practice when spheres are positioned randomly is 64%. In the present study packing density is considered as 60% according to research of M. P. Nijgh et al. [8]. Therefore, the mass density of the steel reinforced resin is calculated considering that the mass density of steel is 7400 kg/m^3 and the mass density of resin RenGel SW404 + HY5159 according to product sheet is 1800 kg/m^3 and their ratio inside the hole is 60% for the former and 40% for the latter.

$$\gamma = 7400 \times 0.6 + 1800 \times 0.4 = 5160 \frac{\text{kg}}{\text{m}^3} \quad (\text{mass density of SR resin})$$

For the numerical static analysis which is presented on chapter 4 of current research, the material properties adopted are the following A Young modulus of elasticity $E=15200 \text{ MPa}$ and Poisson ratio $\nu=0.22$ defined for unconfined conditions according to M. Nijgh et al.([8]).

3.2.3 Steel

Steel is used for all the plates of the specimen meaning the lower plate, the upper plate with the loading pin part and the side plates for the confinement of the hole, as well as for the threaded part of the bolt which transfers the stresses to the resin. All plates are made of steel S355, while the threaded part of the bolt is made of steel 10.9. Since the load is transferred to the resin all steel parts remain undamaged after the end of experiment and can be used for the assembly of the next specimen.

Component	Steel Grade	Nominal Yield Strength (MPa)	Nominal Tensile Strength (MPa)
Lower plate	S355	355	510
Upper plate	S355	355	510
Side plates	S355	355	510
Threaded M20 Bolt threaded part	10.9	900	1000

Table 3.3 Steel grade per component used in specimens (EN 1993-1-1)

The material properties to be adopted in calculations according to EN 1993-1-1 [65] are the following:

- Mass density: $\gamma = 7850 \text{ kg / m}^3$
- Modulus of elasticity: $E = 210.000 \text{ MPa}$
- Poisson's ratio: $\nu = 0.3$
- Shear modulus : $G = \frac{E}{[2(V+1)]} = 81.000 \text{ MPa}$

3.3 Assembly of specimens

For the purposes of experimental program of current research, the steel plates of specimens (Figure 3.12) were designed and ordered to the steel shop in the prescribed dimensions as described in section 3.1. They fabricated and delivered into Stevin Lab with the following quantities:

Order List		
Component	Quantity	Material
Fatigue lower (female) plate D30	5	S355
Fatigue lower (female) plate D26	5	S355
Fatigue lower (female) plate D22	5	S355
Fatigue upper (male) plate	10	S355
Side plate	8	S355

Table 3.4: Order list of steel plates of the specimens



Figure 3.12: Fatigue plates used for the assembly of specimens

Before the assembly and injection of specimens, all steel surfaces which would be in contact with the resin (i.e. the hole of lower plate, the threaded part of pin in the upper plate and the threaded bolt part) were sprayed with a release agent to prevent adhesion and allow for easy separation of resin part from the plates after the experiments. Since the current experimental program is for the fatigue research of resins, a substantial number of specimens is needed therefore fatigue plates demounted after the end of each experiment and used for the assembly of the next.

The release agent used was ACMOS 82-2405 released agent which is a wax-based aerosol spray and according to Nijgh [5], is preferred over PETE, PVA and silicon-based release agents since for instance silicon may have a negative effect in the material properties of resin. According to research of Girbacea [11] who investigated with large scale beam tests many influencing factors and their effects on the assembly and disassembly of demountable steel-concrete composite flooring systems with resin injected shear couplers, the process of spraying surfaces which will be in contact with resin is fast, and one spray tube can be used for approximately 50 bolts and holes. In current research the successful use of release agent was confirmed after the end of each experiment in the demounting process of specimens where all resin parts removed relatively easy with by simple hammering, with some difficulties observed only for some steel-reinforced specimens where extra effort needed.

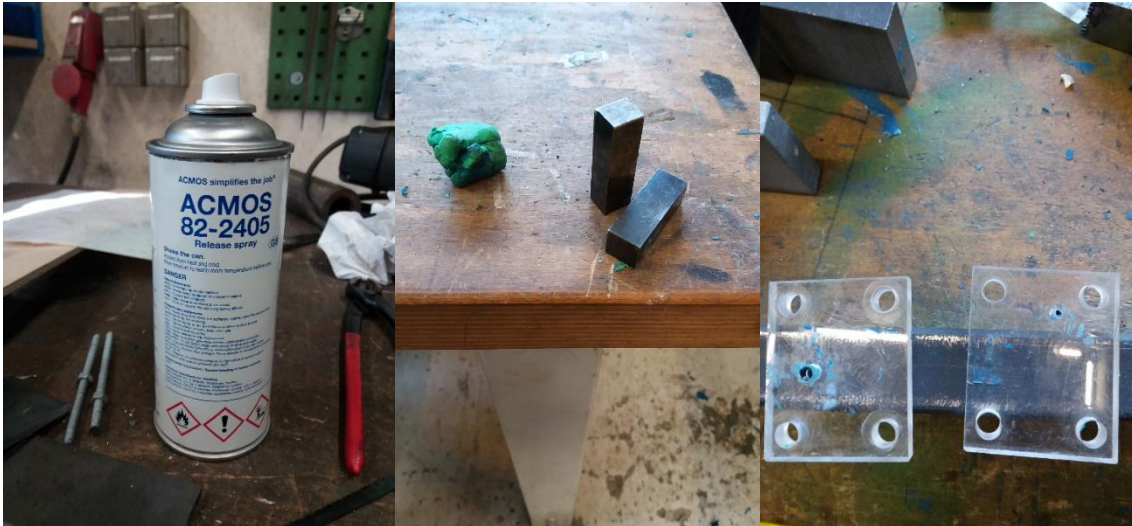


Figure 3.13: Materials used for the assembly of specimens. From left to right: a) ACMOS 82-2405 release agent, b) Clay and small steel plates to facilitate assembly, c) Perspex glass plates with drilled holes for injection

The bolt threaded parts of specimens as mentioned in section 3.1.4 were cut from a M20 threaded rod (Figure 3.6), and then grinded (Figure 3.14) to remove possible sharp extensions remained from cutting, which may come in contact with steel plates and increase friction and hereby the stiffness of specimen.



Figure 3.14: Grinding of bolt threaded part

For the testing of the resin with cyclic loading, the plates must be placed in such a way that the bolt part is positioned at the most unfavourable position inside the hole which is the one that results in the greatest potential of connection slip. This guarantees that the maximal resin layer thickness is placed in the compressed side and depicted in Figure 3.15. Since the bolt threaded part is not tightened into the threaded part of load bearing pin and they are simply in contact, clay (Figure 3.13-b) was used to keep it in position so it will not slip before injection and to seal all the possible regions between upper and lower plate to prevent leakage of resin.

Moreover, when the bolt is fixed by the clay to the threaded part of loading pin, the lower plate and the upper plate must be positioned in such place, so that the most unfavourable position of the bolt part is achieved. This is done by small steel plates, two for each specimen type based on its hole diameter of lower plate. Therefore, according to Figure 3.5 3 different type of small steel plates were cutted with thicknesses of 15mm, 13mm, 11mm, to be used in specimens with hole diameters of D30, D26, and D22 respectively. One type of these steel plates is depicted in Figure 3.13-b, and during the assembly of specimens they were positioned between lower and upper plate prior to injection as depicted on Figure 3.17.

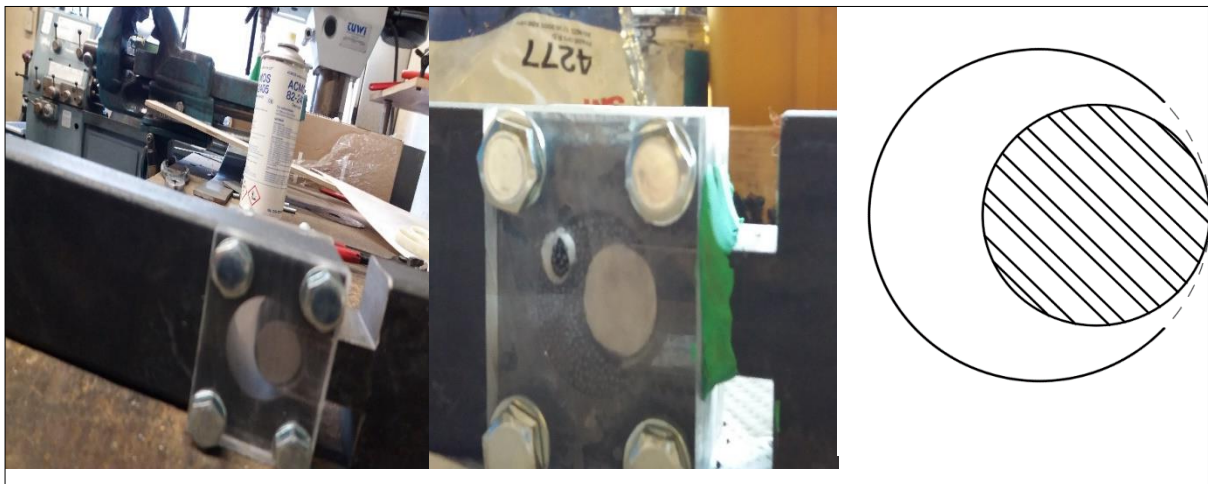


Figure 3.15: Bolt threaded part placed on the most unfavorable position inside the hole – a) in a specimen prior to injection with conventional resin, b) in a specimen prior to injection with steel reinforced resin, c) drawing of the most unfavorable position of bolt part in the hole

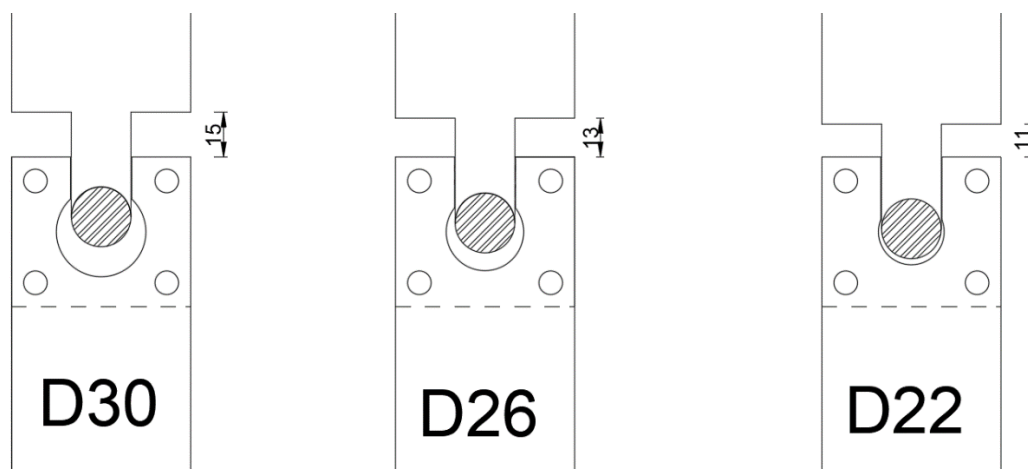


Figure 3.16: Desired distance between upper and lower plate to keep bolt part in most unfavorable position for the resin under testing

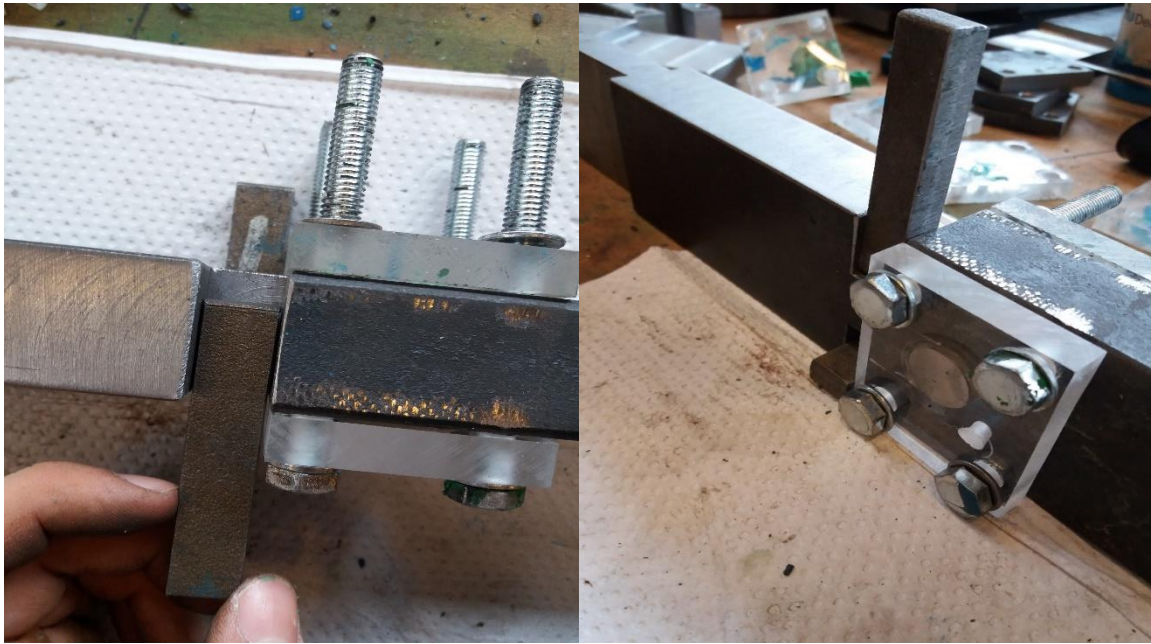


Figure 3.17: Positioning of small steel plates between upper plate and lower plate of specimens ready for injection to secure that the position of the bolt part will be the most unfavorable for the resin

Since there are 3 types of specimens in terms of geometry, after the positioning of the bolt in the worst position for the tested resin, the resin parts which will be created inside the clearance after injection will have 3 different sizes. This is becoming clear from the drawing in Figure 3.18. The resin layer has a max thickness and therefore a maximum slip potential of 10mm for D30 plate, 6mm for D26 plate and 2mm for D22 plate.

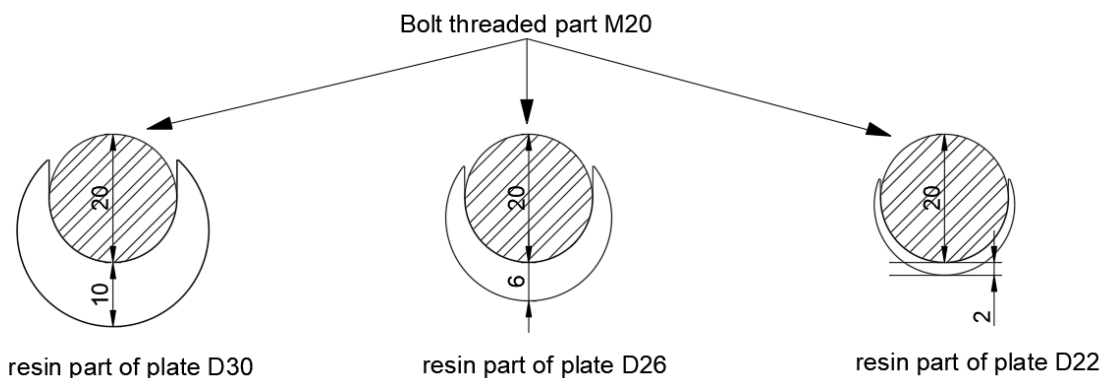


Figure 3.18: Maximum thickness of resin part for the three different geometry types of specimens

The next step of the assembly after ensuring that the plates will be kept in the desirable position to keep the bolt part in the most unfavourable position for the resin, is the injection of the specimens either with resin, or with steel reinforced resin. For this reason, Perspex glass plates were used to make sure visibly that the injection will be successful and not visible voids remain in the hole. The Perspex glass plates have the same geometry as the steel side

plates and after the successful injection and curing of the resin will be replaced by those. One Perspex glass plate with a drilled hole $\varnothing 5\text{mm}$ through which the resin will be injected, is placed in one side of the hole. A second Perspex glass plate with a drilled hole $\varnothing 1\text{mm}$ from which the air can escape during injection and resin will flow indicating that injection was successful, is placed on the other side of the hole Figure 3.19. The two side glass plates per are tightened to the lower steel plate by rotating the nuts of M8 Hex bolts such that any possible voids between glass and steel will be sealed and resin could not escape between these interfaces.

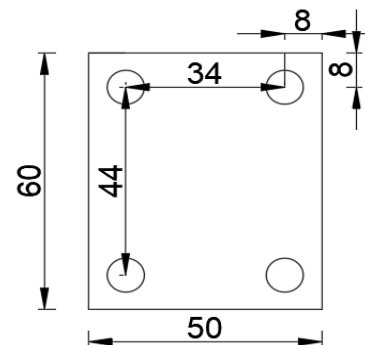


Figure 3.19: Specimen D30 ready for injection after the tightening of Perspex plates with drilled hole

In the case of specimens with resin injected bolted connections, the Perspex glass side plates serve also the filling of the hole with steel shot. Within the experiments conducted at the Stevin Laboratory, the shot-reinforcement was inserted into the free volume through the drilled hole $\varnothing 5\text{mm}$ on glass Perspex plate (note that diameter of steel shots is 1mm) by using a small funnel and gravity, as indicated in Figure 3.20. The steel shots within the clearance were compacted by vibrating them manually using a steel nail which was able to be inserted through the drilled hole and more shot is added until the specimen is completely filled. This method of vibrating was chosen instead of hammering, so there is no danger to destroy the specimen by relatively move the upper and lower plate which should be in a certain distance depending on the desired hole clearance as explained above.



Figure 3.20: Insertion of steel shot reinforcement (left) in the hole through glass plate using funnel

Subsequently, after the assembly as described above, the specimens were ready to be injected with the resin RenGel SW 404 + HY 5159. The resin and the hardener were mixed (Figure 3.21) in ratio 8:1 with the help of a scientific scale and a mixing paddle. According to A. Koper [1] two-component resin systems can suffer from defects in case of inhomogeneous mixing, i.e. incorrect mixing ratio, or in case hardener is not uniformly distributed throughout mixture. These cases can result in a wide scatter of performance locally and introduce stress peaks in the resin. Therefore, special care was given to the proper mixing of the resin and the catalyst in order the latter will be spread uniformly inside the mass of resin. When the resin and the hardener are mixed, they are put in a plastic caulk tube. Then the mixture is injected horizontally through the hole in the Perspex plate with the use of a hand-operated caulking gun as depicted in Figure 3.22



Figure 3.21: Mixing of resin SW404 and catalyst HY 5159 in ratio 8:1 using a scale and a mixing paddle

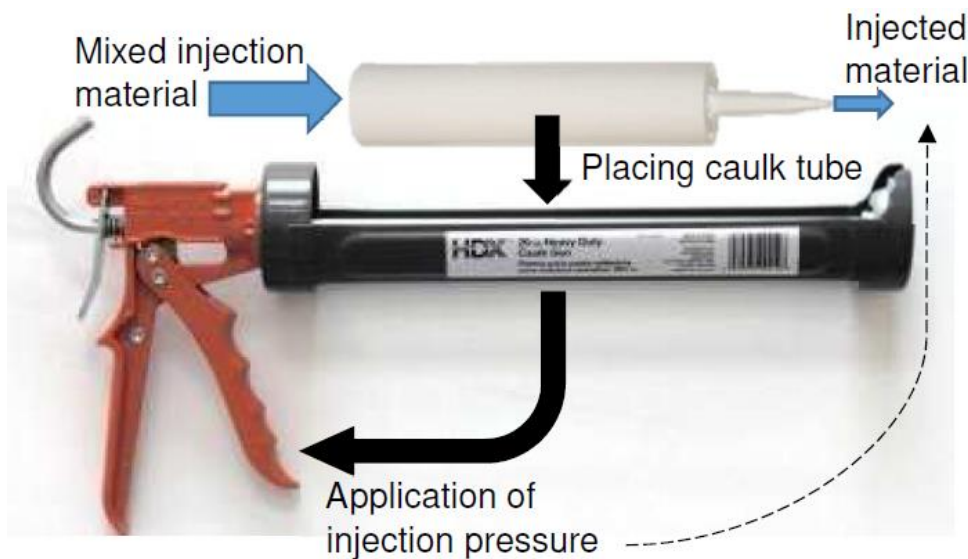


Figure 3.22: Hand-operated caulking gun with a caulk tube containing the mixed injection material [5]

The injection is completed when the resin comes out from the escape hole $\varnothing 1\text{mm}$ on the Perspex side plate. According to Nijgh [5] generally, it can be stated that there must be an air escape path/channel at each highest point bounded by horizontal restraints, as illustrated in Figure 3.23. That's why special care was given that the escape hole in the Perspex plate on one side, will be drilled in a higher position than the insertion hole of the other side plate as it is visible in Figure 3.19

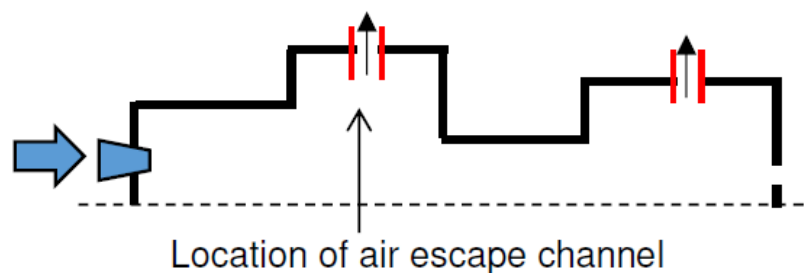


Figure 3.23: Air escape channels positioned such to prevent air inclusions within the volume that is injected for horizontal injection [5]

After the injection, the specimens were left for one day which is the curing time of resin before the remove of glass Perspex plates. Although according to the manufacturer the resin is completely cured after 24 hours, research on the resin that conducted in TU Delft have shown that the strength and stiffness are developed after 3-4 hours as mentioned before. After the removal of the glass plates the specimens were visibly tested for possible surface defects of the resin part. In the case of visible hole defects mixed resin was added to cover them (Figure 3.24) and they left for one more day for curing, before the positioning of the steel side plates and therefore the completion of assembly.



Figure 3.24: Repair of visible defects of resin part in injected specimens

Finally, any possible extensions of the resin part were removed with trimming tool in order to ensure that the external surface is as smooth as possible (Figure 3.25).

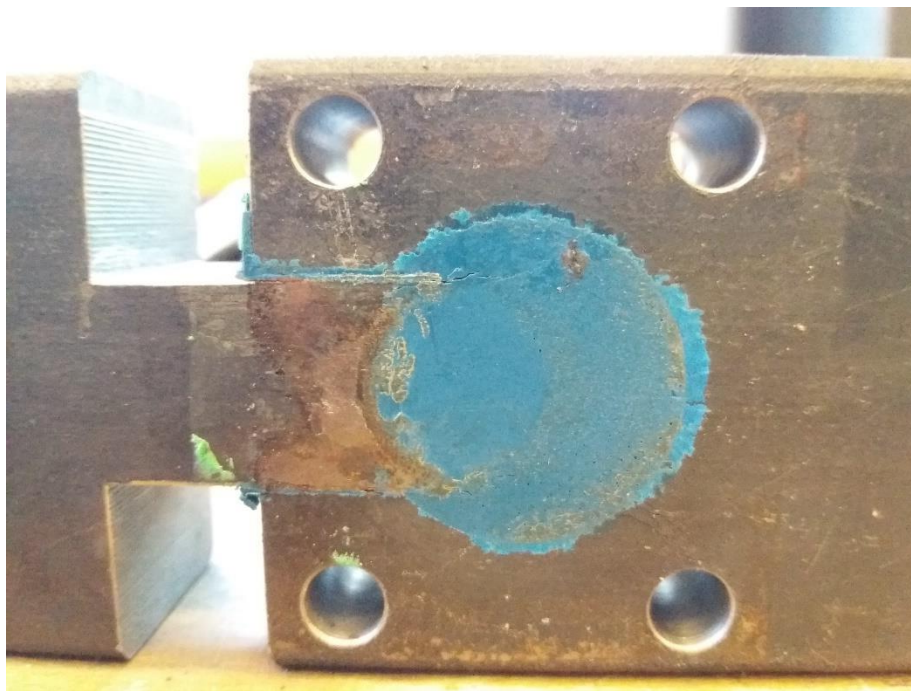


Figure 3.25: Injected specimen before the positioning of side plates

One of the most important considerations of this tailor made testing specimen used in current study, is the friction of the different components of the specimens which may increase the connection stiffness and hereby complicates the investigation of stiffness deterioration of resin due to cyclic loading. For this reason, all surfaces that may come in contact during loading are smoothed and sprayed with wax to reduce friction coefficient. Special attention was given to the friction between the side steel plates and the upper plate with loading pin. Since the lower plate with the tightened steel side plates are fixed in position by machine wedges and the upper part with the load bearing pin is vibrated creating the cyclic stresses in the resin part,

the only surfaces with hard steel to steel contact are between the side plates and the load pin extension of upper plate. In Figure 3.26 a 3D cut visualization of the steel to steel friction surfaces between upper plate and side plates can be seen. Preliminary tests were carried out to investigate, at least visibly the effects of friction to the steel plates since there are not similar studies to compare the effects on stiffness. As it is illustrated in Figure 3.27 there were visible effects of friction on side steel plates from the steel to steel contact. For this reason, Teflon sheets (Figure 3.28) were placed between friction surfaces to reduce as much as possible the effects of friction during cyclic loading.

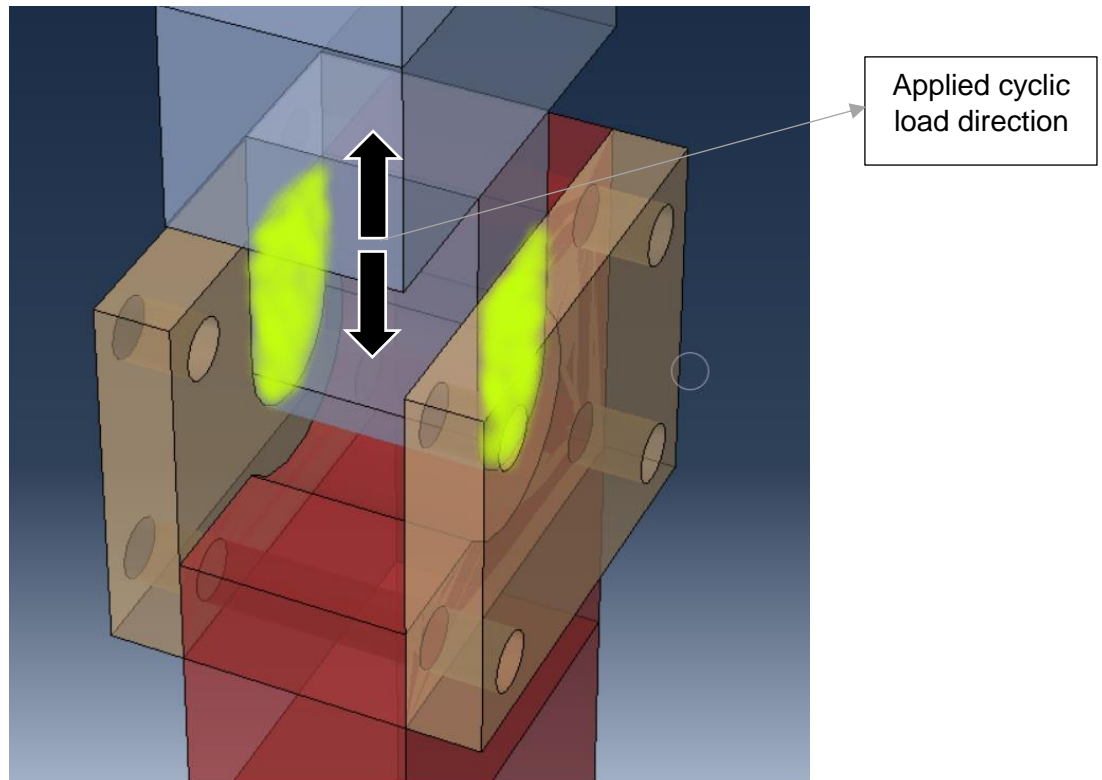


Figure 3.26: Visualization of contact friction surfaces (in yellow) between steel plates during loading



Figure 3.27: Visible effects of friction in surface of side plates after preliminary experiments



Figure 3.28: Teflon sheets placed in the expected friction surfaces (right after the dismantling of specimen, left at a specimen assembled and ready for testing)

Following the above described assembly process, the specimens were ready for testing (Figure 3.29). A designation system created and for every specimen according to geometry of hole, the type of resin and the applied stress range, therefore a different unique name was given to each specimen. Sticker labels with the name were used for each specimen to facilitate the identification and processing of results.

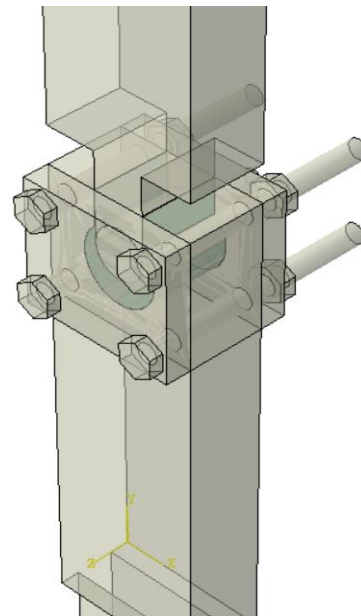


Figure 3.29: Assembled specimens with the sticker indicating their designation ready for testing (Left). Visualization of assembled specimen in Abaqus (Right). In green colour the resin part can be seen

3.4 Test Set-up

For the testing of the experiments the Hydraulic Wedge Grip machine of TU Delft Stevin Laboratory was used (Figure 3.30). The specimens were positioned vertically, such the lower plate with the hole gripped by the lower wedges and the upper plate with the load pin, gripped by the upper wedges. The extension parts of upper and lower plate are clamped between the wedges over the full length of the extended part (Figure 3.30).



Figure 3.30: Hydraulic Wedge Grip Machine (Left-Upper wedge gripping upper plate of specimen, Right- Lower Wedge gripping lower fatigue plate of specimen)

In each specimen 2 LVDTs (Linear Variable Displacement Transducers) were positioned at each side of specimen, measuring the vertical slip between the upper and the lower plate. Slip is defined as the relative displacement between the upper (male) and lower (female) loading plates in the direction of the load. The slip of specimen was taken as the mean of two displacements measured by LVDT's. The stands for the LVDTs were glued to steel at the 2 sides and the sensors were positioned at place as depicted in Figure 3.31.

For the fatigue test programme of current study, the consideration of several parameters was needed. Each of these parameters can affect test results:

- Loading pattern
- Stress ratio
- Stress Range
- Cyclic Loading Frequency
- Control Mode of machine
- Test Temperature
- Failure Criterion

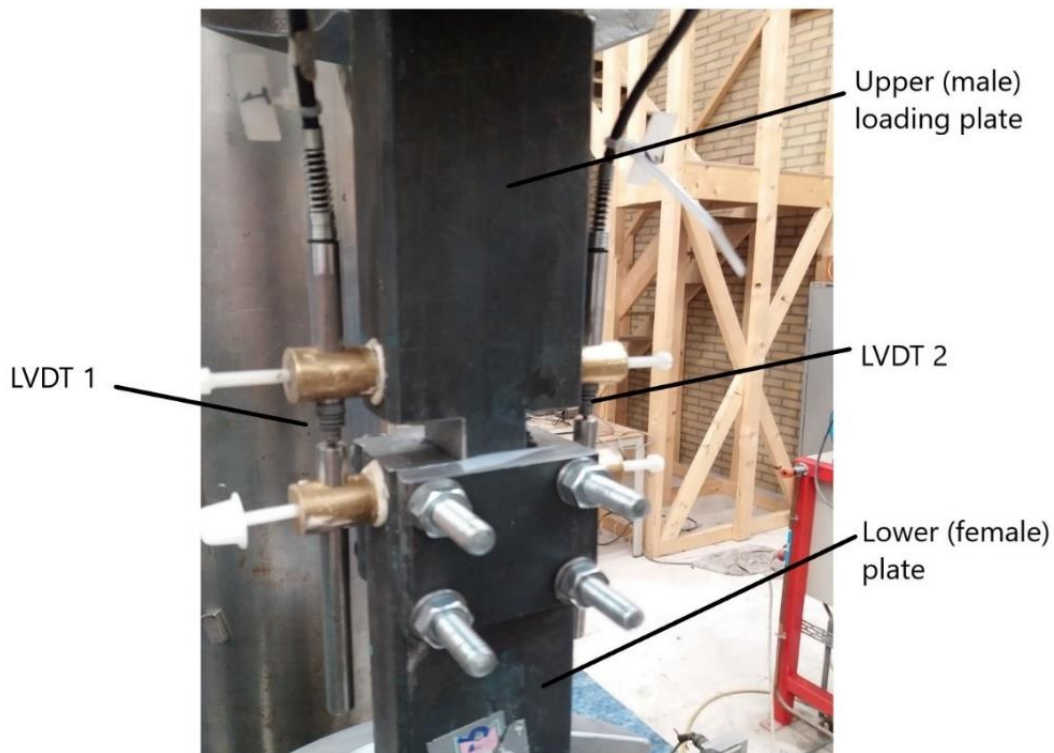


Figure 3.31: Specimen on testing machine with 2 LVDTs at each side measuring the vertical slip between upper and lower plate

3.4.1 Loading pattern

Most experimental data on fatigue testing of injection bolts and in general in fatigue problems, are with constant amplitude loading as reported in literature review in section **Error! Reference source not found.** Therefore, a constant amplitude is chosen for current study. Since the cyclic load is kept constant, the slip will continually increase after first damage initiation which in the case of resin will be the degradation of stiffness at each cycle.

This special test set up allows testing of the resin under cyclic loads, without the risk of fatigue cracks of the bolt and steel parts itself. This is achieved since the upper and the lower plate are not in direct contact, nor fixed together, and the load induced from wedges of machine is transferred from the upper plate to the lower plate of specimen, through the resin part under investigation, and from there to the supports meaning to the grips of the machine. Therefore, only compressive loads can be applied to the specimen, since with the application of tensile load the upper plate will be separated from the lower destroying the specimen. Therefore, the cyclic loading pattern is a constant amplitude sinusoidal history of compression-compression with stress ratio $R_\sigma = \sigma_{\min} / \sigma_{\max}$ as depicted in Figure 3.32

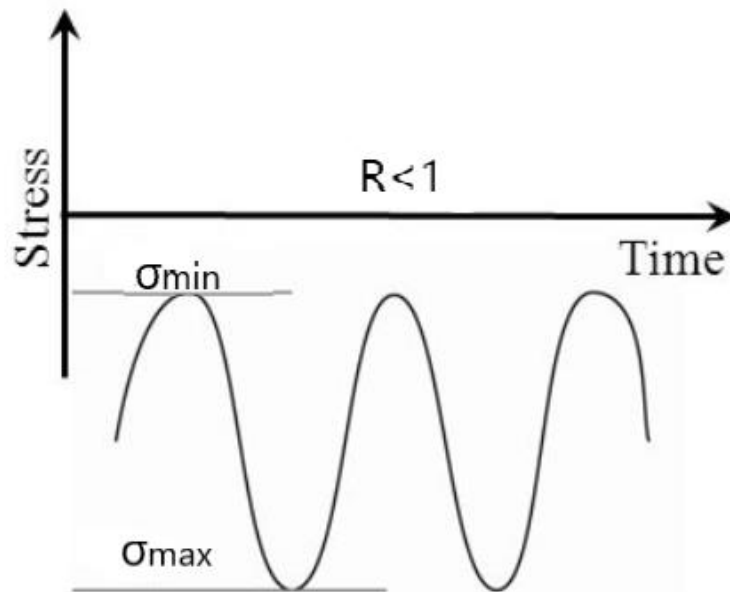


Figure 3.32: Constant amplitude compression-compression sinusoidal loading history chosen for the experiments

3.4.2 Control Mode of machine

The machine is selected to transfer the load to specimen with force control setting of function generator since it is a fatigue test program and it is essential to control the applied stress range, instead of displacement control option which is used mostly in static tests until failure in order to depict the failure in force-displacement diagram. In general fatigue tests are conducted with both methods and with the force-controlled method material failure is observed after fewer cycles. Since load is kept constant, deformation will increase continuously after damage initiation, but this is the case in steel and other metallic details where fatigue crack is expected and this is not the case for epoxy resins as in the present test specimen.

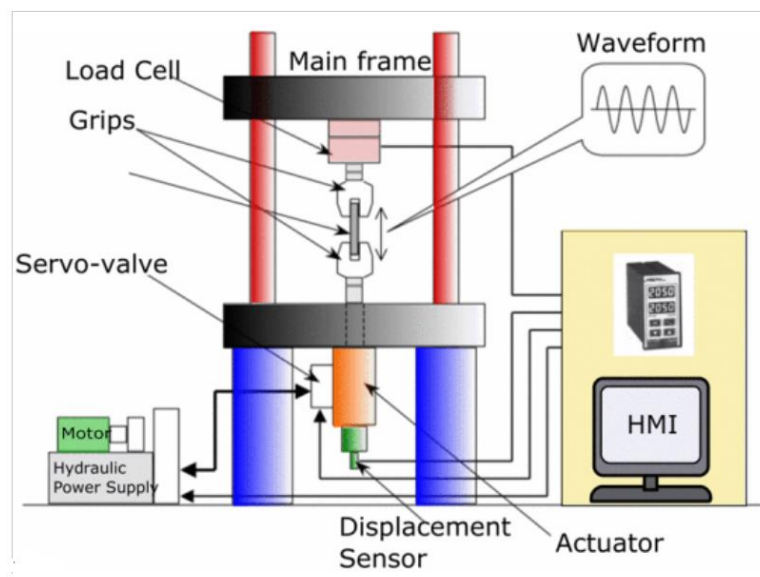


Figure 3.33: Machine operation for fatigue test

3.4.3 Stress Ratio

In most of the fatigue experiments in literature for the fatigue behaviour of resin injected bolted double or single lap connections the stress ratio was either $R=0$ or $R=0.1$ and more details can be found in section 2.6.2. The same stress ratios were used for fatigue testing of epoxy resins alone. In the present experimental program, the stress ratio of $R=0.1$ is qualified since is common in literature. Stress ratio $R=0$ is rejected since in case minimum stress is $\sigma_{\min} = 0$ therefore the minimum load transferred through force control machine setting is 0 kN, so a possible short malfunction of function generator may result in positive tensile loads which will destroy the specimen.

3.4.4 Cyclic Loading Frequency and Temperature

It has been already reported (2.6.1), the fatigue mechanisms of polymer materials are complex because of their molecular structure, hysteresis heating and viscoelastic response, as well as their temperature and environmental sensitivity. It has been reported that the fatigue mechanism of polymers is controlled by the internal damping of materials and the failure occurs with a sharp temperature increase (L. J. Broutman and S. K. Gaggar [43]).

During the fatigue testing of polymers, a temperature rise has been observed in the surface which is attributed to the hysteresis loss of the material. For polymers like epoxy resins this hysteresis loss is not sensitive to ambient temperature as in the case of polyesters, and this results in more uniform hysteresis heating during each cycle [43].

The temperature rise of specimen influences the fatigue life by lowering the ultimate strength and stiffness of resin material. Therefore, there is a clear effect of cyclic frequency to the fatigue life of polymers which is clearer in case of polyesters than epoxy according to Broutman. A cyclic frequency much less than 10 Hz is common when applying fatigue loading in polymers because the testing machine grips otherwise must accommodate high amplitude in movement and viscoelasticity hysteresis can cause heat energy and temperature build up must be avoided. *The American standard ASTM-D7791-12 [51] which has regulations for fatigue tests in structural resins, proposes a test frequency of 1-125 Hz but strongly recommends the use of $f=5\text{Hz}$ or lower.*

Subsequently a cyclic frequency of $f=5\text{Hz}$ is chosen for the fatigue tests of present study. The test temperature was chosen to be the ambient temperature of the Laboratory.

3.4.5 Failure Criterion

For the determination of a failure criterion in terms of number of cycles, considerations of time limitations and conducting of preliminary testing, where the number of cycles after which the connection slip increase stops, needed before the start of experimental program. With the novel test set-up under consideration, there is no possibility of failure of steel plates or bolt part, and additionally the resin would be loaded in compressive cyclic loads, therefore failure in the resin part in the form of a mayor crack which may lead to a structural failure is not expected.

As already reported in section **Error! Reference source not found.** failure can be defined as structural failure of specimen which cannot occur in this case, or some predefined criterion such as certain crack size or certain displacement or slip based on the materials and testing conditions.

This would be the case here, and the failure of specimens will be defined as a certain amount of slip, and the number of cycles until a specimen reaches this slip, will be the N_f cycles to failure.

As it is mentioned in research of B. Zafari et al.[53], fatigue performance of Resin Injected Bolted Connections should be determined against a long-term bearing resistance that is relevant at the end of structure's design working life. In Annex G of EN 1090-2 [3] it is stated that creep displacement caused during the design life of the structure taken as 50 years will not exceed 0.3mm. Therefore, this slip criterion of 0.3mm is adopted in this Thesis. The data points that will be obtained from fatigue tests would include the applied stress range $\Delta\sigma$ of each specimen in y-axis, and number of cycles to failure N_f which needed to reach this slip failure criterion in x-axis. This can be observed in Figure 3.34 where the diagram of slip vs number of cycles of specimen D26R135-2 is depicted. The failure criterion of 0.3mm is reached after 3569 cycles therefore the data point of this specimen to be used in statistical evaluation for defining S-N curve will be (135Mpa, 3569 cycles). In chapter 6 where a statistical evaluation of the results is presented, a second failure criterion of 0.25mm slip will be also adopted for comparison purposes.

The fatigue tests were run until the considered as failure criterion slip of 0.3mm was reached. Initially has been decided that the tests would run until approx. 500.000 cycles which is one day of testing with frequency of $f=5\text{Hz}$ but later during the research the criterion of 0.3mm slip was adopted. Fortunately, most of specimens had reached 0.3mm slip before 450.000. For the stiffest specimens such as D26SR-90 series which barely reached a slip of 0.1-0.15mm the testing repeated until at least 1.000.000 before they were considered as run-outs. During holidays some specimens tested for several days offering results for high cycle fatigue of specimens at $N=4 \times 10^6$ and $N=6 \times 10^6$ cycles.

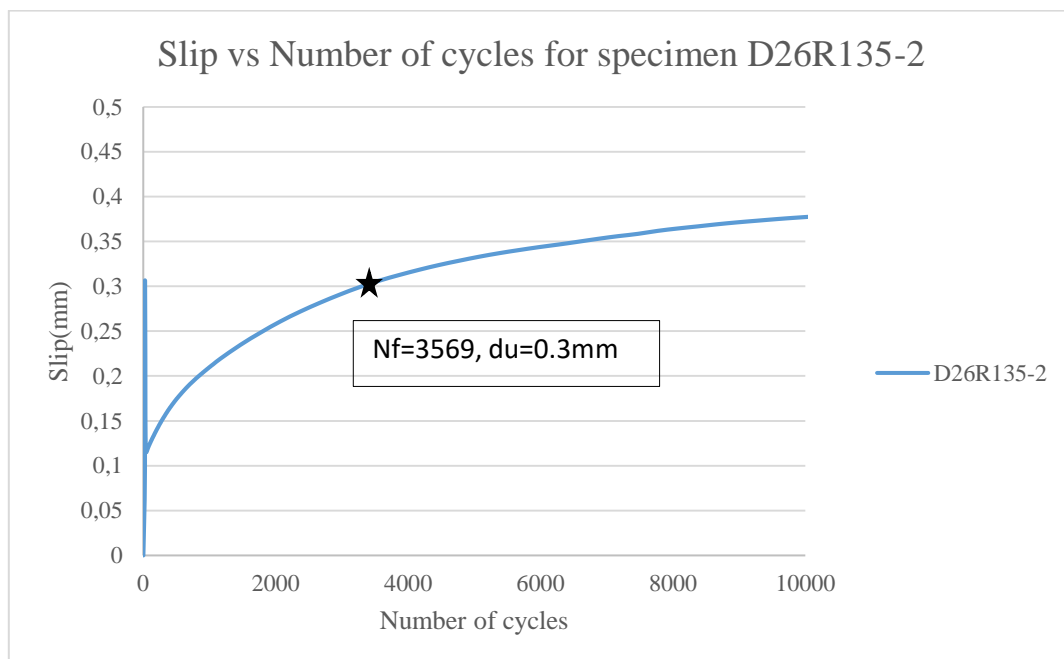


Figure 3.34: Slip accumulation of specimen D26R125-2 with the number of cycles to reach failure criterion indicated

3.4.6 Stress Range

For the present experimental study, the specimens were tested in 3 different bearing stress ranges. The equivalent bearing stress is often used as an indicator for the maximum long-term load that can be transferred through the resin without excessive connection slip. According to research on injected bolted connections as mentioned in chapter 2, it was observed that the long duration bearing stress resistance of this resin can be taken as $f_{b, resin} = 200\text{MPa}$. Therefore, it was chosen that the maximum stress range will be 180MPa for the 1st testing series of resin and steel reinforced resin specimens. For the 2nd testing series a stress range of 135 MPa was chosen which is 3/4 of the 1st stress range. The 3rd stress range was 90 MPa which is 1/2 of maximum bearing stress range. It should be noted that due to the preliminary nature of this research under consideration, the 2nd and 3rd stress ranges were finalized as the testing progressed.

$$\sigma_b = \frac{F_b}{d_b \cdot t_p}$$

(Equation 3.1)

σ_b Equivalent bearing stress [F/L²]

d_b Bolt diameter [L]

F_b External Load [F]

t_p Thickness of the plate [L]

For all specimen types independently of the diameter of the hole the:

- $t_p=30\text{mm}$
- $d_b=20\text{mm}$

With known specimen's geometry and a stress ratio defined as $R=0.1$ and a stress range defined as 180, 135 and 90MPa therefore $\sigma_{\max}=200\text{MPa}$ and $\sigma_{\min}=20\text{MPa}$ for the 1st, $\sigma_{\max}=150\text{MPa}$ and $\sigma_{\min}=15\text{MPa}$ for the 2nd and $\sigma_{\max}=100\text{MPa}$ and $\sigma_{\min}=10\text{MPa}$ for the 3rd the maximum and minimum force F_{\max} and F_{\min} applied by the machine could be calculated (Table 3.5).

Bearing Stress Range (MPa)	Fmax (kN)	Fmin (kN)	$\sigma_{b,\max}$ (MPa)	$\sigma_{b,\min}$ (MPa)
180	120	12	200	20
135	90	9	150	15
90	60	6	100	10

Table 3.5: Maximum and minimum applied forces of the sinusoidal loading history

3.4.7 Specimen Designation

Since there are three different geometry types in terms of diameter of hole, 2 different resin types tested i.e. the conventional and the steel reinforced resin and 3 different stress ranges, a special designation system was used. The name of each specimen consisted of 4 parts.

The first part has always the letter D followed by the number 30, 26 or 22 indicating the diameter of the hole. The second part refers to the type of resin and is consisted of the letter

R for conventional resin and the letters SR for steel reinforced resin. The third part refers to the stress range and therefore is consisted by the numbers 180,135 and 90 indicating that the applied stress range was $\Delta\sigma=180\text{MPa}$, $\Delta\sigma=135\text{Mpa}$ and $\Delta\sigma=90\text{MPa}$ respectively.

Finally, the last part refers to the number of checked specimens with the same geometry, resin type and stress range. The designation system is shown in Table 3.6.

Geometry of Hole	Type of Resin		Stress range (Mpa)			Number of specimens
	R	SR	180	135	90	
D30	R	SR	180	135	90	1-2-3-4-5-6 etc.
D26	R	SR	180	135	90	1-2-3-4-5-6 etc.
D22	R	SR	180	135	90	1-2-3-4-5-6 etc.

Table 3.6: Designation system of specimens

For example, the specimen with name D30R180-1 is the first specimen tested with lower plate of diameter D30 injected with conventional resin in a stress range of 180 MPa while the specimen with name D26SR90-4 is the fourth specimen tested with lower plate of diameter D22, injected with steel reinforced resin in a stress range of 90 MPa.

3.4.8 Loading phases of specimens

Each specimen is loaded in 2 different loading phases. The first phase is a quasi-static phase with very slow frequency which is 100 times lower than the cyclic frequency chosen for the fatigue test. Therefore, the specimens were loaded for the first 25 cycles with $f=0.05$ Hz in the same stress range as the fatigue testing which follows. This quasi-static phase allows to calculate the Initial Stiffness of the specimen since the LVDTs were measuring every second the slip vs the applied force hence a Force-Displacement hysteresis diagram was able to be plotted like the one in Figure 3.35. The slip is calculated as the average slip of the 2 LVDT measurements as already mentioned.

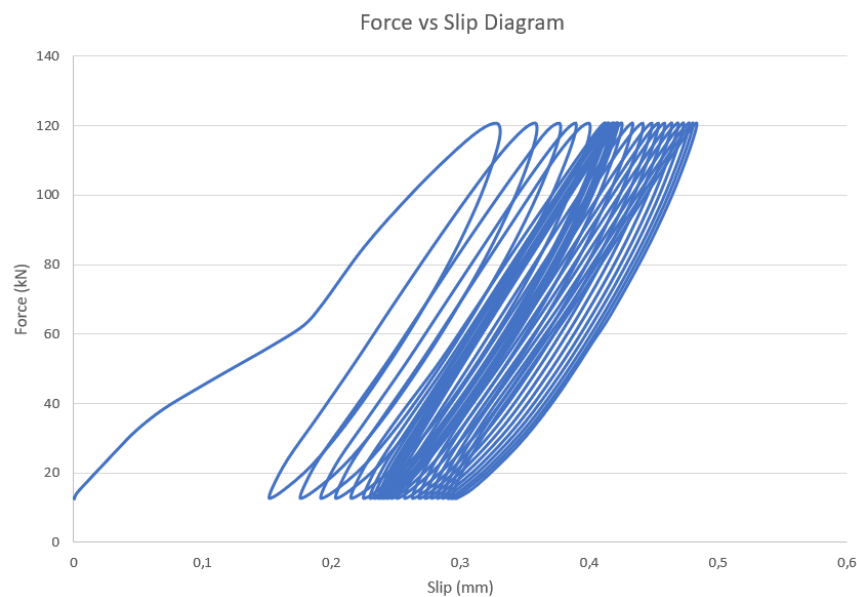


Figure 3.35: Force vs Slip diagram of specimen after the quasi-static loading phase

It can be seen from the diagram that in the first loading cycle the stiffness during the loading phase is not stable but deviates. This can be explained by the internal setting of the specimen

under the load application where all the surfaces set in contact and transfer the stresses. Therefore, for the calculation of initial stiffness this part of the diagram is neglected, and the initial stiffness is measured as the angle of the straight line during the loading phase of 2nd circle. The hole diagram is shifted to the left to start from zero slip (Figure 3.36). Initial stiffness was extracted from the same stress part between 30-60 Mpa (18-36 kN) for most of specimens or a relevant range if it was not possible to extracted from the mentioned one.

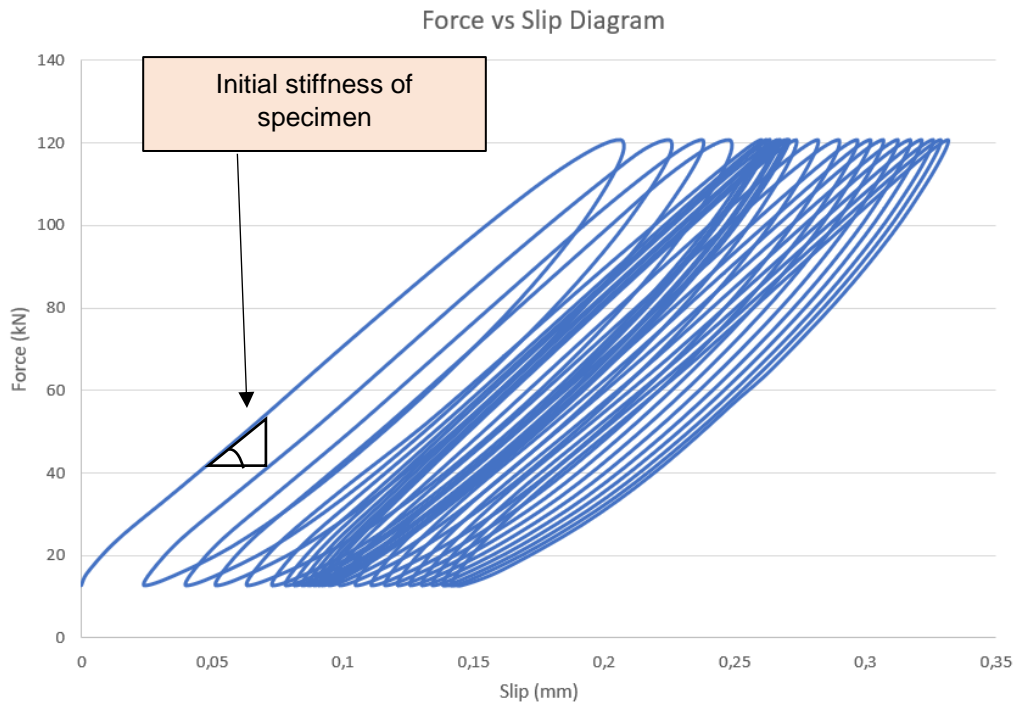


Figure 3.36: Calculation of initial stiffness (kN/mm) of specimen from Force-Slip diagram of quasi static loading phase after the remove of 1st <<setting>> circle

After the end of quasi-static loading phase of specimen, the machine is stopped. The LVDTs are reset to zero offsets to measure the slip due to fatigue loading between upper and lower plate for the second fatigue loading phase. The function generator starts again applying the cyclic stress range but with the selected cyclic frequency of $f=5\text{Hz}$. For the first 1000 circles LVDTs measure every second to capture the fatigue behaviour of resin at the beginning and after that every minute. Since the frequency of 5 Hz means 5 cycles/sec which is quite high for measuring, the LVDTs and the machine provide for each measuring point in time, an average and a range value within the sinusoidal history. From these, the maximum and the minimum value of slip and force for every circle are calculated as following and used for the processing of the results presented in Chapter 5.

- $$\max_{value}(slip, force) = average_{value}(slip, force) + \frac{range_{value}(slip, force)}{2}$$
- $$\max_{value}(slip, force) = average_{value}(slip, force) + \frac{range_{value}(slip, force)}{2}$$

3.5 Summary of experimental procedure

- A tailor made, non-standardized test set-up was used to investigate the fatigue behavior of conventional (R) resin SW404/HY2404 and of steel reinforced resin (SR) without endanger the failure of steel plates or bolt.
- A threaded part of M20 bolt without head or nut was used to simulate the bolt inside a hole of an IBC shear connection.
- Three different geometries in terms of the diameter of the hole were designed (D30, D26, D22). Due to difficulties in injection of the specimens with normal hole and time limitations only the specimens with oversized holes were tested experimentally.
- Wax spray release agent used to allow demountability and reusability of specimen parts, and Teflon sheets were used to reduce as possible friction between the steel plates, in order to have representative results of slip due to deterioration of resin part.
- Two loading phases were applied to specimens. A quasi-static load in 25 cycles with very slow frequency to calculate the initial stiffness of connection and a cyclic sinusoidal compression-compression load with $f=5\text{Hz}$ and $R=0.1$ with testing machine in load control mode.
- A failure criterion was defined at 0.3mm of slip measured as the mean slip between upper and lower steel plates from 2 LVDT's. The specimens which didn't reach this criterion were considered as run-outs after 1million cycles.
- Three different stress ranges were used in the relevant S-N region according to the recommendations of DNVGL for new types of tested details, such as a representative slope could be determined. The selected bearing stress ranges to the resin were 180, 135 and 90 MPa.

4 Numerical Analysis

In order to investigate the fatigue behaviour of resin (conventional and SR) the tailor made test set-up described in section 3.1 used for fatigue tests. When using a non-standardized test specimen, it is important that set-up is verified and compared to standard tests. The description of the finite element models, for the calculation of the initial static stiffness of the specimens and the stress state of the members of setup for comparison with standards, is presented in this section. In total 6 different models (3 geometry types x 2 resin types) were analysed using the software Abaqus/CAE 6.14-5. The geometry, the properties, the boundary conditions, the meshing, the loading steps and the results of the analysis of the models are presented below.

4.1 Model Description

4.1.1 Geometry, material properties and assembly

The FEA models consisted from the same parts as the real specimens but simplification adopted to reduce computational time. Therefore, the upper and lower plate were not fully designed, considering that the extensions for the grip of plates by wedges only transfer the loads to the main body of the steel plates and the stress distribution is uniform to the body of steel plates until the zone with the hole. More specific in reality the main body of lower plate (female) without the extension has a length of 180mm, while the main body of upper plate (male) without the extension has a length of 120mm. In the geometry of the model only a part of 120mm for lower plate and a part of 80mm for the upper plate was designed (Figure 4.1).

Indeed, from an analysis of the full model it was confirmed that the stress distribution at the maximum experimental force (120 kN), is uniform after a zone of 20mm below and under the change of geometry in upper and lower plate respectfully (Figure 4.2). Therefore, the simplification in geometry will not affect the results. Moreover, the bolt part designed without the threads, as a solid cylinder of diameter 20mm. This potentially affects the results and should be investigated in future research. Finally, the M8 bolts were designed also without the threads since the 4 holes inside steel plates have no threads and they are simply in contact with the hole surfaces, but this is assumed to have marginal effect in the results since in reality, the M8 bolts not contribute to transferring mechanism of stresses to the resin part but they only ensure the confinement of resin by tightening the side plates.

An elastic-plastic stress strain material model (see ANNEX A) with a yield strength of 355 MPa was adopted for the steel plates (upper, lower, side), while the M20 bolt part, M8 bolt and nuts were considered only as linear elastic since it is considered that with the proposed stress set-up the stresses in these parts will not reach the plastic region therefore a linear elastic model with young modulus of elasticity $E=210000$ MPa and Poisson ratio $\nu=0.3$ and mass density of $\gamma=7.8 \times 10^6$ kg/mm³ according to material properties of steel (section 3.2.3) will be accurate. A non-linear material model was considered for the resin and steel reinforced resin with Drucker Prager and Drucker Prager hardening plastic criterion to simulate the resin damage and the cohesive surfaces reflecting the relationship between traction and displacement at the interfaces [9], with Young's modulus of elasticity $E=5640$ MPa and Poisson ratio $\nu=0.3$ and mass density of $\gamma=1.8 \times 10^6$ kg/mm³ as explained in section 3.2.1 for resin and a Young's modulus of elasticity $E=15200$ MPa and Poisson ratio $\nu=0.22$ and mass density of $\gamma=5.1 \times 10^6$ kg/mm³ as explained in section 3.2.2 for the steel reinforced resin

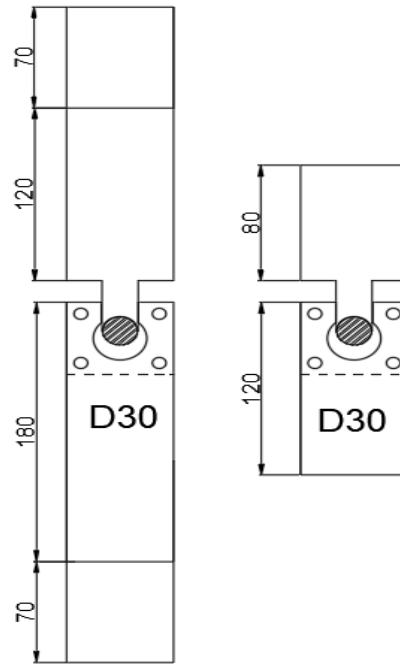


Figure 4.1: Left: Actual 2-D geometry of the specimen. Right: 2-D Geometry of specimen as designed for FEA Analysis

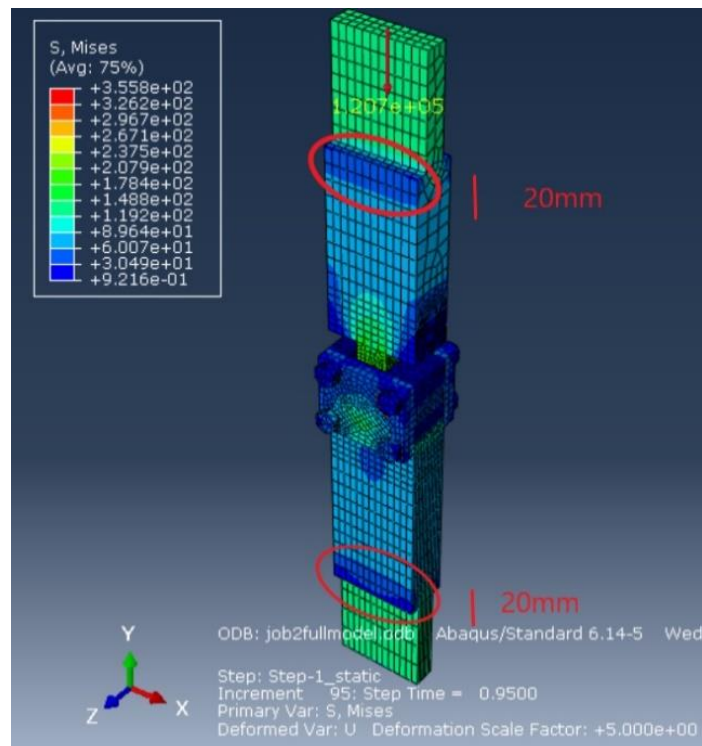
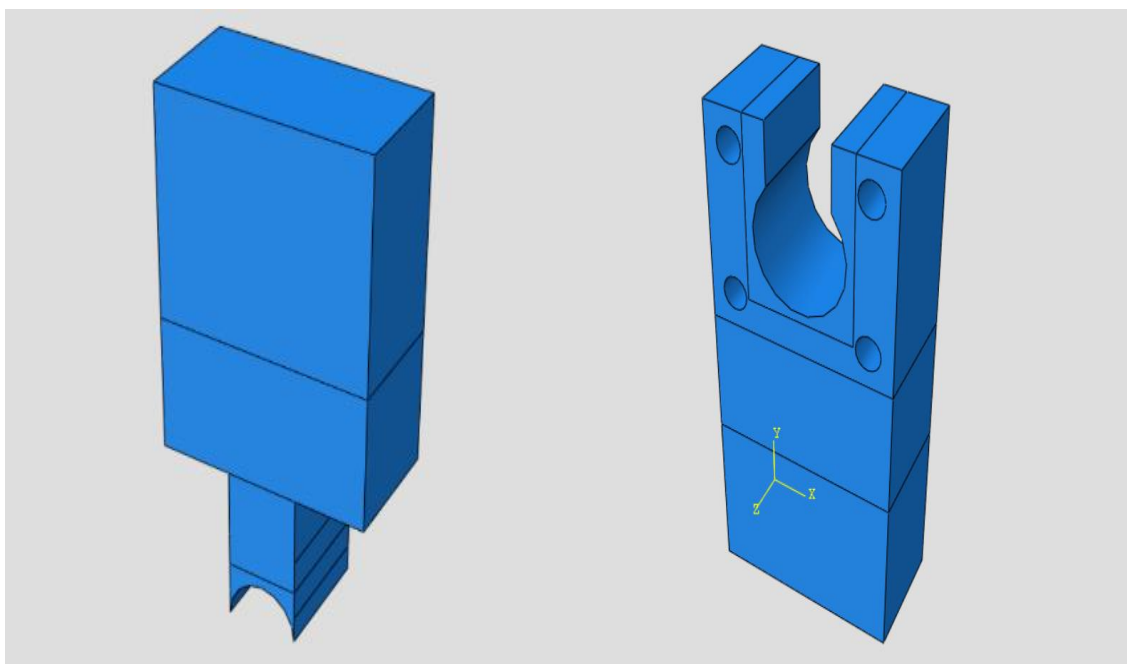


Figure 4.2: Uniform distribution of stresses after the change in geometry of upper and lower plate in full model after the application of maximum load of experiments

The following table lists all the geometrical simplifications made in the model to decrease computational time and facilitate the calculations, and the geometry of all the specimen's parts is depicted in Figure 4.3 and Figure 4.4.

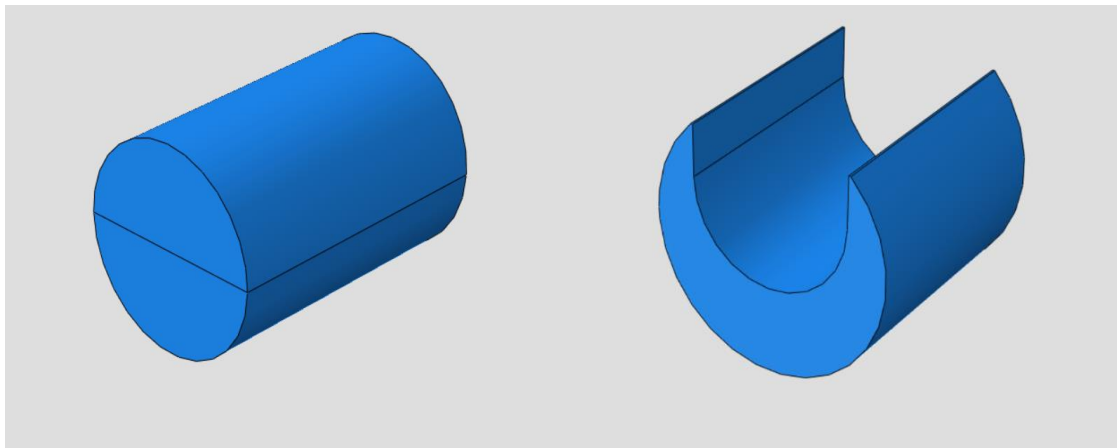
Component	Experimental geometry	Numerical simplified geometry
Bolt part	Part of M20 threaded rod	Bolt part without threads in contact with the cavity in upper plate
Upper (male) plate	With special threaded reception where the threads of plate fit and be in contact with the threads of M20 bolt part	Cavity of upper plate without threads, in contact with bolt part
M8 bolts	Nominal M8X80 Hex Bolts with threads	Shorter M8 bolts without threads
Injection material (resin and steel reinforced resin)	Injected through holes in the Perspex plates, may be voids and defects	Perfect without heterogeneities of inclusions

Table 4.1: Geometrical simplifications in numerical analysis



a) Upper plate (male)

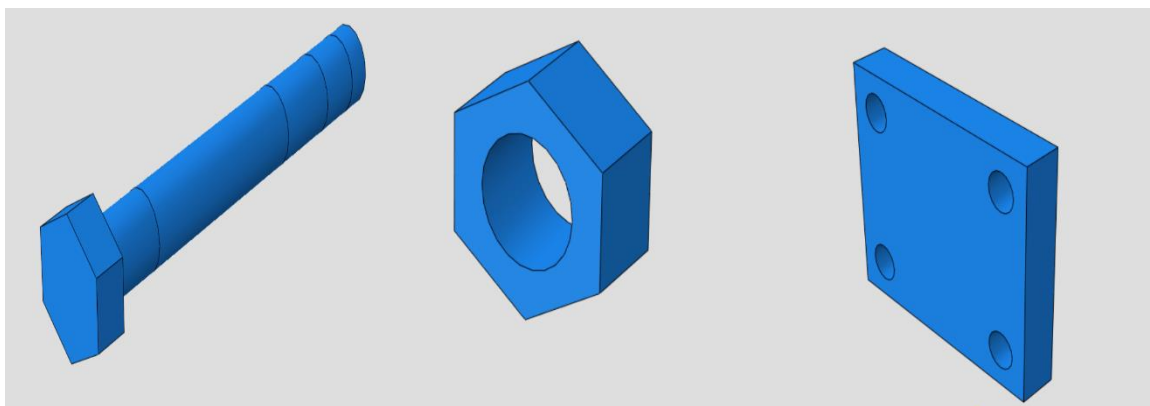
b) Lower plate (female)



c) M20 bolt part (pin)

d) Resin part

Figure 4.3: Geometry of primary components of specimen in Abaqus part module



a) M8 bolt

b) Nut

c) Side plate

Figure 4.4: Geometry of secondary components of specimen in Abaqus part module

4.1.2 Boundary conditions and interaction

After the assembly module of the Abaqus software where all parts assembled in the final specimen the boundary conditions and the interactions between parts are introduced. For the interaction between all contact surfaces the *General Contact (standard)* is chosen which creates interactions for all exterior faces and shell perimeter edges in the model. In Abaqus/Standard general contact can be defined only in the initial step, and this general contact definition is active for all subsequent steps. The Contact Domain is chosen *All with self* to specify contact (including self-contact) for all allowable element faces and model entities. This is the simplest way to define the contact domain according to Abaqus Manual [66]. To set different friction properties between the members where there is steel-steel (with or without presence of Teflon) and resin-steel contact, individual property assignments were defined.

For the contact properties of *General Contact* a *Normal Behavior* is chosen with the default “hard” contact relationship which minimizes the penetration of the slave surface into the master

surface at the constraint locations and does not allow the transfer of tensile stress across the interface. When surfaces are in contact, any contact pressure can be transmitted between them. The surfaces separate if the contact pressure reduces to zero. Separated surfaces come into contact when the clearance between them reduces to zero. For the contact properties a *Tangential Behavior* is also chosen with default settings.

For the surfaces where steel-steel contact occurs a friction coefficient of 0.2 was adopted while for the surfaces between the side plates and the lower plate where Teflon sheet is placed in reality a friction coefficient of 0.04 was used after calibration. For the surfaces where resin and steel come in contact a frictionless behavior was adopted. A release agent was applied at all surfaces which are in contact with the resin to prevent adhesive bonding and enable demounting. Hence, the resin does not adhesively bond with any component; therefore, interfaces with the resin are modelled with general contact interaction as well, since it is considered that the behavior between the resin and the steel which is sprayed with wax in reality is adhesion and not friction and confined conditions occur.

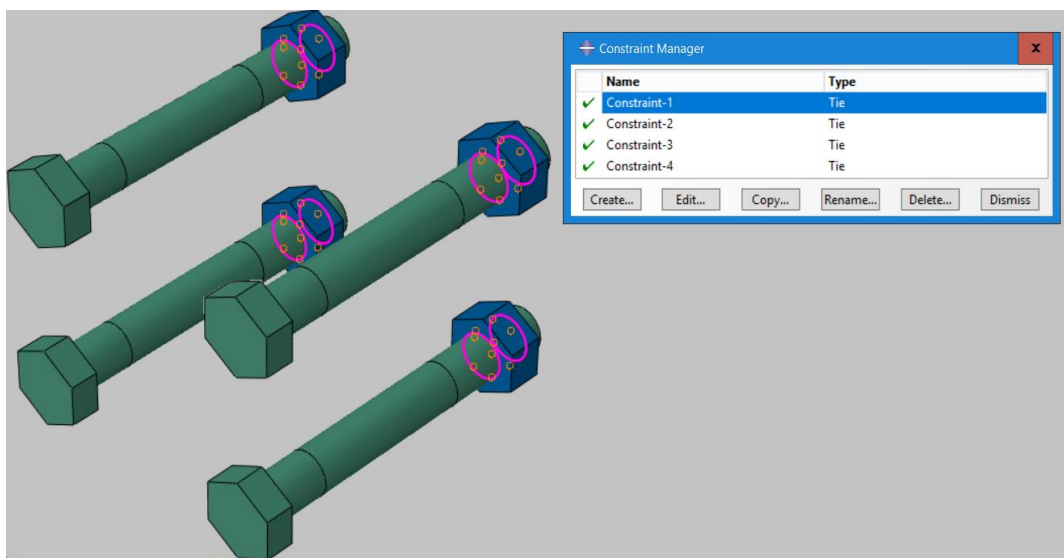


Figure 4.5: Tie constraint between nuts and M8 Bolts

A tie constraint ties two separate surfaces together so that there is no relative motion between them. Since the only surfaces which is not possible to separate due to threads is the region of the M8 Hex Bolts which is contact with the nuts and the internal surface of nuts a Tie Constraint is chosen only for these 4 interfaces in the model (Figure 4.5). To reduce the possibility of convergence issues in contact controls of model the automatic stabilization which introduces viscous damping to oppose incremental relative motion between surfaces, was activated.

Regarding the boundary conditions, the lower edge of lower plate considered to be fully fixed and all possible translations and rotations are restricted thus simulating the fixing of specimen by the wedges of machine.

The load is applied through forced displacement of the upper edge of upper plate. A prescribed displacement of 0.5mm in U2 direction (vertical) is applied on the Static Step of the Analysis in Abaqus/Standard..

4.1.3 Mesh of finite elements

Hexahedral solid brick 8-node elements with reduced integration (C3D8R) are generally used to mesh models because they lead to less computational run time. In this type of element, each node has 3 translational degrees of freedom (DOF) and prevents shear locking. In addition, the brick elements might give a solution of comparable accuracy at a better rate of convergence and less computational time needed than using some other elements. For this reason, all parts of the model were meshed using this kind of elements, except for the M8 bolts. Due to their complex geometry, tetrahedron elements (C3D4) were used for the M8 bolts only. The geometry of upper and lower plate was partitioned in 4 zones to separate different mesh areas.

Different mesh size was used for the parts in relation to their size and importance. The resin, the bolt part and the area around hole of the lower part were meshed with a finer mesh with element size 1.2mm because in these regions higher stresses are expected to occur. The M8 bolts the nuts and the side plates and the most distant zones from hole, were meshed with element size 9.6mm. The middle zones of upper and lower plates were meshed with element size of 2.4mm and 4.8mm. All the meshed parts are depicted in Figure 4.6, Figure 4.7 and Figure 4.7

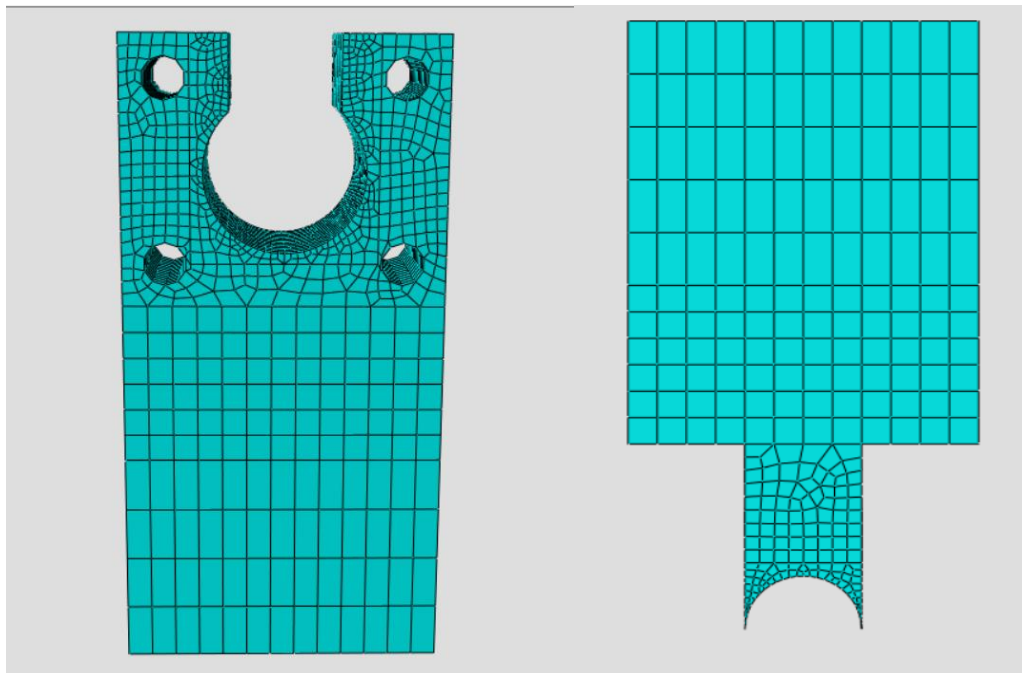


Figure 4.6: Meshed lower-female plate (left) and upper-male plate (right)

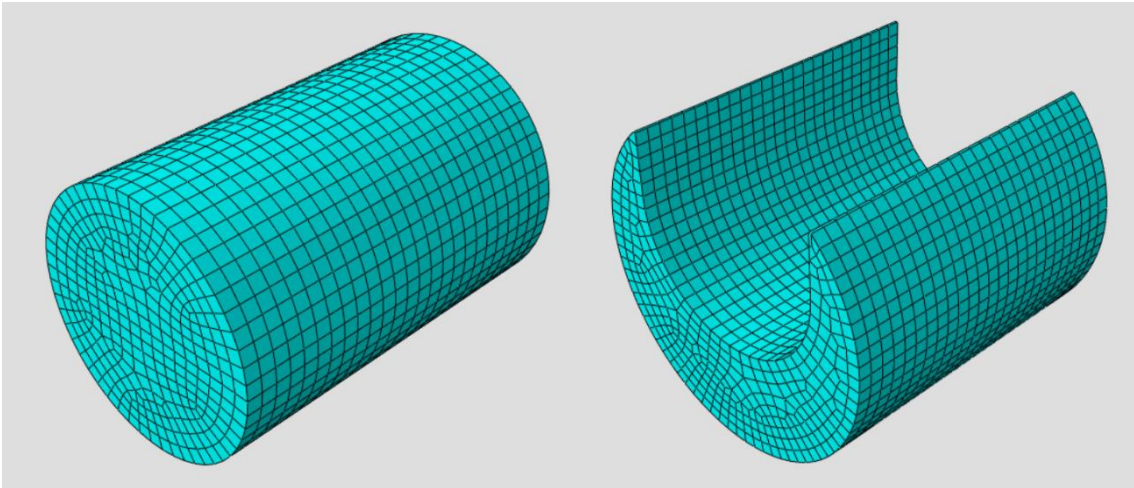


Figure 4.7: Meshed M20 bolt part-pin (left) and resin part (right)

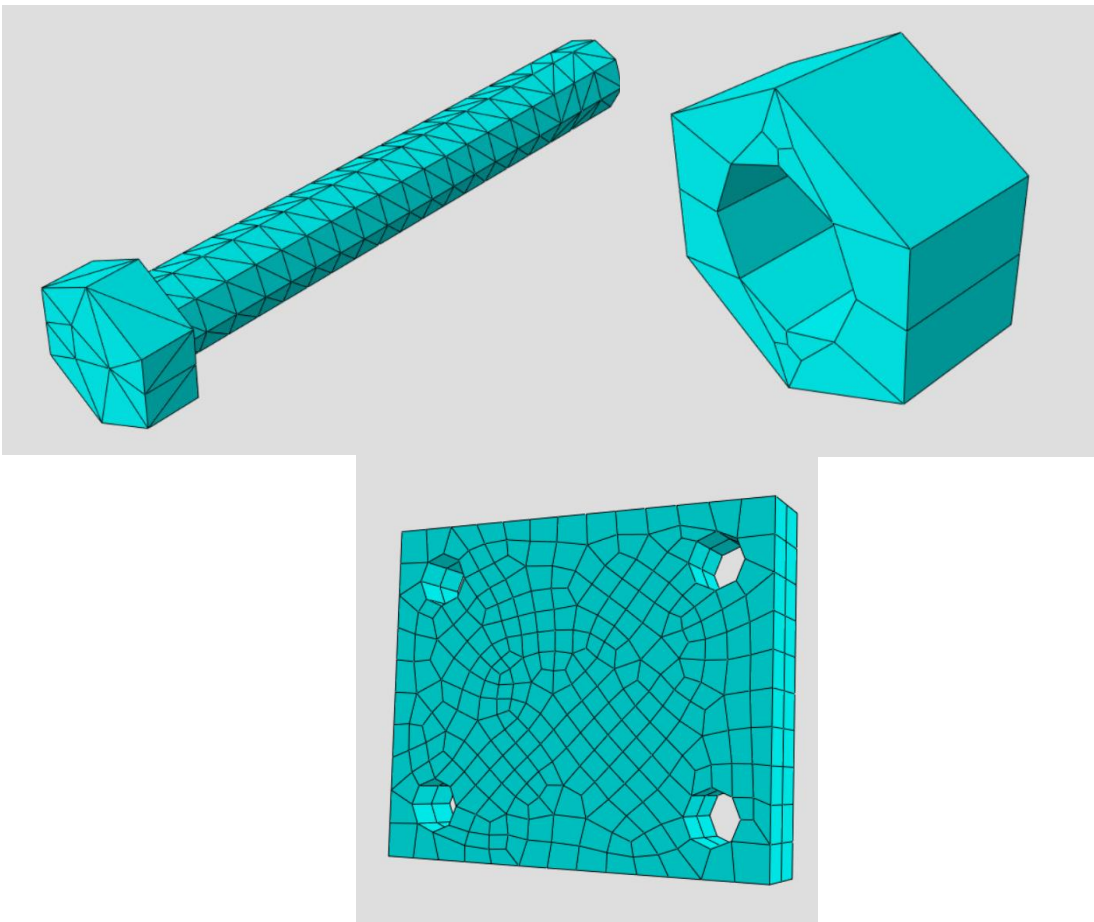


Figure 4.8: Meshed M8 bolt (top-left), nut (top-right) and side plate (bottom)

4.1.4 Loading Step

The load which as described is a forced displacement on upper edge of upper plate is applied through a General Static step of Abaqus/Standard, in a time period of 1 sec for the calculations of initial stiffness. The initial step was 0.01 and the maximum number of increments was 100

to have higher accuracy on the results of the Force vs Displacement diagram to obtain the initial stiffness of the set-up. In step definition an automatic stabilization was chosen with default dissipated energy fraction which applies an extra viscous force, proportional to the nodal displacement divided by the time step to all nodes in the model. This has an extra stabilizing effect to solve any convergence issues.

4.2 Calculation of initial stiffness

Six models were analyzed and the Force – Slip diagram was plotted to obtain numerically the initial stiffness of the specimen. The slip was taken as the average of slip between upper and lower plate in the same way as it was measured also in reality through LVDTs and the stiffness was calculated in the range between 0-0.1mm of slip. The results for the analysis are presented in Table 4.2 for the 3 different geometries and the 2 different resin types.

Type of resin Diameter of hole	Conventional Resin (R)	Steel Reinforced Resin (SR)
D30	342 kN/mm	607 kN/mm
D26	476 kN/mm	762 kN/mm
D22	826 kN/mm	1098 kN/mm

Table 4.2: Results of Initial Stiffness (kN/mm) of set-up from Numerical Analysis

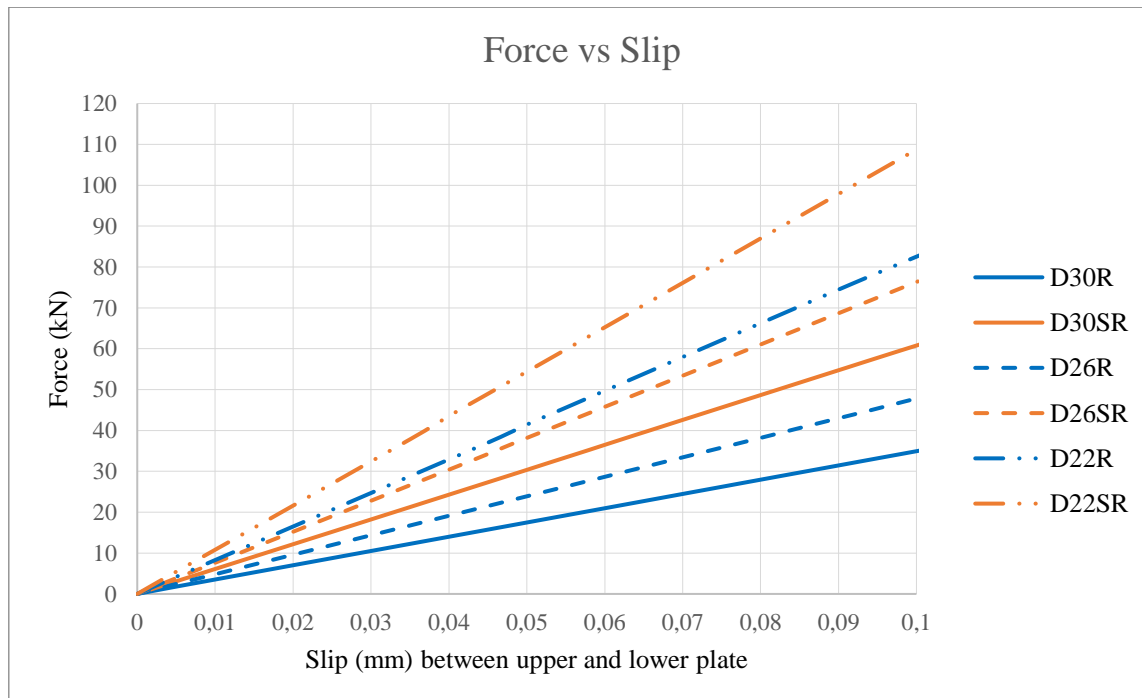


Figure 4.9: Relationship between force and slip measured between the upper and lower plate of setup in the same way as the experiments (mean) zoomed on the range 0-0.1mm from which the numerical initial stiffness was calculated

In the experiments the maximum external force was $F_{max}=120\text{kN}$ which produces a nominal bearing stress to the resin of $\sigma_{br}=200\text{MPa}$ according to (Equation 3.1). In the models D22SR

and D26SR with steel reinforced resin, i.e. the stiffer setups, the behaviour of set-up until the maximum force was linear-elastic indicating that there is no plastic behaviour anywhere in the model up to this stress state. On the other hand, in all other models (D22R, D26R, D30R, D30SR) in force slip diagram a start of plastic behaviour was observed until the max force indicating the develop of plastic strains in the setup. It is important to verify the presence of plastic behaviour in the first loading cycle which can be investigated with the present static numerical analysis since the set-up is used for fatigue analysis and it is essential to know if the deterioration of material properties starts from 1st cycle. Such effort is presented in section 4.5 , where the presence of plastic strains in steel parts in investigated. The results of stiffness and maximum slip reached when the bearing stress was maximum are presented in the following Table 4.3

	Diameter of hole in lower (female) plate					
	22mm		26mm		30mm	
Injection material	R	SR	R	SR	R	SR
Initial stiffness (kN/mm)	826	1098	476	762	342	607
Slip at max bearing stress(mm)	0.149	0.109	0.262	0.158	0.402	0.204
Slip that was expected with linear behaviour (mm)	0.145	0.109	0.252	0.157	0.351	0.197
Increase in slip related to the expected with linear behaviour	2.75%	0%	4%	0.6%	14.5%	3.55%

Table 4.3: Results of static numerical analysis

From the results of analysis, it is concluded that the increase of initial stiffness with the decrease of the hole it is not linear. For conventional resin a 4mm decrease of hole diameter results in 39% increase of stiffness with respect the initial stiffness of D30R (342 kN/mm), and an 8mm decrease of hole diameter results in 142% increase of stiffness with respect to D30R (Figure 4.11). For steel reinforced resin a 4mm decrease of hole diameter results in 26% increase of stiffness with respect the initial stiffness of D30-SR (626kN/mm), and an 8mm decrease of hole diameter results in 80% increase of stiffness with respect to D30SR (Figure 4.12). This confirms the previous research in the field of demountable shear connectors with injection bolts (see section2.3.5) that increase in hole diameter has negative influence to initial stiffness. These results which are for the most unfavorable position of bolt in the hole are in agreement with the results of Nijgh [5] who investigated experimentally the stiffness of double lap IBCs according to Annex G/K of EN 1090-2 with epoxy resin and steel-reinforced resin and concluded that by using steel reinforced resin in oversized holes does not compromise the stiffness of the connection related to the standard sized holes.

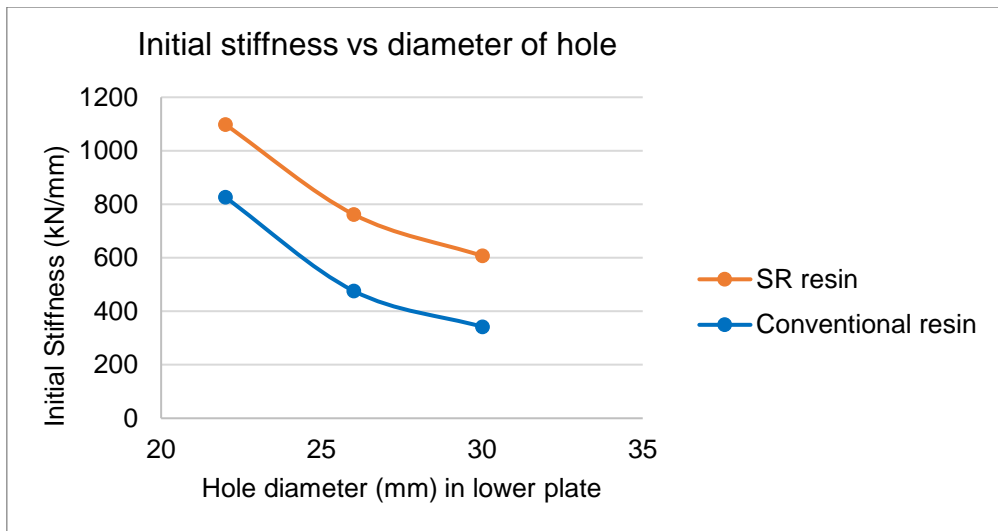


Figure 4.10: Initial stiffness of set-up vs Hole diameter diagram for conventional and steel reinforced resin according to Numerical analysis. The increase of stiffness with decrease of diameter is not linear

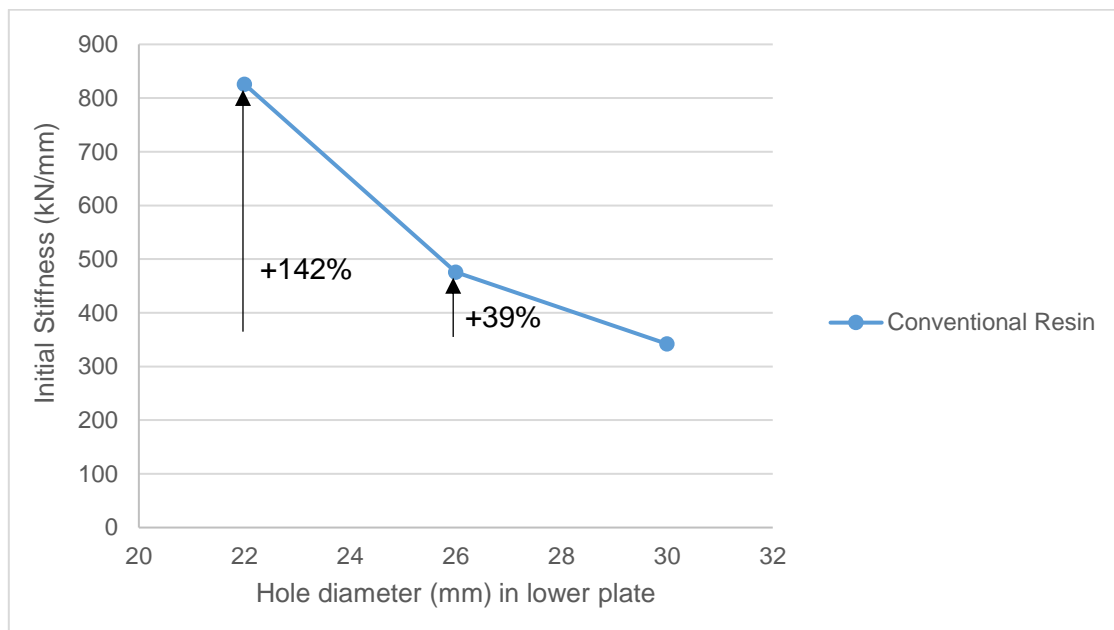


Figure 4.11: Comparison of initial stiffness for conventional resin with varying hole clearance

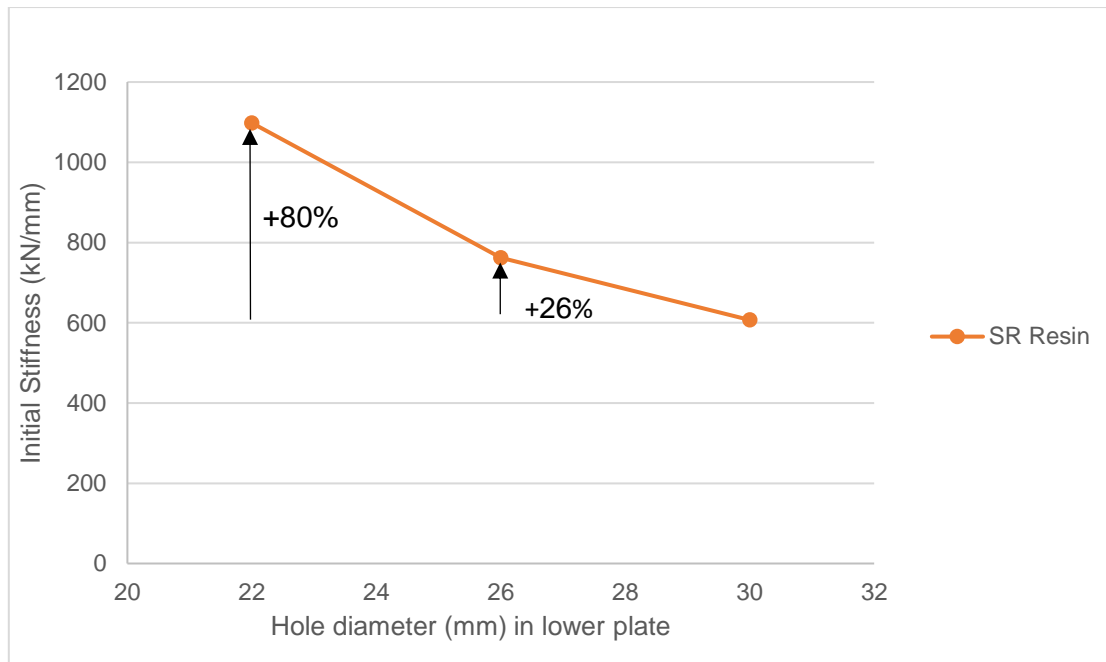


Figure 4.12: Comparison of initial stiffness for steel reinforced resin with varying hole clearance

It is worth to notice also the increase of stiffness for the same hole diameter and varying the resin material. For D30 the initial stiffness with steel reinforced is 77% higher related to initial stiffness with conventional resin. For D26 the initial stiffness with steel reinforced is 60% higher related to initial stiffness with conventional resin. For D22 the initial stiffness with steel reinforced is 32% higher related to initial stiffness with conventional resin. In case of normal clearance(2mm), the percentage increase is almost half related to the increase in 6mm and 10 mm hole clearance. This can be explained by the amount of stiffer steel shot skeleton which transfer the load between the bolt part and the lower plate which is lower in case of normal clearance. (Figure 4.13). These results agree with the research at TU Delft for the static superiority of steel reinforced resin.

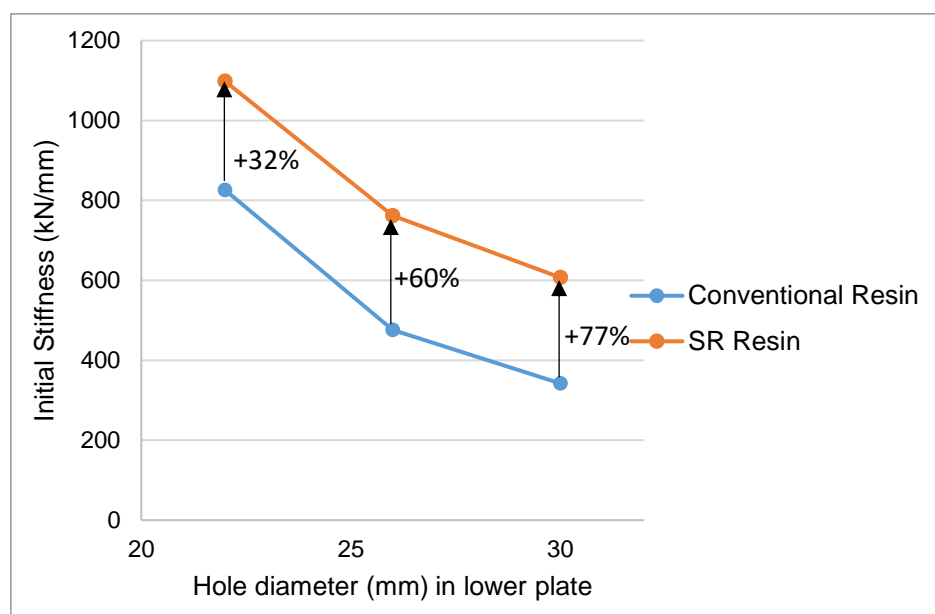


Figure 4.13: Comparison of initial stiffness for same hole clearance and varying injection material

4.3 Numerical verification of set-up

The proposed set-up for fatigue investigation of resin material should be verified numerically, so that the load transfer mechanism agrees with the tested by Nijgh double lap shear connection of Annex G/K EN 1090-2 (Figure 4.14). Furthermore, the confined environment of resin in the set-up is ensured by 2 side plates of thickness 10mm and a short parametric study was conducted to prove that there is no big difference between a fully confined environment and the proposed set-up. This is presented in the following sections.

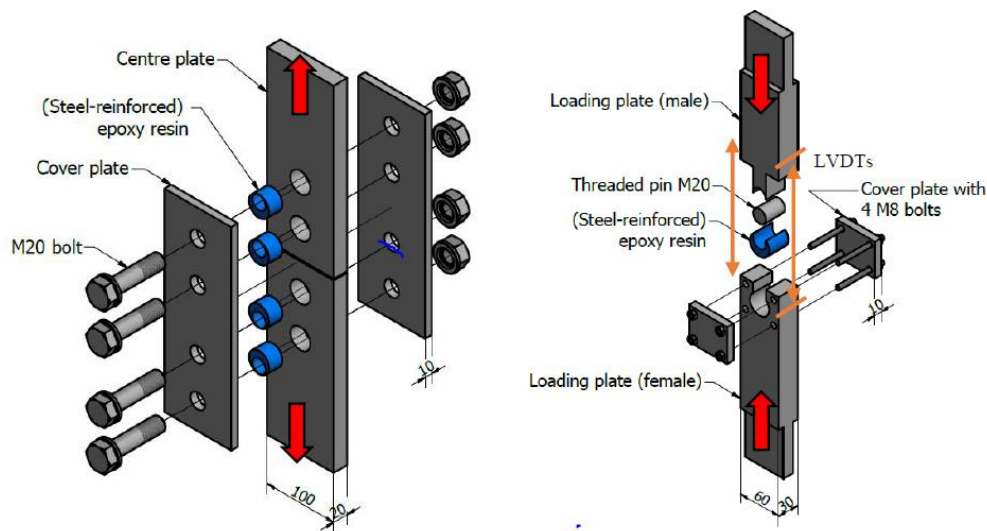


Figure 4.14 Overview of double lap shear connection (left) and proposed set-up used for cyclic experiments (right) [67]

The goal of numerical validation of the proposed set-up which was used for the cyclic tests, is to prove that the bearing stress distribution in the resin and the bolt part (pin) is equivalent to that of the resin and the bolt of double lap shear connection standardized by Annex G of EN 1990-2 [3]. For this reason, a comparison was made between the longitudinal bearing stresses of the numerical model D26-R as this was described in previous sections and a numerical model of a double lap shear connection with hole clearance 26mm in the centre plate and bolt placed in the most unfavourable position (Figure 4.14). The same material properties for the steel and the resin for the two models were defined in Abaqus/Standard. The stresses were calculated in the force level which corresponds to maximum nominal bearing stress for the resin applied in the fatigue experiments, i.e. $\sigma_b=200$ MPa. This corresponds to long duration bearing stress resistance of the resin according to [25] and is considered to be the limit for static applications in normal-clearance connections [67]. The results of the comparison are presented in Figure 4.15 and Figure 4.16.

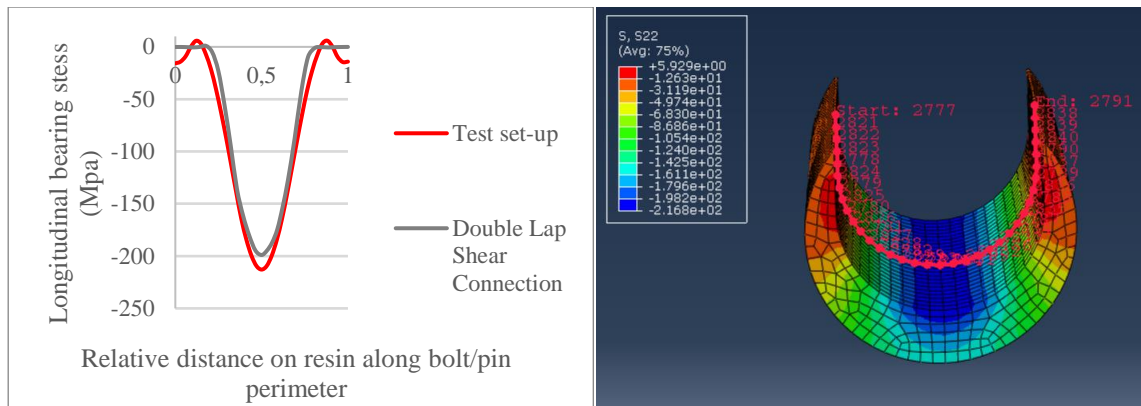


Figure 4.15: Longitudinal bearing stress on resin along bolt/pin perimeter (left) and path of stresses in the resin along bolt part perimeter part as it was taken from Abaqus model D26R (right)

It is clear from the above figure that the model that the stress transfer mechanism is similar in the test set-up which was used for the fatigue experiments and the double lap shear connection since the longitudinal stresses distribution along resin is almost the same in the 2 cases. It should be noted that in both cases the bolt part was designed without threads. The maximum longitudinal bearing stress in the center of resin for the set-up is 212.86 MPa, while for the double lap shear connection is 198.94 MPa which is a difference of 7%. This can be attributed to the friction between steel plates, which contributes to the transfer of forces in case of double lap shear connection and therefore not the full force is transferred by bearing and this is the reason why the bearing stresses are lower in that case.

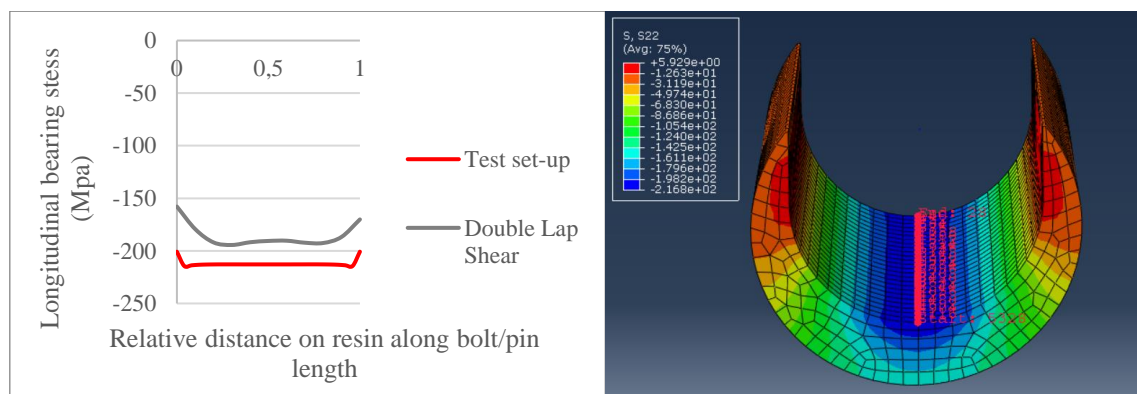


Figure 4.16: Longitudinal bearing stress on resin along bolt/pin length (left) and path of stresses in the resin along bolt part length part as it was taken from Abaqus model D26R of test set-up (right)

It can be observed in Figure 4.16 with the longitudinal bearing stress distribution on the resin along bolt and bolt part (pin) for double lap shear connection and test-set up respectively, that the difference is small and can be attributed again in slip effects. Also, in both cases the stress distribution is uniform over the bolt/bolt part length. Specially for the test set-up the bearing stress is almost constant over the hole bolt length. This agrees with the section 3.6.2 of EN 1993-1-8 [4] where it is referred that in cases of double lap shear connections the bearing stress distribution may be considered as uniform for ratios $l/d < 3$, where l is the clamped bolt length, and d is the bolt diameter. For ratios higher than 3 the bending of the bolt leads to uneven stress distribution.

In terms of initial stiffness, comparing the results of numerically calculated initial stiffness of the set-up with conventional resin and the results of numerical investigation by Nijgh [5] of

double lap shear connection if the M20 bolt is positioned within a connection with an oversize hole at its most negative location with respect to connection slip which is also the case in test set-up the results are also close.

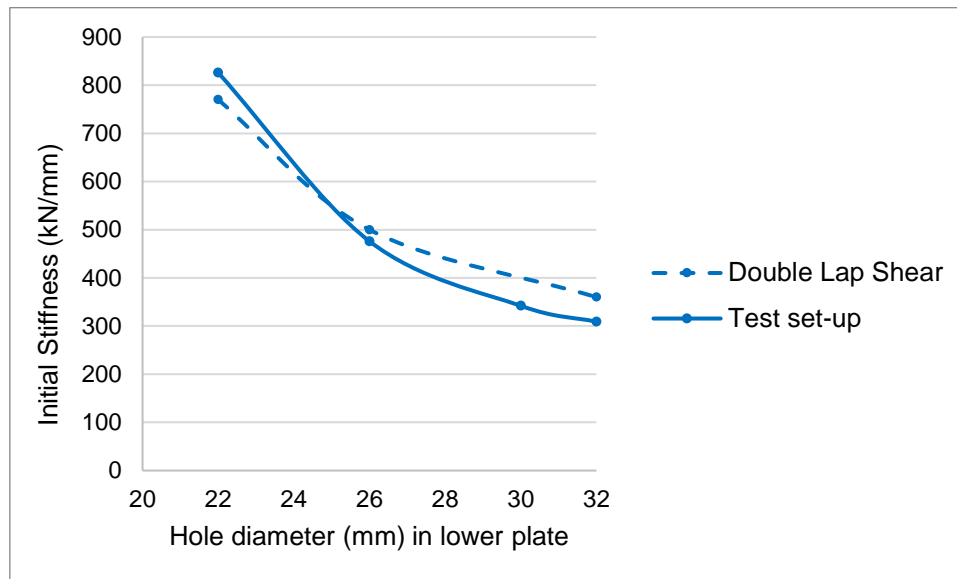


Figure 4.17: Initial stiffness of set-up vs Hole diameter diagram for conventional resin according to Numerical analysis of set-up (solid) and Double Lap Shear Connection by Nijgh

The differences are again small. For 22mm hole the initial stiffness of set-up is 7% higher than that of double lap shear. For 26mm hole double lap shear connection has 5% higher initial stiffness compared to test set-up. For 30mm there are no available data from Nijgh, but for D30 in test set-up the stiffness is 342 kN/mm while for 32mm hole in DLPS of Nijgh the stiffness is 360 kN/mm. Therefore, a numerical model of set-up with lower plate D32 was designed in the same way as described for the rest models and analyzed to have available data to compare with 32mm hole in DLPS of Nijgh. The initial stiffness of D30R is 309kN/mm which is 14% lower than DLPS with 32mm center hole. The results are summarized in following Table 5.4

Ø of center plate for double lap shear and of lower plate for set-up	Initial connection stiffness kN/mm (numerical)		Difference
	Eccentric (most unfavorable) Double Lap Shear Connection (Nijgh)	Test set-up	
22	770	826	7.2%
26	500	476	-4.8%
30	-	342	-
32	360	309	-14%

Table 4.4: Initial stiffness of set-up vs Hole diameter diagram for conventional resin according to Numerical analysis of set-up (solid) and Double Lap Shear Connection by Nijgh

From the above static numerical analysis and comparison of stress state on the resin when the load is maximum causing maximum bearing stress and from the comparison of initial

stiffness, it can be concluded that the test set-up used for the fatigue experiments it is theoretically capable to depict the deterioration of mechanical properties of resin due to cyclic loading of a double lap shear connection as the standard one described in EN 1990-2.

4.4 Parametric Investigation of confinement conditions provided by side plates.

In the test set-up the lateral confinement of the resin part is ensured by 2 steel side plates of 10 mm thickness which are tightened to the lower (female) plate as explained in previous sections. The goal of this short parametric study is to investigate to what extent the deformation of the side plates under the stresses induced by the resin affects the results. To ensure a fully confined environment for the resin the 6 numerical models as described in section 4.1 used again but with fixed side plates. The external surfaces of the side plates were restrained for every translation and rotation by fixed boundary conditions in Abaqus.

Again, a static step with prescribed forced displacement was applied in Abaqus/Standard to obtain the stiffness of set and the stress state in the resin and compare it to the actual model. The increase in stiffness was expected due to the fact that, the resin cannot deform laterally since the sides are fixed. The results of the analysis are presented below.

	Diameter of hole in lower (female) plate					
	22mm		26mm		30mm	
Injection material	R	SR	R	SR	R	SR
Initial stiffness (kN/mm)	826	1098	476	762	342	607
Initial stiffness with fully fixed sides	860	1130	498	785	366	626
Increase of initial stiffness related to the actual set-up	4.1%	2.9%	4.6%	3%	7%	3.15%

Table 4.5: Results of parametric study regarding initial stiffness

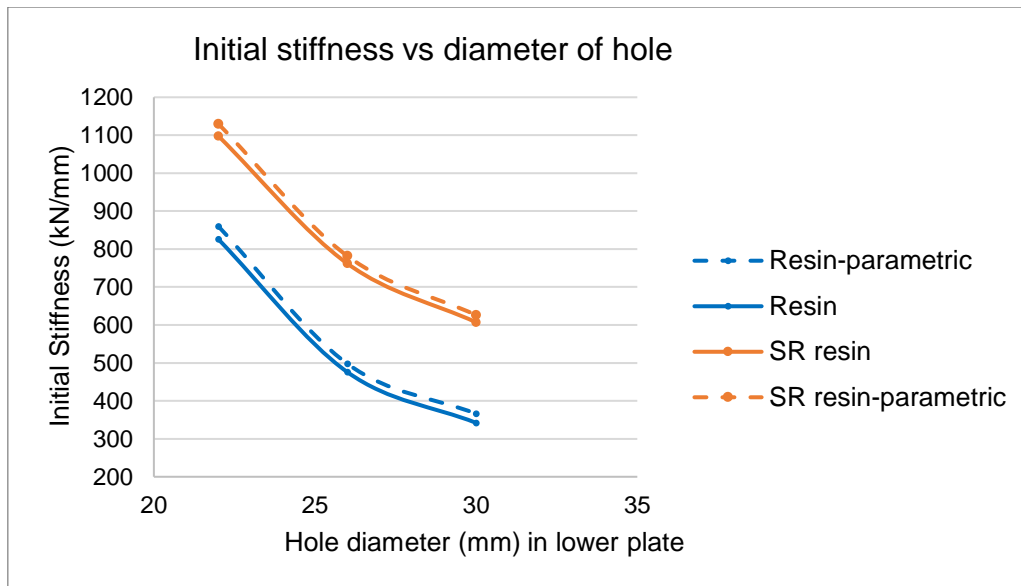


Figure 4.18: Stiffness of set-up vs Hole diameter diagram for conventional resin according to numerical analysis of set-up (solid lines) and numerical analysis with fully confined conditions (dashed lines)

In the material model of resin and steel reinforced resin which was used as an input in FEA software the Young's modulus and Poisson's ratio of unconfined resin and steel reinforced resin were adopted (according to two papers by M. P. Nijgh, H. Xin, M. Veljkovic [8],[9]). The confined conditions were ensured by the steel plates with thickness of 10mm. With this short parametric study, the influence of the thickness of the side plates in the test set-up was investigated. With the fixed boundary conditions to the external surfaces of side plates, theoretically an infinite thickness is considered. Therefore, in this case the resin part is fully confined laterally. From the results of the analysis (Table 4.5 and Figure 4.18) it seems that the effect of confinement ensured only by steel side plates of 10mm thickness on initial stiffness of the set-up is not essential. For resin the increase in stiffness is 4.1-7% based on the clearance with the largest increase observed of the largest clearance and the smaller increase for smaller clearance. For steel reinforced resin the effects are even more marginal probably due to lower Poisson's ratio, with an increase of 2.9-3.15% with same behavior as resin based on hole clearance. This may be explained by the fact that for larger clearance the surface of resin (or SR resin) which is laterally restrained is larger therefore the increase in stiffness is larger related to smaller clearance.

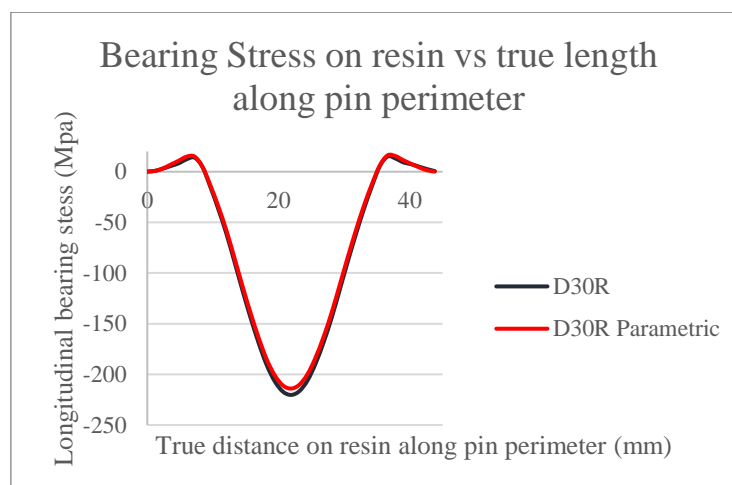


Figure 4.19: Longitudinal bearing stress on resin along pin perimeter for D30R set-up

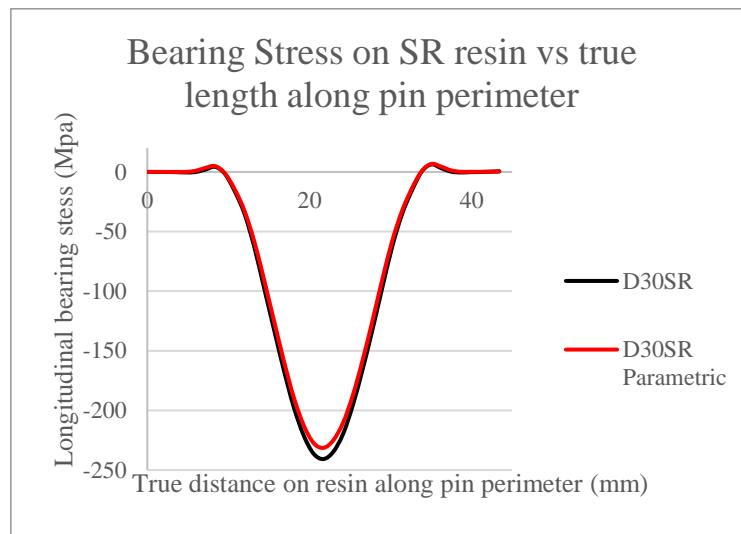


Figure 4.20: Longitudinal bearing stress on steel reinforced resin along pin perimeter for D30SR set-up

In terms of stress state of the resin and steel reinforced resin, the longitudinal bearing stress distribution along the perimeter of bolt part corresponding to the maximum nominal bearing stress of $\sigma_b=200$ MPa is plotted for D30 hole geometry in Figure 4.19 and Figure 4.20 respectively.

The plots for both cases are almost identical which indicates that the load transfer mechanism is the same in both fully confined conditions and in the actual set-up. For D30R the maximum longitudinal bearing stress is 220MPa while for D30R-parametric is 214MPa which is only 2.7% lower. For D30SR the maximum longitudinal bearing stress is 240MPa, while for D30SR-parametric is 231MPa which is 3.75% lower. Note that similar situation is observed for all the other specimens which are not presented here namely D22 and D26 set-ups. The small decrease in maximum longitudinal stress in case of fully fixed sides may be attributed to the fact that the fixed and therefore stiffer side plates in parametric case, attract bigger part of the load than in the case of finite thickness of 10mm in actual set-up. Indeed, the maximum Von Mises stress in the side plates in case of fully fixed sides is 48MPa, while in case of actual set-up is 27MPa for D30SR specimens (Figure 4.21)

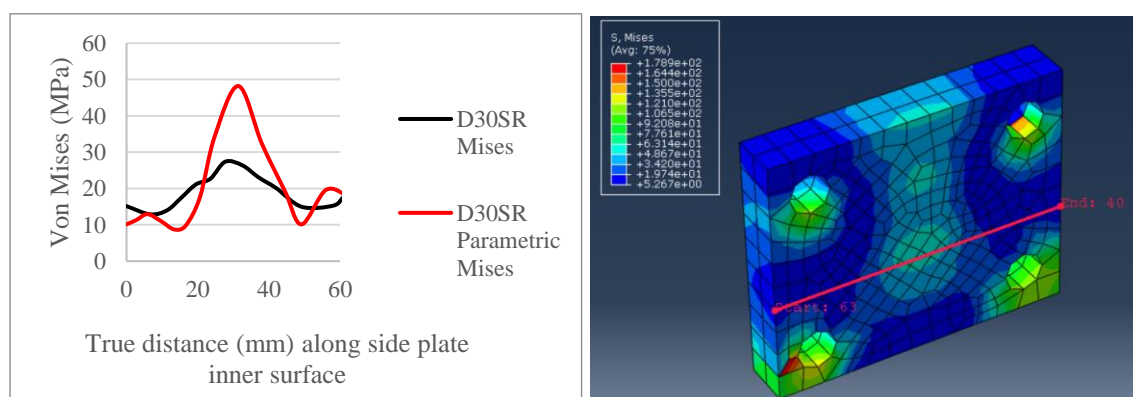


Figure 4.21: Von Mises stresses vs True distance along inner surface of side plate (left) and path of stresses in the side plate as it was taken from Abaqus model D30SR Parametric (right)

The results of the parametric study prove that the thickness of side plates which ensure confinement of resin part in the set-up does not affect significantly the results since for the limit case of infinite thickness, the results in terms of stress state in the resin (or SR resin) part, and in terms of initial stiffness present limited differences.

4.5 Quasi-static numerical analysis of yielding of upper (male) steel plate.

From static numerical analysis of test set-up, it was observed that for all models, in the maximum nominal longitudinal bearing stress of 200 MPa for the resin part, which was used for fatigue experiments, the steel of upper plate reached the nominal yield stress of 355 MPa. Since the yield stress was reached from the first loading cycle which is represented in static numerical analysis, the development of plastic deformations on steel may affect the experimental results of slip between upper and lower plate if a part of that slip is attributed to the yielding of steel plates. In all static models (D22R-SR, D26R-SR, D30R-SR) when the maximum force was 120kN meaning that the bearing stress of resin was 200 MPa, the Von Mises stresses of upper steel plate was 355.7 MPa. The stress diagram and the place where the stress reaches the yield strength are depicted in Figure 4.22

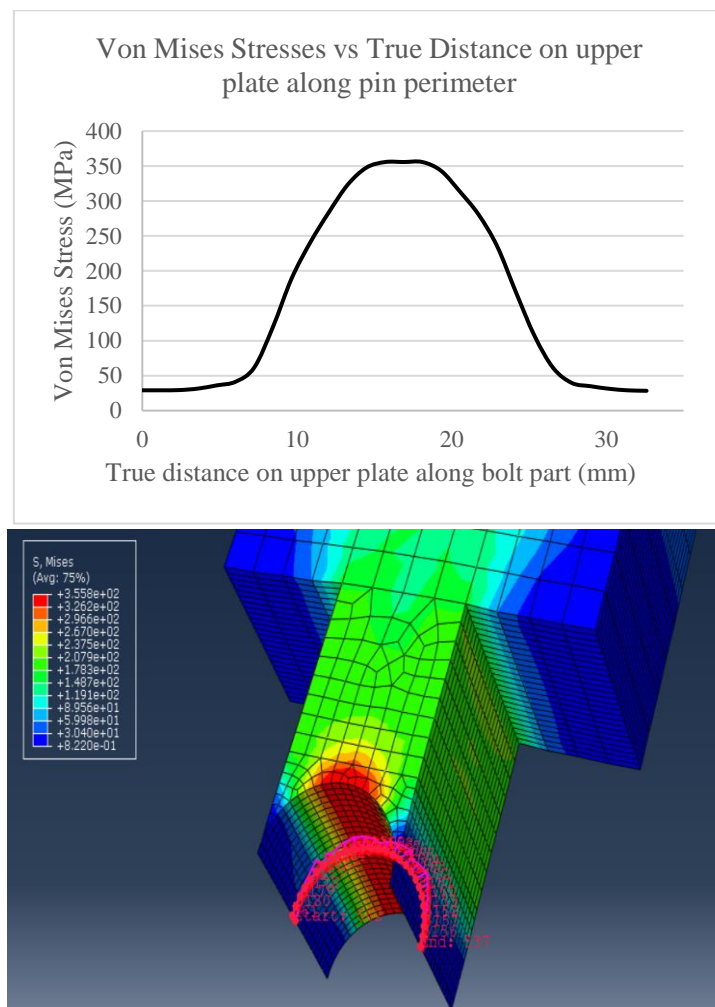


Figure 4.22: Plot of Von Mises stresses (up) and path of stresses on upper plate (down)

For this reason, the behaviour of the set-up in quasi-static low-cycle loading had to be investigated to find in what extent the yielding of steel upper plate affects the results in terms of slip through plastic deformations. Therefore, a numerical model of set-up was analysed in quasi-static loading similar with the loading scheme used in the quasi-static phase of experiments. The model was a similar model of D30R with same geometry and assembly, interactions and meshing as the static D30R as described in section 4.1. The material model of resin was only linear elastic without the Drucker-Prager plastic model because the goal is to investigate the residual deformations due to steel plasticity after cycles of loading-unloading at the end of quasi-static phase. The material model of steel plates was an elastic-plastic stress-strain with a yield strength of 355 MPa and a combined hardening behavior in plasticity module of Abaqus/Standard Figure 4.23. This option is used to model the cyclic loading of a material with nonlinear isotropic/kinematic hardening according to Abaqus Manual [66].

To simulate 20 cycles of loading and unloading a static step was used with time period of 20 and initial and maximum increment size of 0.01. The frequency of application of the load in quasi static phase of experiments was 0.05 Hz and the maximum compressive load was 120 kN and the minimum compressive load is 12 kN for series of 180 MPa which was the maximum stress range of experiments.

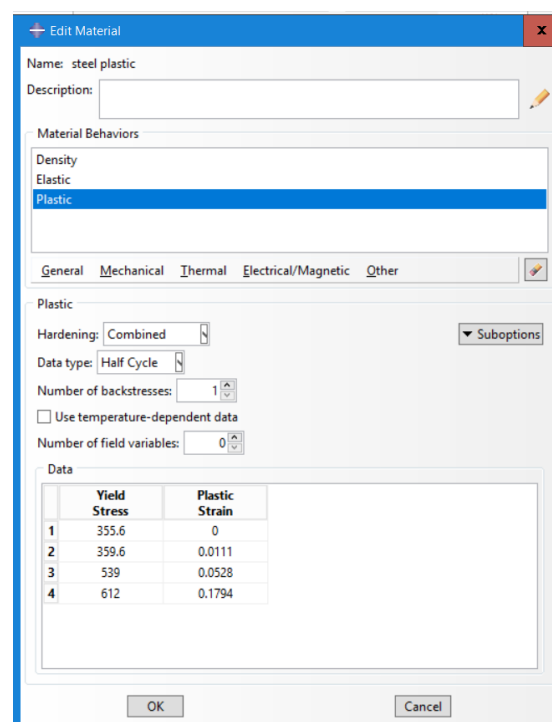


Figure 4.23: Plastic material model for all steel plates S355

From the results of slip between upper and lower plate vs step-time, the difference in slip between the maximum load and minimum data within each cycle was extracted. The plot of $\Delta\delta$ vs Number of cycles where $\Delta\delta$ is the difference in slip from maximum to minimum load within each cycle (Figure 4.24).

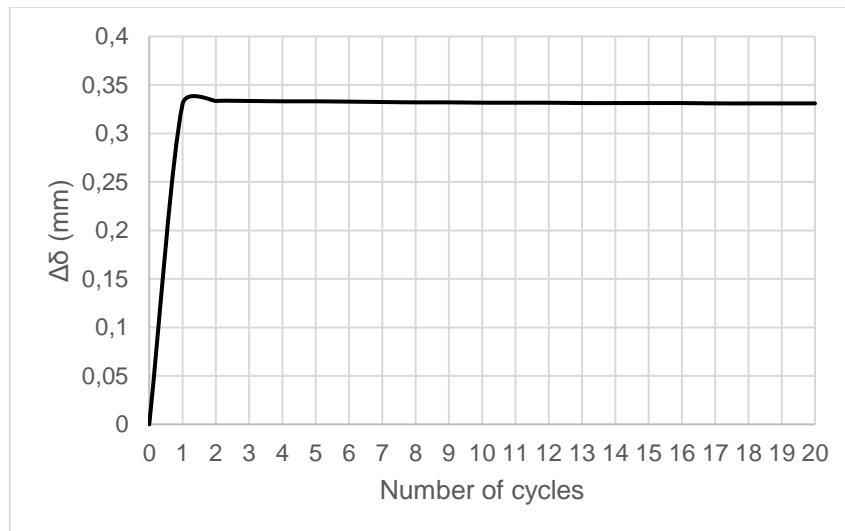


Figure 4.24: Difference in slip between upper and lower plate within each cycle vs Number of cycles

From Figure 4.24 it is concluded that the fact that upper steel plate reaches the yield limit of 355 MPa has not a mayor effect to the slip between upper and lower plate in the quasi-static phase since $\Delta\delta$ is almost stable from the 1st cycle until 20th cycle. Therefore, there are no remaining deformations in the steel during loading and unloading within the cycles. Indeed, there is only a small area in upper plate where plastic strains are developed after 0.5 cycles (where the force is maximum for the 1st time) (Figure 4.25) and the plastic strain is stable and is not increased within the cycles (Figure 4.26) therefore there are no added deformations from cycle to cycle and this is the reason why $\Delta\delta$ is not increased within the cycles.

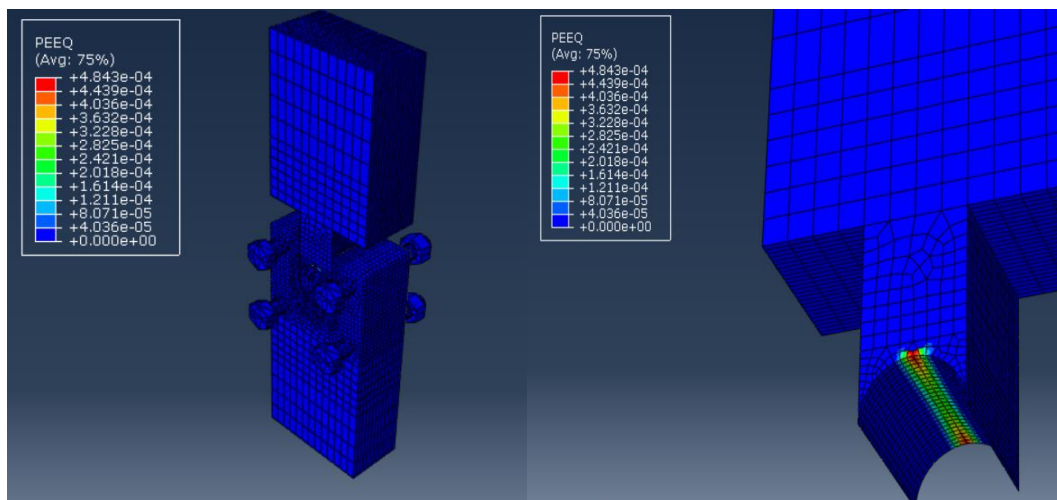


Figure 4.25: Plastic strains in set-up are zero everywhere (left) except a zone in upper steel plate (right)

It is concluded from quasi-static numerical analysis that the slip would not be affected from the yielding of upper steel plate. But the fact that the steel reaches yield stress from the 1st loading cycle will have unpredictable effects in the fatigue loading phase with hundreds of thousands cycles of loading and unloading and frequency of 5 Hz. Of course it has to be mentioned that the numerical analysis was performed without threads in the bolt part and the upper plate. The presence of threads may lead to higher stress concentration and therefore enhance the plastic deformations in reality.

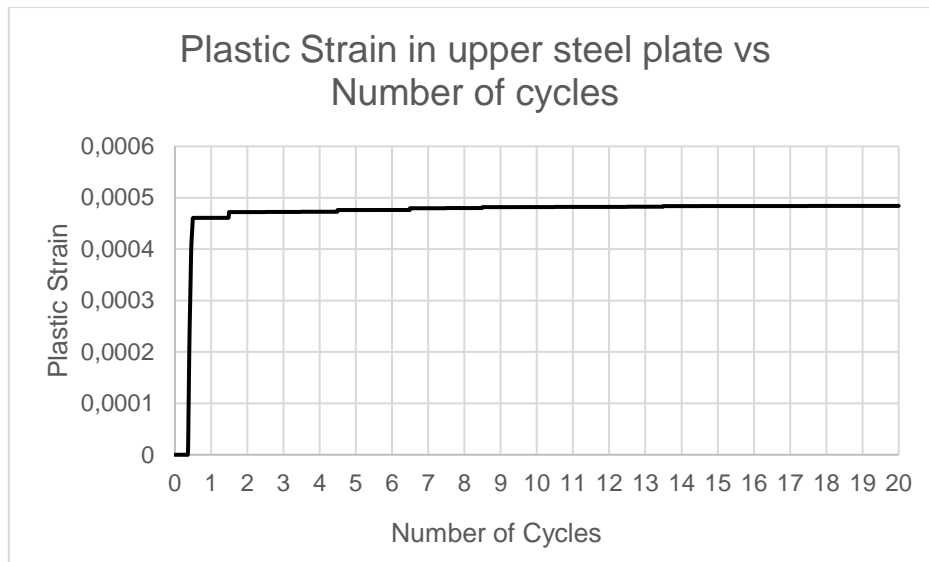


Figure 4.26: Plastic Strain in upper steel plate vs Number of cycles

4.6 Conclusions of numerical analysis

From the numerical analysis which included the static calculation of initial stiffness, the comparison of the test set-up with the standardized double lap shear connection (EN 1990-2), the short parametric study of confinement conditions and the quasi static cyclic analysis the following conclusions were extracted:

- Steel reinforced resin can be used as injection material instead of conventional resin in oversized holes without compromising the initial static stiffness of connection which agrees with research of Nijgh [5] for Double Lap Shear Connections
- The test set-up of a simple pin which allows testing of the resin under cyclic loads, without the risk of fatigue cracks of the injection bolt itself can be used for testing the deterioration of material properties of resin since it is validated that resin part is in a similar stress-state and provides similar initial connection stiffness as a starting point as it is in standard double lap shear connection of EN 1090-2
- The thickness of side plates which ensure confined conditions for the resin part would not have a significant effect in the results.
- The weakest point of the test set-up is located at the upper (male) steel plate in the contact surface with the bolt part from where the load is transmitted. The current steel grade of the test set-up with which the fatigue tests conducted is S355 and at the maximum force applied in specimen for all geometries the steel marginally reaches yield stress. This seems that will not affect the test results in quasi static phase, but it is unknown how affects the fatigue loading phase since yielding occurs in 1st cycle. For future studies with same geometry a higher steel grade is suggested.

5 Experimental Results

In the experimental program, experiments have been carried out for the following specimen series as indicated in Table 5.1 according to designation explained in section 3.4.7.

Diameter of Hole (mm)	Type of Resin (R-SR)	Nominal Bearing Stress Range ($\Delta\sigma_b$)	Specimen Identification	Number of specimens	
Ø30	Conventional	180	D30R180	5	
	Steel Reinforced	180	D30SR180	6	
	Conventional	135	D30R135	4	
	Steel Reinforced	135	D30SR135	4	
	Conventional	90	D30R90	6	
	Steel Reinforced	90	D30SR90	5	
Ø26	Conventional	180	D26R180	5	
	Steel Reinforced	180	D26SR180	6	
	Conventional	135	D26R135	6	
	Steel Reinforced	135	D26SR135	6	
	Conventional	90	D26R90	5	
	Steel Reinforced	90	D26SR90	5	
Total number of specimens	R:31	SR:32	-	-	63

Table 5.1: Overview of fatigue experimental program

5.1 Initial stiffness from quasi-static loading phase

The initial stiffness of all specimens is calculated from quasi-static loading phase as indicated in section 3.4.8, Figure 3.36. The mean value and standard deviation are calculated and presented in Table 5.2 and Table 5.3, along with the comparison with numerical models. Secondly, the diagrams of Slip vs Number of cycles were plotted, where the slip is considered the maximum displacement difference between upper and lower plate measured by LVDTs at each cycle. Since LVDTs were reset to zero offset after the end of quasi static-phase, it should be mentioned the plotted slip is only due to cyclic loads of fatigue loading phase, excluding the residual slip after the end of quasi static phase.

Geometry- Injection Material-Stress Range	Specimen Name	Initial Stiffness <i>Kini</i> (kN/mm)	Geometry- Injection Material-Stress Range	Specimen Name	Initial Stiffness <i>Kini</i> (kN/mm)
D30-R-180	D30R180-1	359.96	D30-SR-180	D30SR180-1	571.41
	D30R180-2	374		D30SR180-2	585.1
	D30R180-3	331		D30SR180-3	570
	D30R180-4	366		D30SR180-4	629.4
	D30R180-6	382		D30SR180-5	610.44
	-	-		D30SR180-6	656
	S. D	17.48		S. D	34.54
	Mean value experimental	362.92		Mean value experimental	603.725
	Numerical (D30-R)	342		Numerical (D30-SR)	607
Difference with numerical	5.87% higher	Difference with numerical	0.66% lower		
D30-R-135	D30R135-1	325	D30-SR-135	D30SR135-2	626.47
	D30R135-2	340.17		D30SR135-3	698.87
	D30R135-4	337.97		D30SR135-4	559.92
	D30R135-5	348.14		D30SR135-5	506.56
	S. D	8.31		S. D	72.11
	Mean value experimental	337.82		Mean value experimental	597.96
	Numerical (D30-R)	342		Numerical (D30-SR)	607
	Difference with numerical	1.4% lower		Difference with numerical	1.48% lower
D30-R-90	D30R90-1	308.95	D30-SR-90	D30SR90-1	625
	D30R90-2	309.25		D30SR90-2	584.3
	D30R90-3	310		D30SR90-3	525.8
	D30R90-4	278		D30SR90-4	697.6
	D30R90-5	338		D30SR90-5	653
	D30R90-6	357		-	-
	S. D	24.95		S. D	58.72
	Mean value	316.87		Mean value	617.14
	Numerical (D30-R)	342		Numerical (D30-SR)	607
	Difference with numerical	7.6% lower		Difference with numerical	1.65% higher
Comparison	Experimental mean value geometry D30-R	339.03	Comparison	Experimental mean value geometry D30SR	606.27
	Numerical	342		Numerical	607
	Difference with numerical	0.87% lower		Difference with numerical	0.12% lower

Table 5.2: Results of experimental initial stiffness of test set-up specimens D30 R-SR and comparison with numerical values

Geometry-Injection Material-Stress Range	Specimen Name	Initial Stiffness <i>Kini</i> (kN/mm)	Geometry-Injection Material-Stress Range	Specimen Name	Initial Stiffness <i>Kini</i> (kN/mm)
D26-R-180	D26R180-1	441.5	D26-SR-180	D26SR180-1	670
	D26R180-2	521.77		D26SR180-2	730
	D26R180-3	485		D26SR180-3	681.1
	D26R180-4	446		D26SR180-4	720.5
	D26R180-5	549.4		D26SR180-5	730
	-	-		D26SR180-6	735
	S. D	42.05		S. D	25.7
	Mean value experimental	488.73		Mean value experimental	711.1
	Numerical (D26-R)	476		Numerical (D26-SR)	762
Difference with numerical	2.68% higher	Difference with numerical	6.67% lower		
D26-R-135	D26R135-1	448.64	D26-SR-135	D26SR135-1	718
	D26R135-2	461		D26SR135-2	741
	D26R135-3	444		D26SR135-3	741.5
	D26R135-4	469.45		D26SR135-4	690.47
	D26R135-5	426.5		-	-
	D26R135-6	472.98		-	-
	S. D	15.98		S. D	20.91
	Mean value experimental	453.76		Mean value experimental	722.74
	Numerical (D26-R)	476		Numerical (D26-SR)	762
Difference with numerical	4.67% lower	Difference with numerical	5.15% lower		
D26-R-90	D26R90-1	464.83	D26-SR-90	D26SR90-1	736
	D26R90-2	416.67		D26SR90-2	657
	D26R90-4	460.15		D26SR90-4	650
	D26R90-5	514		D26SR90-5	616
	-	-		D26SR90-6	692.6
	S. D	58.37		S. D	40.86
	Mean value	439.13		Mean value	670.32
	Numerical (D26-R)	476		Numerical (D26-SR)	762
	Difference with numerical	7.75% lower		Difference with numerical	12% lower
Comparison	Experimental mean value geometry D26R	460.54	Comparison	Experimental mean value geometry D26SR	701.39
	Numerical	476		Numerical	762
	Difference with numerical	3.24% lower		Difference with numerical	8% lower

Table 5.3: Results of experimental initial stiffness of test set-up specimens D26 R-SR and comparison with numerical values

From the calculation of experimental initial stiffness, the static numerical model is validated especially for the specimens with resin as injection material, since the mean experimental stiffness values are very close with the numerical for D30R and D26R with only 0.87% and 3.24% difference respectively. Almost perfect match is observed also for the model D30SR with difference between experimental and numerical values of only 0.12%. The greatest

difference is for the model D26SR with 8%. Note that for all cases the experimental K_{ini} was lower related to numerical. However, the standard deviation between experimental obtained initial stiffnesses is quite big indicating a scatter in the results. The results are summarized in Figure 5.1. Due to time limitations and difficulties in assembly of specimens with geometry D22 (which is a normal hole clearance for bolt M20) since the hole clearance is only 2mm and it is hard to achieve injection, there are no experimental data for this geometry but only numerical.

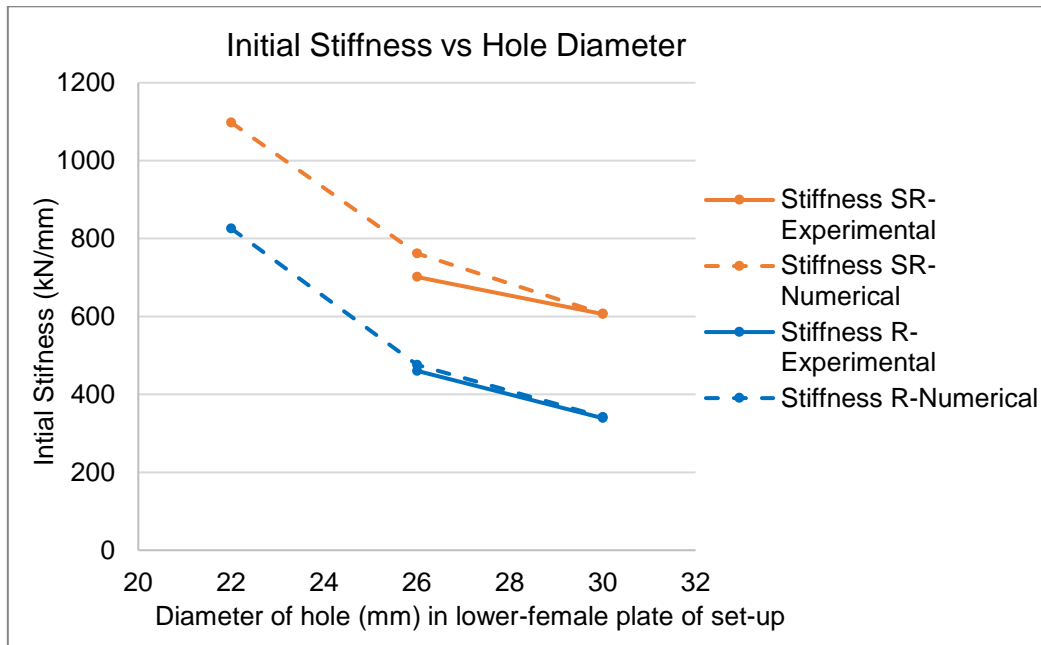


Figure 5.1: Comparison between Numerical and Experimental (mean) results for Initial Stiffness vs Hole diameter in lower plate

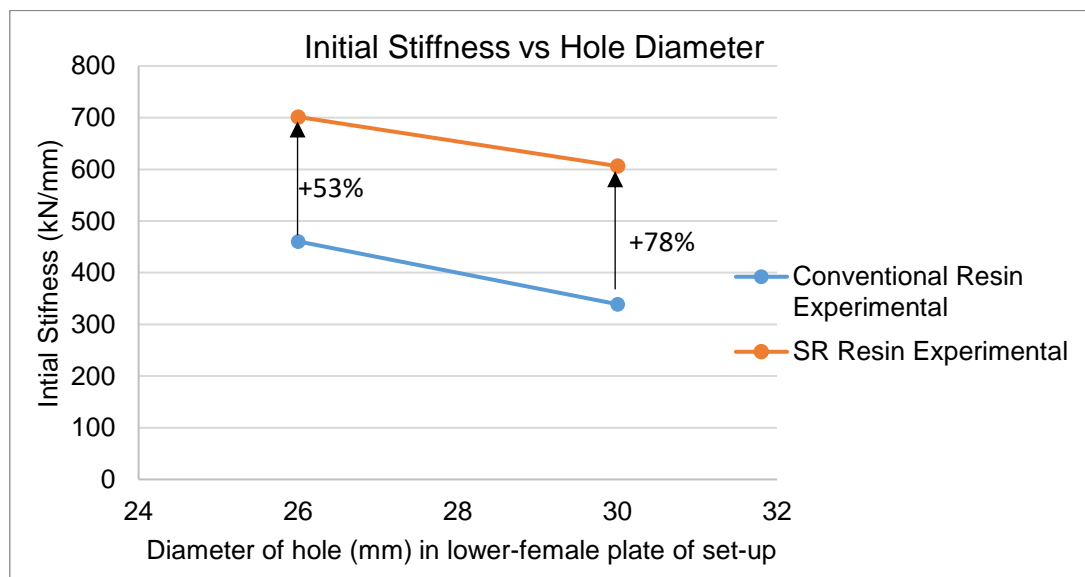


Figure 5.2 a comparison of experimental initial stiffness for the same geometry of specimen but different injection material (R or SR) in depicted. As it can be seen for specimens with hole clearance 10mm (D30) the initial stiffness with steel reinforced resin is 78% higher than the initial stiffness with conventional resin. For 6mm clearance (D26) the increase is 53%. These values are similar to the numerically obtained percentages since it is reminded that the respective values were 77% for D30 and 60% for D26 (Figure 4.13). Therefore, as a starting

point in fatigue analysis the use of SR resin leads to less static slip. This confirmed at the end of quasi-static analysis since after 25 cycles all specimens with steel reinforced resin had lower remaining slip related to specimens with conventional resin for same geometry and stress range. The use of oversized hole reduces the initial stiffness of connection as it was expected. When comparing the 2 different geometries but with same injection material the increase in hole diameter by 4mm (from D26 to D30) leads to a 26% and a 13% decrease in initial stiffness for conventional and steel reinforced resin respectively.

5.2 Results of Fatigue loading phase

5.2.1 Slip vs Number of cycles

The diagrams plotted below indicate how slip displacement alerted during cyclic loading which resulted to decrease of stiffness, for $R=0.1$ and constant amplitude compression-compression. To illustrate how the permanent slips, δ due to cyclic loads, were accumulated during the tests, the registered slips have been plotted against the number of load cycles. The plotted slip corresponds to the mean value of the measured slips registered by the two LDVT-sensors. The mean lines were calculated in MATLAB and plotted along with specimen's results. The results are presented in the figures below. The limit of x-axis is 400.000 cycles for most of series expect for the series with hole diameter 26mm and stress range 90 MPa because in these stiffer specimens with lower stress range slip did not reach 0.3 mm therefore those specimens left in the machine at least for 1.000.000 cycles before considered as run-outs.

D30R180

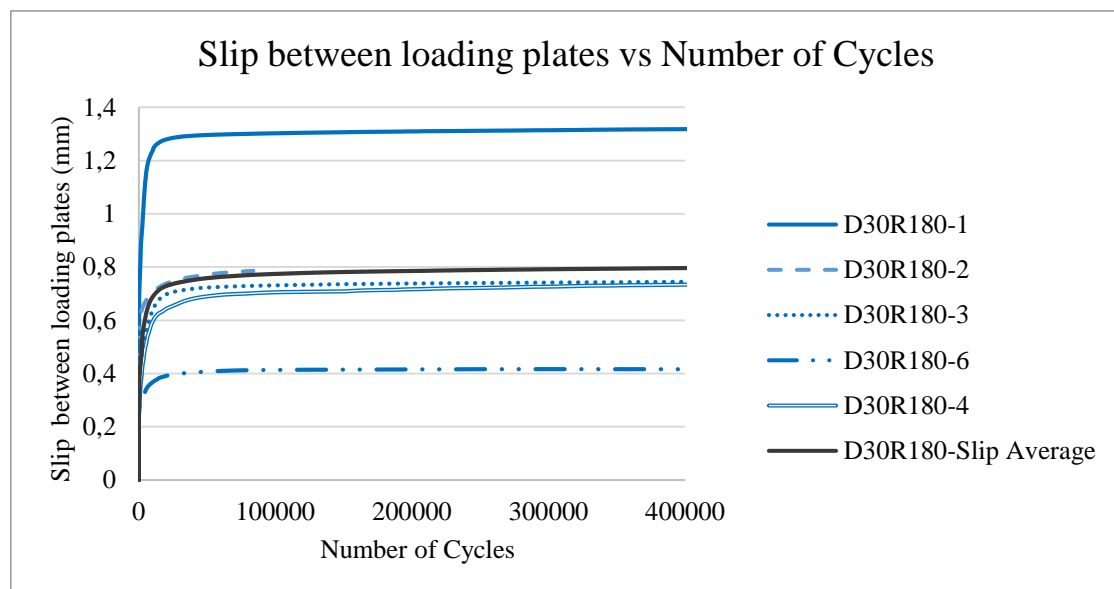


Figure 5.2: Slip vs Number of Cycles for D30R180 series

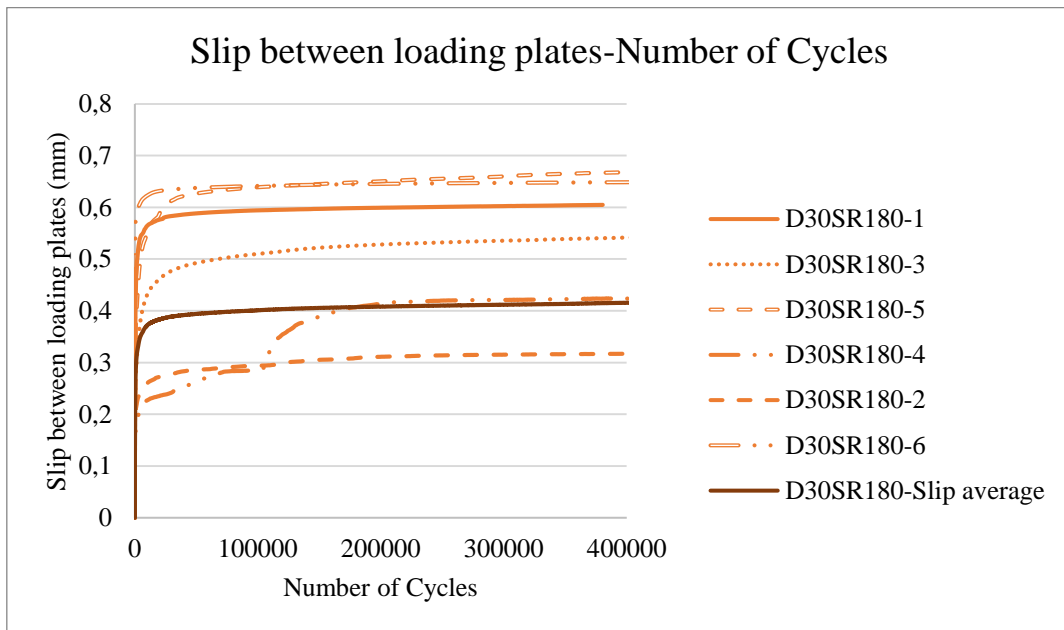
D30SR180

Figure 5.3: Slip vs Number of Cycles for D30SR180 series

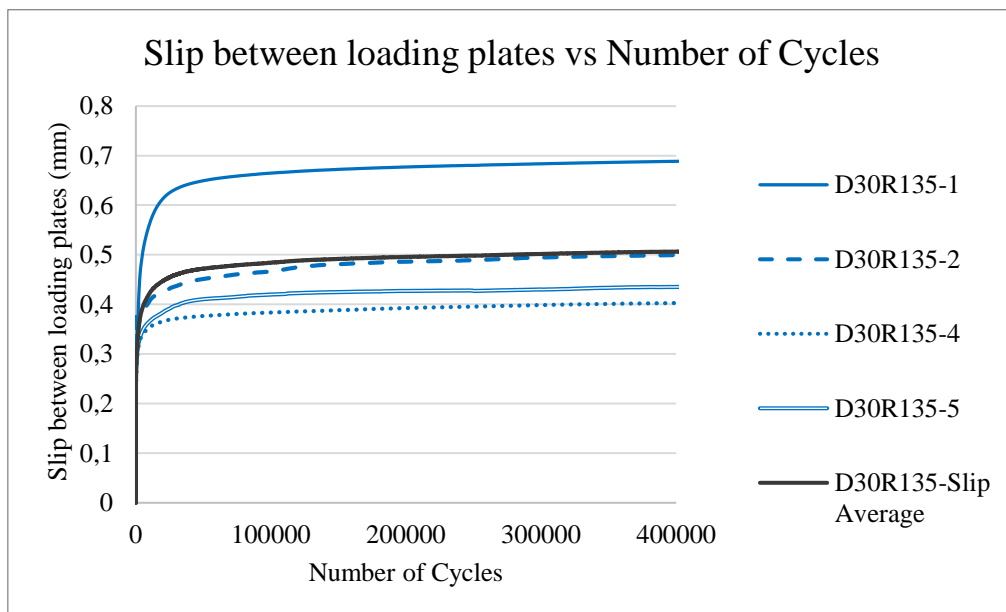
D30R135

Figure 5.4: Slip between loading plates vs Number of Cycles for D30R135 series

For D30SR135

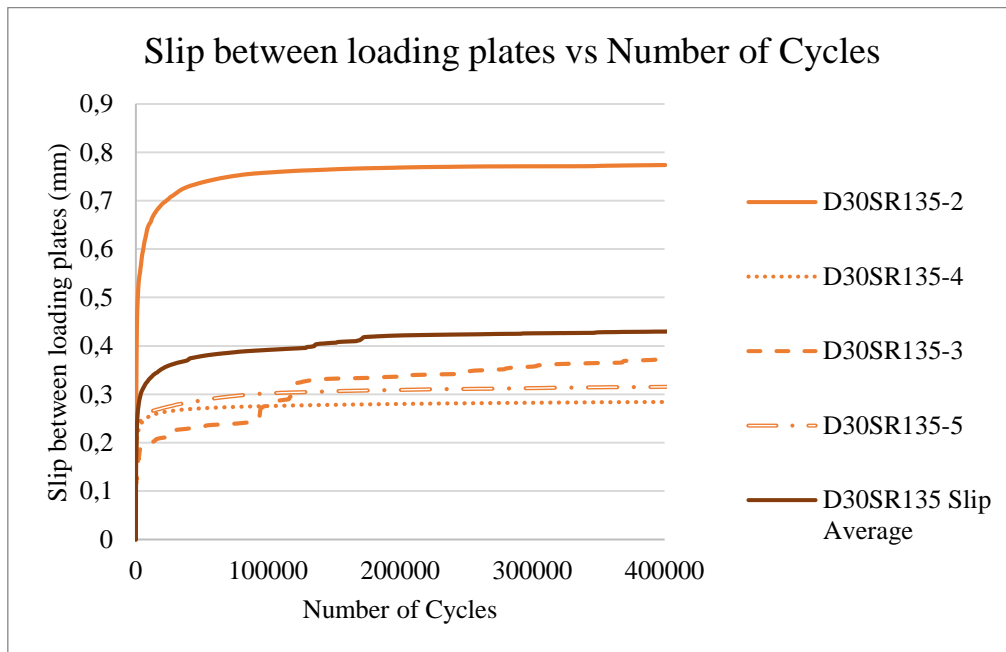


Figure 5.5: Slip between loading plates vs Number of Cycles for D30SR135 series

D30R90

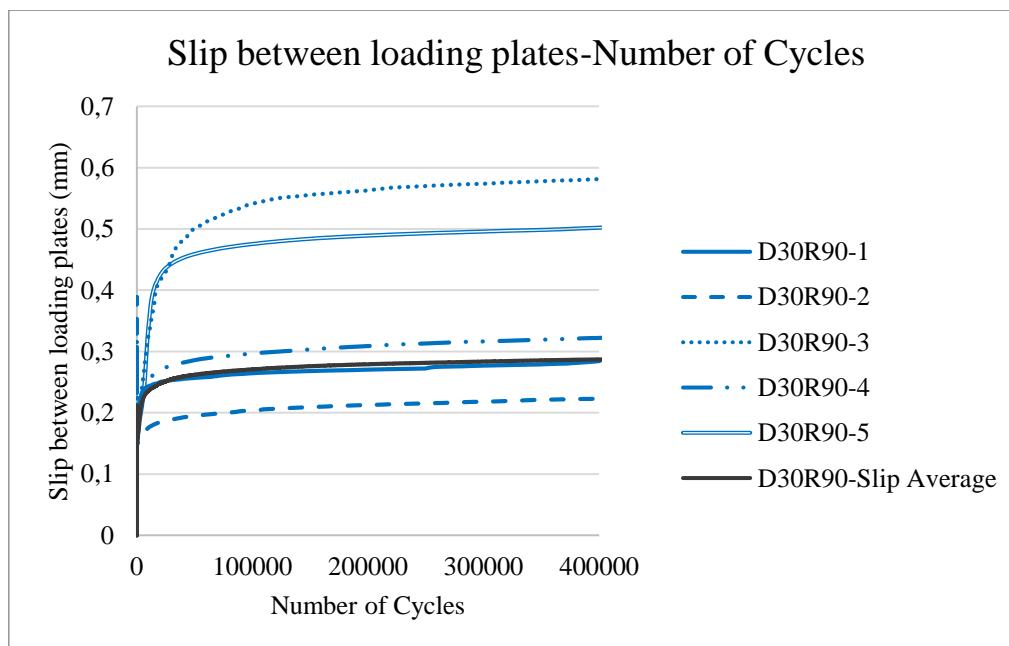


Figure 5.6: Slip between loading plates vs Number of Cycles for D30R90 series

D30SR90

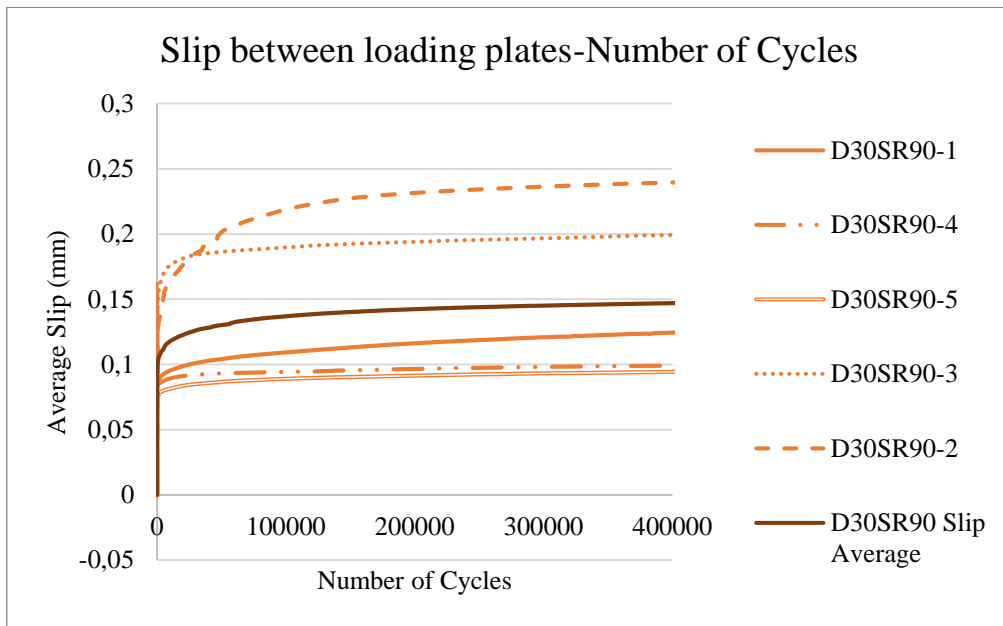


Figure 5.7: Slip between loading plates vs Number of Cycles for D30SR90 series

D26R180

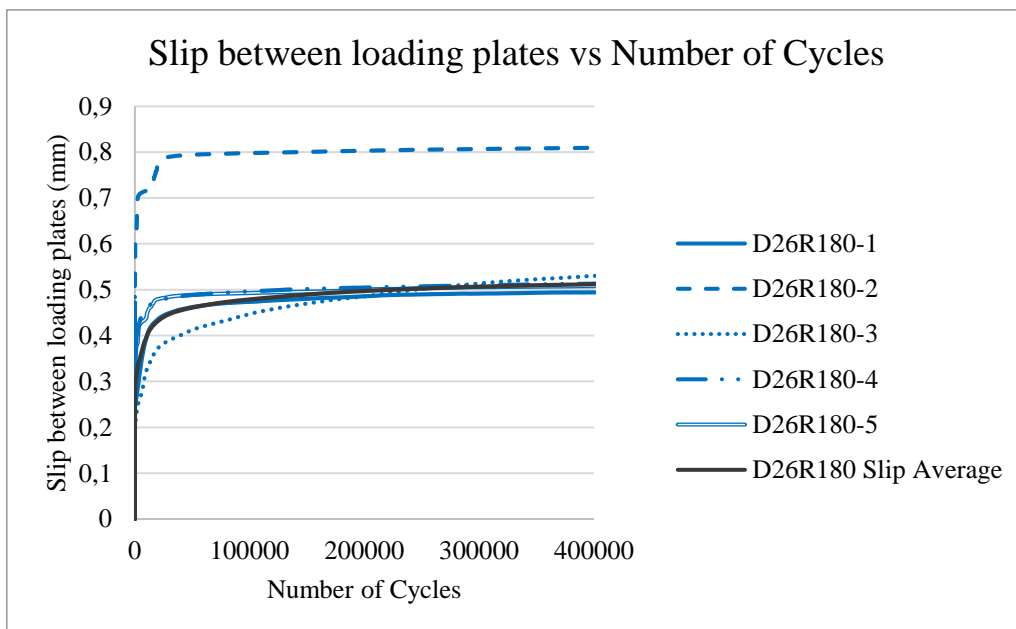


Figure 5.8: Slip between loading plates vs Number of Cycles for D26R180 series

D26SR180

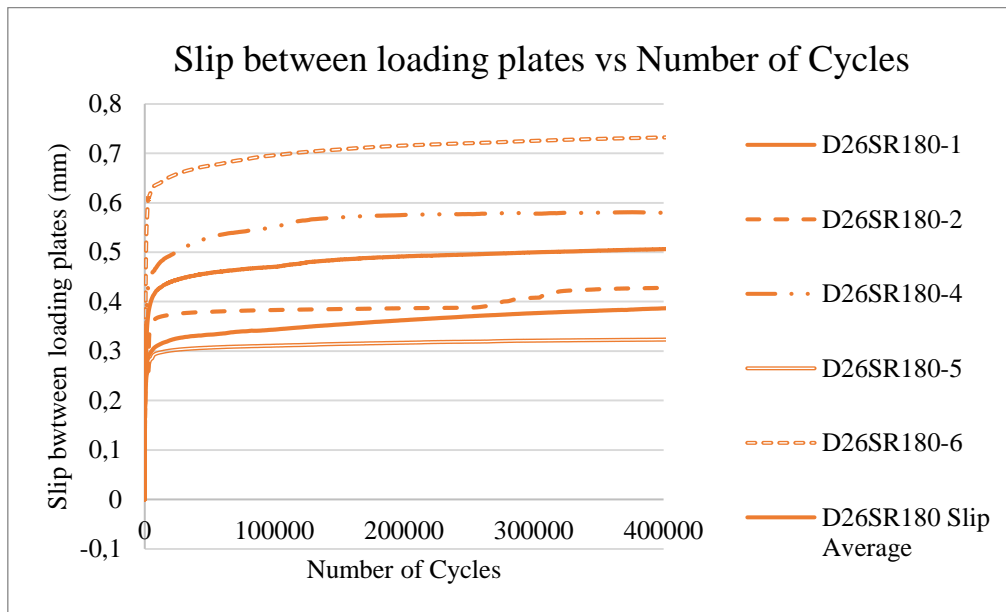


Figure 5.9: Slip between loading plates vs Number of Cycles for D26SR180 series

D26R135

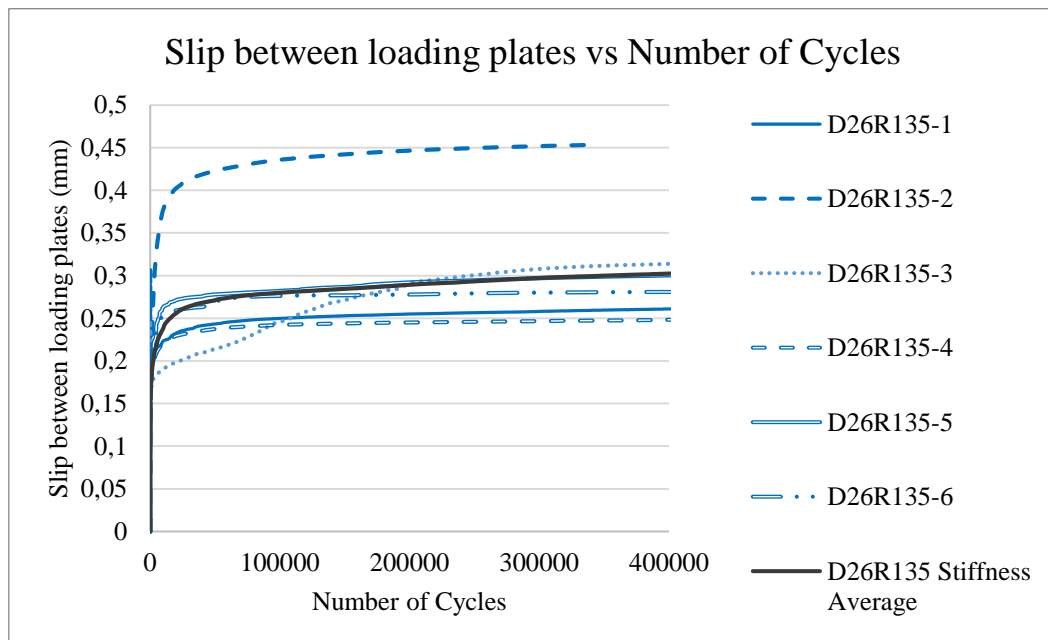


Figure 5.10: Slip between loading plates vs Number of Cycles for D26R135 series

D26SR135

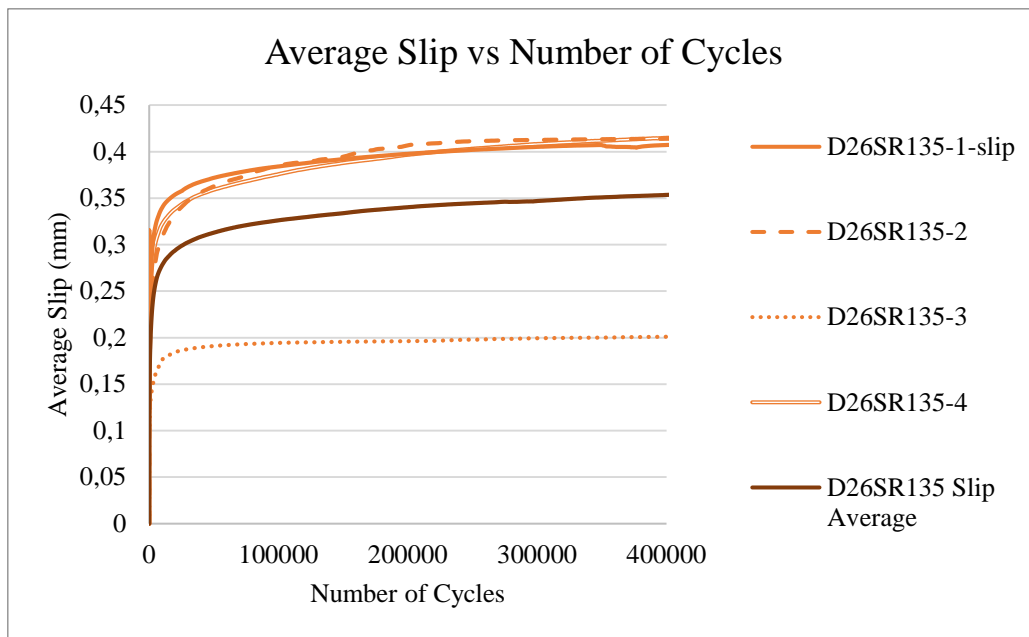


Figure 5.11: Slip between loading plates vs Number of Cycles for D26SR135 series

D26R90

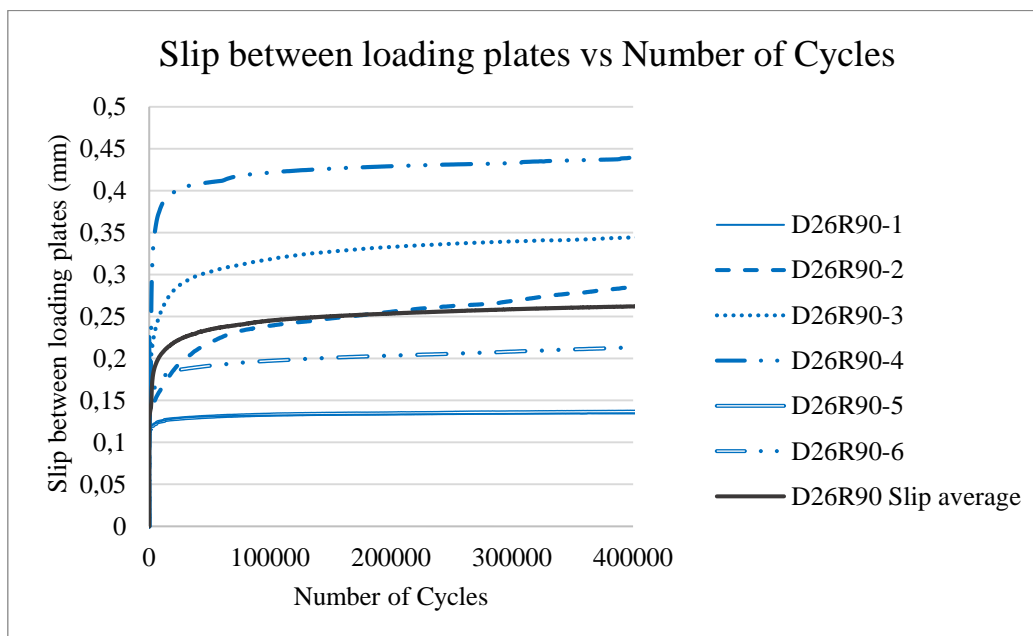


Figure 5.12: Slip between loading plates vs Number of Cycles for D26R90 series

D26SR90

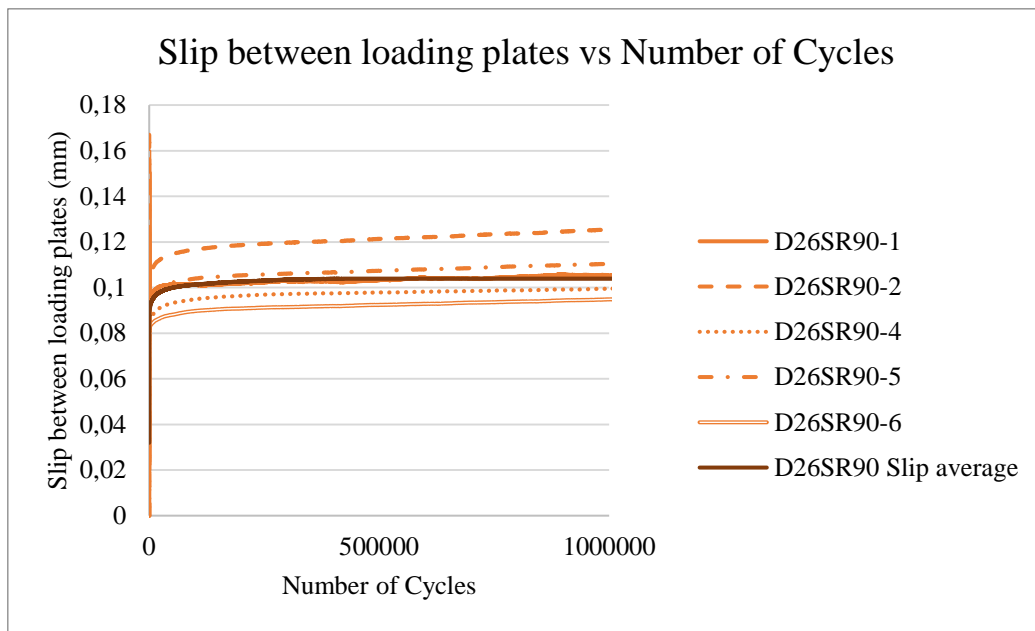


Figure 5.13: Slip between loading plates vs Number of Cycles for D26SR90 series

Comparison of mean lines

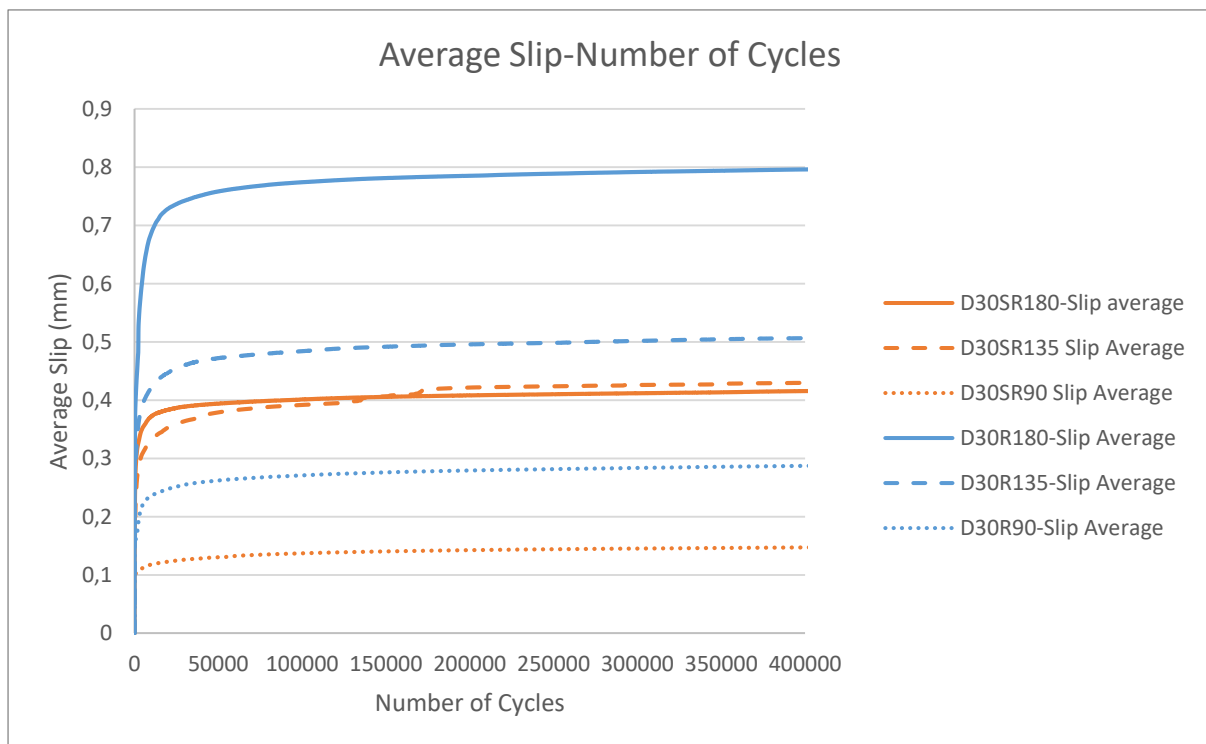


Figure 5.14: Comparison of mean slip line of specimens with geometry D30 with resin and steel reinforced resin

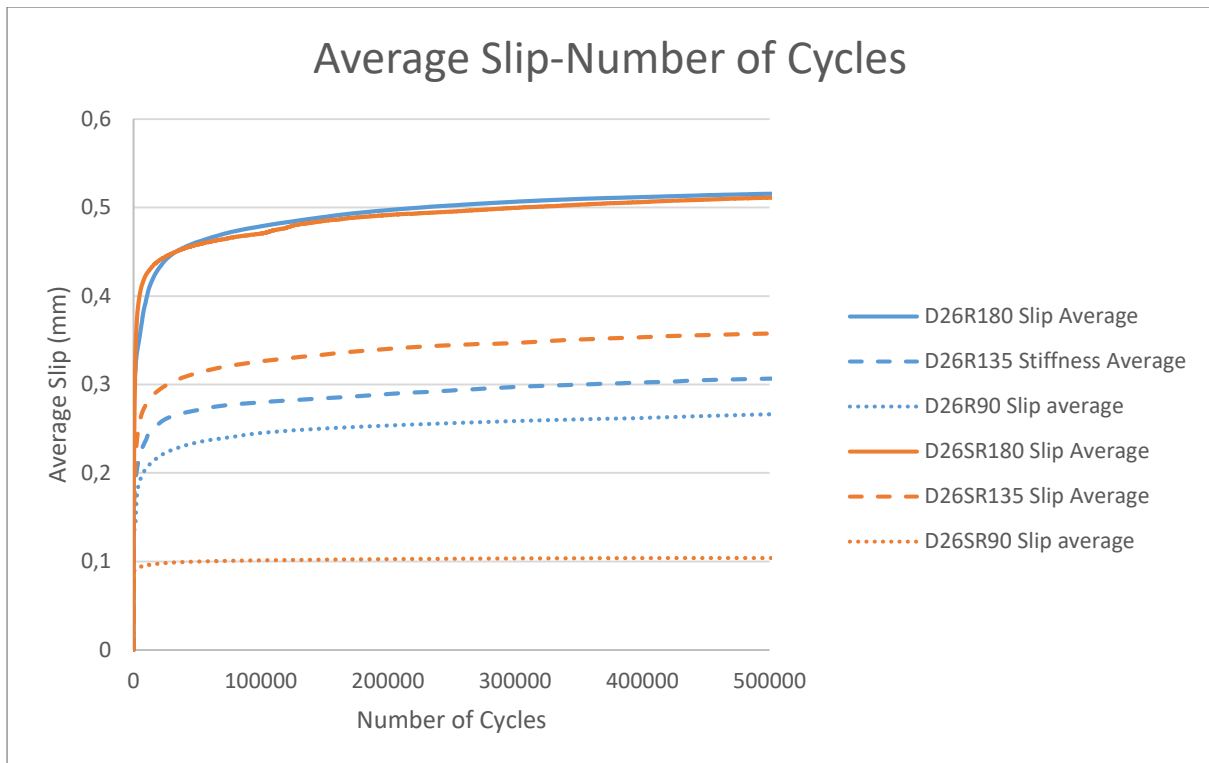


Figure 5.15: Comparison of mean slip line of specimens with geometry D26 with resin and steel reinforced resin

By considering all test data together and deriving the mean lines of slip accumulation over the number of cycles, a safe conclusion about the superiority of steel reinforced resin under cyclic loads, in terms of lower slip related to conventional resin cannot be drawn. Especially for the specimens with larger hole clearance (D30) the scatter is significant. The scatter is more prominent for the higher applied stress range (180MPa) as it can be seen from Figure 5.2 and Figure 5.3. The reason for such big scattering is attributed in large air inclusions which after visual observations when specimens dismantled, were larger in case of larger hole clearance. The reasons for scattering are presented in section 5.3. After the initial slip built-up in the first cycles, a stabilization of slip occurs in the range of 100.000-200.000 cycles indicating that there is no significant deterioration in material properties after this threshold as it can be seen from Figure 5.14, Figure 5.15.

Based on quasi-static phase of specimens and visual inspection an effort was done to exclude the specimens which considered as unreliable. The specimens with large air inclusions and specimens with irrelevant quasi-static behaviour were not considered. This consideration was done for the specimens with geometry D26 (6mm clearance). The results of this comparison are presented in following figures where relative displacement between loading plates as a function of the number of applied loading cycles at a nominal bearing stress range of 90,135 and 180 MPa for a specimen with $\varnothing 26$ mm hole.

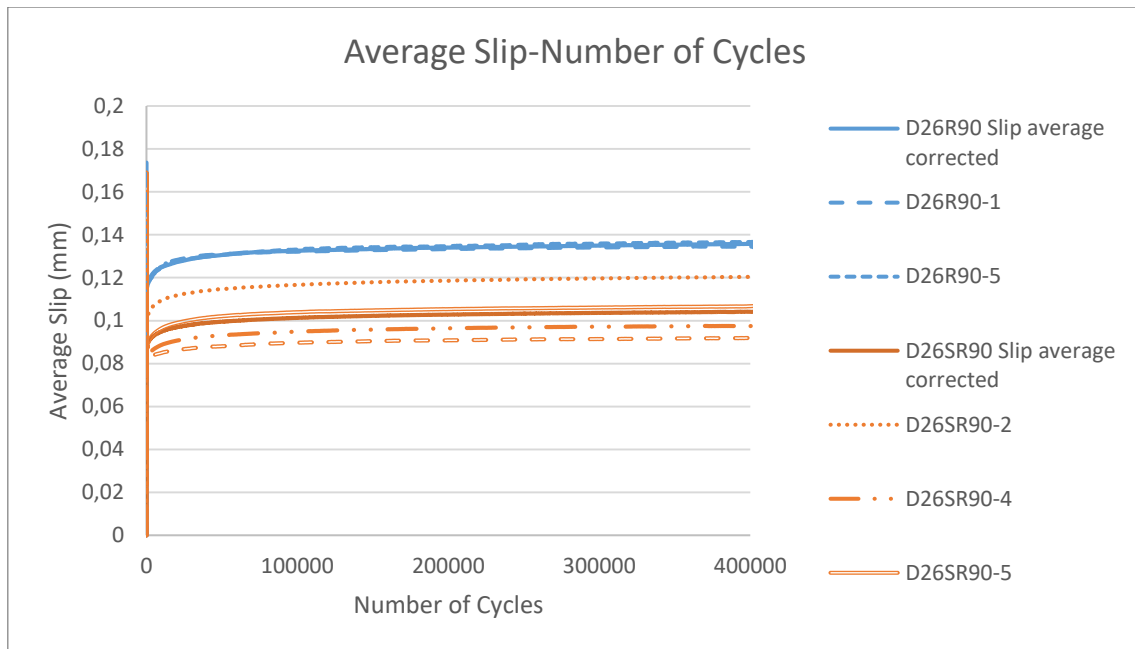


Figure 5.16: Relative displacement between loading plates as a function of the number of applied loading cycles at a nominal bearing stress range of 90 MPa for a specimen with $\varnothing 26$ mm hole

	Slip (mm) after 1 cycle	Slip(mm) at the end of quasi static phase (25 cycles)	Slip due to fatigue after 400.00	Total slip from 1 st to 400.000	Increase of slip (%) from 1 cycle to 4×10^5 cycles
D26R90-1	0.11	0.14			
D26R90-5	0.085	0.11			
Mean value	0.098	0.125			
D26SR90-2	0.047	0.074			
D26SR90-4	0.08	0.1			
D26SR90-5	0.074	0.099			
Mean value	0.067	0.091			

Table 5.4: Comparison of cyclic behaviour between DS6R90 and D26SR90 selected specimens

Mean slip reached after 4×10^5 cycles due to cyclic loads was 0.135 and 0.104 for selected specimens of D26R90 and D26SR90 respectively. The mean deformation had increased from 1st loading cycle to end of fatigue phase by 108% for resin and 114% for steel reinforced resin specimens.

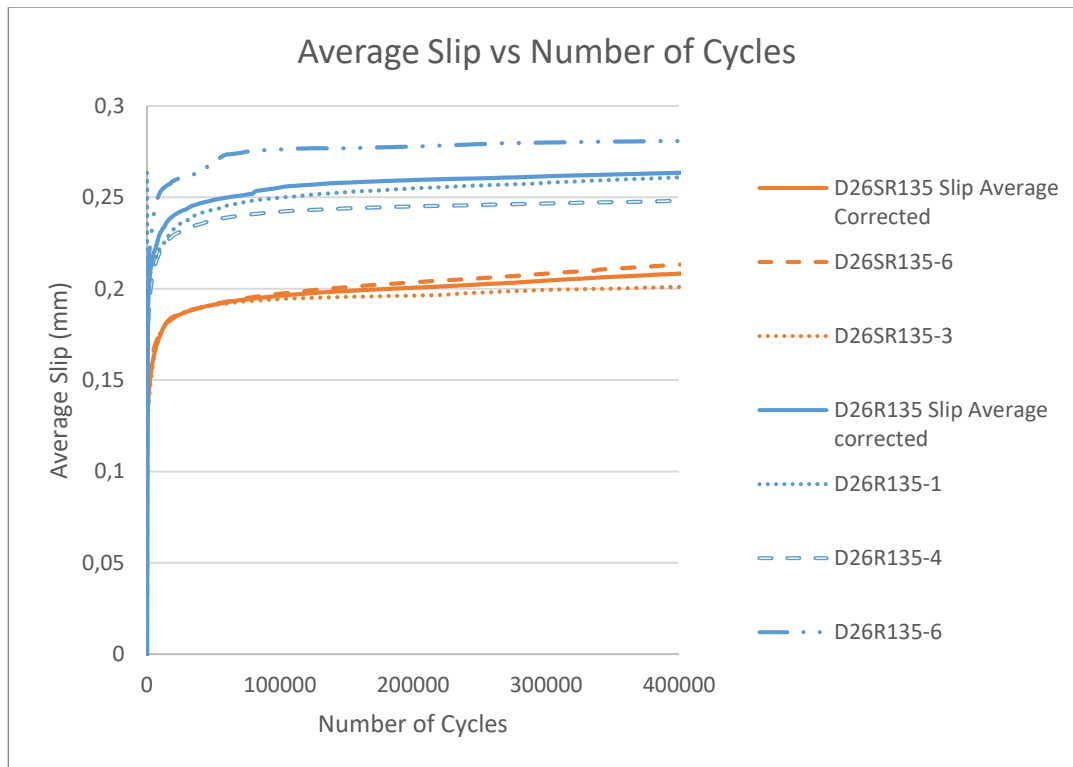


Figure 5.17: Relative displacement between loading plates as a function of the number of applied loading cycles at a nominal bearing stress range of 135 MPa for a specimen with $\varnothing 26$ mm hole

	Slip (mm) after 1 cycle	Slip(mm) at the end of quasi static phase (25 cycles)	Slip due to fatigue after 400.00	Total slip from 1 st to 400.000	Increase of slip (%) from 1 cycle to 4×10^5 cycles
D26R135-1	0.136	0.168			
D26R135-4	0.11	0.17			
D26R135-6	0.1237	0.158			
Mean value	0.123	0.165	0.263	0.428	62%
D26SR135-3	0.08	0.09			
D26SR90-6	0.056	0.078			
Mean value	0.068	0.089	0.208	0.297	233%

Table 5.5: Comparison of mean cyclic behaviour between DS6R135 and D26SR135 selected specimens

Mean slip reached after 4×10^5 cycles due to cyclic loads was 0.263 and 0.208 for selected specimens D26R135 and D26SR135 respectively. The mean deformation had increased from 1st loading cycle to end of fatigue phase by 62% for resin and 233% for steel reinforced resin specimens.

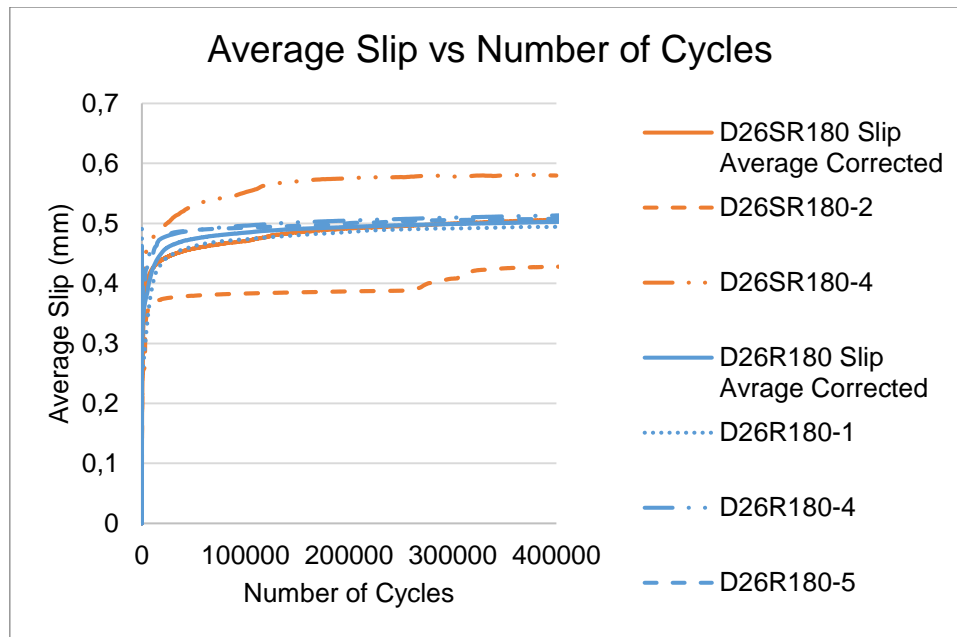


Figure 5.18: Relative displacement between loading plates as a function of the number of applied loading cycles at a nominal bearing stress range of 180 MPa for a specimen with $\varnothing 26$ mm hole

	Slip (mm) after 1 cycle	Slip(mm) at the end of quasi static phase (25 cycles)	Slip due to fatigue after 400.00	Total slip from 1 st to 400.000	Increase of slip (%) from 1 cycle to 4x10 ⁵ cycles
D26R180-1	0.278	0.4			
D26R180-4	0.167	0.3			
D26R180-5	0.23	0.33			
Mean value	0.23	0.34	0.502	0.732	215%
D26SR180-2	0.083	0.13			
D26SR180-4	0.13	0.163			
Mean value	0.111	0.146	0.506	0.617	450%

Table 5.6: Comparison of cyclic behaviour between DS6R180 and D26SR180 selected specimens

Mean slip reached after 4×10^5 cycles due to cyclic loads was 0.502 and 0.506 for selected specimens of D26R180 and D26SR180 respectively. The mean deformation had increased from 1st loading cycle to end of fatigue phase by 215% for resin and 450% for steel reinforced resin specimens.

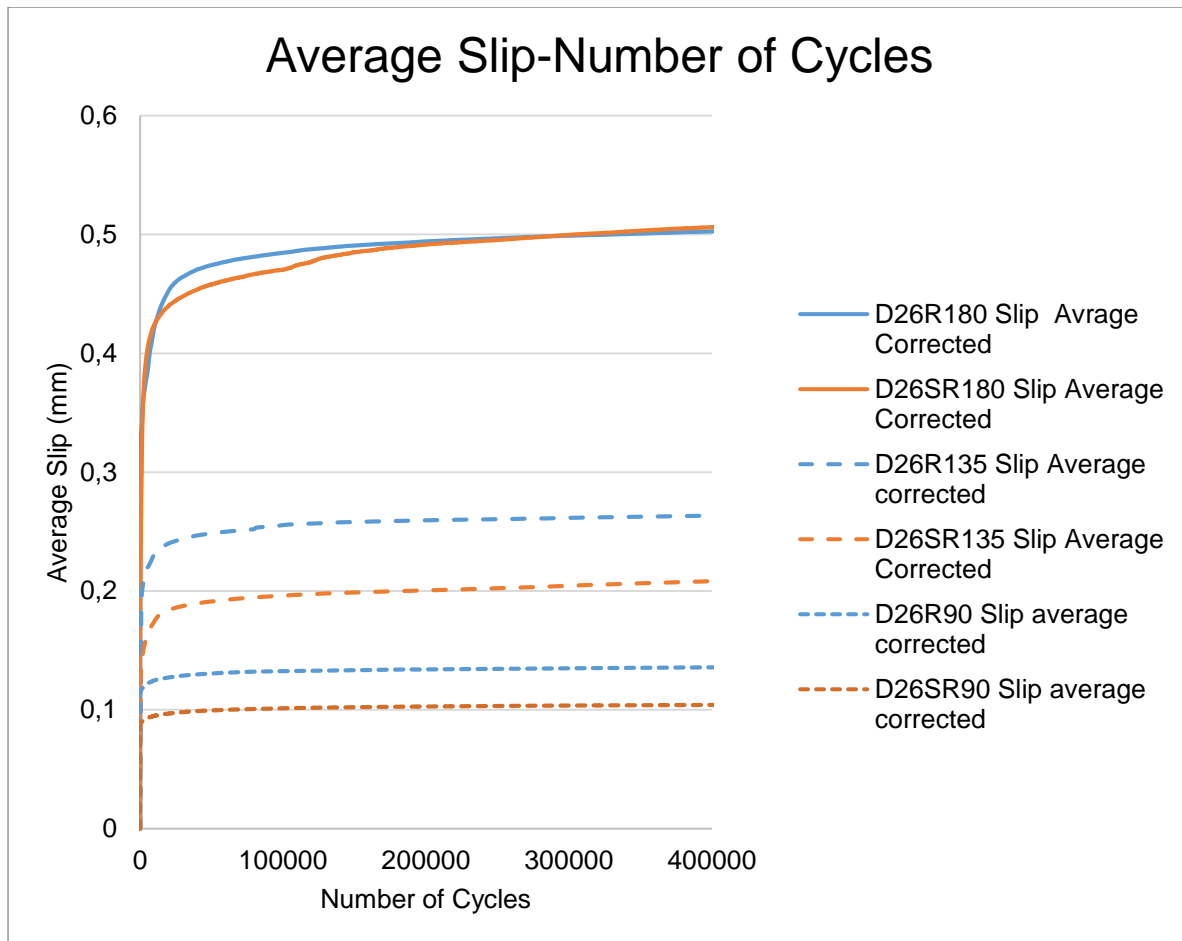


Figure 5.19: Comparison of mean lines of slips of selected specimens for all stress ranges

Specimen type	Mean Slip after 400.000 cycles (mm)	Difference in mean slip (%) between SR and R for same geometry
DS6-R-90	0.135	-24%
D26-SR-90	0.104	
D26-R-135	0.263	-20.95%
D26-SR-135	0.208	
D26-R-180	0.502	+0.5%
D26-SR-180	0.506	

Table 5.7: Summary of results in mean slip after 400.000 cycles for geometry D26 (6mm hole clearance)

As it can be seen from Figure 5.19 and Table 5.7 after 400.000 cycles (1 day of testing) for specimens with nominal bearing stress range of 90 MPa the reached slip in case of steel reinforced resin is 24% lower than of conventional resin. For nominal bearing stress range of 135 MPa the decrease in slip is 20.95% when using steel reinforced resin instead of conventional (Figure 5.19). In the maximum bearing stress range the slip accumulation and

the final slip after 400.000 cycles is the approximate the same. It should be noted that the remaining slip at the end of quasi-static loading phase is smaller for specimens with steel reinforced resin, so the specimens have a different starting point but the final slip (after 400.000 cycles) is the same. Therefore, the slip has increased by 450% and 215% (Table 5.6) compared to the remaining deformation after the end of quasi static phase for the steel-reinforced resin-injected and resin-injected specimens, respectively. This may be attributed to the different Poisson's ratio between steel-reinforced (0.22) and conventional resin (0.3). The lower ν of steel reinforced resin leads to higher 3-D stresses, which leads to earlier onset of plastic material behavior compared to the case of conventional resin.

From these preliminary tests no generic conclusion can be drawn yet on the superiority of steel-reinforced resin compared to conventional resin in an injected bolted connection subject to cyclic loading and further research is necessary to support or reject this hypothesis. Due to big scatter especially for the specimens with the larger hole clearance (D30) the results are not so reliable to support such statement. From a selection of test data from D26 series based on the quasi-static phase and visual observations of the external of resin (or steel reinforced resin) part it seems that use of steel-reinforced resin to the connection leads to less slip up to 400.000 cycles especially for medium or low bearing stress ranges, but the complex stress-state inside the resin part especially in the maximum allowing long term bearing stress (200MPa) has an unknown effect in fatigue properties of steel reinforced resin compared to conventional. Therefore, the material properties under cyclic loads for resin and steel reinforced resin have to be derived with proper testing and modeling.

To improve this test set-up in order to obtain more reliable data in future testing an investigation was carried out to find the possible reasons for scattering based on observations of specimens before and after testing 5.3. Based on the suggested reasons some recommendations for improvement are given.

To overcome as possible the scatter of testing data a statistical evaluation of data was performed based on probabilistic models selected in literature review. This analysis is presented in chapter 6. Since the number of specimens is relatively low, and the scatter was big all results were considered together for statistical analysis. Based on derived S-N curves an effort made to distinguish between resin and steel reinforced resin which was not possible based on diagrams of slip accumulation over tested number of cycles.

5.3 Possible reasons for scattering in the experimental results and recommendations for future improved set-up

As it can be seen from the experimental results for accumulated slip between plates of set-up, measured by the LVDT's, as well as for normalized stiffness of specimens, there is a substantial scattering between the results for specimens of same nominal geometry and same applied stress range both for resin and steel reinforced resin. The scattering is more prominent in case of larger hole clearances (D30) and for higher applied stress range (180 MPa). This scatter in fatigue of resin test data, is in contrast with the scattering in metallic structures where according to research of J. Schijve from TU Delft [59], scatter was larger at low stress amplitudes and lower at high amplitudes as shown by Figure 5.20. In this section possible reasons of scattering due to defects of injection material and test set-up are discussed.

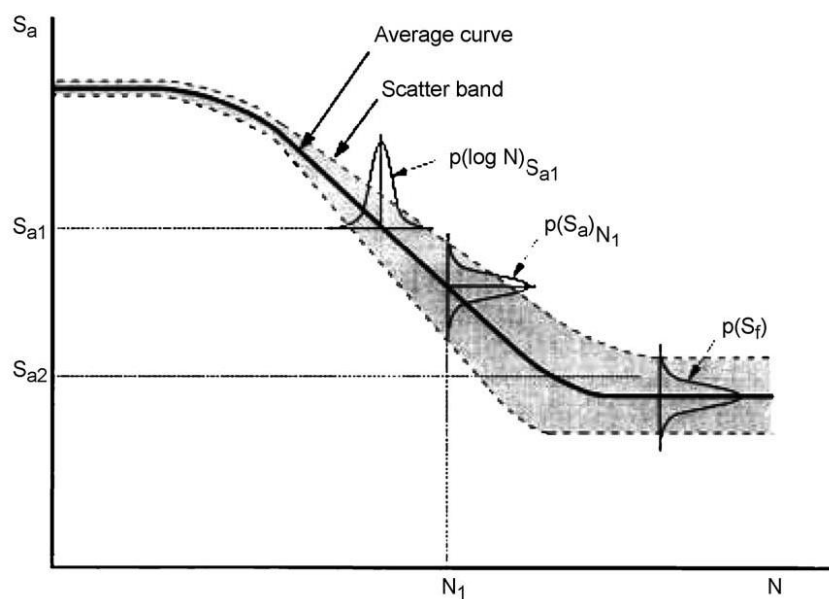


Figure 5.20: Influence of scatter in an S-N curve [59] for steel details (p corresponds to the probability of failure; r_f is the fatigue limit stress)

The injection of specimens is applied through hole ($\varnothing 6\text{mm}$) drilled in the first Perspex side plate when the specimen is positioned horizontally. The escape path of the air and the resin when the injection is completed, is ensured by hole ($\varnothing 2\text{mm}$) in the second Perspex plate in higher position than resin entrance hole (Figure 5.21).

A possible reason for scattering in the experimental results (Figure 5.22) is the inclusion of air voids in the body of resin part after injection and curing due to the position of escape path in the Perspex plate. This agrees with the statement of Nijgh that there must be an air escape path/channel at each highest point bounded by horizontal restraints, as illustrated in Figure 3.23 (section 3.3). This hypothesis becomes stronger by the visual observation of several D30R resin parts which revealed large air inclusions especially at the sides as it can be seen in Figure 5.23.

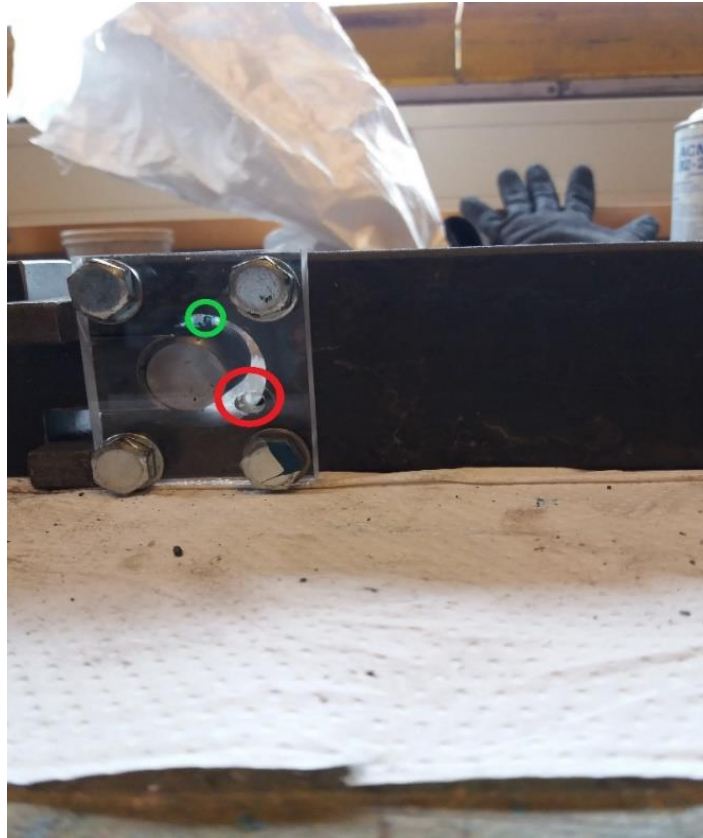


Figure 5.21: Specimen ready for injection. Highlighted in red the injection hole in first Perspex plate, and in green the escape hole in the second Perspex plate in the back side of specimen

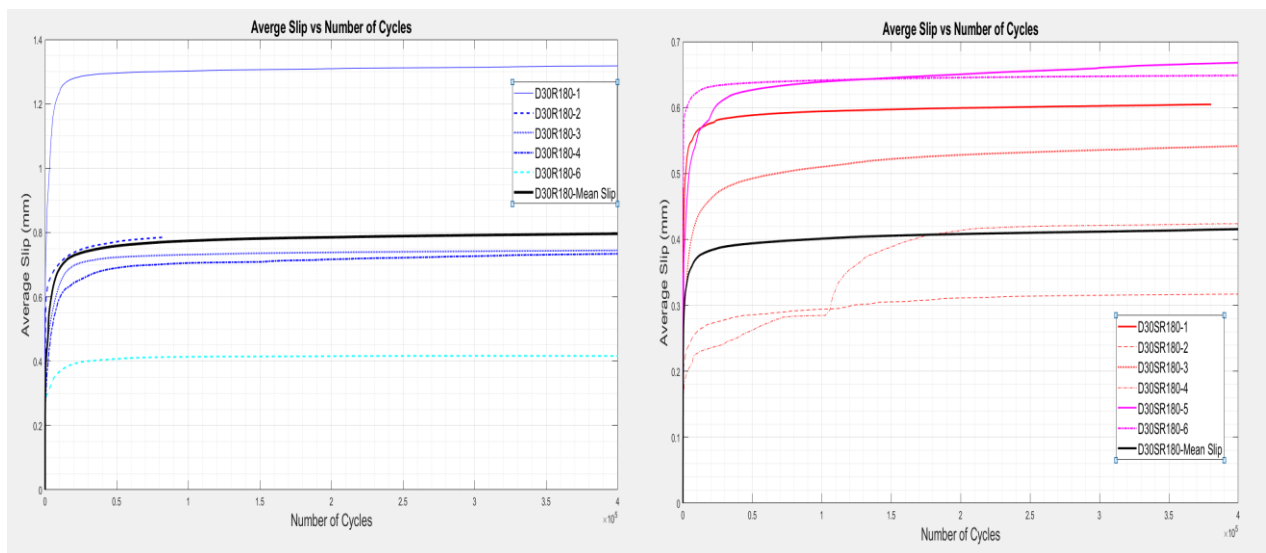


Figure 5.22: Average Slip vs Number of Cycles for specimen series D30R180 (left) and D30SR180 (right) where the scatter is more prominent

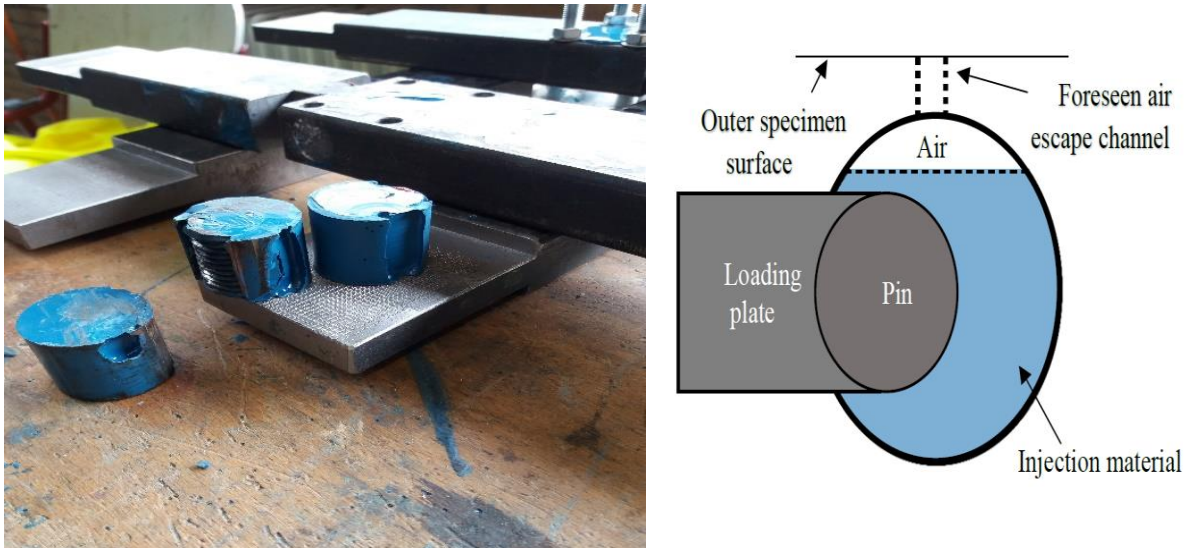


Figure 5.23: Left-Air inclusions in resin samples. Right- Visualization of air inclusions and future alternative escape path [67]

Furthermore, a resin sample with the bolt part extracted from a D26R specimen and investigated for possible voids inside the body of resin. For this the sample placed inside a CT scan with the help of TU Delft professor W. Gard. This allowed to visualize the resin layer in three dimensions through differences in density which made visible by the reflection of radiation. In Figure 5.24 the result of a CT scan on an injection bolt is shown. Here the presence of small air inclusions can be seen in the resin layer orange color. It should be noted that the large parallel to threads orange parts are not air inclusions since steel absorbs a lot more radiation than resin and this does not allow us to observe the area close to bolt part for voids.

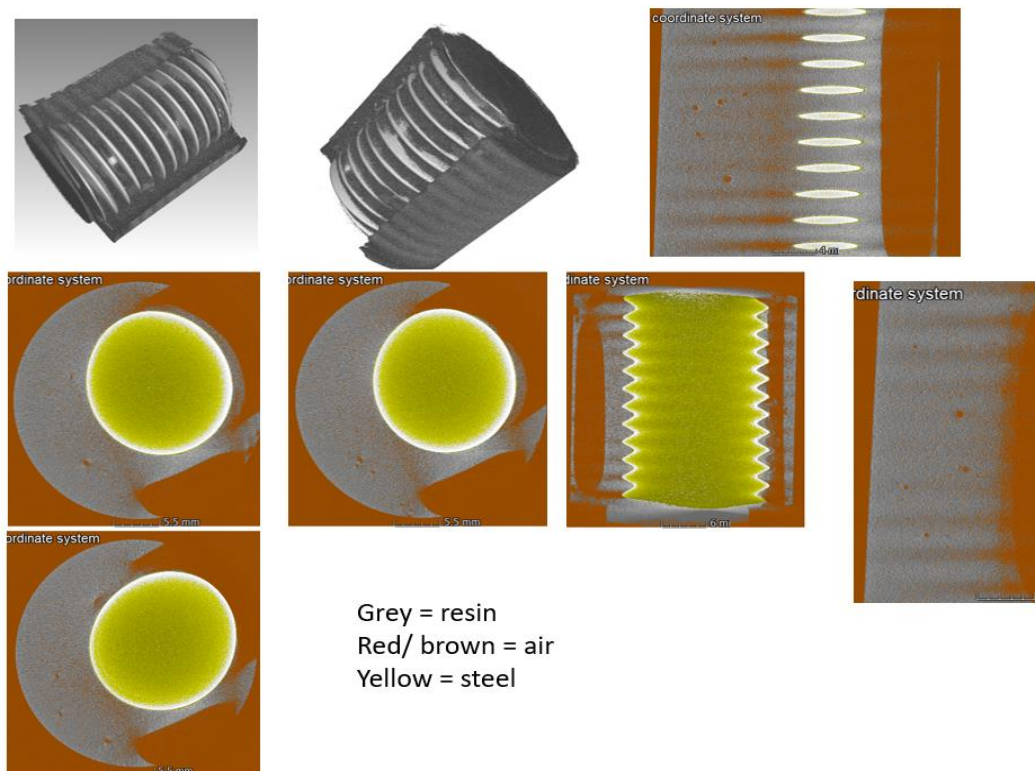


Figure 5.24: CT-scan of sample with injection resin part around a bolt part with void in resin layer



Figure 5.25: The examined in the CT scan sample with the outside missing resin part at the side

From the Figure 5.24 it is clear that there are defects in form of small air inclusions which are not large therefore, the main reason for scattering are the large missing resin parts in the side of resin as can be seen from Figure 5.25

For this reason, an alternative air escape path drilled in the lower plate may would be a solution to avoid such voids. This was applied in 3 specimens, namely D30SR135-3-4-5 with promising results since the slip curves are similar and the visual inspection revealed compact and without external defects resin parts (Figure 5.26,Figure 5.27).



Figure 5.26: Alternative air escape path (left) and compact resin specimens after the application of the improved solution

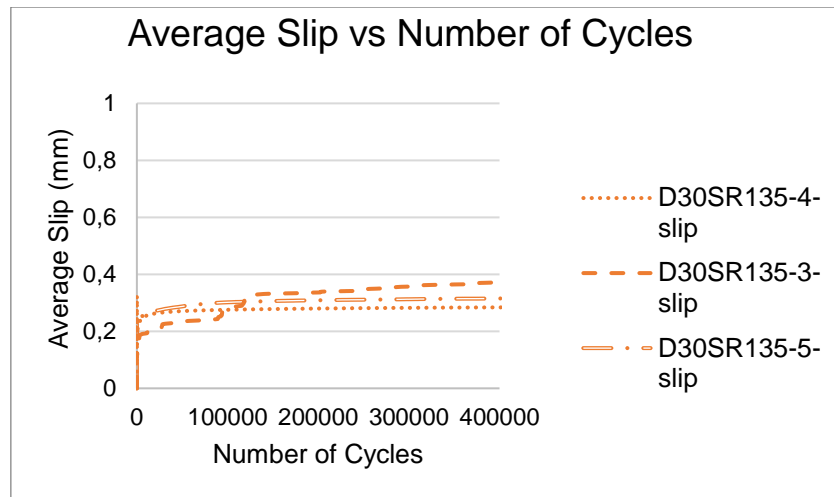


Figure 5.27: Results of slip vs number of cycles for the specimens with the alternative escape path which mitigate the scatter

A second possible reason for scattering may lie in the assembly of specimen. Since the upper and the lower plate are not fixed in position as in the case of actual shear connections where the tightening of the bolts results in placing of all parts in line. In the case of the set-up at hand a possible deviate of the plates from the central horizontal axis is possible as illustrated in Figure 5.28. After the injection and the curing of resin this angle between upper and lower plate remains and the assembled specimen is not in straight line. When the specimen with this angle defect are placed in the Hydraulic Wedge Grip machine, they are forced to aligned by the wedges of the machine. This forced alignment creates cracks in the resin part like the specimen in Figure 5.29. This specimen placed at the machine and fixed by wedges and removed before the start of loading revealing cracks due to the alignment of upper and lower plate in straight line. These cracks are not supposed to appear in nominal geometry of specimen where upper and lower plate are in line in a perfect specimen assembly.

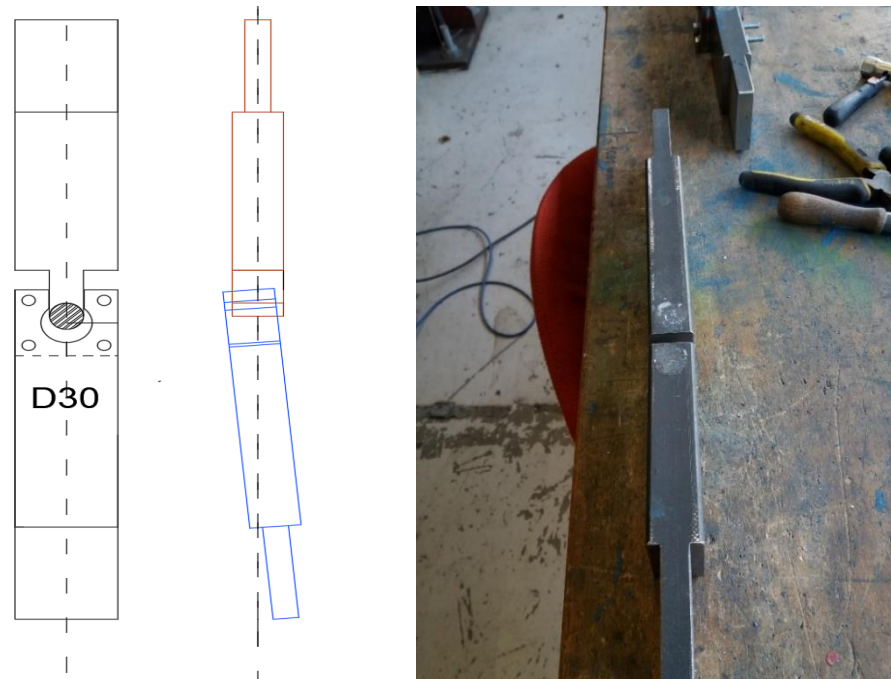


Figure 5.28: Left-Drawing of angle defect (not to scale). In blue the lower plate not in straight line with the red upper plate. Right-The defect in an actual specimen



Figure 5.29: Crack due to misalignment after the position of specimen to the wedges, highlighted in red. The specimen was placed in machine fixed by wedges and removed before start of loading revealing the cracks

A solution for this defect, in order to obtain a reliable specimen could be a special frame-base for the preparation and assembly and injection of the specimen. This would place upper and lower plate in the same line, preventing a possible misalignment during injection. A special care could be given to facilitate the positioning of plates to the desired place according to the geometry of specimen as explained in section 3.3, by engraved lines in the base plate (Figure 5.30).

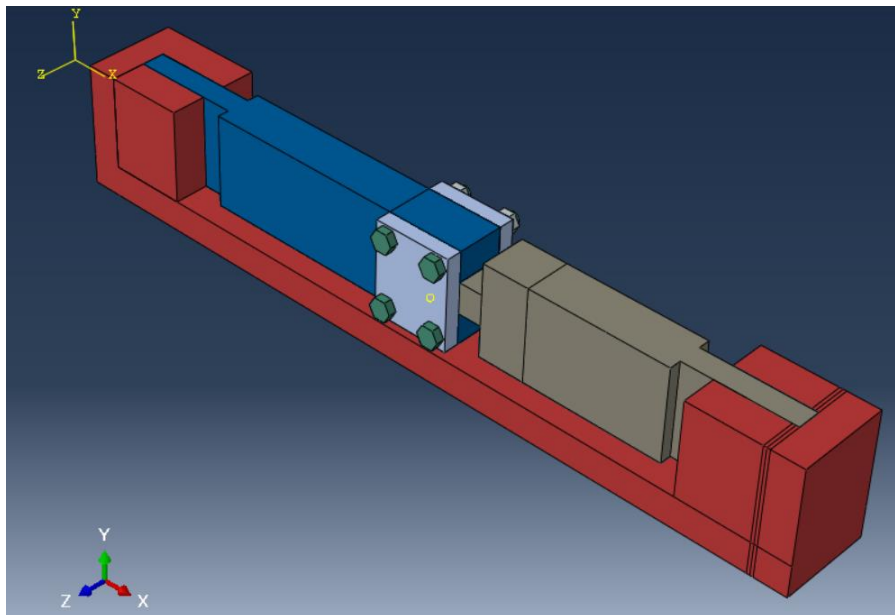


Figure 5.30: Visualization of proposed base (in red) for assembly of specimen

A final possible reason for scattering may be the fact that the upper plate and the bolt part which has threads are two separated parts and the bolt is positioned manually in the special reception of upper plate and stay in place with the use of clay and it is not fixed. Therefore, a rotation of the bolt part in its position is possible which results in a non-uniform distribution of stresses and an even more complex stress state in the resin when it is loaded with the cyclic loads, and has non-predictable effects in the results (Figure 5.31)

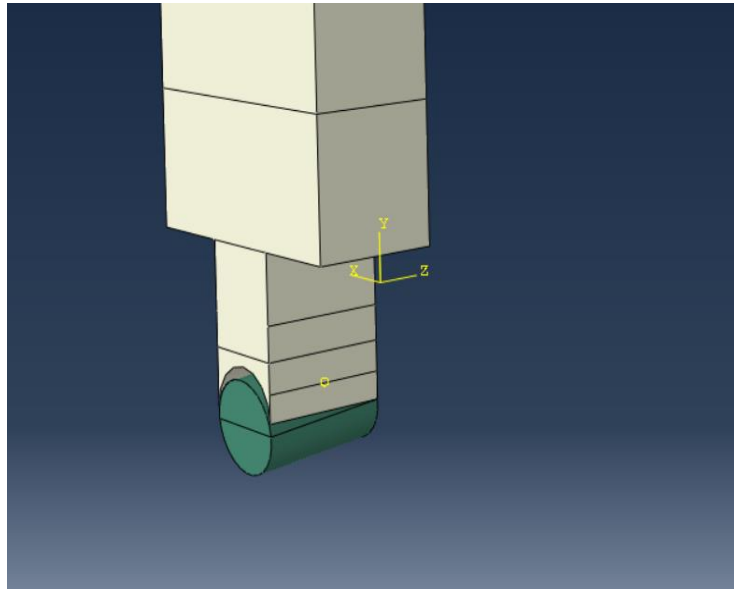


Figure 5.31: Visualization of the defect of position of the bolt part in the reception of upper male plate

A solution to this defect could be a slightly different and improved set-up for the future research namely a specimen without separated bolt part and upper plate, but in one piece to avoid this possible rotation (Figure 5.32). A drawback of this is that is difficult to include threads in such specimen.

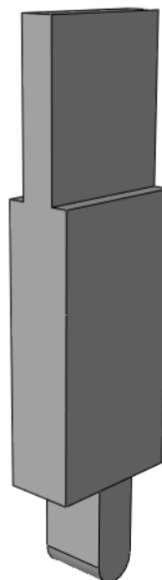


Figure 5.32: Improved upper plate for future specimens (visualization)

5.4 Behaviour of specimens in high cycle fatigue

Two specimens were left in the machine for several days offering results for high cycle fatigue of the resin. In terms of slip vs Number of cycles (Figure 5.33) for $N=400,000$ the slip due to cyclic loading is $\delta u_{400000}=0.5\text{mm}$ while for $N=6,000,000$ (14 days of testing), slip is $\delta u_{6000000}=0.529\text{mm}$ which is a 5.8% increase in slip for 1400% increase in the number of cycles. In fact, increase in slip stops after 3 million cycles and after that point slip slightly reduces.

Specimen D30SR90-5 left for $N=4,285,540$ (9 days) and the slip vs number of cycles presented in Figure 5.34. In terms of slip due to cyclic loading, for $N=400,000$ the slip is $\delta u_{400000}=0.09\text{mm}$ while for $N=4,285,540$ slip is $\delta u_{6000000}=0.1\text{mm}$ which is an 11% increase in slip for a 970% increase in number of cycle.

In both cases after an initial built-up period of 500000 cycles there is no virtually slip change over the next million cycles. This indicates that the future testing program should be designed to last at least for some million cycles for example 2×10^6 which define the fatigue life of steel details in real applications. The preliminary tests of the current experimental program provide results up to 400.000-500.000 cycles.

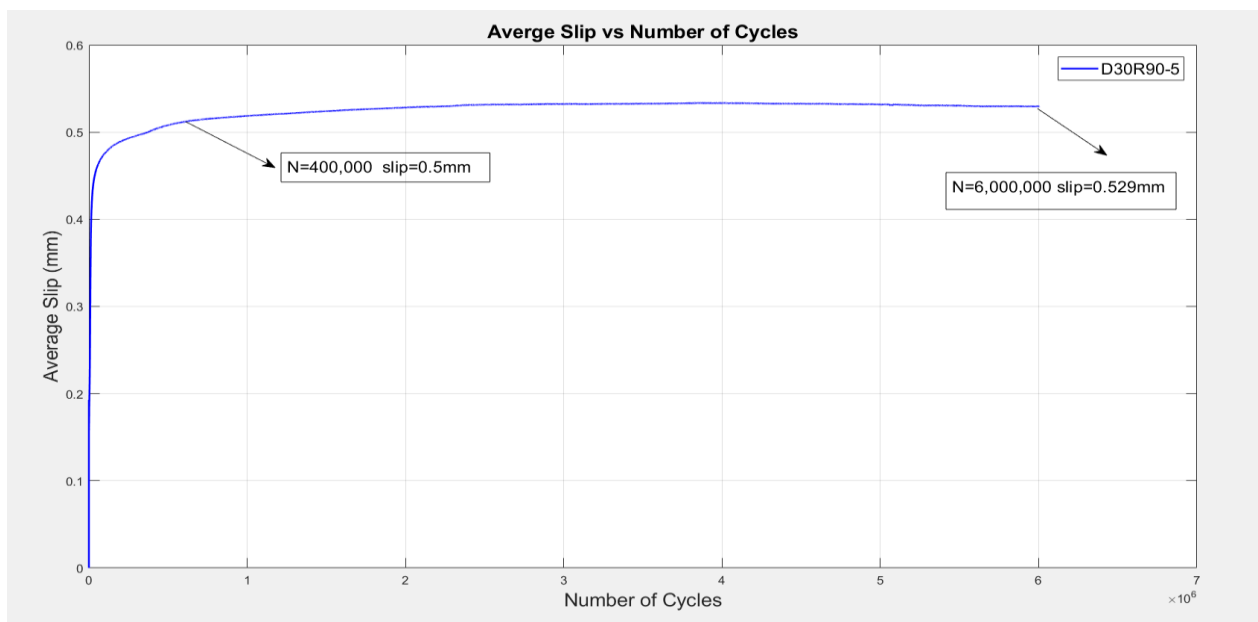


Figure 5.33: Plot of Slip vs Number of cycles for specimen D30R90-5 which left in the machine for 6 million cycles

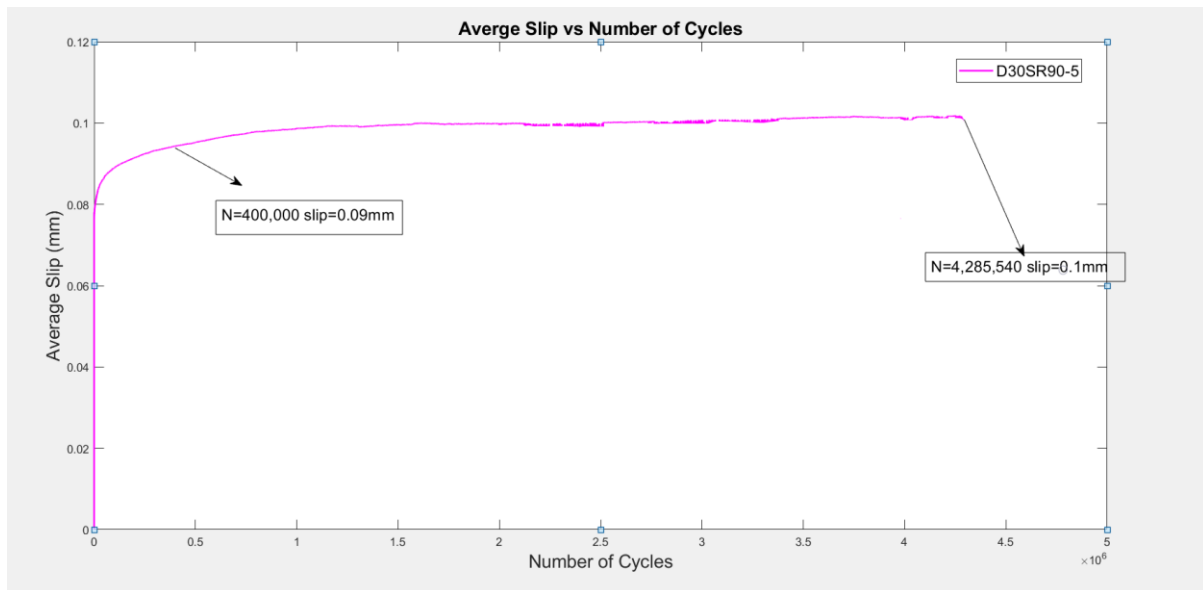


Figure 5.34 Plot of Slip vs Number of cycles for specimen D30SR90-5 which left in the machine for 4 million cycles

5.5 Conclusions of experimental results

In total 63 specimens were tested, with half of them injected with conventional resin and the other half injected with steel reinforced resin, in two different geometries namely D26 (6mm hole clearance) and D30 (10mm hole clearance). The nominal stress ranges applied in the specimens were 180, 135 and 90 MPa. All the experiments carried out in two phases. A quasi-static phase with frequency 0.05 Hz and $R=0.1$ for 25 cycles, followed by a fatigue loading phase in form of a sinusoidal history compression-compression load with $f=5\text{Hz}$ and $R=0.1$. Two LVDT's (Linear Variable Displacement Transducers) at every side of specimens offered measurement results for the relative displacement between upper and lower plate, and the mean between two measurements is considered to be the slip of connection.

From the quasi-static phase analysis of results, the initial stiffness of specimens was calculated. The experimental initial stiffness was in a good accordance with the numerically calculated initial stiffness, which allowed the validation of numerical model. Specifically, the difference between mean experimental and numerical initial stiffness was 0.87% and 0.12% for resin and steel reinforced resin respectively in 10mm oversized hole (geometry D30R-SR). For geometry D26R and D26SR the difference was 3.24% for the former and 8% for the later. In all cases the mean experimental initial stiffness was lower than numerical. The standard deviation between experimentally obtained initial stiffness of specimens with same geometry and same stress range was quite significant indicating a scatter in the results which was observed also in results of fatigue loading phase.

As it was expected from the previous research at TU Delft and confirmed in the current, the use of steel reinforced resin leads to higher connection stiffness since specimens D26SR (steel reinforced resin in 6mm hole) had 58% higher mean initial stiffness related to specimens with conventional resin and same geometry. For higher hole clearance this was more prominent since the difference between mean experimental initial stiffness of steel reinforced resin and conventional resin injected specimens was 78%. Therefore, as a starting point for fatigue analysis the steel reinforced resin results to stiffer connection. This confirmed at the end of quasi-static analysis since after 25 cycles all specimens with steel reinforced resin had

lower remaining slip related to specimens with conventional resin for same geometry and stress range. Also, it was confirmed the result of previous research in demountable shear connectors with use of injection bolts, that the use of oversized holes reduces the initial stiffness of connection, since for a 4mm increase in hole clearance (from D26 to D30) there is a 26% and a 13% decrease in mean experimental initial stiffness in case of resin and steel reinforced resin respectfully.

The results of accumulated slip due to cyclic loads over the tested number of cycles and the resulting normalized stiffness over the number of cycles were presented for all specimen geometries and stress ranges. The experiments last for approx. 400.000 cycles (1 day of testing) for most of specimens and almost all of them reached the failure criterion of 0.3mm slip. For the specimens which didn't reach this limit the tests run until 10^6 before considered as run-outs. The scatter in test data is big and more prominent for specimens with larger hole (D30) clearances and higher stress range.

Based on quasi static phase and visual observations of specimens D26 (6mm hole clearance) where the scatter was not so large as for bigger hole clearance, a limited number of specimens were considered reliable and the mean lines of slip were plotted based only on those, to offer some preliminary results for the slip gained after cycles of fatigue loading. From this effort it was observed that after 400.000 cycles the specimens with steel reinforced resin had a slip 24% and 20.95% lower related to specimens with conventional resin for low and medium stress ranges of 90 and 135 MPa respectfully. The mean lines of selected specimens loaded with the higher stress range of 180MPa were almost the same with both resins and the remaining slip after 400.000 cycles were 0.5mm in both cases. The fact that after the end of quasi static phase (25 cycles) the specimens with steel reinforced resin had less remaining slip indicated that the steel-reinforced resin-injected specimens undergo relatively larger additional relative displacement (+450%) due to cyclic loading compared to the resin-injected specimens (+215%). This is attributed to lower Poisson ratio of steel reinforced resin (0.22) compared to conventional (0.3) which leads to higher deviatoric stresses which affect the more the cyclic elastic-plastic behavior.

Two specimens one with resin and one with steel-reinforced resin with low stress range (90MPa) were tested for 6×10^6 and 4.3×10^6 cycles respectively offering results in high-cycle fatigue of specimens. The slip stabilized after 500.000 cycles indicating no significant mechanical deterioration in both cases. The remaining slip at the end of 6 million cycles was 5% higher related to that at 400.000 for resin-injected specimen, while the slip after 4.3 million cycles was 11% higher related to that at 400.000 cycles for steel reinforced resin specimen.

Due to limited number of cycles of experiments and the significant scattering a total conclusion about the fatigue superiority of steel reinforced resin can't been drawn. The indications are promising about steel reinforced resin in fatigue behaviour but testing of specimens at least at 2 million cycles which is the relevant number in engineering practice and testing and numerical analysis in order to find out the fatigue material properties of both resins are required. Therefore, the current study can be considered as preliminary. The scatter is attributed to large air inclusions due to position of air escape channel, to cracks in resin part due to relative rotation of upper and lower plate and to a possible rotation of the bolt part which is not fixed to the upper (male) plate. To improve the quality of data and mitigate the scatter three improvements at the novel test set-up proposed by the author. The 1st one related to the position of escape air escape channel at the top steel plate and not at the side Perspex plate since the injection is done horizontally, has tested already and lead to a reduction in scatter and visually observed compact specimens without externally missing parts. An effort to overcome scatter based on statistical analysis is done in next chapter.

6 Statistical evaluation of test results

6.1.1 Overview of S-N curves obtained by test data

The mean and probabilistic S-N curves were obtained by a statistical analysis performed using two methods selected from literature review (section **Error! Reference source not found.**).

- According to principles of American Testing Standards (ASTM E739-91 [52]) to obtain fitted and characteristic curves
- According to the study of C.R.A. Schneider and S.J. Maddox [56] using a linear regression analysis to obtain the fitted curve and a probabilistic analysis using Student's t distribution.

The two methods were used for comparison purposes since there are no available fatigue data for the resins under investigation. Two failure criteria were used namely the selected 0.3 mm slip which is adopted based on Annex G of EN 1090-2 [3], where a 0.3 mm creep slip should not be exceeded during design life of structure, since fatigue performance of Resin Injected Bolted Connections should be determined against a long-term bearing resistance that is relevant at the end of structure's design working life. For comparison purposes a second failure criterion of 0.25 slip used. The specimens which did not reached the failure criteria after $N=10^6$ cycles were considered as run-outs and left out of the fatigue probabilistic analysis.

Since the number of tested specimens was relatively low and the scatter as it can be seen in previous chapter is very significant, all results were considered together to propose a fatigue characteristic curve with the selected 95% probability of survival of specimens. ASTM E739-91 covers only S-N relationships that may reasonably approached by a straight line only in the specific interval of testing and do not recommends to extrapolate the S-N curve outside this interval. This statement is adopted also in present analysis and the obtained curves are presented in the interval 0-500.000 cycles. For comparison also, the fatigue detail categories 112 and 90 suggested by EN 1993-1-9 for Injected Double Lap shear connections preloaded and non-preloaded respectively will be presented. It should be mentioned that the fitted curves obtained with ASTM proposed method and with linear regression analysis from Schneider and Maddox *are exactly the same*.

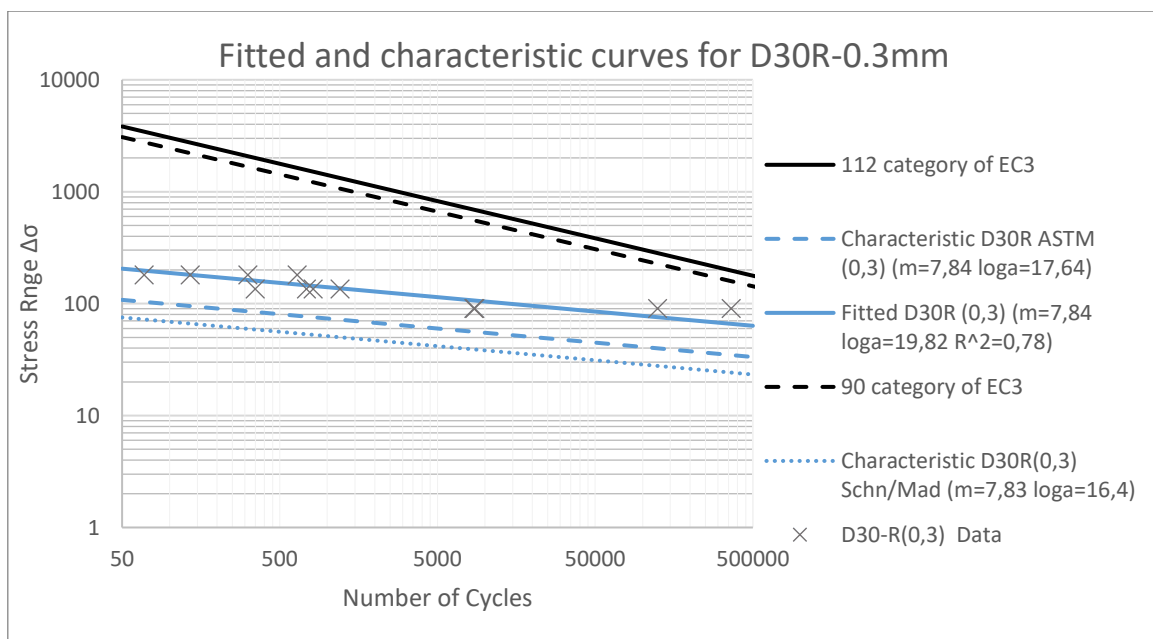


Figure 6.1: Statistical analysis of D30-R specimens with failure criterion 0.3mm

The fitted curve of specimens D30-R with failure criterion 0.3mm tested in stress range regime 180-135-90 MPa according to regression analysis is:

- $\log N = 19.82 - 7.84 \log \Delta \sigma$ with $R^2 = 0.78$ which indicates a relatively good fit between the linear regression line and the test results data since 78% of $\log N$ can be explained by $\log \Delta \sigma$.

The characteristic curves obtained through mean (fitted) curve with 95% probability of survival are:

- $\log N = 17.64 - 7.84 \log \Delta \sigma$ from ASTM E739-91 analysis
- $\log N = 16.40 - 7.84 \log \Delta \sigma$ from Schneider and Maddox analysis

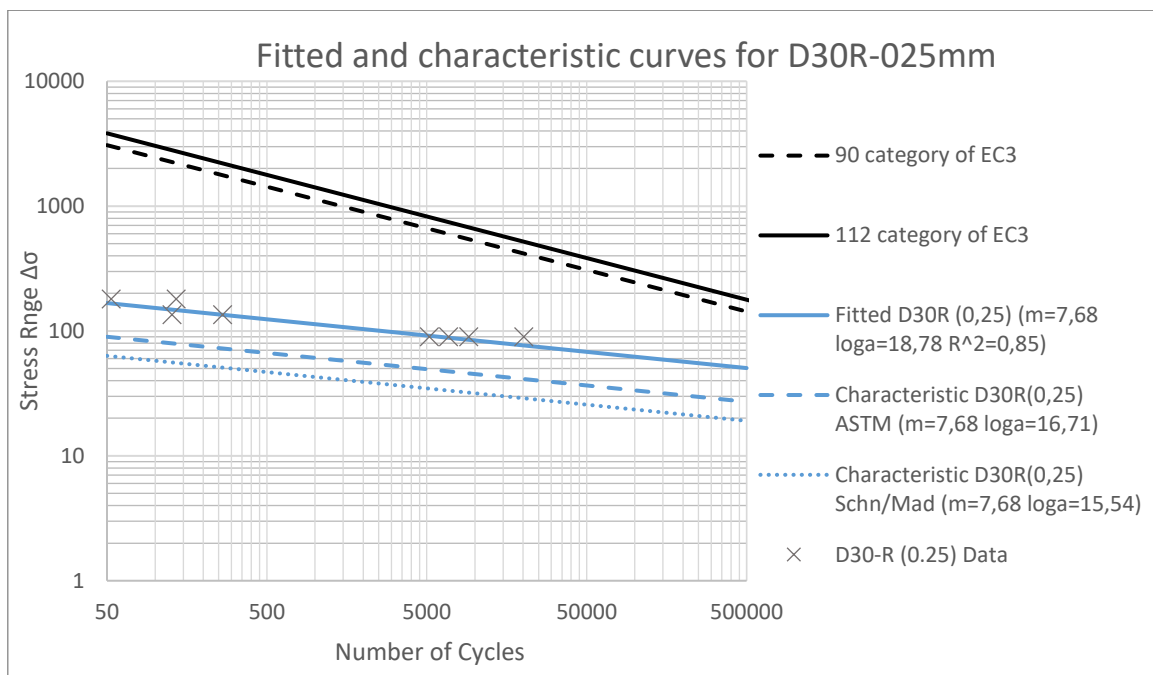


Figure 6.2: Statistical analysis of D30-R specimens with failure criterion 0.25mm

The fitted curve of specimens D30-R with failure criterion 0.25mm tested in stress range regime 180-135-90 MPa according to regression analysis is:

- $\log N = 18.78 - 7.68 \log \Delta \sigma$ with $R^2 = 0.85$ which indicates a good fit between the linear regression line and the test results data since 85% of $\log N$ can be explained by $\log \Delta \sigma$.

The characteristic curves obtained through mean (fitted) curve with 95% probability of survival are:

- $\log N = 16.71 - 7.68 \log \Delta \sigma$ from ASTM E739-91 analysis
- $\log N = 15.54 - 7.68 \log \Delta \sigma$ from Schneider and Maddox analysis

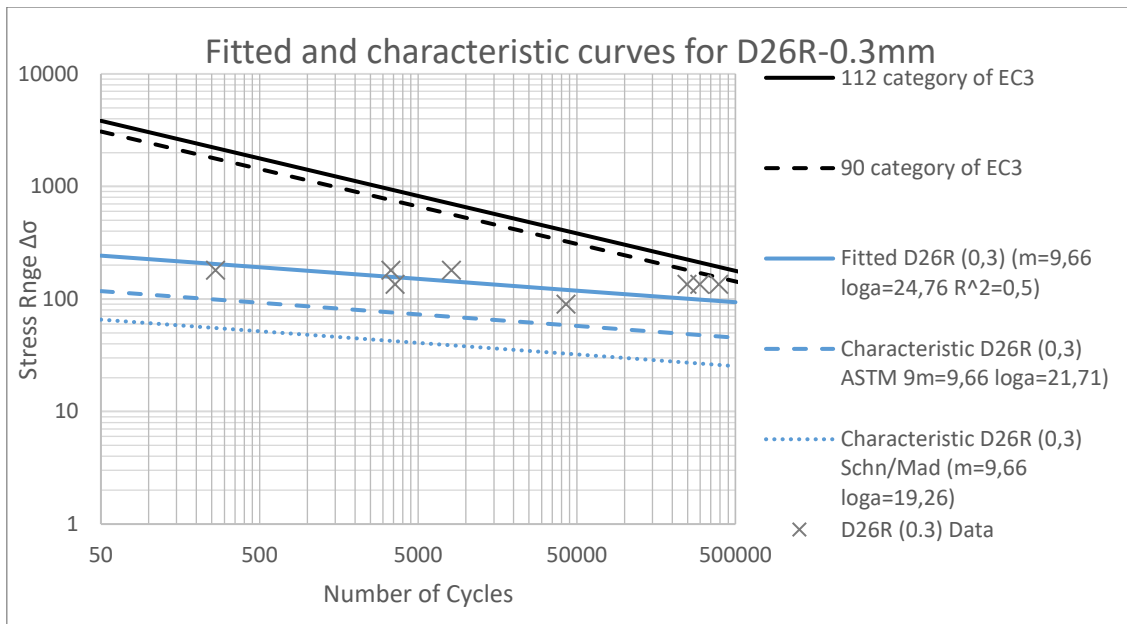


Figure 6.3: Statistical analysis of D26-R specimens with failure criterion 0.3mm

The fitted curve of specimens D26-R with failure criterion 0.3mm tested in stress range regime 180-135-90 MPa according to regression analysis is:

- $\log N = 24.76 - 9.66 \log \Delta \sigma$ with $R^2 = 0.5$ which indicates a not so good fit between the linear regression line and the test results data since 50% of $\log N$ can be explained by $\log \Delta \sigma$.

The characteristic curves obtained through mean (fitted) curve with 95% probability of survival are:

- $\log N = 21.71 - 9.66 \log \Delta \sigma$ from ASTM E739-91 analysis
- $\log N = 19.26 - 9.66 \log \Delta \sigma$ from Schneider and Maddox analysis

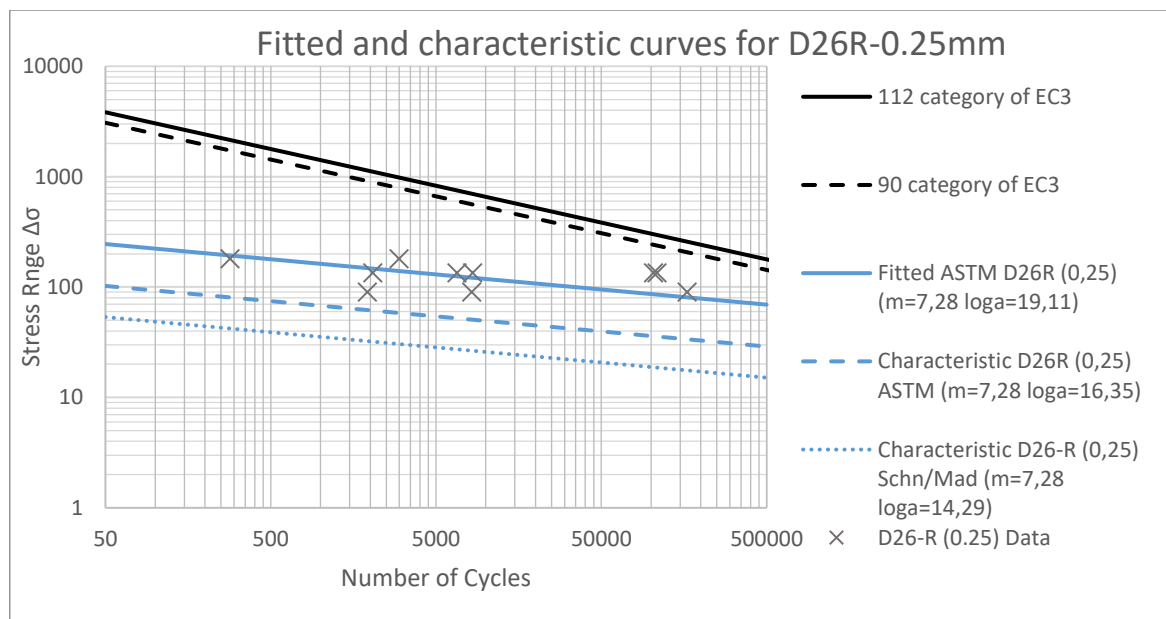


Figure 6.4: Statistical analysis of D26-R specimens with failure criterion 0.25mm

The fitted curve of specimens D26-R with failure criterion 0.25mm tested in stress range regime 180-135-90 MPa according to regression analysis is:

- $\log N = 19.11 - 7.28 \log \Delta \sigma$ with $R^2 = 0.33$ which indicates a bad fit between the linear regression line and the test results data since 33% of $\log N$ can be explained by $\log \Delta \sigma$.

The characteristic curves obtained through mean (fitted) curve with 95% probability of survival are:

- $\log N = 16.35 - 7.28 \log \Delta \sigma$ from ASTM E739-91 analysis
- $\log N = 14.29 - 7.28 \log \Delta \sigma$ from Schneider and Maddox analysis

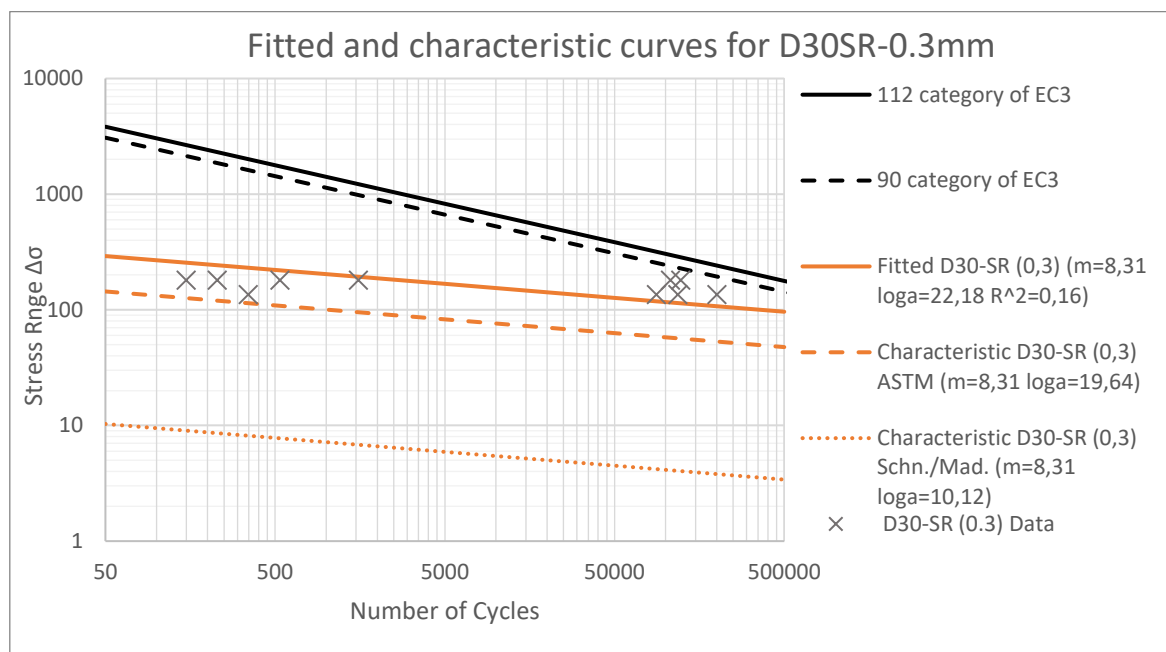


Figure 6.5: Statistical analysis of D30-SR specimens with failure criterion 0.3mm

The fitted curve of specimens D30-SR with failure criterion 0.3mm tested in stress range regime 180-135-90 MPa according to regression analysis is:

- $\log N = 22.18 - 8.31 \log \Delta \sigma$ with $R^2 = 0.16$ which indicates a bad fit between the linear regression line and the test results data since only 16% of $\log N$ can be explained by $\log \Delta \sigma$.

The characteristic curves obtained through mean (fitted) curve with 95% probability of survival are:

- $\log N = 19.64 - 8.31 \log \Delta \sigma$ from ASTM E739-91 analysis
- $\log N = 10.12 - 8.31 \log \Delta \sigma$ from Schneider and Maddox analysis

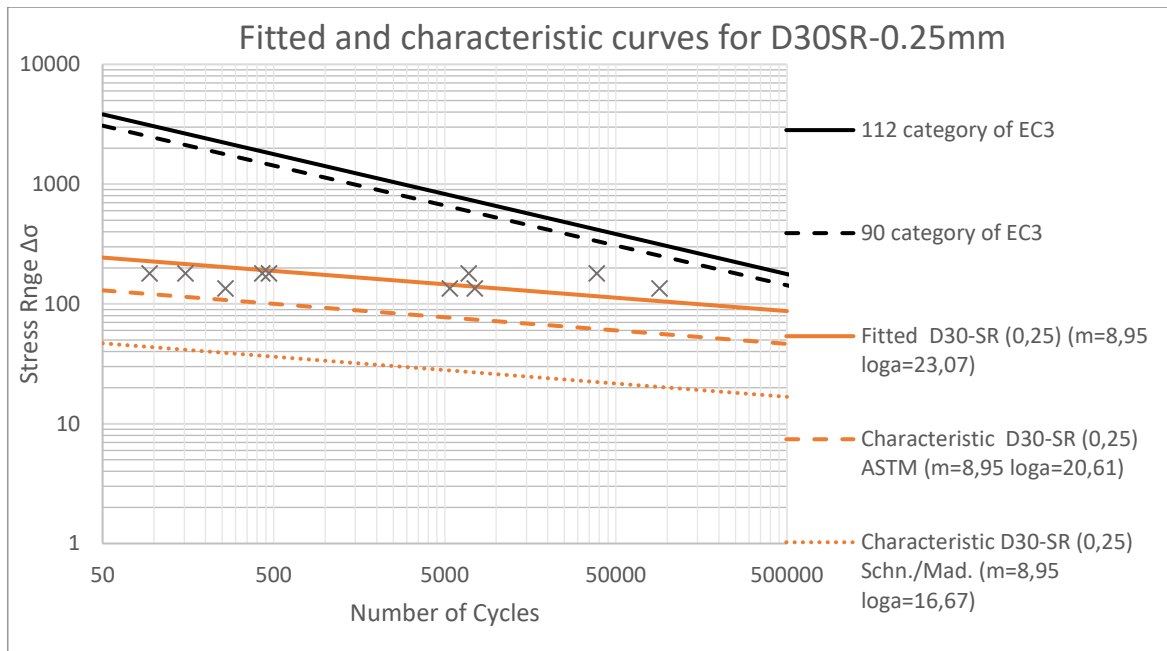


Figure 6.6: Statistical analysis of D30-SR specimens with failure criterion 0.25mm

The fitted curve of specimens D30-SR with failure criterion 0.25mm tested in stress range regime 180-135-90 MPa according to regression analysis is:

- $\log N = 23.07 - 8.95 \log \Delta \sigma$ with $R^2 = 0.5$ which indicates a not so good fit between the linear regression line and the test results data since only 50% of $\log N$ can be explained by $\log \Delta \sigma$.

The characteristic curves obtained through mean (fitted) curve with 95% probability of survival are:

- $\log N = 20.61 - 8.95 \log \Delta \sigma$ from ASTM E739-91 analysis
- $\log N = 16.67 - 8.95 \log \Delta \sigma$ from Schneider and Maddox analysis

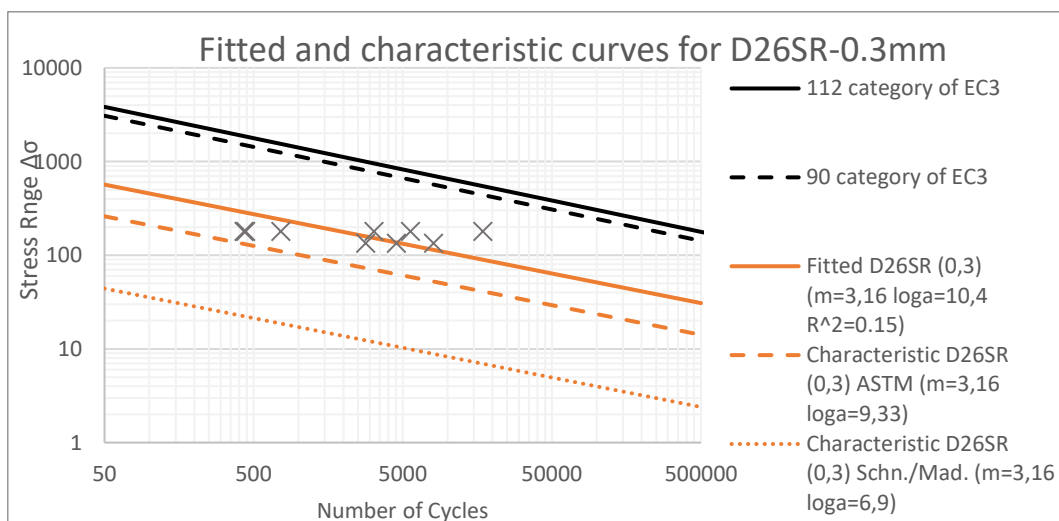


Figure 6.7: Statistical analysis of D26-SR specimens with failure criterion 0.3mm

The fitted curve of specimens D26-SR with failure criterion 0.3mm tested in stress range regime 180-135-90 MPa according to regression analysis is:

- $\log N = 10.4 - 3.16 \log \Delta \sigma$ with $R^2 = 0.15$ which indicates a bad fit between the linear regression line and the test results data since only 15% of $\log N$ can be explained by $\log \Delta \sigma$.

The characteristic curves obtained through mean (fitted) curve with 95% probability of survival are:

- $\log N = 9.33 - 3.16 \log \Delta \sigma$ from ASTM E739-91 analysis
- $\log N = 6.9 - 3.16 \log \Delta \sigma$ from Schneider and Maddox analysis

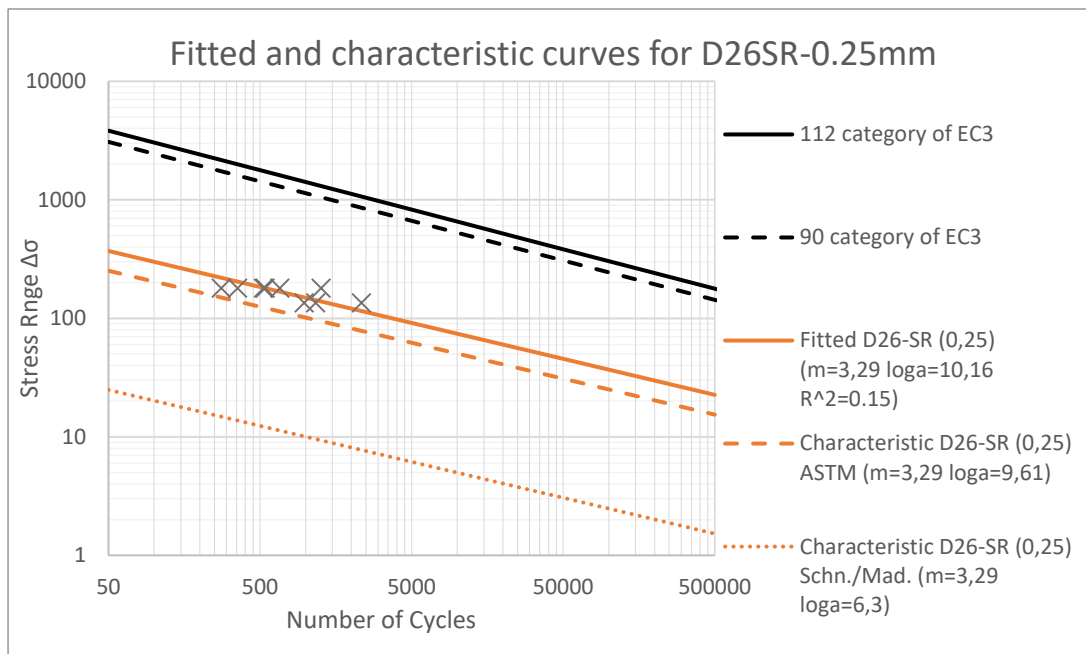


Figure 6.8: Statistical analysis of D26-SR specimens with failure criterion 0.25mm

The fitted curve of specimens D26-SR with failure criterion 0.25mm tested in stress range regime 180-135-90 MPa according to regression analysis is:

- $\log N = 10.16 - 3.29 \log \Delta \sigma$ with $R^2 = 0.15$ which indicates a not so good fit between the linear regression line and the test results data since only 15% of $\log N$ can be explained by $\log \Delta \sigma$.

The characteristic curves obtained through mean (fitted) curve with 95% probability of survival are:

- $\log N = 9.61 - 3.29 \log \Delta \sigma$ from ASTM E739-91 analysis
- $\log N = 8.23 - 3.29 \log \Delta \sigma$ from Schneider and Maddox analysis

From the above statistical analysis of test results initially some generic conclusions can be drawn. All fatigue curves and fatigue test data are below the code detail categories 90 and 112 which represent double lap shear connections preloaded or not. All fatigue curves of specimens with conventional resin (with both failure criteria of 0.3mm and 0.25mm) have a slope roughly between 7.28-9.66 which differs from $m=3$ of IBC's. This holds for specimens D30 with steel reinforced resin which have a slope around 8-9. Of course, this was expected since fatigue curves of codes are based on crack propagation and failure of steel members of connections while in the current research the failure criterion is the slip of the connection due to deterioration of mechanical properties of a totally different material namely the resin (conventional or steel reinforced).

It should be mentioned that the $m=7.28-9.66$ slopes of the resin and steel reinforced resin are in between the extracted $m=6$ for Sinkadur52 and $m=11$ of Sinkadur30 from the research of M. Rodriguez et al. [50] based on statistical analysis of test results with ASTM E739-91 probabilistic method. Of course the loading in that case was cyclic flexural and not uniaxial as in the current research. More details of this research can be found in section 2.6.1.

For geometry D26-SR the slope is close to $m=3$ that's why extracted S-N curves are parallel to code-based, but this should not be considered as reliable since for these specimens there were not available results for 3rd stress range of 90MPa. As it can be seen from previous chapter these specimens D26SR-90 never reached slip above 0.1-0.11mm even at $N=10^6$ so they all were considered as run-outs and excluded from statistical analysis. According to DNVGL [57] at least 3 stress ranges needed to propose fatigue curves for new types of connections.

Furthermore, in all cases the probabilistic approach proposed by Schneider and Maddox [56], leads to more conservative results related to recommended method by ASTM E739-91. This may be attributed to the fact that the former method is mainly recommended by the authors for welded details where there are big uncertainties due to residual stresses induced by welding. That's why they selected Student's T distribution function instead of normal for example since Student's in more prone to producing values that fall far from its mean related to normal distribution.

6.1.2 Comparison of two failure criteria

Also, as it was expected, for all cases the S-N curves extracted for the lower failure criterion of 0.25mm, lead to lower fatigue strength (lower $\Delta\sigma$ for the same N), when compared to the curves with 0.3mm criterion. It should be mentioned that in all cases characteristic curves obtained with Schneider and Maddox model were conservative related to those obtained with ASTM for the same specimen series. An example of this comparison for geometries D30-R, D26-R and D30-SR can be shown in Figure 6.9, Figure 6.10, Figure 6.11 respectively. Since for the geometry D26-SR the slopes are not representative as explained above, these curves are not presented.

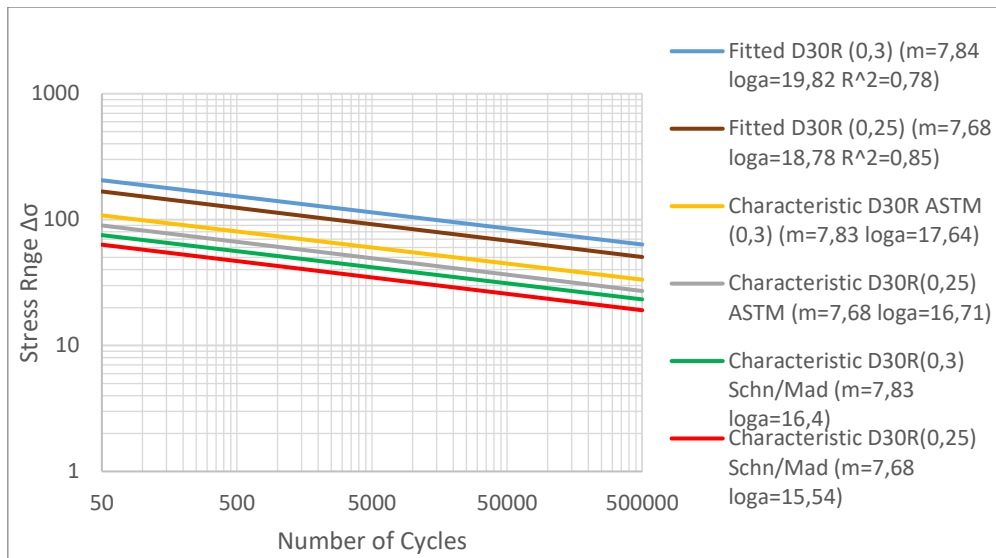


Figure 6.9: Comparison of S-N curves of D30-R specimens for 2 different failure criteria

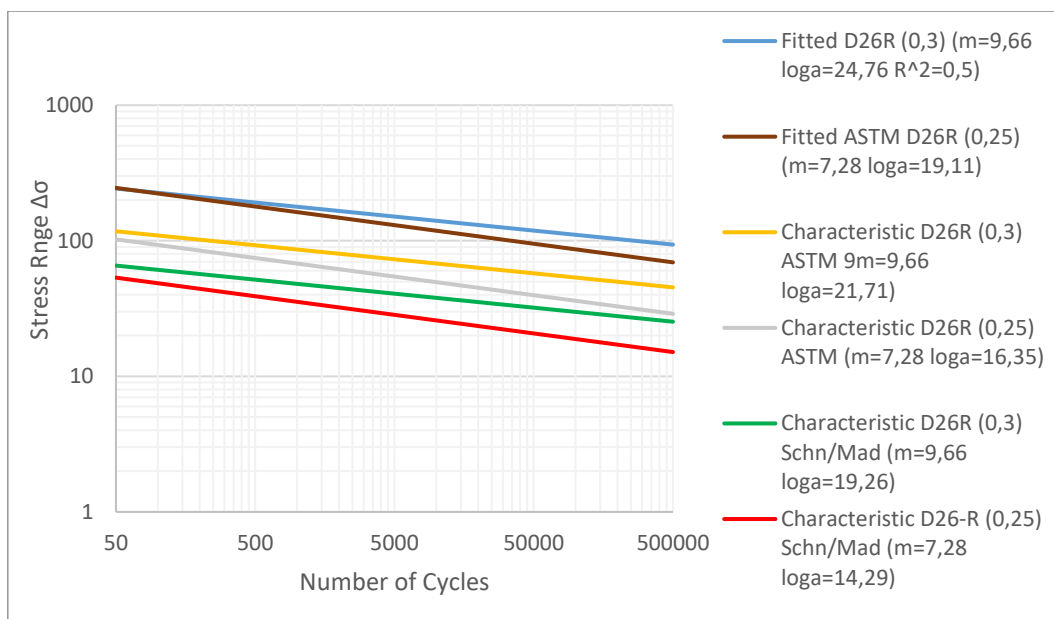


Figure 6.10: Comparison of S-N curves of D26-R specimens for 2 different failure criteria

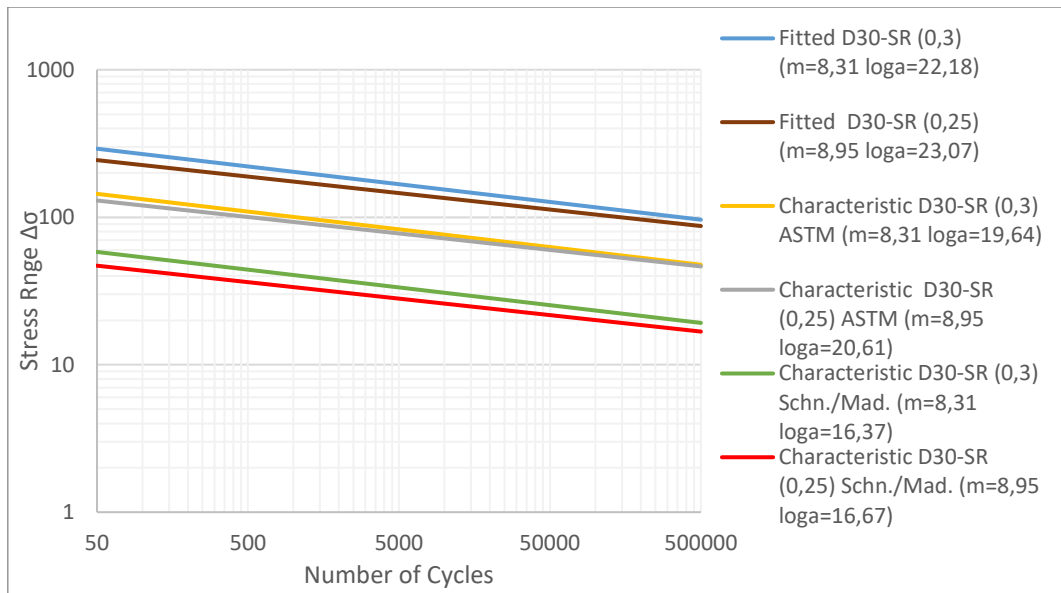


Figure 6.11: Comparison of S-N curves of D30-SR specimens for 2 different failure criteria

6.1.3 Comparison between different hole clearances for the same injection material.

The S-N curves of same injection material namely conventional resin or steel reinforced resin with varying hole clearance are compared in this section. The fitted and characteristic curves presented are based on probabilistic analysis with ASTM model. The comparison will be made only for the failure criterion of 0.3 mm reached slip which was selected based on literature review.

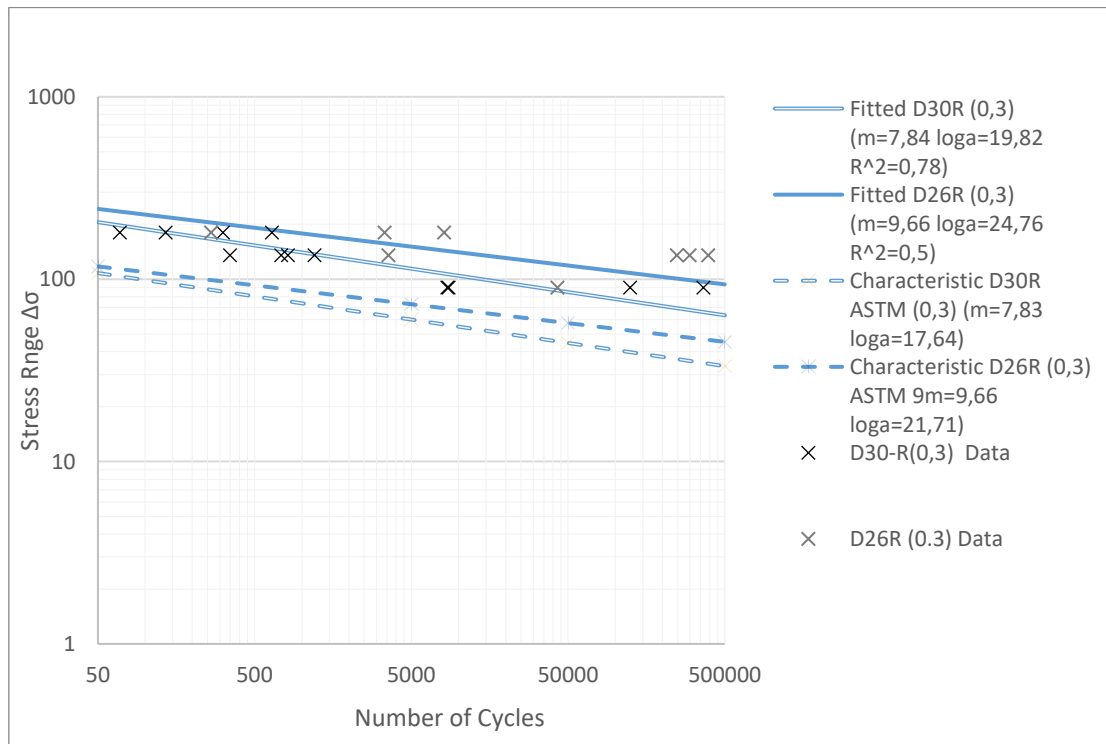


Figure 6.12: Comparison of the effect of oversized holes in fatigue strength of specimens injected with conventional resin

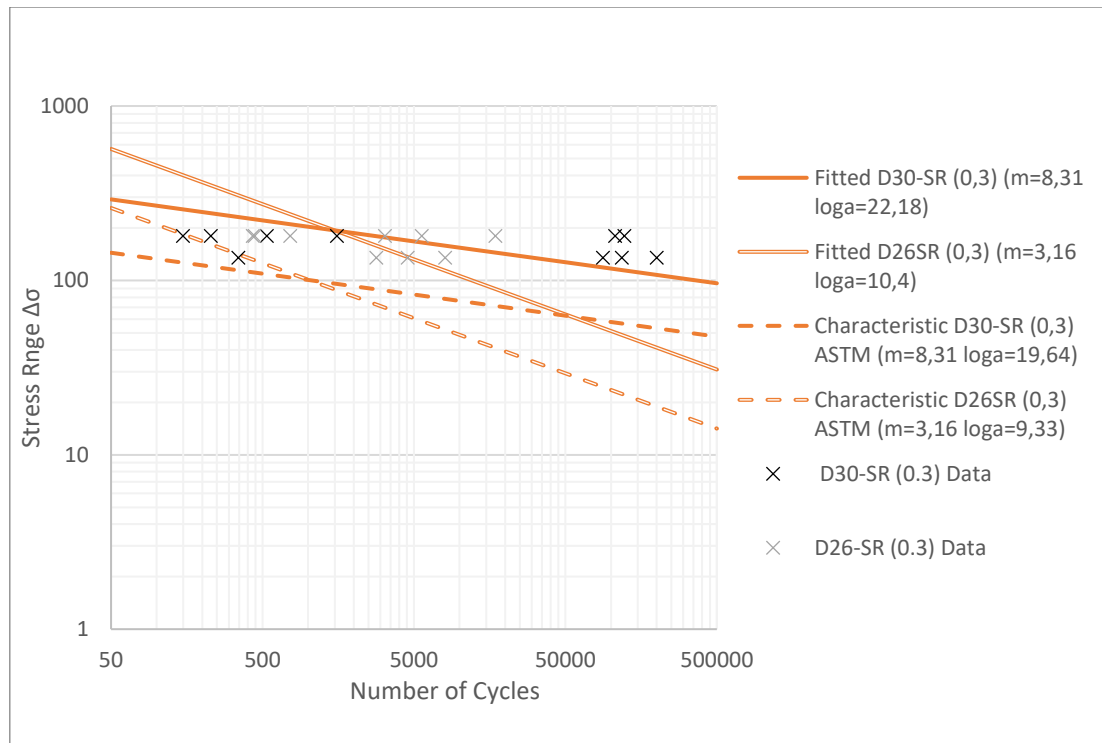


Figure 6.13: Comparison of the effect of oversized holes in fatigue strength of specimens injected with steel reinforced resin

From comparison of test results and S-N curves obtained from statistical analysis according to probabilistic model proposed by ASTM for the same injection material but oversized hole with 6mm and 10mm clearance a safe conclusion can be drawn only for conventional resin SW404/HY2404. In this case the improve in fatigue strength is obvious for conventional resin as it can be observed from Figure 6.12. For low cycle fatigue the difference are not big but as the number of cycles increased until 500.000 the fatigue strength reduction for larger hole is more prominent. This is not the case for steel reinforced resin where fatigue strength is higher for D26SR in low cycles and for higher fatigue cycles D30SR curve is higher (Figure 6.13). However, the later comparison is not reliable since the slope of curves for steel reinforced resin in D26 holes derived only from 2 stress ranges while DNVGL proposes at least 3.

Therefore, from comparison of S-N curves for same injection material and different hole clearance it seems that for larger clearances (10mm instead of 6mm in this case) the fatigue behaviour of conventional resin is worst, while for the fatigue behaviour of SR resin more no safe conclusion can be drawn with the available test data. It is recommended more testing with different stress regime since for the 3rd stress range of 90MPa the specimens injected with the stiff steel reinforced resin never reached 0.3mm failure criterion as it can be seen from slip built-up of these specimens compared to number of cycles (section 5.2.1).

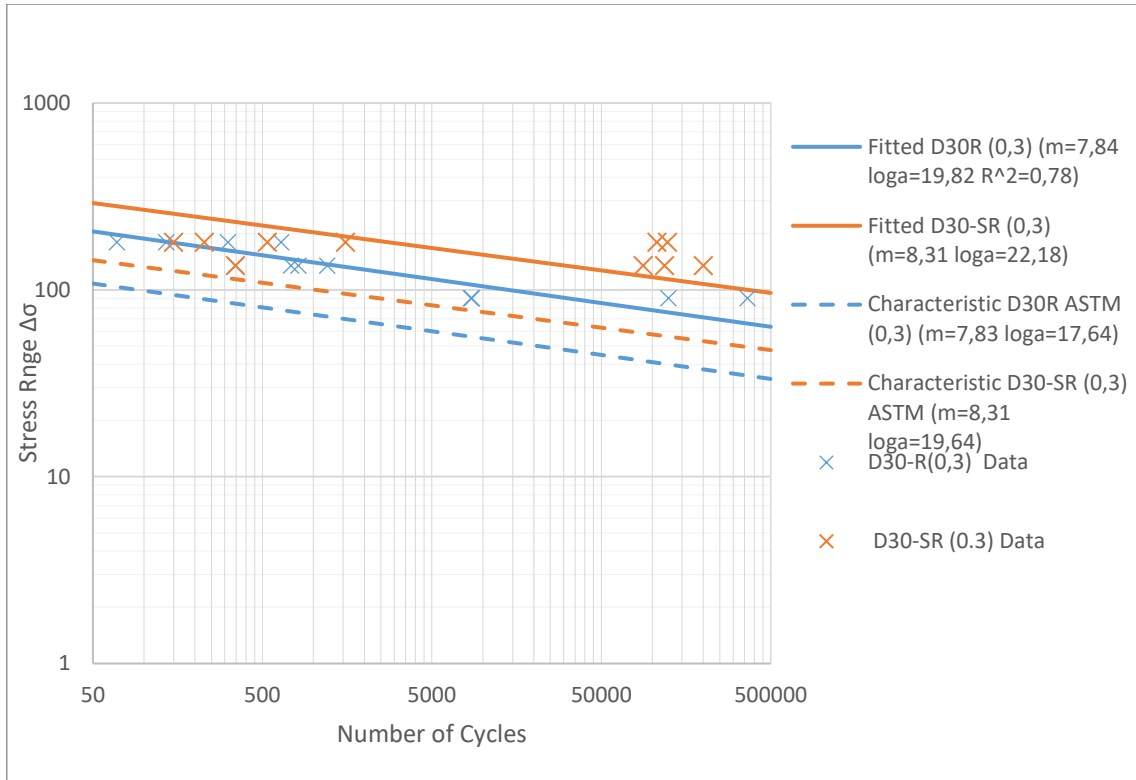


Figure 6.14: Comparison of fatigue strength for same geometry (D30) and varying injection material

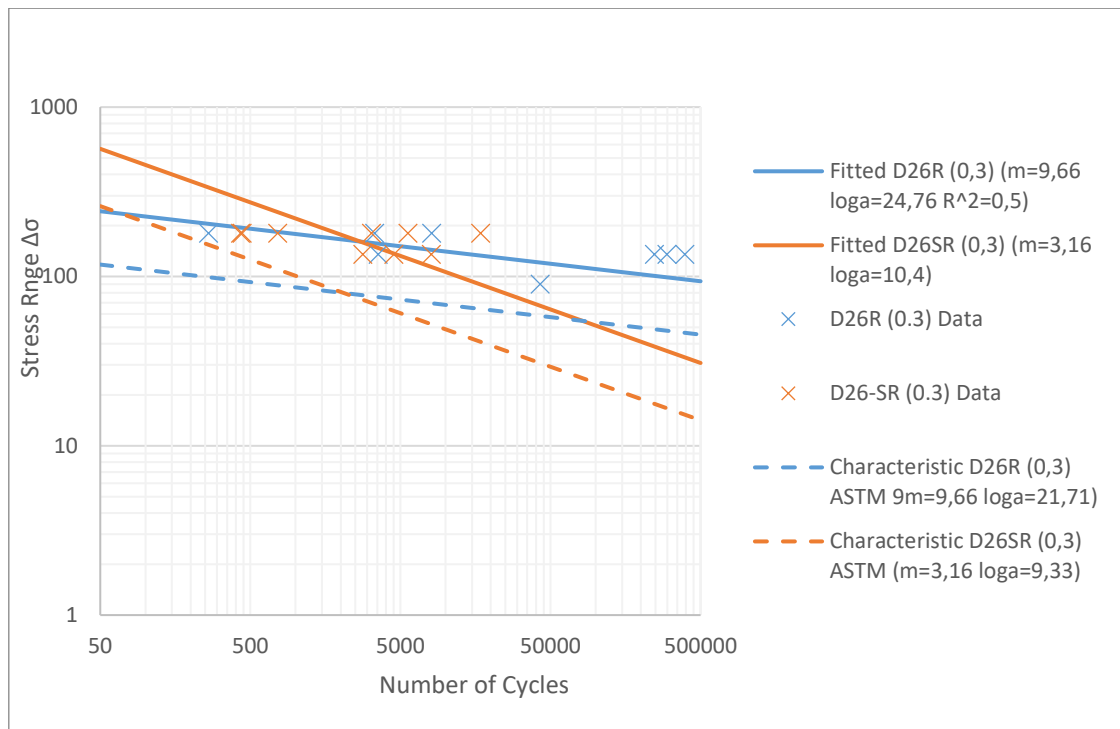


Figure 6.15: Comparison of fatigue strength for same geometry (D26) and varying injection material

From the comparison of specimens with same geometry but different injection material as depicted in Figure 6.14 and Figure 6.15 a conclusion can be drawn for specimen type D30 (10mm oversized hole with bolt part M20). As it can be seen the fatigue strength is higher for steel reinforced resin compared to conventional resin for hole tested fatigue regime, since both fitted and proposed characteristic curves (95% probability of survival) of SR resin are above the curves of conventional R resin. The curves are almost parallel for both SR and R with slopes $m=8.31$ for the former and $m=7.84$ for the latter.

From the comparison of fatigue behaviour of SR and R in geometry D26 (6mm hole clearance for M20 bolt part) no safe conclusion can be drawn since the slope of SR resin ($m=3.16$) is not reliable because it was obtained using only 2 stress ranges as explained above while DNVGL code proposes 3. With the current test data, it seems that SR resin has better fatigue behaviour in low fatigue regime until approx. 5000 cycles and after that conventional resin is superior.

6.2 Summary and Conclusions of statistical evaluation of experiments

- A statistical evaluation of fatigue data for resin and steel reinforced resin tested with the novel test set-up was performed and some preliminary conclusions were drawn.
- For the statistical evaluation of experimental data two probabilistic methods used. The proposed by ASTM E739-91 model were the mean curve shifted based on rectilinear coefficient bands, and the stochastic model proposed by Schneider and Maddox based on t Student's probability function. For both models a 95% probability of survival was used
- The mean (fitted) S-N curves a linear regression analysis performed based on least square method. The equations of both models used for regression model independently and the result for fitted curves in all cases was exactly the same.
- The ASTM model has limited application in high cycle fatigue and outside test limits and extrapolation is not recommended therefore all obtained curves are in tested region 0-500.000 cycles. For this reason, future testing of specimens for several million cycles is recommended.
- The specimens did not reach failure criterion (0.3mm) were defined as run-outs and were not considered in statistical evaluation
- In all cases characteristic curves of Schneider and Maddox were more conservative compared to ASTM curves. This was more prominent with bad fit of mean curve (small R^2). This was expected since Student's function produces results that fall far from its mean compared to Normal distribution function
- The obtained slopes for all cases are between $m=7-9$ ($m=7.84$ for D30R, $m=9.66$ for D26R, $m=8.31$ for D30SR). Only for D26SR specimens the slope is $m=3.16$ but for these series slope is considered as unreliable since was obtained only by 2 stress ranges because all specimens with steel reinforced resin in 6mm oversized hole were run-outs.
- The increase in hole clearance (from 6mm oversized to 10mm oversized) leads to worst fatigue behaviour for connection with conventional resin in relative S-N field. No safe conclusion can be derived for steel reinforced resin
- For 10mm hole clearance (D30 specimens) the fatigue endurance of connection with steel reinforced resin is higher related to that with conventional resin in the relative S-N field. No safe conclusion can be drawn for 6mm hole clearance.

7 Discussion

7.1 Scatter in experimental results

From this research significant scatter in the experimental results has been observed. All specimens with same geometry and same injection material were constructed in the same way (mixing ratios, distance between lower and upper plate to create the hole clearance, filling the clearance with steel shot in case of steel reinforced resin) and the friction was limited using Teflon sheets between steel plates in the only position where there is a steel to steel contact. Also, the use of 2 LVDT'S per specimen reduces the measurement errors. Therefore, the scatter did not occur due to assembly process or testing process. This was a major consideration during the experimental research and despite any adaptations to decrease the scatter (using exactly the same upper lower and side plates for certain specimen series with same geometry in terms of hole clearance and same injection material), a large scatter remained. Only at the end of testing program the major reason for scattering was identified. Experimentally and visibly. This was the occurrence of large air inclusions in the top position (related to the position they had during the injection) of resin parts. This was attributed to injection procedure. The specimens injected in horizontal position through holes in side Perspex plates to inspect the successful injection. One entrance hole in first side plate where the nozzle of injection gun placed and one air escape hall in the second side plate from where the resin flows at the end of injection. This placement of escape hall was the reason for large air inclusions in the top part of resin. These resin missing parts were not immediately visible since it was a thin layer of resin which covered them. But after small effort to remove the layer the large holed revealed.

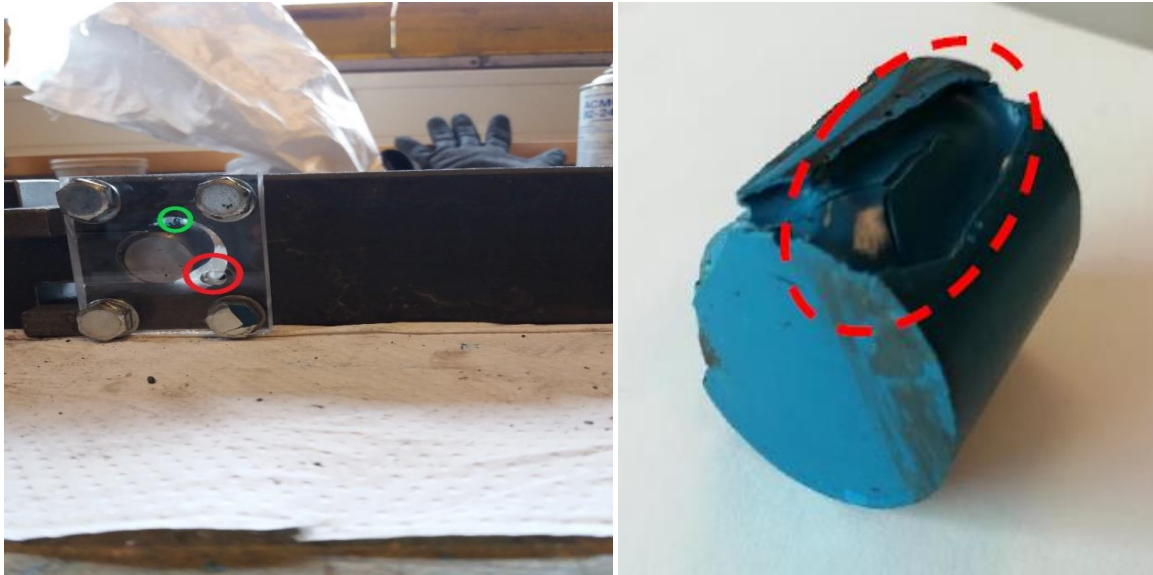


Figure 7.1: Left- Specimen ready for injection highlighted with red the entrance hole and with green the air escape hole on side plates. Right- Large air inclusion in top of the resin part

After this discovery, an adaptation in assembly was adopted to limit the scatter in the last three specimens of experimental program. An air escape path was drilled in the steel lower female plate in order to be at the top position relative to hole during the injection.

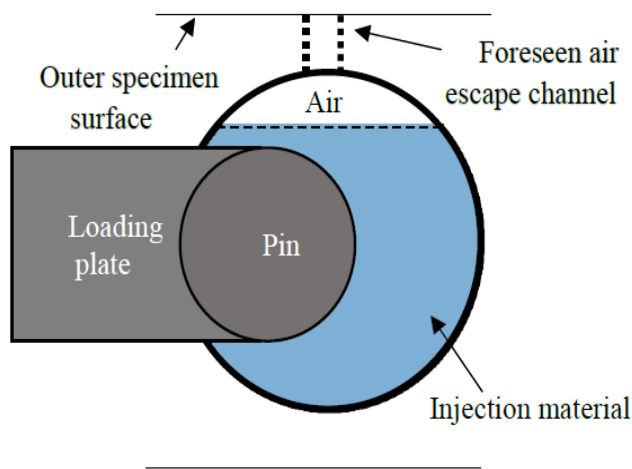


Figure 7.2: Air escape channel at the top position of steel plate to limit the air inclusions

The scatter on the results of slip for specimen tested with this adaptation was limited and the visual observation revealed compact resin parts, verifying the hypothesis of effects of air inclusions due to injection process. From a CT scan of a resin part also air inclusions are identified inside the body the resin layer but their size is relatively small related to the large air inclusions explained above. Another possible reason which identified only visibly is cracks on resin part due to misalignment of lower and upper plate since they are not fixed together. A specimen with obvious misalignment were placed at the machine and after the wedges gripped the specimen and fixed it in place ready for testing, therefore upper and lower plates were in straight line, it was removed from the machine and the side plates removed to observe any defects after this forced rotation. A large crack was revealed and captured in Figure 7.3.



Figure 7.3: Crack due to misalignment during assembly and forced alignment by wedges of machine

By using a base with predefined dimensions in future tests, this defect may be eliminated. These two reasons were identified as the main reasons for scattering. A 3rd reason may lie in a possible rotation of bolt part inside the bolt hole, but this couldn't verify. However, by using an upper plate where the bolt part is already adapted on steel plate as one piece and not separately this can be left out of consideration.

Another reason for scattering may lie in the yielding of upper steel plate which was made by S355 steel. Numerical quasi-static analysis proved that the point of contact with the bolt part in the middle of extension of male plate yields from the 1st cycle already. This did not affect significantly the results of quasi-static phase since the plastic strain was stable over the first 20 cycles but it is unknown to what extent plastic deformations developed after thousands of cycles affecting the slip since plastic deformations of steel may occur in the experiments and added to measured slip.

7.2 Selected parameters for fatigue testing and statistical limitations

Since the test set-up used in this Thesis had never been used before, it is not standardized, and all testing parameters had to be defined based on the literature review. Frequency $f=5\text{Hz}$ for cyclic loading was selected based on the maximum recommended by American Standards for testing of epoxy resins in order to avoid a temperature built up which negatively influences the material properties. After the end of experiments a digital temperature scale was used to measure temperature in resin part and no significant differences with ambient temperature could be identified.

The novel test set-up proposed in this Thesis allows testing of resin (and steel reinforced resin) parts under fatigue loading without the danger of fatigue crack in the bolt or steel plates which is the usual failure mode in shear connections with injection bolts. Therefore, a general structural failure of specimens was not expected during testing. For this reason, a failure criterion had to be defined, to stop the tests. According to literature fatigue performance of Resin Injected Bolted Connections should be determined against a long-term bearing resistance that is relevant at the end of structure's design working life and this according to Eurocode is 0.3mm slip at the end of structure's life. This was selected in the present research.

Three stress ranges were selected for the experimental program. This is in accordance with the recommendations of DNVGL code which recommends 3 stress ranges to establish a reliable slope of the S-N curve. The 1st and higher stress range was 180 MPa. In this stress range the maximum nominal bearing stress in the resin part is 200MPa which according to literature and previous research on the field of resin-injected connections with SW404/HY2404, is the long-term limit stress for static and creep loading. Based on the maximum bearing stress range the lower stress range was identified as 90MPa which is 50% of maximum and a medium stress range of 135 which is 75% of maximum to have a wide stress field for statistical evaluation. However, for specimens with 6mm hole clearance which was the lower between the two hole clearances tested, and when steel reinforced resin was used, the failure criterion of 0.3mm was never reached from any of the specimens. All specimens of this geometry were considered as run-outs. Therefore, for this material and this geometry there is no available test data and the derived from statistical evaluation S-N curves for D26SR specimens are considered unreliable.

Moreover, DNVGL code proposes to perform tests on at least 15 specimens in order to establish S-N curves for new types of connection. The derived S-N curves at current thesis

were based on a number of 9-12 specimens. Therefore, future tests with this type of test set-up should be carried out with more than 15 specimens for each geometry. The test results and derived S-N curves for the specimens referred only in testing in one testing frequency and one stress ratio in constant amplitude with three stress ranges and based only to failure criterion of 0.3mm to obtain the S-N data points. However, to obtain a design recommendation more testing in other frequencies and stress ranges is required for safer conclusions. Moreover, the selected from literature statistical model of ASTM strongly recommends not to extrapolate the fatigue curves outside the tested field. Therefore, the results are presented only in the range 0-500.000 cycles. Future tests with million cycles have to be carried out to have results in relative to real applications, fatigue field.

7.3 Linking resin material properties to fatigue performance

From the results in this research no clear relation could be drawn between the derived from literature mechanical properties of the resin and steel reinforced resin and the fatigue performance of novel testing specimens. The main reason is the significant scatter in experimental results and the time and statistical limitations in the analysis. The tested set-up was used for first time in research and the fact that it is not standardized and due to big scatter the results of this Thesis are considered as preliminary fatigue results on the wide research which is performed by TU DELFT. From the experiments when using some selected specimens to mitigate scatter as possible, it seems that connection with steel reinforced resin leads to lower mean slip after 400.000 cycles compared to the connection with conventional resin at least for medium and low stress ranges of 135 and 90 MPa. For maximum applied nominal bearing stress range the mean slip after 400.000 cycles is the same. With this as a reference point and considering the superior static behavior of steel reinforced resin which led to lower slip after the end of quasi static phase namely after 25 cycles it can be realized that specimens with steel reinforced resin had to undergo relatively larger additional relative displacement due to cyclic loading compared to the resin-injected specimens (850% compared to 320% relative displacement increase after quasi-static phase). This was attributed to lower Poisson's ratio of SR resin which leads to higher 3D stresses but confirmed the complex stress state and the unknown stress concentration mainly inside the body of steel reinforced resin. For this reason, more experiments and multi-scale numerical analysis is required to obtain the fatigue material parameters of resin and steel reinforced resin. The static superiority of steel reinforced resin over conventional which has been already proved in former TU Delft research was confirmed by numerical and experimental quasi-static analysis. From the derived S-N curves which as it was mentioned were calculated with certain limitations it seems that performance of connection with steel reinforced resin leads to higher fatigue life in the relevant S-N field.

8 Conclusions and Recommendations

8.1 Conclusions

The fatigue behaviour of conventional and recently developed steel reinforced resin was investigated in uniaxial compressive stress ranges using a tailor-made test set up as described in previous chapters. Based on static and quasi static numerical study, experiment results and statistical evaluation of test data the following conclusions can be drawn:

- FEA analysis
 - 1) Use of oversized hole in test set-up decreased the initial stiffness of connection using conventional resin. For 6mm oversized hole there was a 40% decrease in stiffness related to normal hole, while for 10mm oversized hole there was a 60% decrease in stiffness. When using steel reinforced resin, the decrease was 30% and 45% respectively for 6 and 10mm hole clearance
 - 2) Use of steel reinforced resin instead of resin increased initial stiffness by 32%, 60%, 77% for 2mm, 6mm and 10mm hole clearance respectively.
 - 3) The thickness of side plates which is 10mm in current test set-up would not affect the results. For limit case of infinite thickness, the longitudinal bearing stress distribution on resin layer along bolt was the same with that of 10mm side plate thickness both when using resin and steel reinforced resin
 - 4) Tailor made non standardized test setup is verified compared to standard double lap shear connection of EN 1090-2. For same hole clearance and using conventional resin as injection material the longitudinal bearing stress distribution presented a very good match for both cases. The difference of 7% in maximum stress is attributed to friction between plates of double lap connection.
 - 5) The upper steel S355 plate yields from 1st cycle. Plastic deformations did not affect results in quasi-static phase since plastic strain in the plate is constant from 1st to 20th cycle but it should be noted that the model designed without bolt threads which may affect the stress concentration.

- Experimental results
 - 1) The experimental initial stiffness was in a good accordance with the numerically calculated initial stiffness, which allowed the validation of numerical model. Specifically, the difference between mean experimental and numerical initial stiffness was 0.87% and 0.12% for resin and steel reinforced resin respectively in 10mm oversized hole (geometry D30R-SR). For 6mm oversized hole (geometry D26R-SR) the difference was 3.24% for the former and 8% for the later
 - 2) The use of oversized holes reduces the initial stiffness of connection, since for a 4mm increase in hole clearance (from 6mm to 10 mm hole clearance) there is a 26% and a 13% decrease in mean experimental initial stiffness in case of resin and steel reinforced resin respectfully.
 - 3) The use of steel reinforced resin leads to higher connection stiffness since specimens D26SR (steel reinforced resin in 6mm hole) had 58% higher mean experimental initial stiffness related to specimens with conventional resin and

same geometry. For 10mm hole clearance this was more prominent since the difference between mean experimental initial stiffness of steel reinforced resin and conventional resin injected specimens was 78%.

- 4) At the end of quasi-static analysis, after 25 cycles all specimens with steel reinforced resin had lower remaining slip related to specimens with conventional resin for same geometry and stress range.
 - 5) There is a stabilization of slip due to cyclic loading for all specimens after 100.000-200.000 cycles
 - 6) No conclusion for fatigue behaviour superiority of steel reinforced resin over resin can be drawn to the tested cycles regime of 400.000 cycles due to large scatter in results specially for larger hole clearance.
 - 7) For selected specimens with limited scatter in results, with 6mm hole clearance, after 400.000 cycles less slip with steel reinforced resin compared to resin was observed (-24%, -21% for 90 and 135MPa stress range). Same slip for resin and steel reinforced at 180MPa stress range.
 - 8) For these selected specimens with higher stress range mentioned in previous conclusion, after the end of quasi static phase (25 cycles) the specimens with steel reinforced resin had less remaining slip, indicated that the steel reinforced resin specimens undergo relatively larger additional relative displacement (+450% in average) due to cyclic loading compared to the conventional resin-injected specimens (+215% in average). This is attributed to lower Poisson ratio of steel reinforced resin (0.22) compared to conventional (0.3).
- Statistical Evaluation of test data
 - 1) Fitted curves are exactly the same using the equations of 2 different models namely ASTM probabilistic model and Schneider and Maddox model.
 - 2) For all the proposed characteristic curves a 95% probability of survival used. Characteristic curves proposed by Schneider and Maddox model always more conservative than ASTM. More prominent with bad fit of mean curve namely for low values of R^2 .
 - 3) The obtained slopes for all cases are between $m=7-9$ ($m=7.84$ for D30R, $m=9.66$ for D26R, $m=8.31$ for D30SR). Only for D26SR specimens the slope is $m=3.16$ but for these series slope is considered as unreliable since was obtained only by 2 stress ranges because all specimens with steel reinforced resin in 6mm oversized hole were run-outs.
 - 4) The increase in hole clearance (from 6mm oversized to 10mm oversized) leads to worst fatigue behaviour for connection with conventional resin in relative S-N field based on the fitted and characteristic curves from ASTM model. No safe conclusion can be derived for steel reinforced resin.
 - 5) For 10mm hole clearance (D30 specimens) the fatigue endurance of connection with steel reinforced resin is higher related to that with conventional resin in the relative S-N field based on the fitted and characteristic curves from ASTM model. No safe conclusion can be drawn for 6mm hole clearance.

8.2 Recommendations for future research

Based on the numerical and experimental research on of the tailor made test set-up in this preliminary study on fatigue behaviour of conventional and steel reinforced resin the following recommendations are proposed to improve reliability the test set-up and to investigate further the fatigue behaviour.

- Modifications in test set-up to improve reliability test data and limit scattering
 - Avoid the presence of escape path in the side of specimen. Instead an air escape path should be placed on the top of the hole, drilled at the steel plate. This adaptation in assembly it is proved experimentally and visually that limits the scattering in test results by creating compact with no observable air inclusions resin layers
 - Use a base to assemble the specimens without any relative rotations between male and female plate which occurred in the assembly of specimens in present Thesis
 - Use an upper plate with adapted bolt part as one piece with upper (male) plate to avoid rotations of bolt part inside the specimen
 - By numerical quasi-static analysis, it is proved that the weakest points on steel parts is at the male steel plate, in the position where the bolt part is in contact. From this point the greater part of the load is transferred to the bolt part and the steel which was S355 yielded from the 1st loading cycle. It was proved numerically that this has limited effect on quasi-static phase, but it is unknown to what extend this yielding of the weakest part affects the measured slip. Therefore, it is recommended to use a steel of higher grade of S420 or even S690.

- Further research on numerical modelling
 - The numerical model was designed without threads and calculated only with static step. This allowed the verification of tailor-made test set-up compared to standardized by Eurocode double lap shear connection but in the actual test set-up the bolt part is threaded. Therefore, a more complex numerical model with designed threads is recommended for future research.
 - Numerical modelling of fatigue loading of test set-up. For this of course, further experimental testing is required on uniaxially loaded cylinders of (steel-reinforced) resin under confined and unconfined conditions to allow for material modelling of the (steel-reinforced) resin under cyclic loads.

- Statistical approach
 - The S-N curves defined using two probabilistic methods which are common in literature. It was recommended not to extrapolate the curves outside the testing field which in the current study reached only 400.000 cycles. To propose S-N curves for design recommendations more testing is required with tests at least of 2 million cycles.
 - More testing is required with different stress range field and in different frequencies to limit the statistical uncertainties in the definition of relevant S-N curves.

9 Bibliography

- [1] A. Koper, "Assessment of epoxy resins for injected bolted shear connections," 2017.
- [2] ECCS, "European Recommendations for Bolted Connections with Injection Bolts." Brussels: ECCS Publication No. 79, 1994.
- [3] European Committee for Standardization, "NEN-EN 1090-2 Execution of steel structures and aluminium structures - Part 2: Technical requirements for steel structures," 2019.
- [4] European Committee for Standardization, "EN 1993-1-8 : 2003 Eurocode 3 : Design of steel structures Part 1 . 8 : Design of joints Stage 49 draft," 2003.
- [5] M. P. Nijgh, "New Materials for Injected Bolted Connections A Feasibility Study for Demountable Connections," 2017.
- [6] I. Kortiš, "the Numerical Solution of the Bolted Connection With the Low-Quality Injected Bolts," 2011.
- [7] J. A. de Freitas, D. de Araújo, M. S. Cerri, "Propriedades Mecanicas de um Molde de Composito Multicamadas para Colagem Sob Pressao de Pecas Ceramicas," Joinville (Brasil), 2012.
- [8] M. P. Nijgh, H. Xin, and M. Veljkovic, "Non-linear hybrid homogenization method for steel-reinforced resin," *Constr. Build. Mater.*, vol. 182, pp. 324–333, 2018.
- [9] H. Xin, M. P. Nijgh, and M. Veljkovic, "Computational homogenization simulation on steel reinforced resin used in the injected bolted connections," *Compos. Struct.*, vol. 210, no. Wccm Xiii, pp. 942–957, 2019.
- [10] "https://www.viba.nl/media/files/resources/176099%2022172rengel-sw-404_hy-2404_hy-5159_eur_e1.pdf." [Online]. Available: https://www.viba.nl/media/files/resources/176099_22172rengel-sw-404_hy-2404_hy-5159_eur_e1.pdf.
- [11] I. A. Gîrbacea, "Assessment of demountable steel-concrete composite flooring systems," 2018.
- [12] L. P. Bouman, "Het monteren, het injecteren en het demonteren van injectiebouten (Installation, injection and dismantling of injection bolts)," 1972.
- [13] European Committee for Standardization, "EN 1993-1-9:2003, Eurocode 3 : Design of steel structures Part 1.9: Fatigue."
- [14] M. De Jesus, A. Fernandes, A. Ribeiro, A. Augusto, "Fatigue behavior of resin-injected bolts: an experimental approach," 2010.
- [15] J. Correia *et al.*, "Fatigue behaviour of single and double shear connections with resin-injected preloaded bolts," in *IABSE Congress Stockholm, 2016: Challenges in Design and Construction of an Innovative and Sustainable Built Environment*, 2016.
- [16] B. Pedrosa, J. A. F. O. Correia, C. Rebelo, and A. De Jesus, "Experimental fatigue tests of resin-injected and standard single bolted connections combining S355 mild steel and old material from Eiffel Bridge," p. 355, 2017.
- [17] A. S. for T. and Materials, "ASTM E739-91: Standard Practice for Statistical Analysis of Linear or Linearized Stress-Life (S-N) and Strain Life (ϵ -N) Fatigue Data," in *Annual Book of ASTM Standards*, 1991, pp. 597–603.

- [18] R. Bjorhovde, R. Colson, A. Zandonini, *Connections in steel structures III Behaviour, Strength and Design*. Pergamon, 1996.
- [19] G. L. Kulak, J. W. Fisher, and J. H. A. Struik, *Guide to design criteria for bolted and riveted joints*, Second Edi., vol. 15, no. 1. AISC, 1988.
- [20] A. Gresnigt, G. Sedlacek, and M. Paschen, "Injection Bolts To Repair Old Bridges," <http://citeseerx.ist.psu.edu/viewdoc/download?doi=10.1.1.552.4959&rep=rep1&type=pdf> (May 5, 2016), pp. 349–360, 2000.
- [21] J. F. Mattes, "Substituição de Rebites por Parafusos Injectados com Resina," Technical University of Lisbon, Lisboa, 2007.
- [22] "https://www.rijkswaterstaat.nl/english/about-us/gems-of-rijkswaterstaat/maeslant-barrier/index.aspx." [Online]. Available: <https://www.rijkswaterstaat.nl/english/about-us/gems-of-rijkswaterstaat/maeslant-barrier/index.aspx>.
- [23] I. D. G. Mans and J. Rodenburg, "The Amsterdam Arena: a multi' functional stadium," vol. 172, pp. 323–331, 2000.
- [24] H. J. Lint, J. C. Wolfswinkel, and A. Gresnigt, "Besparen op Injectiebouten," *Bouwen met Staal*, pp. 44–48.
- [25] N. Gresnigt, D. Beg, and F. Bijlaard, "Injection Bolts in steel structures with short duration high loads."
- [26] D. Beg and N. Gresnigt, "Design Bearing Stresses for Injection Bolts with Short and Long duration High Loads," *Res. Appl. Struct. Eng. Mech. Comput.*, vol. vol.2013, pp. 471–472, 2013.
- [27] L. P. Bouman, "De invloed van de dikteverhoudingen van hoofd- en stuikplaten op de toelaatbare stuikspanning bij verbindingen met injectie-bouten," Delft, 1974.
- [28] M. von Arnim, "Demountable Composite Steel-Concrete Flooring System for Reuse," Delft University of Technology, Karlsruhe Institute of Technology, 2017.
- [29] J. Nassen, J. Holmberg, A. Wadeskog, and M. Nyman, *Direct and indirect energy use and carbon emissions in the production phase of buildings: An input-output analysis*. 2007.
- [30] B. Kourmpanis, A. Papadopoulos, K. Moustakas, M. Stylianou, K. Haralambous, and M. Loizidou, "Preliminary study for the management of construction and demolition waste, *Waste Management & Research*," pp. 267–275, 2008.
- [31] X. Liu, A. Bradford, and M. Lee, "Behavior of High-Strength Friction-Grip Bolted Shear Connectors in Sustainable Composite beams," *J. Struct. Eng.*, p. 141, 2015.
- [32] M. Pavlović, "Resistance of bolted shear connectors in prefabricated steel-concrete composite decks," University of Belgrade, 2013.
- [33] M. Pavlovic, M. Veljkovic, D. Budevaca, and Z. Markovica, "Bolted shear connectors vs headed studs behavior in push out tests," *J. Struct. Eng.*, vol. 88, pp. 134–149, 2013.
- [34] A. Kozma, C. Obenbreit, M. Braun, M. Veljkovic, and M. Nijgh, "Push-out test on demountable shear connectors of steel-concrete composite structures.," in *12th international conference on Advances in Steel-Concrete Composite Structures*, 2018.
- [35] A. Gritsenko, "Towards a Demountable Composite Slab Floor System," 2018.
- [36] A. Sarri, "Assessment of steel-concrete shear connector system with resin injected

- bolts,” 2019.
- [37] M. P. Nijgh, M. Veljkovic, M. Pavlovic, and R. Oly, “Flexible shear connectors in a tapered composite beam optimized for reuse,” 2018.
- [38] A. Kozma and C. Odenbreit, “Documentation and background information of push-out tests, Documentation of the REDUCE Project,” 2017.
- [39] H. Kolstein, J. Li, A. Koper, W. Gard, M. Nijgh, and M. Veljkovic, “Behaviour of double shear connections with injection bolts,” *Steel Constr.*, vol. 10, no. 4, pp. 287–294, 2017.
- [40] R. Committee, *RCSC Specification for Structural Joints Using High-Strength Bolts*. 2014.
- [41] European Committee for Standardization, “NEN-ENV 1090-1.”
- [42] G. Grondin, M. Jin, and G. Josi, “Slip Critical Bolted Connections — A Reliability Analysis for Design at the Ultimate Limit State,” Edmonton, Alberta, Canada, 2007.
- [43] L. J. Broutman and S. K. Gaggar, “Fatigue Behavior of Epoxy and Polyester Resins,” *Int. J. Polym. Mater. Polym. Biomater.*, vol. 1, no. 4, pp. 295–316, 1972.
- [44] R. Talreja, “Damage Mechanics and Fatigue Life-Assesment of Composite Materials,” *Int. J. Damage Mech.*, vol. 8, 1999.
- [45] P. T. Curtis and G. Dorey, “Fatigue of composite materials,” *J. Aerosp. Eng.*, vol. 203, pp. 31–37, 1987.
- [46] L. Lorenzo and H. T. Hahn, “Effect of ductility on the fatigue behavior of epoxy resins,” *Polym. Eng. Sci.*, vol. 26, no. 4, pp. 274–284, 1986.
- [47] D. Hughes and J. L. Way, “Fatigue of fibre - reinforced plastics: a review,” *Composites*, vol. 4, no. 4, pp. 167–173, 1973.
- [48] A. Mortezaei and S. M. Zahrai, “Risk reduction and externally FRP retrofitting of RC columns subjected to extreme loading conditions,” *Asian J. Civ. Eng.*, vol. 13, no. 4, pp. 531–555, 2012.
- [49] L. Sahu and J. Broutman, “Progressive damage of a glass reinforced plastic during fatigue,” *24th Annu. Tech. Conf. Reinf. Plast. Div. Soc. Plast. Ind.*, 1969.
- [50] M. Rodrigues *et al.*, “Fatigue Characterization of Structural Resins Used in Reinforcement of Old Steel Bridges,” in *XI Congresso de Constructao Metalica e Mista, Portugal*, 2017.
- [51] A. International, “ASTM D7791-12: Standard Test Method for Uniaxial Fatigue Properties of Plastics,” 2012.
- [52] *ASTM E739-91: Standard Practice for Statistical Analysis of Linear or Linearized Stress-Life (S-N) and Strain Life (ϵ -N) Fatigue Data*. American Society for Testing and Materials, 1991.
- [53] B. Zafari, J. Qureshi, J. T. Mottram, and R. Rusev, “Static and fatigue performance of resin injected bolts for a slip and fatigue resistant connection in FRP bridge engineering,” *Structures*, vol. 7, no. May, pp. 71–84, 2016.
- [54] R. Rahul and R. Kitey, “Effect of cross-linking on dynamic mechanical and fracture behavior of epoxy variants,” *Compos. Part B Eng.*, vol. 85, pp. 336–342, 2016.
- [55] A. Lowe, O. H. Kwon, and Y. W. Mai, “Fatigue and fracture behaviour of novel rubber modified epoxy resins,” *Polymer (Guildf)*, vol. 37, no. 4, pp. 565–572, 1996.

-
- [56] C. Schneider and S. Maddox, "Best practice guide on statistical analysis of fatigue data," Granta Park, Great Abington, Cambridge, UK, 2003.
- [57] DNV GL, "Dnvgl-Rp-C203," no. DNVGL-RP-C203, p. 176, 2016.
- [58] Y. X. Zhao, B. Yang, M. . Feng, and H. Wang, "Probabilistic fatigue S-N curves including the super-long life regime of a railway axle steel," *Int. J. Fatigue*, no. 1 (10):1550–8, 2009.
- [59] J. Schijve, "Statistical distribution functions and fatigue of structures," *Int. J. Fatigue*, no. 27(9):1031–9, 2005.
- [60] E. Castillo and A. Fernández-Canteli, *A unified statistical methodology for modeling fatigue damage*. Berlin: Springer, 2009.
- [61] J. A. F. de O. Correia *et al.*, "Fatigue Strength Evaluation of Resin-Injected Bolted Connections Using Statistical Analysis," *Engineering*, vol. 3, no. 6, pp. 795–805, 2017.
- [62] R. Hällmark, P. Collin, and S. J. Hicks, "Fatigue Push-out Tests of Coiled Spring Pins," 2017.
- [63] T. R. Gurney, "*A re-analysis of fatigue data for welded joints in steel*". Welding Institute, 1973.
- [64] G. D. Scott and D. M. Kilgour, "The Density of Random Close Packing of Spheres," *J. Phys. D. Appl. Phys.*, vol. 2, no. 6, p. 863, 1969.
- [65] European Committee for Standardization, "Eurocode 1: Actions on structures - Part 1-1: General actions - Densities, self-weight, imposed loads for buildings Eurocode," 2001.
- [66] Dassault Systèmes Simulia, "Abaqus 6.14 User Guide," p. 1146, 2014.
- [67] M. P. Nijgh, H. Xin, and M. Veljkovic, "Mechanical Properties of (steel-reinforced) resins used in Injected Bolted Connections," in *Twenty-second international Conference on Composite Materials (ICCM22)*, 2019.

10 Annex A - Input data for ABAQUS

A.1 Resin conventional

Density:	1.8E-006
Elastic:	
Young's modulus	Poisson's ratio
5640	0.3

Table 10.1: Density and Elasticity for conventional resin

Angle of Friction	Flow Stress Ratio	Dilation Angle
12.15675	1	0

Table 10.2: Drucker Prager criterion parameters for conventional resin

80	0
85	0.000354185
90	0.00105188
95	0.002263137
100	0.00429174
105	0.007590723
110	0.012822443
115	0.020938058
120	0.033281319
125	0.051722468
130	0.078829109
135	0.118082063
140	0.174145514

Table 10.3: Drucker Prager Hardening for conventional resin

A.2 Steel reinforced resin

Density:	5.1E-006
Elastic:	
Young's modulus	Poisson's ratio
15200	0.22

Table 10.4: Density and Elasticity for steel reinforced resin

Angle of Friction	Flow Stress Ratio	Dilation Angle
52.04	1	0

Table 10.5: Drucker Prager criterion parameters for steel reinforced resin

Yield Stress	Abs Plastic Strain
124	0
123.7	0.00634
50.1	0.032
12.96	0.04
4.09	0.045

Table 10.6: Drucker Prager Hardening for steel reinforced resin

A.3 Steel plates and bolts

Steel plates S355

Density:	7.8E-006
Elastic:	
Young's modulus	Poisson's ratio
210000	0.3

Table 10.7: Density and Elasticity for steel grade S355

Yield Stress	Plastic strain
355.6	0
359.6	0.0111
539	0.0528
612	0.1794

Table 10.8: Plasticity of steel grade S355

Bolts 10.9

Density:	7.8E-006
Elastic:	
Young's modulus	Poisson's ratio
210000	0.3

Table 10.9: Density and Elasticity for steel grade 10.9

11 Appendix B – Probabilistic models

B.1 Schneider and Maddox

Linear Regression Analysis

Parameters	Equations
Number of tests	N
Mean value of $\log \Delta \sigma$	$\overline{\log \Delta \sigma} = \frac{\sum \log \Delta \sigma_i}{N}$
Variance of $\log \Delta \sigma$	$Var(\log \Delta \sigma) = \frac{\sum (\log \Delta \sigma_i - \overline{\log \Delta \sigma})^2}{N - 1}$
Mean value of $\log N$	$\overline{\log N} = \frac{\sum \log N_i}{N}$
Variance of $\log N$	$Var(\log N) = \frac{\sum (\log N_i - \overline{\log N})^2}{N - 1}$
Covariance of $\log \Delta \sigma$ and $\log N$ (R^2)	$Cov(\log \Delta \sigma, \log N) = \frac{\sum (\log \Delta \sigma_i - \overline{\log \Delta \sigma})(\log N_i - \overline{\log N})}{N - 1}$
Coefficient of determination	$R^2 = \frac{Cov(\log \Delta \sigma, \log N)^2}{Var(\log \Delta \sigma) \cdot Var(\log N)}$

Slope m	$m = \frac{Cov(\log \Delta\sigma, \log N)}{Var(\log \Delta\sigma)}$
Interception loga	$\log a = \overline{\log N} - m \cdot \overline{\log \Delta\sigma}$
Fitted curve	$\log N = \log a + m \cdot \log \Delta\sigma$

Table 11.1: Linear regression analysis equations and parameters for Schneider and Maddox model

Characteristic curves 95% survival probability

Parameters	Equations
Number of tests	N
Student's t score	$t(0.05)$ for n-2 degrees of freedom
Standard deviation for logN	$\sigma_{\log N} = \sqrt{\frac{N}{N-2} (1-R^2) \cdot Var(\log N)}$
Stress at Nc (MPa)	$\Delta\sigma_c = 10^{(\log 2 \cdot 10^6 - \log a)/m}$
Correction factor f for σ at Nc	$f = 1 + \frac{1}{N} + \frac{(\log \Delta\sigma_c - \overline{\log \Delta\sigma})^2}{Var(\log \Delta\sigma)}$
Characteristic $\log \Delta\sigma_{c,k}$	$\log \Delta\sigma_{c,k} = \log \Delta\sigma_c + \frac{t(0.05) \cdot \sigma_{\log N} \cdot \sqrt{f}}{m}$
Characteristic $\Delta\sigma_{c,k}$ (MPa)	$\Delta\sigma_{c,k} = 10^{\log \Delta\sigma_{c,k}}$
Characteristic $\log a_k$	$\log a_k = \overline{\log N_c} - m \cdot \overline{\log \Delta\sigma_{c,k}}$
Correction factor	$f = 1 + \frac{1}{N} + \frac{(\log \Delta\sigma_c - \overline{\log \Delta\sigma})^2}{\sum_{i=1}^N (\log \Delta\sigma_i - \overline{\log \Delta\sigma})^2}$
Characteristic curve	$\log N_{c,k} = (\log a + m \cdot \log \Delta\sigma) - t_{5\%} \sigma \sqrt{f}$

Table 11.2: Parameters and equations used to establish characteristic curves with Schneider and Maddox model

	Level of Significance									
2 Tailed	0.40	0.30	0.20	0.15	0.10	0.05	0.02	0.01	0.002	0.001
1 Tailed	0.20	0.15	0.10	0.075	0.05	0.025	0.01	0.005	0.001	0.0005
df										
1	1.376	1.963	3.133	4.195	6.320	12.69	31.81	63.67	—	—
2	1.060	1.385	1.883	2.278	2.912	4.271	6.816	9.520	19.65	26.30
3	0.978	1.250	1.637	1.924	2.352	3.179	4.525	5.797	9.937	12.39
4	0.941	1.190	1.533	1.778	2.132	2.776	3.744	4.596	7.115	8.499
5	0.919	1.156	1.476	1.699	2.015	2.570	3.365	4.030	5.876	6.835
6	0.906	1.134	1.440	1.650	1.943	2.447	3.143	3.707	5.201	5.946
7	0.896	1.119	1.415	1.617	1.895	2.365	2.999	3.500	4.783	5.403
8	0.889	1.108	1.397	1.592	1.860	2.306	2.897	3.356	4.500	5.039
9	0.883	1.100	1.383	1.574	1.833	2.262	2.822	3.250	4.297	4.780
10	0.879	1.093	1.372	1.559	1.813	2.228	2.764	3.170	4.144	4.586
11	0.875	1.088	1.363	1.548	1.796	2.201	2.719	3.106	4.025	4.437
12	0.873	1.083	1.356	1.538	1.782	2.179	2.682	3.055	3.930	4.318
13	0.870	1.079	1.350	1.530	1.771	2.160	2.651	3.013	3.852	4.221
14	0.868	1.076	1.345	1.523	1.761	2.145	2.625	2.977	3.788	4.141
15	0.866	1.074	1.341	1.517	1.753	2.131	2.603	2.947	3.733	4.073
16	0.865	1.071	1.337	1.512	1.746	2.120	2.584	2.921	3.687	4.015
17	0.863	1.069	1.333	1.508	1.740	2.110	2.567	2.899	3.646	3.965
18	0.862	1.067	1.330	1.504	1.734	2.101	2.553	2.879	3.611	3.922
19	0.861	1.066	1.328	1.500	1.729	2.093	2.540	2.861	3.580	3.884
20	0.860	1.064	1.325	1.497	1.725	2.086	2.529	2.846	3.552	3.850
21	0.859	1.063	1.323	1.494	1.721	2.080	2.518	2.832	3.528	3.820
22	0.858	1.061	1.321	1.492	1.717	2.074	2.509	2.819	3.505	3.792
23	0.857	1.060	1.319	1.489	1.714	2.069	2.500	2.808	3.485	3.768
24	0.857	1.059	1.318	1.487	1.711	2.064	2.493	2.797	3.467	3.746
25	0.856	1.058	1.316	1.485	1.708	2.060	2.486	2.788	3.451	3.725
26	0.856	1.058	1.315	1.483	1.706	2.056	2.479	2.779	3.435	3.707
27	0.855	1.057	1.314	1.482	1.703	2.052	2.473	2.771	3.421	3.690
28	0.855	1.056	1.313	1.480	1.701	2.048	2.468	2.764	3.409	3.674
29	0.854	1.055	1.311	1.479	1.699	2.045	2.463	2.757	3.397	3.660
30	0.854	1.055	1.310	1.477	1.697	2.042	2.458	2.750	3.386	3.646
40	0.851	1.050	1.303	1.468	1.684	2.021	2.424	2.705	3.307	3.551
50	0.849	1.047	1.299	1.462	1.676	2.009	2.404	2.678	3.262	3.496
60	0.848	1.045	1.296	1.458	1.671	2.000	2.391	2.661	3.232	3.460
70	0.847	1.044	1.294	1.456	1.667	1.994	2.381	2.648	3.211	3.435
80	0.846	1.043	1.292	1.453	1.664	1.990	2.374	2.639	3.196	3.417
90	0.846	1.042	1.291	1.452	1.662	1.987	2.369	2.632	3.184	3.402
100	0.845	1.042	1.290	1.451	1.660	1.984	2.365	2.626	3.174	3.391
∞	0.842	1.036	1.282	1.440	1.645	1.960	2.327	2.576	3.091	3.291

Figure 11.1: Student's *t* distribution used in Schneider and Maddox model

B.2 ASTM Probabilistic model

Linear Regression Analysis

Number of tests	k
Dependent variable Y	$Y = \log N$
Independent variable X	$X = \log \Delta \sigma$
Intercept logA	$A = \bar{N} - B \cdot \bar{\Delta \sigma}$
Slope	$B = \frac{\sum_{j=1}^k (\Delta \sigma_j^* - \bar{\Delta \sigma})(N_j^* - \bar{N})}{\sum_{j=1}^k (\Delta \sigma_j^* - \bar{\Delta \sigma})^2}$
Fitted curve	$Y = A + B \cdot X$

Figure 11.2: Linear regression analysis equations and parameters for ASTM model

Characteristic curves 95% survival probability

S	Standard deviation of logNi
α (95%)	2
Characteristic curve	$N = A + B \cdot \Delta \sigma \pm a \cdot S$

Figure 11.3: Parameters and equations used to establish characteristic curves with ASTM model

12 Appendix C – Materials

C.1 Resin conventional



Advanced Materials

RenGel[®] SW 404 / Ren[®] HY 2404 or HY 5159

GELCOAT RESIN
FILLED EPOXY SYSTEM, WITH OUTSTANDING ABRASION RESISTANCE

KEY PROPERTIES	<ul style="list-style-type: none"> • Outstanding mechanical strength and qualities • Good chemical resistance • Very hard, abrasion-resistant surfaces
-----------------------	---

APPLICATIONS	<ul style="list-style-type: none"> • Foundry patterns • Copy-milling models • Foaming and concrete-casting moulds • Tools and tooling aids
---------------------	--

PRODUCT DATA

Property	Unit	RenGel [®] SW 404	Ren [®] HY 2404	Ren [®] HY 5159
Appearance		Paste	Clear liquid	Clear liquid
Colour	visual	Blue	Pale yellow	Pale yellow
Viscosity at 25°C*	mPas	70'000-110'000**	3400-5000**	120-175**
Density	g/cm ³	1.85-1.95	1.0-1.05	0.98

** Specified data are on a regular basis analysed. Data which is described in this document as 'typical' is not analysed on a regular basis and is given for information purpose only. Data values are not guaranteed or warranted unless if specifically mentioned.

TYPICAL SYSTEM DATAS

PROCESSING

Mix ratio	Parts by weight	
RenGel [®] SW 404	100	100
Ren [®] HY 2404	10	-
Ren [®] HY 5159	-	8

Mix the two components thoroughly in the ratio indicated.
Apply in thin layers with a brush or spatula, wait until gelcoat has gelled, but ensure that it is still slightly tacky before proceeding.
Post-curing will improve final properties.



PROPERTIES

Resin/Hardener mix:	Volume	Unit	SW 404 HY 2404	SW 404 HY 5159
Appearance			Blue	Blue
Pot life at 25°C	250 ml	min	15	50
Demoulding time		h	12	12

*After cure: with HY 2404: 14 hours at 60 °C
with HY 5159: 14 hours gradually to 80 °C*

Density	ISO 1183	g/cm ³	1.8	1.8
Hardness	ISO 868	Shore D	85-90	85-90
Deflection temperature	ISO 75	°C	80	100
Abrasion	Taber	mm ³ /100U	4-6	4-6

STORAGE

Provided that RenGel® SV 404, Ren® HY 2404 and Ren® HY 5159 are stored in a dry place in their original, properly closed containers at the storage temperatures mentioned in the MSDS they will have the shelf lives indicated on the labels. Partly emptied containers should be closed immediately after use.

WORKING CONDITION

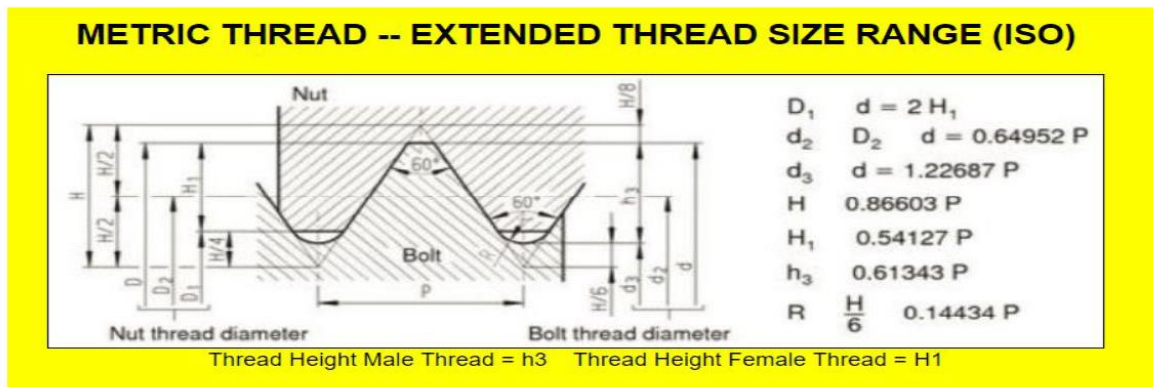
The products should be handled when in the temperature range of 20 - 25°C.

PACKAGING

System	SW 404	HY 2404	HY 5159
Quantity and Weight	2 x 10kg	6 x 1kg	6 x .800gr
Quantity and Weight	2 x 3kg	6 x 300gr	6 x 240gr
Quantity and Weight	6 x 500gr	6 x 50gr	6 x 40gr

Figure 12.1: Product sheet of RENGEL

C.2 Metric threads M20x2.5



Size (mm)	ISO Metric Profile		Pitch (mm)	Class	Internal (nut thread)			Basic Tap Drill		
	Thread designation	Simple Thread Designation			Minor Dia D1	Pitch Dia d2=D2	Major DIA d=D			
20	M20x2.5	M20	2.5	6H	max min	17.294 17.744	18.376 18.6	max min	20 20.585	17.5

Figure 12.2: Standard dimensions of metric threads M20x2.5 according to ISO

